UNIVERSITÀ DEGLI STUDI DI SALERNO

Dipartimento di Ingegneria Civile

Dottorato di Ricerca
in
Rischio e Sostenibilità
nei Sistemi dell'Ingegneria Civile, Edile ed Ambientale

XXXIV Ciclo (a.a. 2021/2022)

SPATIO-TEMPORAL CHARACTERIZATION AND PREDICTION OF DROUGHT IN SOUTHERN ITALY, CASE STUDY: CAMPANIA REGION

OUAFIK BOULARIAH

Il Tutor
Prof. Antonia Longobardi
Il co-tutor
Prof. Paolo Villani

Il Coordinatore
Prof. Fernando Fraternali

ABSTRACT

Drought is a natural phenomenon that has widespread and significant effects on the global economy, environment, industries, and communities. early drought detection allows for the implementation, mitigation strategies and measures before its occurrence. Therefore, drought assessment is critical in the planning and management of water resource systems, particularly during dry climatic periods. However, assessing droughts is not always simple.

This study described and evaluated drought conditions in Campania (southern Italy) using an in-situ measurement database that spans a centennial period from 1918 to 2019. With the assistance of these tools, water managers may more accurately assess droughts and prepare in advance for water management operations during droughts. Since water resource management in our area was crucial, the Campania region in southern Italy was selected as the case study region. To achieve the objectives of this study, an analysis of the precipitation coefficient of variation, assumed as index of inter-annual climate variability, was first performed over the period 1918-2015. Based on the findings of the above analysis and with the aim of reconstructing continuous long-term monthly scale precipitation time series, the in-situ point measurements (observed at the rain gauge locations) for the two datasets were projected on a 10×10 km resolution grid covering the whole region by using a geostatistical interpolation approach.

Standardized Precipitation Index (SPI) and Standardized Precipitation Evapotranspiration Index (SPEI) time series were reconstructed for different accumulation timescales (from 3 to 48 months) to explore the full range of drought types. The modified Mann–Kendall and Sen's tests were applied to identify SPI and SPEI changes over time. In addition, the impact of the vegetation stress to better understand causes of the drought phenomenon was evaluated. Drought characteristics (Duration, severity and peak) were furthermore investigated for both moderate (SPI/SPEI ≤ -1) and extremely severe conditions (SPI/SPEI ≤ -2).

Spatial autocorrelation was used too, to evaluate whether the different events studied have similar characteristics in terms of spatial aggregation, i.e., if there are areas increasingly affected by drought and how they are affected. The same events in which drought was already assessed with the SPI and SPEI indices were taken into consideration, i.e., the events of 1962, 1989, 2003 and 2017.

DECLARATION

I, Ouafik Boulariah, declare that the PhD thesis entitled ‘SPATIO-TEMPORAL CHARACTERIZATION AND PREDICTION OF DROUGHT IN SOUTHERN ITALY, CASE STUDY: CAMPANIA REGION’ is no more than 100,000 words in length including quotes and exclusive of tables, figures, appendices, bibliography, references, and footnotes.

This thesis contains no material that has been submitted previously, in whole orin part, for the award of any other academic degree or diploma. Except where otherwise indicated, this thesis is my own work.

Signature

Ouafik Boulariah
April 2022

ACKNOWLEDGMENTS

I would like to express heartiest gratitude and indebtedness to my Principal Supervisor, **Dr. Antonia Longobardi** for her scholastic guidance, constant encouragement, inestimable help, valuable suggestions, and great support through my study at university of Salerno (UNISA). She has never looked at me separately from her other students. She has always taken time to introduce me to the people within the discipline, kept me focused, carefully listened to my problems and has been a flexible but a strong advocate to me. In reviewing my writing, she offered painstaking comments, whilst respecting my voice. What kept me moving constantly, were her amazingly insightful comments with detailed attention to my arguments, showing the ways of dramatically improving them. I have been especially fortunate to work with such a great supervisor.

Without her continual efforts, this would have been a very lonely journey. She has given me great freedom to pursue independent work. More importantly, she demonstrated her faith in my ability and encouraged me to rise to the occasion.

I would also like to express special thanks to Professor **Paolo Villani** for his valuable suggestions, and great support through my study at university of Salerno, he has been a strong and supportive Associate Supervisor throughout my study at Unisa. I also like to thank Professor **Salvatore Barba** for providing me all necessary support which have given me several opportunities to achieve my research work.

Following individuals and institutions also deserve special mention for theircontributions to this dissertation and their support is gratefully acknowledged:

- Faculty of Civil Engineering in Unisa for providing financialsupport for this research project.
- Faculty of Civil Engineering for their financial support for attending different international and national conferences.
- Environmental and Maritime Hydraulics laboratory (LIDAM) and all the staff for research training provided.

- **Giovanni Salzano** and all the staff of Post-graduate Research for their quick responses to my queries regarding my scholarship.
- Prof. **Mohamed Meddi** and Prof. **Rassoul Abdelaziz** in National high school of hydraulics Blida, Algeria. for their quick response to my queries.
- Family and friends who gave me social and intellectual support.

At last, but not the least, I feel highly indebted to my beloved parents, little brother **Soheib** and sister **Khaoula**, my adoptive mother **"ASSIA"** (may God have mercy on her) and other family members for their unconditional support, patience and love which were always there for me

LIST OF PUBLICATIONS AND CONFERENCES

Publications

1. Boulariah, O., Meddi, M., & Longobardi, A. (2019). **Assessment of prediction performances of stochastic and conceptual hydrological models: monthly stream flow prediction in northwestern Algeria**. Arabian Journal of Geosciences, 12(24), 1-14.
2. Longobardi, A., Boulariah, O., & Villani, P. (2021). **Assessment of centennial (1918–2019) drought features in the Campania region by historical in situ measurements (southern Italy)**. Natural Hazards and Earth System Sciences, 21(7), 2181-2196.
3. Boulariah, O., Mikhailov, P. A., Longobardi, A., Elizariev, A. N., & Aksenov, S. G. (2021). **Assessment of prediction performances of stochastic models: Monthly groundwater level prediction in Southern Italy**. Journal of Groundwater Science and Engineering, 9(2), 161-170.
4. Longobardi, A., Boulariah, O. **Long-term regional changes in inter-annual precipitation variability in the Campania Region, Southern Italy**. *Theor Appl Climatol* **148,** 869–879 (2022). https://doi.org/10.1007/s00704-022-03972-2
5. **Reconstruction of precipitation gridded data from two database at different scale: the case of Campania Region (Italy), based on centenary monthly data,** Journal of water resources management, **Boulariah, O**, Longobardi, Antonia, Villani, Paolo (**Under review).**

Conference Papers

1. **Ricostruzione di un database di piogge mensili per la regione Campania: analisi delle condizioni di siccità descritte dall'SPI**. pp.78-78. In Studio dei fenomeni idrologici in relazione alla tutela e salvaguardia del territorio, Longobardi, A.; Boulariah, O.; Villani, P.,Conference date : 30/09 - 1/10, 2021
2. **Drought characteristics in southern Italy during 1918–2019 by SPEI spatio-temporal assessment**. pp.1-1. In ICSH-STAHY 2021, Longobardi, A.; Boulariah, O., Conference date:Sept 16-17, 2021
3. **Implementation of the standardized precipitation index (SPI) for regional drought assessment in a Mediterranean area**. pp.1-1. In MetMed2021, Longobardi, Antonia; Boulariah, Ouafik; Villani, Paolo., Conference date:23-25 maggio 2021
4. **Long term monthly precipitation database reconstruction for drought assessment**. pp.1-1. In ClimRisk2020: Time for Action! Raising the ambition of climate action in the age of global emergencies., Boulariah, O.; Longobardi, A.; Nobile, V.; Sessa, M.; Villani, P.
5. **Trend analysis of the year -to -year rainfall variability under a Mediterranean climate in southern Italy**. pp.151-158. In SUSTAINABLE MEDITERRANEAN CONSTRUCTION - ISSN:2420-8213 vol. 10 (151)., BOULARIAH, OUAFIK; LONGOBARDI, Antonia; VILLANI, Paolo

TABLE OF CONTENTS

INTRODUCTION

1.1 Background

The climate has changed and will continue to change in the future due to greenhouse gases, atmospheric aerosols, and human (anthropogenic) activities; thus significant climate change is expected in the future (IPCC 2014)

According to the Intergovernmental Panel on Climate Change (IPCC) (IPCC 2014), the atmospheric concentration of CO2 has increased from 345 ppm in 1750 to 405 ppm in 2011 and is projected to reach 463-640 ppm by 2050 and 800-1313 ppm by 2100. The IPCC further states that the global average air temperature has increased over the 21st century by about 0.9 ± 0.6°C. This is the largest increase of any century in the last 1,000 years. Under different emission scenarios, all atmospheric general circulation models (AGCMs) project a further increase in global average temperature of 2-6 °C by the end of the 21st century and high interannual climate variability (Giorgi 2006, Raymond et al. 2016, Ullmann et al. 2018). These changes in atmospheric temperature and terrestrial radiation balance may affect several components of the hydrological cycle, such as changes in rainfall patterns, increases in atmospheric water vapor, increases in evaporation and changes in soil moisture and runoff, leading to an increase in extreme events (heat waves, intense precipitation, droughts) (Longobardi and Van Loon 2018). In addition, according to the Sixth and latest assessment report (AR6) of IPCC (IPCC 2021), no region will

be invulnerable to the effects of climate change, with enormous human and economic costs that far outweigh the costs of the action.

Droughts and fires will worsen in Southern Africa, the Mediterranean, the Amazon, the western United States, and Australia, affecting livelihoods, agriculture, water systems, and ecosystems (IPCC 2021); moreover, snow, ice, and river flooding are expected to have an impact on infrastructure, transportation, energy production, and tourism in North America, the Arctic, Europe, the Andes, and elsewhere. Storms are expected to intensify over most of North America, Europe, and the Mediterranean (IPCC 2021).

Drought is the most challenging natural phenomenon where its frequency has increased significantly in recent years representing a direct effect of climate change (Tramblay and Somot 2018). Compared to other natural hazards (e.g., floods, landslides, earthquakes, etc.), drought has a broader impact on multiple areas. It can cause famine, conflicts, and displacement of populations. It affects economic development and health systems (Wilhite et al. 2014). It disrupts and threatens biodiversity through the disappearance of species or the proliferation of others, the aridification of wetlands, etc. It is a complex multidimensional phenomenon whose most representative features are: frequency, severity, duration, and spatial extent (Mathbout et al. 2018). Human-induced climate change and substantially associated heatwaves are increasing the frequency of drought events, multiplying their durations and intensifying their severity (Spinoni et al. 2019, Sillmann et al. 2021). This will increase the probability of occurrence of extreme drought events in the future and consequently increase the complexity of the hydrological cycle in many regions of the world and increase the risk of changing flow characteristics and extremes (AghaKouchak et al. 2020). This implies the need for better identification and quantification of changes in the extremes of projected precipitation, temperature, and runoff indices.

In addition, water deficit during drought periods as well as increasing temperatures is one of the most important stressors in global crop production. Indeed, the geographic shift in climatic conditions makes many crops, agricultural plains,

and grasslands more vulnerable in terms of crop type, spatial extent, or even existence (Bachmair et al. 2018, van Ginkel and Biradar 2021). These effects will vary depending on the location, current climate, and species composition of each plain or grassland (Inoue et al. 2021). Considering that the world's population is estimated to reach 9.1 trillion by 2050 (Desa and Affairs 2019), understanding the effects of agricultural drought and water stress on food and agricultural production on a global scale has become of general interest in the scientific community.

Drought manifests itself in several ways, including meteorological drought, hydrological drought, agronomic drought, and edaphic drought (Mishra and Singh 2010). For efficient management of agricultural production, the identification of climatic variables and their influence on the duration and severity of hydrological drought is necessary. Indeed, meteorological drought is recognized by the Intergovernmental Panel on Climate Change (IPCC) (Salvador et al. 2020) as the main factor causing other types of droughts (e.g. hydrological, agricultural, and socio-economic). However, they occur either simultaneously or with a different time lag (Hao et al. 2018). Prolonged rainfall deficits can lead to a drop in storage reservoir levels below normal. This, together with overexploitation of groundwater, results in a hydrological drought that puts agricultural production and food security at risk and can lead to long-term socio-economic problems (i.e., inability to satisfy the demand for economic assets, such as drinking water, cereals, hydropower generation, etc.)(Yves et al. 2020).

The combined effects of meteorological and hydrological droughts set off agricultural drought, a period when soil moisture decreases, and crops fail due to a shortage of surface and groundwater resources. Therefore, agricultural plains will be affected, so among agricultural, meteorological, and hydrological droughts, more attention should be given to hydrological drought because of its direct relationship with humans (Mishra, Tiwari et al. 2019). Many investigations around the world have been conducted to understand, characterize, and predict hydrometeorological variations (Mishra and Singh 2011, Wood, Schubert et al. 2015, Diaz, Corzo et al. 2019, Forootan, Khaki et al. 2019, Haile, Tang et al. 2020). Indeed, the occurrence

of intense precipitation events has increased globally in recent decades (Trenberth et al., 2015). The seasonality and spatial distribution of precipitation will also shift, making it challenging to reach inferences about how climate change will affect meteorological drought. (Fischer and Knutti 2015, Lehmann, Mempel et al. 2018, Papalexiou and Montanari 2019).

The Italian territory is vulnerable to drought episodes, and unfortunately the temporal consistency and the spatial resolution of available data by rain gauge stations are frequently inadequate for drought characterization analysis. Beyond ground rainfall observations, data from global weather datasets can be considered, but their coarse spatial resolution makes them poorly effective especially in capturing the high precipitation variability that affects the southern European region. In this context, historical in situ long-term measurements are crucial for understanding historical drought conditions as they allow us to learn about how a specific region has been affected by precipitation shortage periods in the past, how severe the response was and how quickly it took to recover from drought conditions (Bonaccorso, Peres et al. 2013, Marini, Fontana et al. 2019).

Several approaches, such as measurement of lack of rainfall, shortage of streamflow, reduced levels of water storage, and Drought Indices, have been used in the past as drought assessment tools. Drought Indices are widely used for drought assessment among these (Hayes 2002, Keyantash and Dracup 2002, Ntale and Gan 2003, Tigkas, Vangelis et al. 2015). A drought Index is a function of a set of hydro-meteorological variables (for example, rainfall and streamflow) and is expressed as a number that is more useful than raw data during decision making (Belayneh, Adamowski et al. 2012). However, defining an appropriate drought Index is not always an easy task, and researchers and professionals face difficulties in developing an appropriate Drought Index (Heim Jr 2002). As a result, the primary task in this thesis is to describe drought conditions and their evolution in Campania (southern Italy) using appropriate drought indices, relying on hydro climatological data at the grid cell level.

Unfortunately, slight attention has historically been paid to the aspect of drought assessment, particularly on a regional scale, which is critical for drought planning and early warning. Because of this focus on crisis management, many communities have shifted from one scenario to another with little or no risk mitigation (Wilhite, Sivakumar et al. 2014). Furthermore, it is not rare that another drought event occurs before the region recovers fully from the previous event. However, an early warning of drought conditions may reduce future impacts and the need for government control (Gutiérrez, Engle et al. 2014, Wilhite, Sivakumar et al. 2014). Therefore, contributing to the development of a drought assessment tool that can be useful for drought preparedness is considered as the main task of this thesis.

1.2 Motivation of the study

Drought and drought management have always been important issues in the context of water resource management in the Mediterranean basin, particularly in southern Italy. Drought assessment activities in Italy have increased in recent years as a result of the country's longest ever recorded drought over the last decade (Spinoni, Naumann et al. 2015). However, as previously stated, the drought assessment is still in its early stages. As a result, the main motivation for this research project was the lack of a suitable drought assessment tools for predicting drought conditions.

The current research was also inspired by the fact that there are two different sources of hydro climatological data where the spatial location, the typology of the measuring instruments, and the complex topography of the region all show a change in the coherence of the two datasets that make it more difficult to merge and homogenize. For this reason, we decided to reconstruct a continuous long-term monthly scale precipitation time series, the in-situ point measurements (observed at the rain gauge locations) for the two datasets were projected on a 10×10 km resolution grid covering the whole region by using a geostatistical interpolation approach. Projecting the two distinct database point measurements to a common grid

made it possible to reconstruct centennial monthly precipitation time series from 1918 to 2019, which is crucial for long-term historical drought condition analysis.

This research was also motivated by the lack of an adequate drought assessment tool (such as a drought indices) that can be used to define critical drought conditions for providing government support to drought-affected communities. Actually, there is no EU directive or policy specifically dedicated to drought management at the present time, but current legislation, sectoral policies, and instruments – binding or not – in the fields of water, agriculture, climate change, energy, industry, transport, nature protection, and biodiversity are partially or marginally related to drought management and can thus support drought management policies (Vogt and Somma 2013).

Experts analysed EU policies related to water, agriculture, climate change, energy, industry, transportation, nature protection, and biodiversity in this revision based on five criteria: 1) monitoring; 2) incentives for water efficiency and circular economy; 3) knowledge and research; 4) drought management measures and plans; and 5) financial instruments (Fava, Gardossi et al. 2021). Moreover, selecting a suitable drought assessment tool (i.e., DI) to define drought conditions, including drought exceptional circumstances, is critical. Consequently, this study was also motivated by the fact that, while many drought indices have been developed around the world, many existing DIs have been developed for specific regions. Although a few studies have been conducted in other parts of the world, the suitability of these DIs have not been tested for the Campania region southern Italy (Heim Jr, 2002; Keyantash and Dracup, 2002; Smakhtin and Hughes, 2004; Morid et al., 2006).

1.3 Aims of the study

The main aim of the current thesis is to assess drought features in the Campania region of southern Italy by analysing the spatial and temporal pattern characteristics of different drought indices (derived from hydro-meteorological data and remote sensing data) time series computed at various accumulation scales over

a centennial period from 1918 to 2019. Furthermore, an auxiliary objective of this study is the reconstruction of high-resolution hydro-climatological gridded data for the Campania region (southern Italy) based on a monthly data set of over 380 stations covering the entire region and parts of the surrounding regions from 1918 to 2019.

1.4 Research methodology in brief

In order to achieve the above objectives, the following tasks were conducted in this research project:

- Review of drought and drought assessment methods.
- Selection of the study area, and data collection and processing
- Evaluation of the change in long-term precipitation variability
- Reconstruction of the hydro-climatological database
- Evaluation of selected drought indices
- Assessment of drought hotspots using remote sensing.

1.4.1 Review of Drought Assessment

As mentioned previously, several methods have been used in the past as drought assessment tools. Among these, several drought indices have been the most used for drought assessment by researchers and professionals worldwide (e.g., Gibbs and Maher, 1967; Shafer and Dezman, 1982; McKee et al., 1995; Keyantash and Dracup, 2004). However, in recent decades, there has been an increase in interest among researchers worldwide in comparing drought indices (Dubovyk et al. 2019; Seiler et al. 1998; Zhou et al. 2012). Distinct ways to quantifying drought exhibit different characteristics, and different drought indices are appropriate for varying conditions because different data constraints are put on the construction of various drought indices.. Therefore, a review of existing indices was first conducted in this research to understand the suitability of existing indices for use in regions outside of those for which they were originally developed. Similarly, several drought prediction

modeling techniques have been used to develop drought assessment models (e.g., Kim and Valdes, 2003; Mishra and Desai, 2005; Barros and Bowden, 2008; Cutore et al., 2009). A review of these techniques was conducted to select the appropriate technique to assess the phenomenon and its characteristics.

The Campania region in southern Italy was selected as a case study area in this research with the aim of reconstructing a long-term database and assessing drought and its characteristics. This region was selected because the management of water resources in the region is of great importance for the population and the agriculture. Hydrometeorological data (for several locations in the region) was collected from several organizations for use in this research. Data processing was then carried out to obtain the representative values of the region which were used for the reconstruction of the hydro-meteorological database and the evaluation of the drought indices and drought characteristics.

1.4.2 Selection of the study area, and data collection and processing

In this study, the Campania region and some limitrophe area in southern Italy was chosen as the case study area to evaluate drought indicators and reconstruct a historical database of different meteorological variables. The region was chosen since the management of water resources in this region is critical to the majority of the Campanian population, and different regions rely on the region's agricultural production. Hydro-meteorological data (for several locations in the Campania region) were gathered from a variety of sources for use in this study. The data was then processed to obtain region representative values, which were used for evaluating drought indicators and reconstructing hydro climatological variables.

1.4.3 Evaluation of the change in long-term precipitation variability

Due to the obvious high precipitation variability that affects specific regions of the globe, coarse spatial resolution data from global weather datasets or climate models are ineffective; thus, historical in situ measurements are critical for reliable drought conditions assessment (Marini et al. 2019). The Mediterranean basin, in particular, is well known to be characterized by high climate variability (Luterbacher et al.,2006) and has been identified as one of the most outstanding "Hot-Spots" in future climate change predictions (Giorgi, 2006). Given the scarcity of empirical regional-scale studies based on historical observations, this step aims to demonstrate the results in terms of inter-annual precipitation variability for a specific area in the Mediterranean basin. The outlined context was carried out in the current research to better understand the change in inter-annual precipitation variability.

1.4.4 Reconstruction of the climatological database

Climate data are vital inputs for most of the hydrological operational purposes and water resource planning trials in continuous space. Usually, the spatial distribution of environmental data is estimated by using ground-based point data from sparsely located gauge stations. The objective of this study is to reconstruct a historical gridded database of climate variables by merging two distinct gauge sets of Campania region (Italy) available from different national agencies for the period 1918-2000 and 2000-2019, where two datasets are characterized by the change in consistency, spatial location, type of gauge stations lying in the complex topography of the region. The merging approach is based on testing four

geostatistical methods (Ordinary Kriging [OK], Ordinary Cokriging [OCK], Empirical Bayesian Kriging [EBK], Detrended Kriging [DK]) and one deterministic interpolation method (Inverse Distance Weighting [IDW]) for enhanced monthly rainfall and temperature spatial interpolation. The in-situ point measurements for the two datasets were projected on a 10km x 10km resolution grid covering the whole region. The resulted datasets will be used then for chapter 6 to calculate the different drought indicators.

1.4.5 Evaluation of selected Drought indices

Existing drought indices have been developed primarily for use in specific regions, and thus may not be directly applicable to other regions due to the inherent complexity of drought phenomena, different hydro-climatic conditions and watershed characteristics (Redmond, 2002; Smakhtin and Hughes, 2007). There had been a few studies evaluating these indices worldwide (Heim Jr, 2002; Keyantash and Dracup, 2002; Smakhtin and Hughes, 2004; Morid et al., 2006). However, no such study has been conducted for the Campania region. Therefore, an evaluation of a few selected indices was carried out to search for the most appropriate drought indices to define the drought conditions in the Campania region. A variety of decision criteria were used in this drought index assessment study. The significance of the research project and its overall outcomes are discussed in this section. This section also includes a list of innovative ideas that have developed as a result of this research.

1.4.6 Assessment of drought hotspots using remote sensing

As mentioned in section 1.1, depending on the consequences of drought, we can distinguish different categories: meteorological drought, in case of a relative decrease in precipitation; hydrological drought, in the presence of a relatively scarce

supply of water in the soil or in watercourses; agricultural drought, in case of deficit of water content in the soil that determines stressful conditions in the growth of crops; socioeconomic drought, if referred to the overall consumption on the territory. The anomalies of precipitation are due to the characteristics of the climate that influences the hydrological cycle. The climatology of precipitation, temperature and atmospheric humidity provides information on the frequency, intensity of precipitation and the correlation between temperature and precipitation. Among the vegetation indices, the main one is the NDVI (Normalized Difference Vegetation Index) calculated from satellite images, from which the photosynthetic activity, which is reduced in case of water stress, is evaluated. The following thesis work aims from one hand to analyse the drought seen through the climatic indicators SPI and SPEI and the water stress on vegetation measured through the NDVI vegetation index, limiting the considerations to the Campania Region, in order to outline any connections that are present between the two drought phenomena. In addition, we want to study how drought conditions develop over time and space, to find out if there are areas of the region that are particularly exposed and if dry periods impact the region always with the same severity.

1.5 Research Significance and Outcomes

1.5.1 Significance

This research project contributes to a scientific advancement in the field of water resource management, particularly in the management of water resources during drought conditions. These contributions are as follows:

- An analysis of the precipitation coefficient of variation, assumed as index of inter-annual climate variability, was performed over the period 1918-2015 and compared with the annual precipitation regime and the intra-annual precipitation variability of the same region. Therefore, the Mann-Kendall and the Modified Mann

Kendall tests were applied to detect the sign and significance of the temporal changes and the Sen's test was applied to quantify the temporal changes in inter-annual variability;

- Due to the significant influence of orography in the study area, the Ordinary Cokriging method was found to be the best interpolating method for the interpolation of the merged series over a century. This historical gridded database of climate variables was reconstructed by combining two distinct gauge sets of Campania region (Italy) available from different national agencies for the periods 1918-2000 and 2000-2019.
- This study was the first to evaluate existing drought indices in the Campania region. The SPI was found to be the best drought index among the existing indices investigated in this study. The overall result of this indices evaluation study was a valuable contribution to the hydrologic and water resource management community worldwide in general, and the Campania region in particular.

1.5.2 Outcomes

The outcomes of this study are outlined below:

- The average coefficient of variation (CV) characterization and spatial pattern revealed a generalized condition of statistically significant increase in inter-annual variability almost across the entire analyzed area, with only a very moderate spatial consistency detected, besides, it was found that larger CV values appear associated to large mean annual precipitation (MAP) and large precipitation concentration index (PCI) values.
- Using a comparative approach, it was determined that the Ordinary Cokriging method was the best interpolation technique for the interpolation of the merged series over a century in order

to reconstruct long historical in situ long-term measurements that are essential for comprehending historical drought conditions and developing mitigation strategies to further combat future climate change impacts.

- SPI and SPEI yield almost the same results, with SPI being slightly more severe than SPEI, in addition, when comparing the indices from 191 grid points, similar variability was observed. The variability was most likely caused by moisture loss to evapotranspiration during the spring/summer season, which is accounted for by the SPEI.
- The comparative study that was conducted between SPI, SPEI and the vegetation index NDVI showed that the SPI was a better drought indicator than others, furthermore the SPI was found to be the most suitable drought indicator for defining drought conditions within the Campania region. In addition, it was not possible to affirm that due to the pluviometric deficits shown by the SPEI there was a water deficit for the vegetation because the climatic condition of the Campania Region is part of a sub-humid climate.
- Spatial autocorrelation using the Moran index was an important step in determining whether the different events studied have similar spatial aggregation characteristics.

1.6 Outlines of the thesis

The outline of the thesis is presented in Figure 1.1. This figure shows that the thesis consists of eight chapters. The first chapter describes the background of the research project, the motivation for the study, the aims, a brief methodology, thesignificance, and outcomes of this project. The second chapter presents a critical review of literature related to the research project. Details on

the case study catchment and its importance, drought history in the Campania region, data used inthis research, and their sources and processing are illustrated in the third chapter.The fourth chapter provides details on the regional changes in inter-annual precipitation variability for the case study area. The reconstruction of gridded climatological database (precipitation and temperature) is presented in the fifth chapter. The sixth chapter provides the evaluation of drought indicators, their performance evaluation, and the selection of the best index in this study. Drought hot spot analysis using local indicators of spatial autocorrelation are presented in the seventh chapter. Finally, a summary of the thesis and the main conclusions, and the recommendations for future work are presented in the eighth chapter.

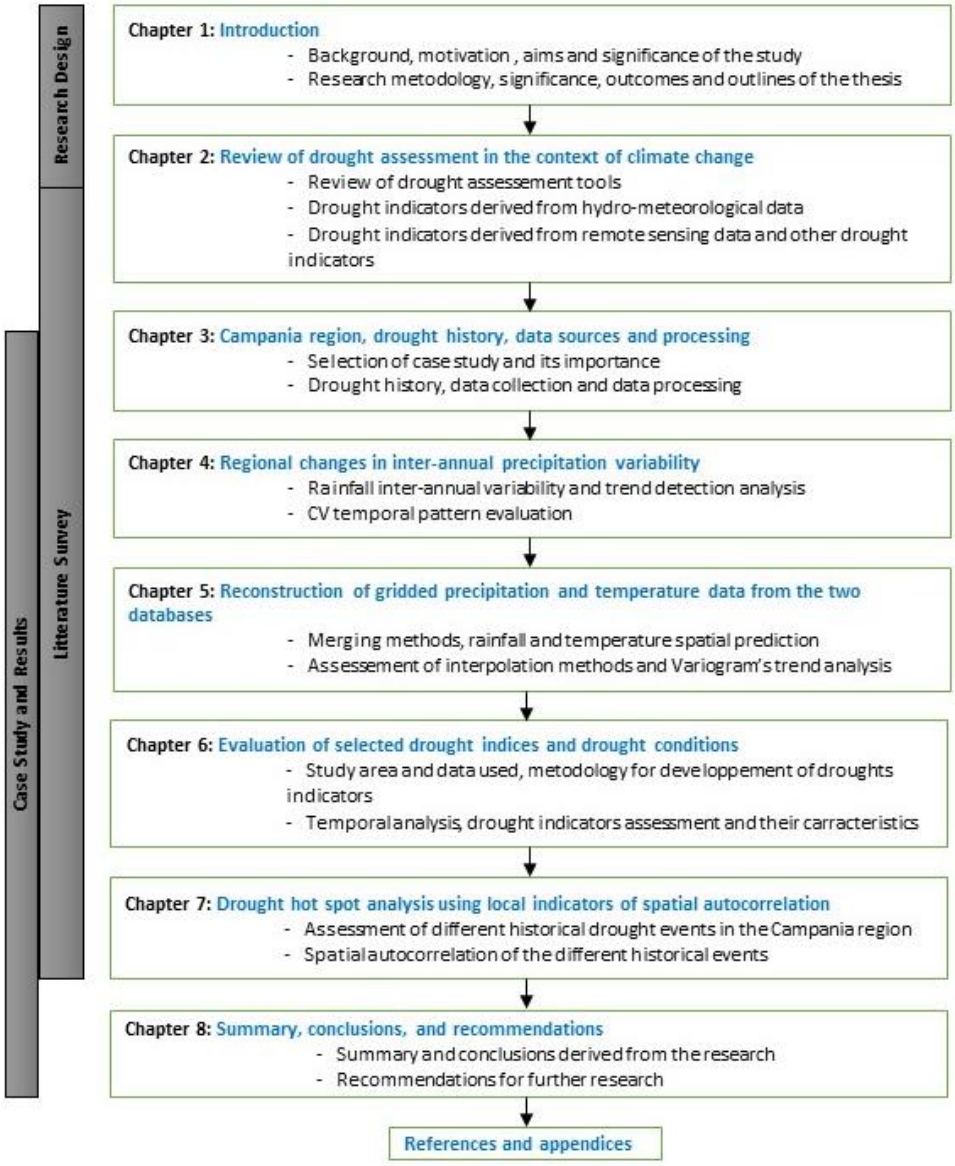

Figure 1.1: Outline of the thesis

Chapter 2

REVIEW OF DROUGHT ASSESSMENT TOOLS

2.1 Overview

Drought is a complex natural phenomenon with serious consequences for effective water resource management. Drought, in general, gives the impression of scarcity of water due to insufficient precipitation, high evapotranspiration, and over-exploitation of water resources, or a combination of all the above (Bhuiyan, 2004). Droughts are classified into three types: meteorological, hydrological, and agricultural. The meteorological drought is defined solely by the amount of dryness measured in terms of rainfall deficit (Keyantash and Dracup, 2004). The hydrological drought, on the other hand, is defined by a lack of available water in the form of streamflow, reservoir storage, and groundwater depths (Wilhite, 2000). The agricultural drought is expressed in terms of soil moisture deficits and takes into account rainfall deficits, soil water deficits, evapotranspiration variation, and other factors (Hounam, 1975). Furthermore, the American Meteorological Society (1997) established a new drought category known as socioeconomic drought. This type of drought occurs when physical water shortages begin to have an impact on people's health, well-being, and quality of life. This drought is beginning to have an impact on the supply and demand for economic products such as water, hydroelectric power generation, and so on. Drought puts an enormous strain on rural and urban water resources, as well as agricultural and energy production. As a result, timely determination of the level of drought will aid decision-making in reducing the effects of drought.

This type of drought occurs when physical water shortages begin to have an impact on people's health, well-being, and quality of life. This drought is beginning to have an impact on the supply and demand for economic products such as water, hydroelectric power generation, and so on. Drought puts an enormous strain on rural and urban water resources, as well as agricultural and energy production. As a result, timely determination of the level of drought will aid decision-making in reducing the effects of drought.

As mentioned in Section 1.1, several methods have been used in the past as drought assessment tools, including the measurement of lack of precipitation, lack of river flow, temperature increase, and drought indicators, among others. However, traditionally, the most common drought assessment tools have been drought indicators, which have been used to estimate future dry conditions. This is because drought indicators are expressed as a number, which is considered much more functional than raw data in decision-making (Hayes, 2003). In general, the drought index is a function of several hydro-meteorological variables such as rainfall, temperature, streamflow, and storage reservoir volume. Some researchers and professionals make the argument that drought is simply a lack of rainfall and that it can be defined with rainfall as the single variable. The majority of the available drought indicators, such as Deciles (Gibbs and Maher, 1967), Percent of Normal (PN) (Hayes, 2003), Standardized Precipitation Index (SPI) (McKee et al., 1993; Ganguli and Reddy, 2014), and many others, were developed with rainfall as the only variable. These rainfall-based drought indicators are more widely used than other drought indices due to their lower input data requirements, flexibility, and ease of calculation (Smakhtin and Hughes, 2004). Other drought researchers and professionals, on the other hand, argue that rainfall-based drought indicators do not encompass all types of drought conditions because they can only be used to define meteorological droughts (Keyantash and Dracup, 2004; Smakhtin and Hughes, 2004). According to Smakhtin and Hughes (2004), drought assessment should consider important components of the water cycle (rainfall, temperature and storage reservoir volume). Byun and Wilhite (1999) previously held the view, stating that a valid drought index should include a combination of hydro- meteorological variables. Based on these concepts, (Shafer and Dezman, 1982) and (Keyantash and

Dracup, 2004) developed two drought indicators, the Surface Water Supply Index (SWSI) and the Aggregated Drought Index, which take into account a variety of hydro-meteorological variables such as rainfall, streamflow, and others. In addition (Vicente-Serrano et al., 2010) stated that the SPEI index is designed to consider both precipitation and potential evapotranspiration (PET) in determining drought. It should also be noted that the majority of drought indicators developed were regional, and some drought indicators are better suited for specific uses than others (Redmond, 2002; Hayes, 2003; Mishra and Singh, 2010). As a result, before adopting any of the existing drought indicators for use in specific areas other than those for which they were originally developed, a review of the existing drought indicators is expected.

The current chapter has two goals: (1) to review the existing drought assessment tools that have been used to define the drought conditions, The outcome of this chapter will be the identification of the best drought indicator for accurately describing the spatial and temporal characterization of drought conditions in the Campania region, which will be critical information for long-term and efficient water resource management planning strategies.

2.2 Drought assessment tools

As previously stated, several drought assessments tools have been used in the past, and Drought Indices have been the most commonly used to assess drought conditions around the world, because they are more functional than raw data in decision making. These drought indicators were used to stimulate drought relief programs and quantify water resource deficits in order to assess the severity of the drought. They were also used to monitor the drought. Palmer (1965) was the first to introduce a drought index called Palmer Drought Severity Index (PDSI) in the United States in the mid-twentieth century to define meteorological droughts using a water balance model. PDSI became popular almost immediately after its development and was the most widely used DI in the United States until Alley (1984) identified its limitations. Other drought indicators developed over time include the widely used Percent of Normal (PN) (Willeke et al., 1994), Deciles (Gibbs and Maher, 1967), Standardized Precipitation Index (SPI) (McKee et al., 1993). etc.…

According to Vincente Serrano (2010), the SPI was unable to identify the role of a temperature increase in future drought conditions, and it cannot account for the influence of temperature variability and the role of heatwaves, such as the one that hit Central Europe in 2003. They developed the SPEI index to account for the potential effects of temperature variability and temperature extremes other than global warming. In addition, one of the most important indicators of drought events is vegetation growth. Greenness-related vegetation indices (VIs) such as the Normalized Difference Vegetation Index (NDVI) and the Enhanced Vegetation Index (EVI) are frequently used to assess agricultural drought. There is a need to assess the sensitivity of water-related vegetation indices to drought and its consequences. In the current chapter we will review only the drought indicators adapted to our study area, such as SPI, SPEI, NDVI and EVI.

2.2.1 Meteorological, Agricultural and hydrological drought indices

The availability of data is critical for the development and implementation of a drought index (Steinemann et al. 2005). Previously, drought indices relied on readily available meteorological data from synoptic meteorological stations (Niemeyer 2008). RAI (Van-Rooy 1965), BMDI (Bhalme and Mooley 1980), DSI (Bryant et al. 1992), NRI (Gommes and Petrassi 1994), EDI (Byun and Wilhite 1999), and DFI (González and Valdés 2006) are all precipitation-only indices. Additional meteorological variables have been considered for reasons such as better correlation with drought impacts and accounting for temperature temporal trends. Modifications to SPI (McKee et al. 1993) are being made in order to develop a more comprehensive RDI (Tsakiris and Vangelis 2005) that incorporates evapotranspiration, resulting in a better association with agricultural and hydrological drought impacts. SPEI was developed by Vicente-Serrano et al. (2010) and is sensitive to long-term trends in temperature change. SPEI performs similarly to SPI in the absence of such trends. KBDI (Keetch and Byram 1968) was the first to consider temperature and has found widespread use in wildfire monitoring. PAI

(Pálfai 1991) took groundwater into account in addition to these two indicators and was primarily applied to basins within Hungary.

Approaches to characterizing agricultural drought revolve primarily around tracking soil water balance and the resulting deficit in the event of a drought. This is true for the seven non-remote-sensing agricultural drought indices studied in this study: RSM (e.g., Thornthwaite and Mather 1955), CMI (Palmer 1968), which is similar to PDSI but models short-term agricultural by considering moisture deficit only in the top 5 feet of soil column (Byun and Wilhite 1999; Narasimhan and Srinivasan 2005), and CSDI (Meyer et al. 1993), which was originally designed for corn and its variant for soybean (Meyer and Hubbard 1995). The daily transpiration deficit (DT) for x days is calculated by DTx (Matera et al. 2007). SMDI and ETDI were designed with higher spatial and temporal resolutions in mind (Narasimhan and Srinivasan 2005). This method takes into account the soil component of the SWAT hydrologic model, which has a resolution of 16 km^2. (Compared to then 7 000 to 160 000 km^2 resolutions of SPI and PDSI). SMDI characterizes soil moisture deficit at varying depths within the top 2 m of the soil component, "soil profile": top 2 ft ($SMDI_2$), 4 ft ($SMDI_4$), and 6 ft ($SMDI_6$). $SMDI_2$ and ETDI (which takes evapotranspiration into account) were proposed for short-term drought monitoring, and $SMDI_6$ for long-term monitoring. As mentioned below, NDVI (Tucker 1979), EVI (Liu and Huete 1995), VegDRI (Brown et al. 2008), TCI (Kogan 1995), and NDWI (Gao 1996) are also used to monitor general vegetation state and health (Si vakumar et al. 2011).

In term of hydrological drought indices, the set of this indices aims to provide a comprehensive characterization of the delayed hydrologic effects of drought. Previously, the sophisticated PHDI (Palmer 1965) model took into account precipitation, evapotranspiration, runoff, recharge, and soil moisture. The PDSI family of indices has always lacked snow component accumulation, which led to the development of SWSI (Shafer and dezman 1982), which is probably the most popular of this group. Later, RDI (Weghort 1996) improved SWSI by incorporating temperature and thus calculating a variable water demand as input. RSDI (Stahl 2001) bases its model on homogeneous drought-stricken regions with multiple low-flow gauging stations nearby. RSDI determines drought-affected areas by

calculating the difference in streamflow between current and historic values and then using cluster analysis. GRI (Mendicino et al. 2008) and Water Balance Derived Drought Index are two additional indices that take a water balance model into account (vasiliades et al. 2011). The former is concerned with groundwater resources and employs geo-lithological conditions information in a distributed water balance model, whereas the latter employs a model that artificially simulates runoff for ungauged and low-data watersheds.

2.2.2 Drought indicators derived from hydro-meteorological data

2.2.2.1 The Standardized Precipitation Index

McKee et al. (1993) developed the Standardized Precipitation Index (SPI) for Colorado, USA, as an alternative to the PDSI. The SPI was developed as a drought monitoring tool to quantify rainfall deficits and has been used to monitor drought conditions in Colorado since 1994. (McKee et al., 1995). The Colorado State University home page has monthly maps of the SPI (http://ulysses.atmos.colostate.edu/SPI.html). It is also used by the National Drought Mitigation Center and the Western Regional Climate Center in the United States. SPI is calculated by fitting a long-term historical rainfall record to a probability distribution (generally the gamma distribution), which is then transformed into a normal distribution (McKee and Edwards, 1997). Rainfall deficits at various time scales have varying effects on various water resource components such as groundwater, soil moisture content, and streamflow. Soil moisture conditions, for example, respond relatively quickly to rainfall anomalies (e.g., days/weeks to a month), whereas groundwater, streamflow, and reservoir storage reflect longer-term rainfall anomalies (e.g., months to seasons). As a result, the SPI was initially calculated for monthly or multiple monthly time scales (i.e. 1-, 3-, 6-, 12-, 24-, and 48-month) as in the PN (McKee et al.,1993). The SPI does have more applications around the world than other DIs due to its lower input data requirements and flexibility in SPI calculations (Hughes and Saunders, 2002; Hayes, 2003; Bhuiyan, 2004; Smakhtin and Hughes, 2004; Mishra and Desai,

2005; Morid et al., 2006; Bacanli et al., 2008). The SPI was used by Marini et al. (2019) to identify and characterize droughts in Apulia region, southern Italy. Cacciamani et al. (2007) used the SPI to forecast drought conditions in Emilia Romagna region, Northern Italy. Although, the SPI has more popularity than any other DI, it is not strong enough to define the wider drought conditions since many other important hydro-meteorological variables (e.g., streamflow, soil moisture condition, evapotranspiration and reservoir storage volume) that affect droughts were not considered in SPI (Keyantash and Dracup, 2004; Smakhtin and Hughes, 2004). Further details on SPI are given in Section 6.3.1.

2.2.2.2 The Standardized Precipitation Evapotranspiration Index

The Standardized Precipitation Evapotranspiration Index (SPEI) is a variation on the widely used Standardized Precipitation Index (SPI). In determining drought, the SPEI considers both precipitation and potential evapotranspiration (PET) Vicente-Serrano et al. (2010). In contrast to the SPI, the SPEI captures the primary impact of rising temperatures on water demand. The SPEI, like the SPI, can be calculated over timescales ranging from 1 to 48 months. The SPEI has been shown to correlate with the self-calibrating PDSI over longer timescales (>18 months) (sc-PDSI) Vicente-Serrano and NCAR (2015). PET can be estimated using the simple Thornthwaite method if only limited data, such as temperature and precipitation, are available. Variables that can affect PET, such as wind speed, surface humidity, and solar radiation, are not taken into account in this simplified approach. In cases where more data are available, a more sophisticated method of calculating PET is often preferred in order to account for drought variability more completely. These additional variables, however, can have significant uncertainties. Further details on SPI are given in Section 6.3.2.

2.2.3 Vegetation indices useful for Drought monitoring

Effective monitoring of vegetation indexes is also required for understanding environmental changes. Vegetation indexes are arithmetic combinations of two or

more bands related to vegetation spectral characteristics (Matsushita et al. 2007) that have found widespread application in crop phenology monitoring, vegetation classification, and the derivation of vegetation biophysical parameters. Vegetation index values are typically in the range of 1 to +1. Negative values indicate the presence of clouds, snow, water, or urban land, whereas positive values indicate the presence of green vegetation (Chen et al. 2006a). According to Phompila et al. (2015), the vast majority of remote sensing techniques for monitoring changes in vegetation cover have relied on VIs, most notably the Normalised Difference Vegetation Index (NDVI) and the Enhanced Vegetation Index (EVI). The NDVI is the more widely used of the two. When used to monitor vegetation, it can cancel out a large portion of the noise caused by topographic effects, clouds or cloud shadow, changing sun angles, and atmospheric conditions (Huete, Justice 1999, Matsushita et al. 2007). Even though it is accurate, computationally simple, efficient, and useful for agricultural land use mapping in tropical environments, it has found widespread application (Meera et al. 2015). However, at high biomass levels, it becomes more saturated (Gao et al. 2000), and it is also sensitive to canopy background variations (Huete 1988). The EVI improves on atmospheric correction, index saturation in densely forested areas, and soil reflectance influence as an enhancement to the NDVI. (Boegh et al. 2002, Huete et al. 2002, Gao et al. 2003, Xiao et al. 2004, Rankine et al. 2017). The EVI also has a greater dynamic range than the NDVI, and its improved performance has drawn the attention of many researchers. Li et al. (2010) investigated the relationship between NDVI and EVI derived from the Moderate Resolution Imaging Spectroradiometer (MODIS) instrument and natural vegetation coverage in China's Northern Hebei Province. They found that MODIS-NDVI was more correlated with field data of vegetation cover and had obvious advantages for predicting natural vegetation coverage than MODIS-EVI. They concluded that there is still a need to combine the complementary performances of NDVI and EVI for a more detailed understanding of vegetation characteristics and to inform planning decisions for more sustainable environments.

2.2.4 Other Drought indicators

Many other drought indicators were cited in the literature, but their applications were limited. Table 2.1 contains a list of some of these drought indicators as well as brief descriptions of each. This table shows that the majority of the DIs were created with rainfall as the sole variable. It can also be seen that the majority of these drought indicators are only used in the United States. Alley (1984), Keyantash and Dracup (2002), Heim Jr (2002), Tsakiris et al. (2002), Morid et al. (2006), Hayes (2003), Smakhtin and Hughes (2004), and Loucks and van Beek (2004) provide additional information on the applicability and limitations of these drought indicators (2005).

Drought Index	Drought Definition	Application
Munger Index (Munger, 1916)	Length of period in days with daily rainfall less than 1.27 mm.	Daily measure of comparative forest firerisk in the Pacific Northwest, U.S.A.
Kince Index (Kincer, 1919)	30 or more consecutive days with daily rainfall less than 6.35 mm.	Producing seasonal rainfall distributionmaps in the U.S.A.
Marcovitch Index (Marcovitch, 1930)	*Drought Index = ½(N/R)^2; where N is the total numberof two or more consecutive days above 32.2 ^{0}C in a month and R is the total rainfall for the month.*	Alarming bean beetle in the eastern UnitedStates of America.
Blumenstock Index (Blumenstock Jr, 1942)	*Length of drought in days, where drought is terminatedby occurrence of 2.54 mm of rainfall in 2 days.*	Short term drought management in theU.S.A.
Keetch - Byram Index (KBDI) (Keetch and Byram, 1968)	*Rainfall and soil moisture analyzed in a water budgetmodel with a daily time step.*	Used by fire control managers for wildfire monitoring and prediction in the U.S.A.

Crop Moisture Index (CMI)(Palmer, 1968)	The CMI was developed from procedures within the calculation of the PDSI. The PDSI was developed to monitor long-term meteorologicall wet and dry spells,however the CMI was designed to evaluate short-term moisture conditions across major crop producing regions. The CMI is computed using the mean temperature and total rainfall for each week within thecatchment, as well as the CMI value of the previous week.	Used in the U.S. to monitor week to weekchanges in moisture conditions affecting crops.
Reclamation Drought Index (RDI) (Weghorst, 1996)	RDI is calculated at the river basin (or the catchment)level using a monthly time step, and incorporates temperature, rainfall, snow water content, streamflowand reservoir levels.	Used as a tool for defining drought severity and duration, which assisted the Bureau of Reclamation in the U.S.A. in providing drought mitigation measures.
Effective Drought Index (EDI) (Byun and Wilhite, 1999)	The EDI is the rainfall amount needed return to normal condition (or to recover from the accumulated deficit since the beginning of a drought).	Used to monitor day to day drought conditions in the U.S.A. It was also tested in Iran (Morid *et al.*, 2006).

Chapter 3

CAMPANIA REGION, DROUGHT HISTORY, DATA SOURCES AND PROCESSING

3.1 Overview

As stated in Chapter 1, this thesis used the Campania region in southern Italy as a case study. Campania is a major source of water supply for southern Italy's territory. This region's water resource management is critical in terms of a broader range of water uses, as well as downstream user requirements and environmental flows. However, due to frequent droughts and rising water demand in recent years, pressure on water resource management activities in southern Italy has increased (Colella, Ripa et al. 2021). Many initiatives have recently been launched to protect the environmental health of this territory's waterways, particularly during drought periods (Rossi 2020).

In this study, hydro-meteorological data from the Campania region were used to evaluate drought indices and assess drought features and characteristics in the region. Throughout the research, historical drought records from southern Italy were also used to evaluate the various drought indices.

This chapter begins by describing the Campania region in terms of land use conditions, importance, and water resources. The drought history is then described, followed by the sources of hydro-meteorological data used in this thesis. The

processing of hydrometeorological data is then presented. Finally, at the end of the chapter, a summary is provided.

3.2 Campania region southern Italy

3.2.1 Description of the Campania region

The Campania region is located between 40.0 and 41.5∘ N and 13.5 and 16.0∘ E, covering about 13 600 km^2 in the southwest of Italy (Figure 3.1). The region is well known for a complex orography; the altitude of the region ranges from well above 2000 m a.s.l. (above sea level) in the Apennine Mountains to the coastline. Furthermore, the territory of the Campania region is predominantly hilly. There are few plains in the Caserta area, along the Cilento coast and along the course of the Garigliano, Volturno and Sarno rivers. The most important plains are the Pianura Campana and the Sele plain. Among the mountainous reliefs are the Appennino Campano, the Appennino Lucano and the Antiappennino Romano-Campano. The highest peaks are Mount Miletto (2050 m), Mount Cervati (1899 m), Mount Cervialto (1809 m) and Mount Terminio (1786 m). Along the coast there are volcanic massifs, including Vesuvius (a dormant volcano and one of the most dangerous in the world because the surrounding area is densely populated), Campi Flegrei (a vast volcanic area in which the solfatara of Pozzuoli is of particular interest, with powerful sulphur dioxide fumaroles, jets of boiling mud and high soil temperatures) and Roccamonfina. From the Tyrrhenian coast to the mountains of the Campano-Lucano Apennines, the Cilento and Vallo Diano National Park covers 181,000 hectares. The region is characterized by a complex climatic pattern because of the orography. In addition, the region can be divided into two climatic zones Figure 3.2; in the coastal areas the Mediterranean climate prevails even in winter

due to the influence of the sea, in the inland and mountainous areas the continental climate prevails, where winters are harsher and sometimes accompanied by snowfall (especially in Irpinia).

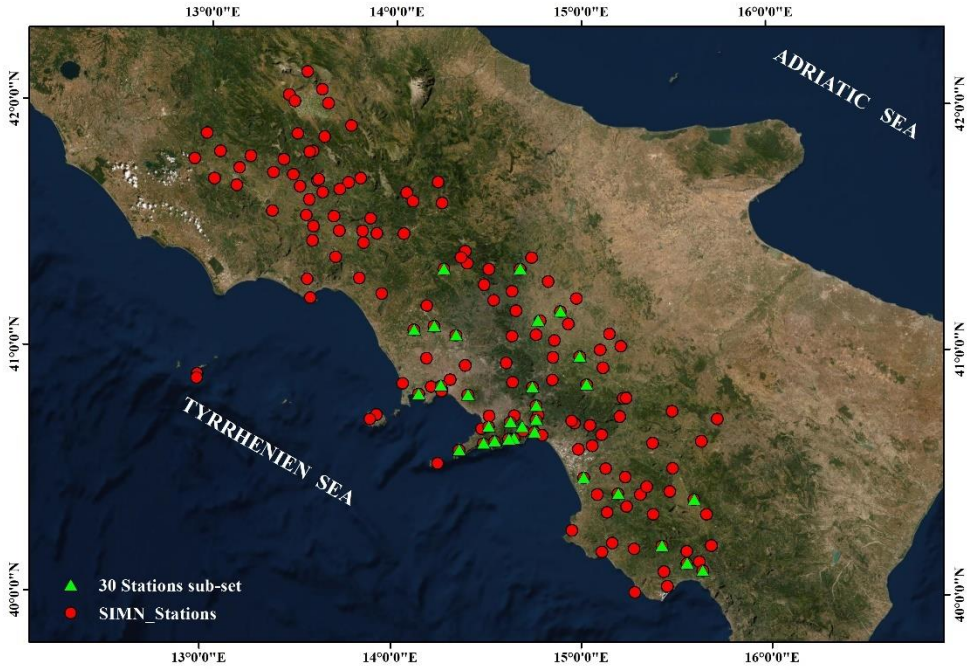

Figure 3.1 The studied area with the two rain gauge networks.

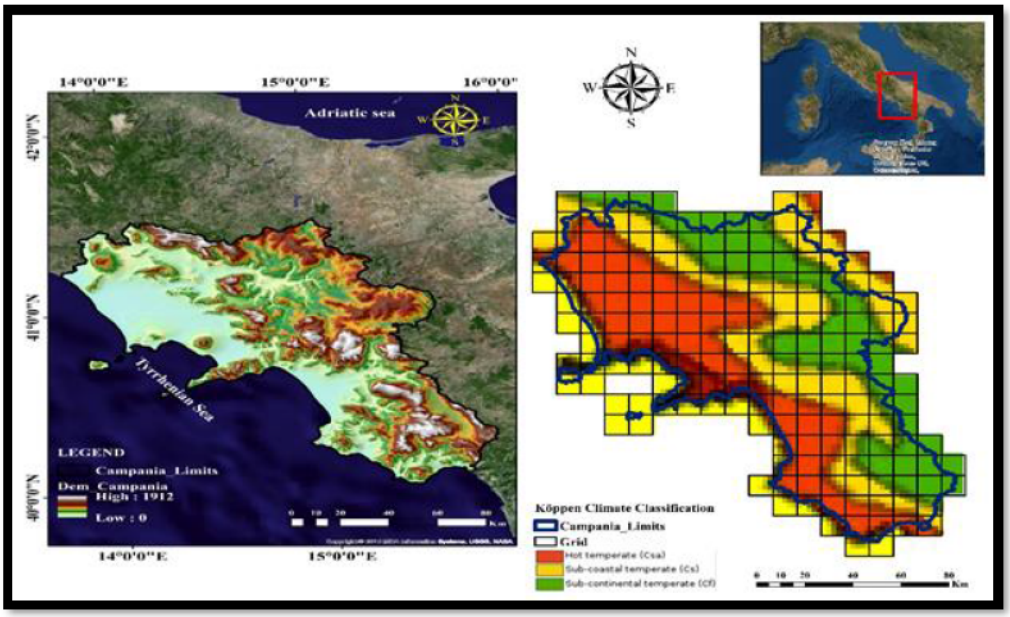

Figure 3.2. The studied area. Left panel: Study area location in the Italian peninsula. Right panel: Köppen climate classification of the study area.

3.2.2 Water supply of the Campania region

For southern Italy, the Campania region is crucial for its water resources, with over 10% of the Italian population (approximately 6 million) living in this region. Water resources in the region support a variety of uses valued by the Campanian community, including urban water supply, agricultural and horticultural industries, downstream user requirements, and flow requirements for maintaining environmental flows. The Region has a robust site for soil conservation, where it addresses the many challenges pertaining to the region. Campania is crossed by few but relatively important watercourses. The Volturno river is the most important one

and it is about 170 km long while the area of the hydrographic basin, which is about 5600 km^2, represents almost the 40% of the whole regional territory. The hydrographic basin is constituted from the whole of two important basins: that one of the high Volturno, that is identified mainly in carbonate rocks, and that one of the Calore Irpino in which prevail the clayey lithotypes. The second river of Campania is the Sele which originates from Monte Cervialto from the source of Caposele and has a length of about 65 km while its basin has an areal extension of about 3200 km^2.

In Campania, the aquifers supply perennial sources with an average flow of more than 40.000 liters per second (Figure 3.3). The source water supplies the Campania aqueducts and with about 7000 liters per second also the Apulia aqueduct, as well as almost all the irrigation system of the Campania plain, Agro Nocerino-Sarnese, Sele plain, and Vallo di Diano. The summer qualified agricultural production in Campania always depends on the water supplied by the springs as well as the water used in the food industry that in part also comes from groundwater withdrawals which is always mainly fed by carbonate aquifers. There are also numerous agricultural dams in the region, and extraction of water from rivers and streams for agriculture is common. A variety of recreational activities, metropolitan parks and biodiversity conservation are also present around the region's waterways.

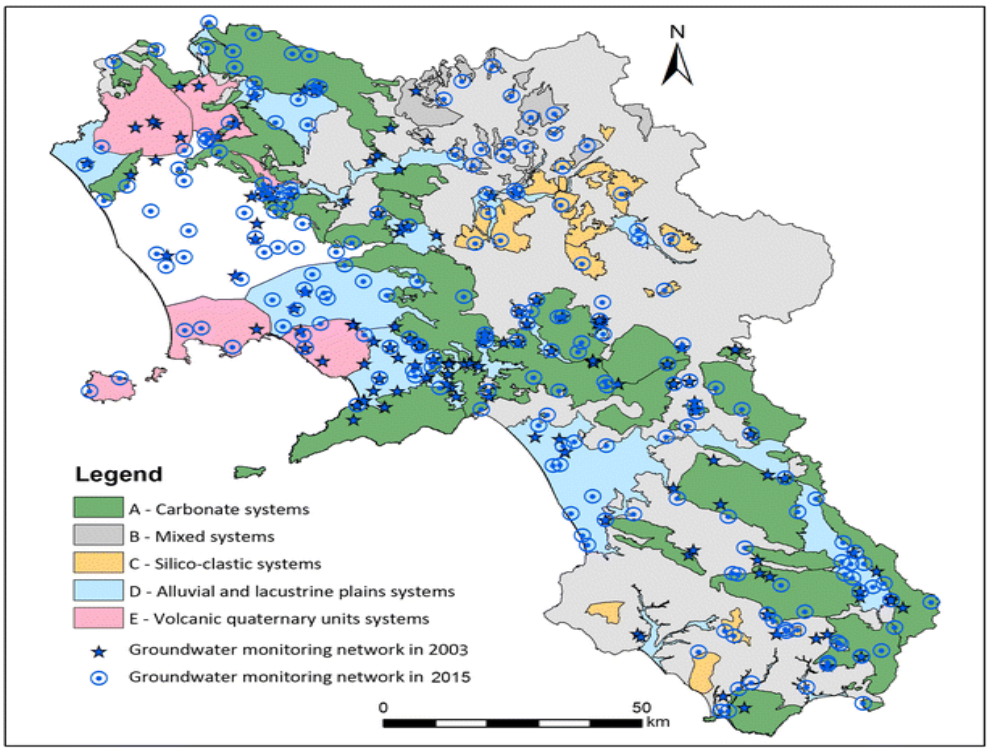

Figure 3.3 The 80 groundwater bodies (GWBs) of the Campania region and the groundwater monitoring network. In white, the GWB of the "Volturno-Regi Lagni" plain (P-VLTR). In light gray, not significant GWBs (Daniela et al. 2019).

3.2.3 Sources of Water Resources in Campania Region

As it was mentioned in section 3.2.1, the region is characterized by a complex climatic pattern because of the orography. However, the seasonality is well defined, with the larger amount of precipitation recorded during the winter periods. The mean annual rainfall of the study area ranges from 600 to 2400 mm, whereas the average annual temperature is around 17 ∘C. Trends in historical precipitation and their seasonal variability were described in Longobardi and Villani (2010) and

Longobardi et al. (2016). The area is experiencing a moderate negative trend in precipitation (− 35 mm/10 years, Longobardi and Villani 2010), especially concerning the northeastern and southwestern areas. At the same time, the seasonal variability also appeared to be featured by a negative trend, with a transition of the precipitation regime from a seasonal to more uniform one. Figure 3.4 shows the annual average rainfall for the Campania region and its limitrophe based on the 163 rainfall measuring stations (which will be discussed in next chapter) for the period from 1918 to 1999. This figure shows that the annual average rainfall was around 1200 mm when consider all years from 1918 to 1999.

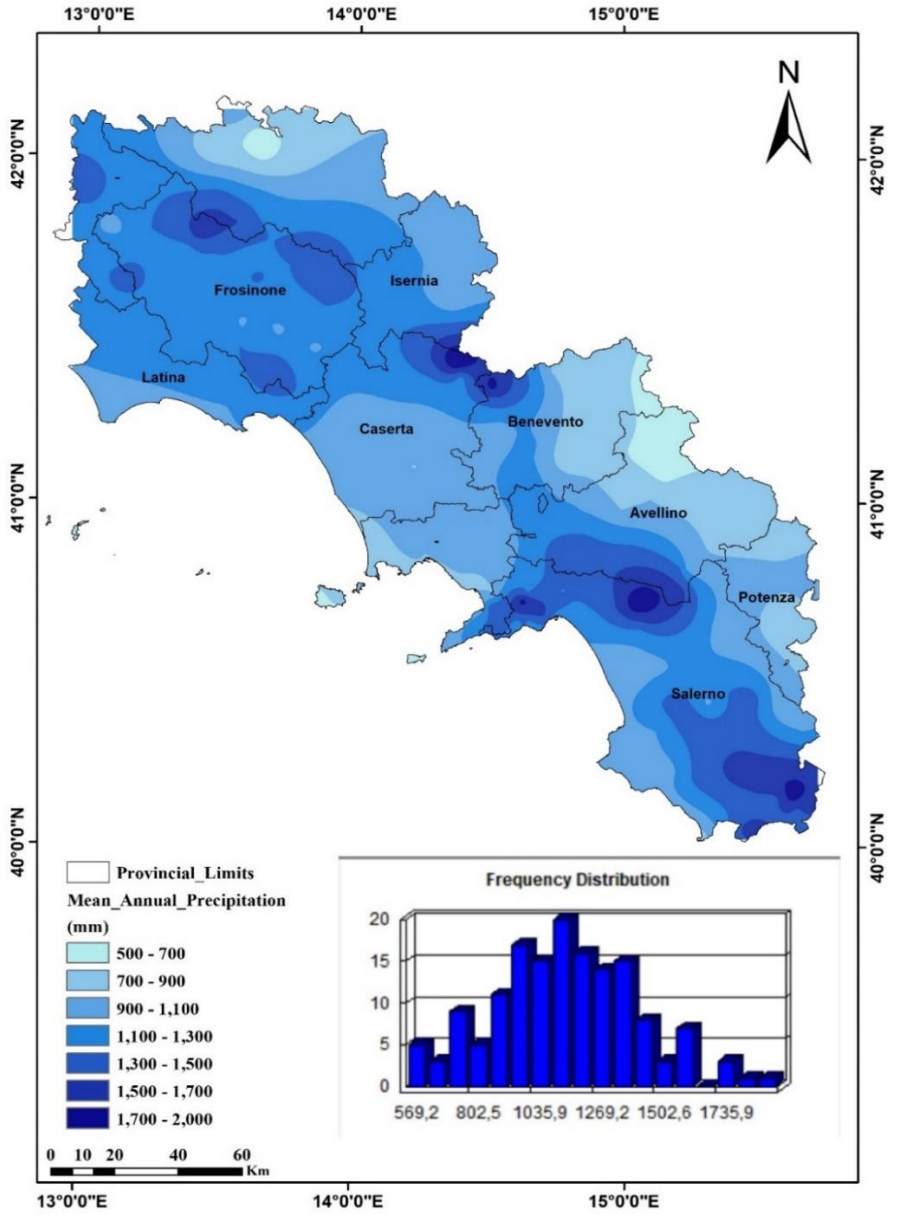

Figure 3.4 Mean annual precipitation of the Campania Region and its surrounding region, Southern Italy.

3.3 Drought history in Campania region and southern Italy

Several droughts have occurred in the Campania region in the past, including 1962, 1976, 1980-1981, 1988-1989, 1994, 2001-2002, 2003, 2011, 2015, and 2017. The European Drought Observatory (EDO, 2018) recorded these historical droughts after analysing rainfall and storage records from the time and comparing them to their average values. They also noted that during these droughts, there was a severe lack of water resources in terms of rainfall and storage reservoir volume, as well as negative socioeconomic impacts due to water scarcity. Based on the EDO report, the following observations are made:

1. During the 1962 drought, the monthly average rainfall had fallen below 10% of its normal in February 1962.
2. During the 1976-1977 drought, the monthly average rainfall had fallen below 24% of its normal (in November 1977). This drought was relatively long in duration. this is due to a very hot anticyclone which at beginning of June a very hit Europe, the heat was exceptional, with temperature close to +40°C.
3. Of all droughts recorded until 2015, the worst drought occurred the Campania Region was in 2003. 4 weeks the average temperature in Italy were above 40°C, and the deaths recorded during the summer season were 4000 more than the average. the duration of the phenomenon is particularly extensive, from May to the beginning of September.
4. During the period of 2016-2017, The rainfall data recorded by the various stations in Campania show that, since December 2016, the amount of rain that have fallen, especially in the flat areas of the region, are close to zero. In Campania, 18,177 hectares have gone up

in smoke to date, equal to 14.57% of the total with damage of over 363 million euros (source: processing of data collected by the EU commission as part of the Copernicus project), the third most affected region after Sicily and Calabria.

Along with the reduction in annual average rainfall, and the diversity of water uses and activities, pressure upon water resource management within the Campania region has become more intense in recent years especially during the droughts. Therefore, the management of water resources in terms of droughts is important within the Campania region.

3.4 meteorological data sources

In order to reconstruct a historical long-term database and evaluate the drought indices and its characteristics, it was necessary to collect the required hydro climatological data (precipitation and temperature). This task starts from the study of historical series of monthly and annual precipitation values for the Campania Region, from 1918 to 2019, starting from the data collected by the gauge network stations located on the territory. The collection of precipitation data, over time, has been the responsibility of two different agencies:

- Until the year 2000, data were collected by the Servizio Idrografico e Mareografico Nazionale (S.I.M.N.) and published in the Annali Idrologici;
- From 2000 onwards, data were collected by the Centro Funzionale Multirischi of the Protezione Civile Regione Campania.

The Servizio Idrografico e Mareografico Nazionale (National Hydrographic and Tidal Service), initially called Servizio Idrografico Italiano (Italian Hydrographic

Service), was established by the D.L. of 17 June and 25 October 1917. In the second half of the nineteenth century, leading experts in the field of hydrology and hydraulics noted the need for the establishment of national hydrographic service to study the national water heritage. The establishment of the Italian Hydrographic Service is placed in this historical context.

The performance of the functions of the S.I.M.N. continued until 2002, the year in which the activities of the Service stopped permanently in the state, following the adoption of the legislative measures of D. Decree 112/98 which transferred its responsibilities in part to the Regions (D.P.C.M. July 24, 2002) and in part to A.P.A.T. - Agency for the protection of the environment and technical services (D.P.R- 207/2002). In particular, the Compartmental Office of Naples of the National Hydrographic and Mareographic Service was transferred to the Campania Region to be incorporated, with the D.G.R. 21 December 2001, in the Service 04 - *Functional Centre for meteorological forecasting and meteo-hydropluviometric and landslide monitoring - of the Civil Protection Interventions Programming Sector*.

The Functional Center began its activities in October 2002 and ensures the functions already carried out by the former Compartmental Office of Naples of S.I.M.N., relating to the historical activities of detection, validation, archiving, and publication of climatic, hydrological, and hydrographic quantities concerning the surface and underground hydrographic network.

The Functional Center has started its activities in October 2002 and guarantees the functions already carried out by the former Compartimental Office of Naples of S.I.M.N., related to the historical activities of survey, validation, filing and publication of climatic, hydrological and hydrographic quantities concerning the surface and underground hydrographic network.

Chapter 3: CAMPANIA REGION, DROUGHT HISTORY, DATA SOURCES AND PROCESSING

In this study, the information obtained from the hydrological annals consisted of daily rainfall observations, from 1918 to 1999, recorded in 154 rainfall stations located in the Campania Region and the provinces of Latina, Rome, Frosinone, Isernia, and Potenza. Subsequently, with the transfer of responsibilities from the Compartimental Office of Naples of the S.I.M.N. to the Multihazard Functional Centre of the Civil Protection of the Campania Region, the spatial distribution, as well as the number of stations distributed over the territory, has undergone changes. In this study, the rainfall data recorded in 186 stations located in Campania were taken into account for the years 2000-2019 (Figure 3.5 comparison of the distribution of stations between the two databases).

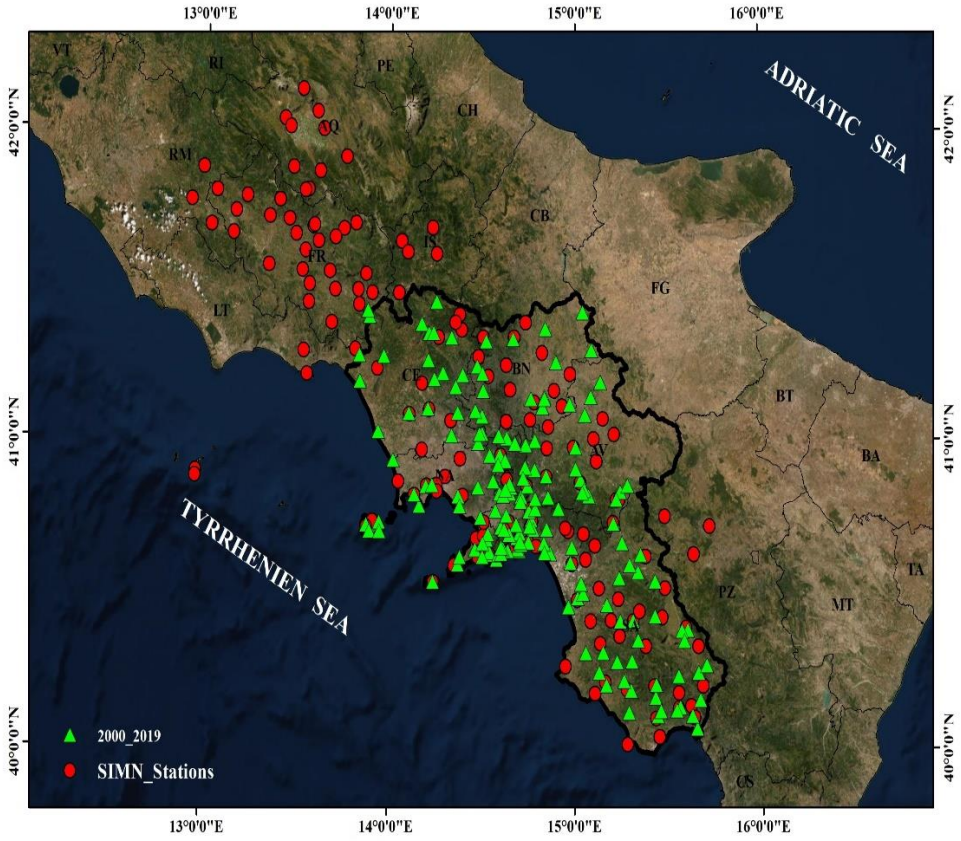

Figure 3.5 The two rain gauge networks: Red colour: SIMN raingauge station, Green colour: Centro Funzionale Multirischi of the Protezione Civile Regione Campania Rain gauge station.

First, data from 1918 to 1999 (82 years) and 2000 to 2019 (20 years) were used in this study to reconstruct a continuous database, and the resulting gridded data will be used for drought purposes. This data were either available or estimated for all variables (i.e. precipitation, temperature and potential evapotranspiration). However, drought indices were developed on a monthly time scale because monthly

drought indices are more appropriate for operational purposes and have a lower sensitivity to observational errors (McKee et al., 1993; Mishra and Singh, 2010).

3.5 Meteorological data processing

In total, almost 400 precipitation and temperature stations were used to calculate monthly values for the region. The numbers, names, and geographical coordinates of each of the measuring stations are presented in Appendix 1, for the precipitation and temperature stations respectively, and their spatial locations are shown in Figure 3.5 and Figure 3.6. The data from these stations were used because all of them had long historical records, from 1918 to 1999 and 2000 to 2019 for precipitation on the one hand, and 1924 to 1999 and 2000 to 2019 for temperature on the other.

3.5.1 Rainfall data

Analyses on precipitation data of annual and monthly time series were carried out considering two databases. Annual and monthly precipitation time series for over 400 sites across Campania and Lazio were available. Longobardi and Villani (2010) performed a data quality control process, and only 163 rain gauge stations passed a time series homogeneity statistical analysis. As it was mentioned in section 3.4, after 1999, the Regional Civil Protection Department oversaw reorganizing and managing the rain gauge network. Around that time, there was a change in the consistency, spatial location, and typology of rain gauge stations, which hampered the possibility of database merging. In fact, only a subset of 30 stations were discovered to share the same location in both databases and to exhibit statistical homogeneity features from 1918 to 2015. (Longobardi et al., 2016). The change in gauge location

prevented the possibility of reconstructing a long precipitation time series by merging the two data bases for the remaining stations.

3.5.2 Temperature data

A further 62 stations of the S.I.M.N. have been considered, of which 22 are outside the borders of the Campania Region. The period to which this first database refers covers the period from 1924 to 1999. After 1999, The temperature stations managed by the Centro Funzionale Multirischi della Protezione Civile (Multihazard Functional Center of the Civil Protection) were numerous, 98 in total, of which only 6 are outside the Campania Region (From 2000 to 2019).

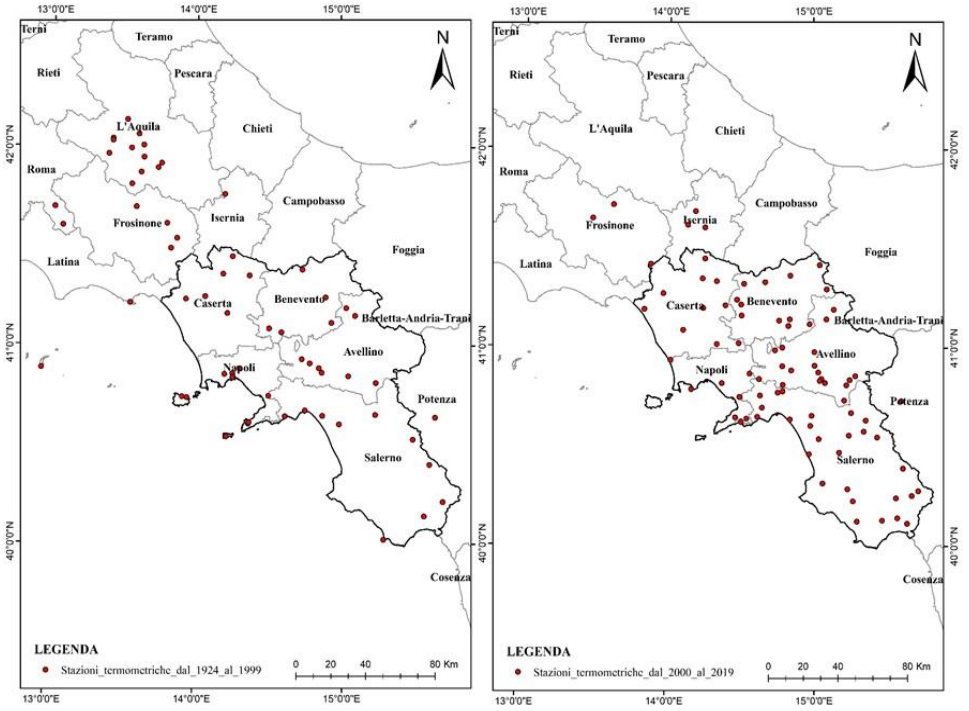

Figure 3.6. Spatial location of the rainfall and temperature gauge station in the studied Area

3.5.3 Evapotranspiration data

Evapotranspiration depends strongly on the intervention of three factors, climatic, geographical, biological and soil. Different equations for estimating potential evapotranspiration can be used, most commonly the Thornthwaite equation (Thornthwaite 1948) because it is a purely climatic equation that represents the evaporative demand of the atmosphere (Allen et al. 1998; Allen et al. 2011). It is directly related to the duration of sunshine; it is a very well-known equation used in several research works all over the world.

The estimation of potential evapotranspiration (PTE) was therefore based on the above equation; Figure (3.7) shows the average variation of PTE across the study area in the month of January considered as the coldest month of the year and in the month of July as the hottest month, for the period from 1924 to 2019.

In January, the average potential evapotranspiration does not exceed 23 mm, this maximum value characterizes the mountainous region where the climate is extremely humid. The territory is adjacent to the sea (the Golf of Naples, the Amalfi Coast, and the Cilento area) and has a dense vegetation cover. For the hottest month of the year, July, the average ETP exceeds generally and over the entire region the 160 mm.

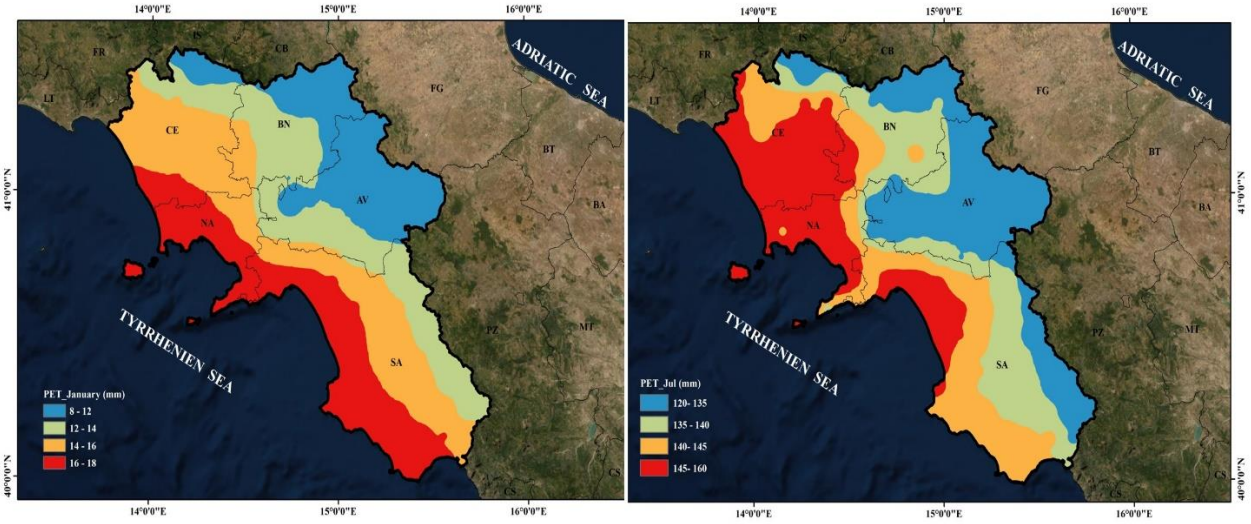

Figure 3.7 Mean monthly Potential evapotranspiration distribution in the Campania Region. (two representative months are shown: a) January b)July).

3.6 Summary

The Campania region, located in southern Italy, is a valuable asset for all inhabitants of the region and the surrounding areas. The region's water resources are important for a wide range of water uses as well as for the needs of users. Numerous initiatives have been taken by several water authorities, including the Campania Region authorities, to protect the region's water sources and to mitigate the demand for water in times of drought (both for potable water and for use in agricultural irrigation). The frequent droughts and the increase in water demand in recent years, however, have increased the pressure on the management of water resources in the region. However, frequent droughts and increased water demand in recent years have increased the pressure on water resources management in the region, and

therefore water resources management in terms of drought is important in the Campania region.

Data on several meteorological variables (i.e., precipitation, potential evapotranspiration, and temperatures) have been collected for the Campania region from different sources to reconstruct a long-term climatic database and to elaborate the Drought Indices which aim to characterize the drought in the region. The data were collected for the period 1918-1999 and 2000-2019 (Precipitation) on the other hand 1924-1999 and 2000-2019 (temperature), the collected data will be estimated for the period 1918 -2019 on a 10 x 10 km grid. These data were available in two-time scales (i.e., daily and monthly) for these weather variables. However, the database reconstruction and drought indices were developed using a monthly time step, as monthly drought forecasting was appropriate for operational purposes, and also monthly data have a lower sensitivity to observational errors. Therefore, data that were not on a monthly time scale were transformed to represent the monthly time scale. These data (i.e., precipitation, potential evapotranspiration, and temperature) were collected and/or estimated, and analysed for three specific purposes in this thesis for appropriate use in the Campania region:

1. To reconstruct a long-term database of climatological data (i.e., precipitation, potential evapotranspiration, and temperature).
2. To evaluate existing drought indices.
3. To characterize drought and drought events in the Campania region.

Chapter 4

REGIONAL CHANGES IN INTER-ANNUAL PRECIPITATION VARIABILITY

4.1 Overview

Water scarcity is a recurring and global phenomenon, with spatial and temporal characteristics that differ significantly from one region to the next (Tallaksen and Van Lanen, 2004). Climate change is likely to accelerate the climate-meteo-hydrological processes that can lead to intense drought episodes (Longobardi and Van Loon, 2018), and understanding historical precipitation variability is required to plan mitigation strategies for future climate change impacts. The inter-annual precipitation variability is intended to represent the year-to-year variability in cumulative precipitation occurrences and can be used as an index of climatic risk if it indicates the possibility of a random sequence of years of rainfall abundance and years of rainfall scarcity, with the corresponding consequences. However, no such study had been conducted for a region with a Mediterranean climate nor for the Italian territory, which is often considered as the inhabited basin that faces a rather complex rainfall variability. In the outlined context of change in interannual precipitation variability, only two studies, one in a tropical climate region and one in a Mediterranean climate region, examined CV temporal patterns derived from

historical precipitation time series, and both confirmed an increase in the CV (Gajbhiye et al., 2016; He and Gautam, 2016; Chandniha et al., 2017).

The work presented in this chapter is the first part of a larger research project highlighting the results of inter-annual precipitation variability for a specific area in the Mediterranean basin. The CV average and spatial variability at the regional scale were first illustrated in the current chapter. In order to analyze the temporal changes in the CV patterns, 30 years of moving windows CV time series were reconstructed for each station. The Mann-Kendall and Mann-Kendall modified tests for auto-correlated time series were used to evaluate the significance and the sign of the changes, as well as the Sen's slope test was used to assess the magnitude of temporal changes in CV (Hamed and Rao, 1998; Yue and Wang, 2004; Theil, 1950; Sen, 1968). Finally, the inter-annual precipitation changes were compared to the previously studied annual precipitation regime and intra-annual precipitation variability changes to depict a general characterization of the long-term climate variability for the studied region.

4.2 Study area and available data set

The study area is a 25.000 km^2 region in Southern Italy that has previously been analyzed for climatological characterization (Longobardi and Villani, 2010; Califano et al., 2015; Longobardi and Mautone, 2015; Longobardi et al., 2016; Fattoruso et al., 2017; Longobardi et al., 2021). The region's annual precipitation appeared to show a general negative trend, which was statistically significant for only a limited number of rain gauge stations. Changes in intra-annual precipitation variability, as summarized by the PCI index, were also assessed, revealing a general trend for a precipitation regime shift from seasonal to more uniform, but statistical significance was limited to a small number of rain gauge stations once again. The

study area's climate regime is typically seasonal, with some main distinctions depending on the location of the station. Because of the significant orographic effect on precipitation, large amounts of precipitation are recorded during winter periods and near or in correspondence with the tallest reliefs (more than 2000 mm).

For the period 1918-1999, the SIMN "Servizio Idrografico e Mareografico Nazionale" managed the rain gauge network for the investigated region. Annual and monthly precipitation time series for over 300 sites across Campania and the surrounding province are available. Longobardi and Villani (2010) performed a data quality control process, and only 163 rain gauge stations carried a statistical analysis of time series homogeneity. After 1999, "the Regional Civil Protection Department" was in charge of reorganizing and managing the rain gauge network. Through that period, there was a change in the consistency, spatial location, and typology of rain gauge stations, which hampered the possibility of database merging. By simply joining the two series, only a subset of 30 stations was discovered to have the same location in both databases and to have statistical homogeneity features from 1918 to 2015. (Longobardi et al., 2016). The change in gauge location prevented the possibility of reconstructing a long precipitation time series by merging the two data bases for the remaining stations. From 2000 to 2015, finer time scale resolution precipitation at 10 minutes was available, which was aggregated at the monthly scale for comparison with the former meteorological service's data recorder.

The current analysis was carried out in two steps to illustrate, on the one hand, the long-term variability over the longest available period and, on the other hand, the broadest spatial pattern variability. Initially, the investigation was focused on the 163 stations for which data were available from 1918 to 1999 in order to represent spatial variability at the regional scale. Besides that, the subset of 30 stations was investigated to represent the temporal variability over the longest available period.

A comparison of the results from 1918 to 1999 and 1918 to 2015 was also carried out. For the years 1918 to 2015, daily, monthly, and annual time series are available. The current analysis is focused on the annual scale.

4.3 The methodology used for exposure assessment of interannual rainfall variability

4.3.1 Inter-annual variability index estimation

The coefficient of variation (CV), also recognized as the relative standard deviation (RSD) in Bayesian statistics, is a standardized measure of the dispersion of a probability or frequency distribution. It is frequently expressed as a percentage and is defined as the ratio of standard deviation σ to mean μ (Searls 1964). CV or RSD is commonly used to express the precision and repeatability of a test (Taverniers, De Loose et al. 2004). It is also commonly used in quality assessment studies in fields such as engineering and physics.

In the current chapter, the average CV for each rain gauge station was computed as the ratio between the annual precipitation standard deviation σ and mean annual precipitation μ

$$CV = \frac{\sigma}{\mu} \quad (4.1)$$

It reflects an average index of inter-annual variability. The CV, as defined by eq. (4.1), has also been computed on a 30-year moving window to detect changes in the inter-annual variability precipitation time series. In this manner, CV time series for each rain gauge station were reconstructed in order to test the significance and magnitude of the temporal trends. A 30-year period has been chosen as a

compromise between the definition of a climate normal WMO (1989) and the average temporal extension of the available historical observation.

4.3.2 Trend detection Analysis

CV time series were tested for trend detection over time. A trend is a significant change in a random variable over time that can be detected using statistical parametric and non-parametric procedures. The current study, in particular, provided and compared results for non-parametric Mann–Kendall (MK), modified Mann–Kendall (MMK), and Sen's test approaches.

4.3.2.1 Original Mann-Kendal trend test (MK)

The Mann-Kendall test (Mann 1945, Kendall 1948) is one of the most widely used methods to detect trend in climatology analysis. It is used to analyse data collected over time for consistently increasing or decreasing trends (monotonic). It is a non-parametric test, which means it works for all distributions, thus tested data does not have to meet the assumption of normality but should have no serial correlation. The Mann-Kendall statistic S is defined as:

$$S = \sum_{i=1}^{n-1} \sum_{j=i+1}^{n} sign(x_j - x_i) \tag{4.2}$$

where:

$$sign(x_j - x_i) = \begin{cases} +1, \text{ if } (x_j - x_i) > 1 \\ 0 \text{ , if } (x_j - x_i) = 0 \\ -1, \text{ if } (x_j - x_i) < 1 \end{cases} \tag{4.3}$$

x_i and x_j are the annual values in years i and j, with $i > j$. When $n \geq 10$, the statistic S is almost normally distributed with mean E(S) and variance Var(S) as follows:

$$E(S) = 0, \quad Var(S) = \frac{n(n-1)(2n+5)}{18}$$

(4.4)

however, the expression of Var(S) should be adjusted when tied value do exist:

$$Var(S) = \frac{1}{18}\left[n(n-1)(2n+5) - \sum_{p=1}^{q} t_p(t_p-1)(2t_p+5) \right]$$

(4.5)

where q is the number of tied groups and t_p is the number of data values in the p^{th} group. The standardized test statistic Z follows a standard normal distribution and is computed as follows:

$$Z = \begin{cases} \dfrac{S-1}{\sqrt{Var(S)}} & if\ S > 0 \\ 0 & if\ S = 0 \\ \dfrac{S+1}{\sqrt{Var(S)}} & if\ S < 0 \end{cases}$$

(4.6)

At the significance level α, the existing trend is statistically significant if $P \leq \alpha/2$ in the case of the two-tailed test.

4.3.2.2 Modified Mann-Kendal trend test for autocorrelation data

To take account of the presence of both positive and negative autocorrelation in analysed data, which might increase the probability to detect trends when actually none exists, the Modified Mann-Kendall test can be applied (Hamed and Rao 1998).

For this purpose, a modified form of the variance S, set as Var(S)*, is used as follows:

$$Var(S) = Var(S)\frac{n}{n^*}$$

(4.7)

where n* is the effective sample size and n the number of observations. The ratio between the effective sample size and the actual number of observation was computed as proposed by (Hamed and Rao 1998) as follows:

$$\frac{n}{n^*} = 1 + \frac{2}{n(n-1)(n-2)}\sum_{i=1}^{n-1}(n-i)(n-i-1)(n-i-2)r_i$$

(4.8)

where: r_i is the lag-i significant auto-correlation coefficient of rank i of time series.

4.3.2.3 Sen's slope magnitude

(Sen 1968) developed the non-parametric procedure for estimating the slope of trend in a sample of N pairs of data:

$$T_i = \frac{x_j - x_i}{j - i},\ i = 1,2,...N,\ j > i \qquad (4.9)$$

where x_j and x_i are data values at time j and i (j>i) respectively. The Sen's estimator of slope is defined by the median of the N values of T_i :

$$T = \begin{Bmatrix} Q_{\frac{N+1}{2}} & \text{if N is odd} \\ \frac{1}{2}\left[Q_{\frac{N}{2}} + Q_{\frac{N+2}{2}} \right] & \text{if N is even} \end{Bmatrix}$$

(4.10)

The T sign reflects the data trend behavior (increase or decrease), while its value indicates the steepness of the trend.

4.3.2.4 Pettitt test

The Pettitt test is a non-parametric approach derived from the Mann-Withney (Pettitt, 1979; Ceresta 1986; Servat et al., 1997) test to identify a breakpoint in a sequence of independent random variables X_i,. i = 1...N

The null hypothesis of the test is the absence of a break in the time series. The implementation of the test assumes that for any time t varying from 1 to N series $(x_i), i = 1, t$ and $(x_i); i = t+1$ N belongs to the same population.

Either Dij = Sgn (x_i - x_j) with Sgn (x) = 1 if x>0; 0 if x=0, -1 if x<0.

We consider the variable $U_{t,N}$ such that:

$$U_{t,N} = \sum_{i=1}^{t} \sum_{j=t+1}^{N} D_{ji}$$

(4.11)

Let K_N denote the variable defined by maximum in absolute value of $U_{t,N}$ for t varying from 1 to N-1 if K denotes the value of K_N taken on the series studied under the null hypothesis, the probability of exceeding the value K is given approximately by:

$$\text{Prod (KN>K)} \approx 2\exp(-6k^2/(N^3+N^2)) \qquad (4.12)$$

For a given first-order risk, if prob (kN>k) is less than α, the null hypothesis is rejected. This test is known for its robustness.

4.4 CV temporal pattern evaluation

4.4.1 Average CVs for the period 1918-1999

The boxplot in Figure 4.1 depicts the average CV empirical distribution. The case study's minimum and maximum CV values, 14.37 % and 35.16 % respectively, appear to be higher than the extremes of CV range found by Gajbhiye et al. (2016) and Chandniha et al. (2017) in a tropical climate area, confirming the Mediterranean basin's highest variability. The median value is approximately 21%. The interquartile range, which represents a measure of data dispersion, is only 4.12 %. The data is skewed by a few outliers (8 rain gauge stations) that are only above the boxplot upper fence. They are all associated with average CV values greater than 29.29 %. Figure 4.1 illustrates the spatial pattern of the average CV of the investigated area as estimated using an ordinary kriging geostatistical interpolation. The spatial patterns of average CVs do not appear to be well-organized. Moreover, the higher average CV values appear to be concentrated in the extreme areas of the studied area, that is in the southern and northern sections. Lower average CV values characterize the central area between these two sections and the entire inland area.

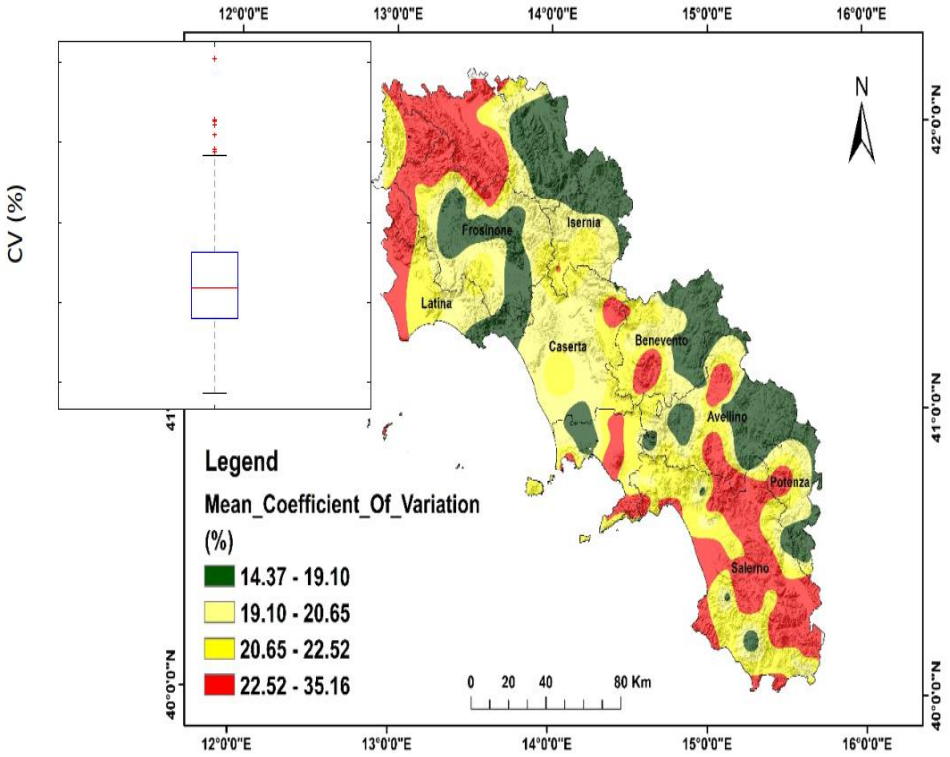

Figure 4.1 Spatial distribution of average CV over the studied region.

4.4.2 CV temporal pattern for the period 1918-1999

In terms of the temporal patterns of the 30-year moving window CVs, each rain gauge station clearly showed a different pattern, but they can be roughly classified into four different typologies, as shown in Figure 4.2. Aside from monotonic increasing (e.g., ID 3610) and decreasing (e.g., ID 3768) behaviour, several stations displayed complex patterns in which either a stationary condition (e.g., ID 3623) or a decreasing trend (e.g., ID 3747) precedes an increase in the CV trend, which generally occurs during the 1970s.

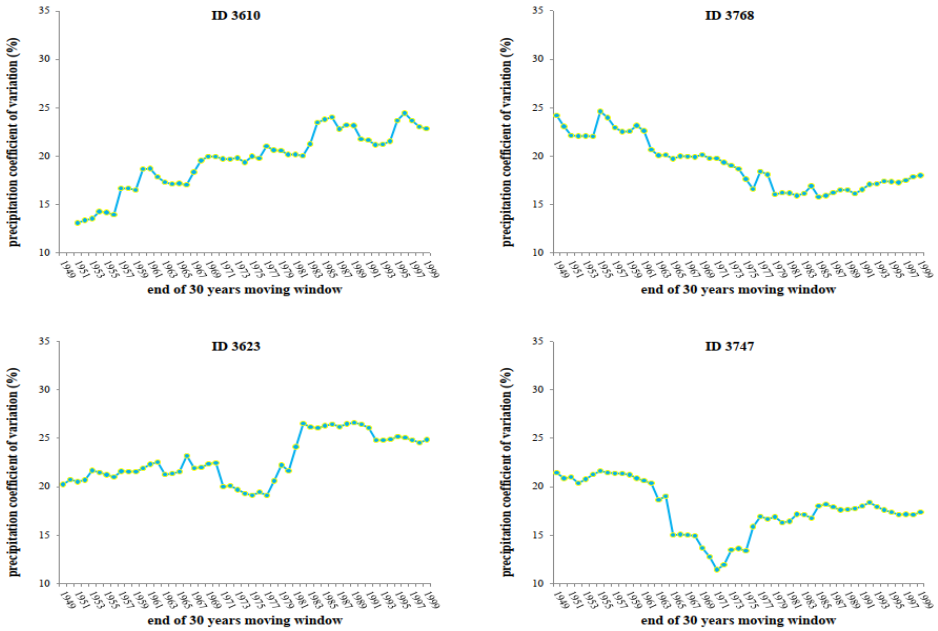

Figure 4.2. Typical CVs pattern over the studied region. ID = rain gauge station code

Table 4.1 shows the relevant results of the Mann-Kendall (MK) and Modified Mann-Kendall (MMK) tests for trend sign and significance (significance level = 5%).

Table 4.1. Results for the Mann-Kendall (MK) and Modified Mann-Kendall (MMK) tests (α = 5%).

	MK %	MMK %
stations with significant trend	80	73
stations with not significant trend	20	27
stations with positive trend	70	72
stations with negative trend	30	28

MK and MMK both show how a substantial portion of rain gauge stations, 80 % and 73%, respectively, show a significant trend. The MMK test locates a lower number of stations clearly displaying a significant trend, highlighting the potential effect of autocorrelation in the data that the MK does not account for. However, the difference in the number of stations exhibiting a significant trend between the MK and MMK tests does not appear to be significant, as it reports for only 8% of total stations. In terms of spatial variability, the results of the MMK test are discussed further below. Figure 4.3 (left panel) shows the spatial distribution of rain gauge stations with a significant/not significant trend as provided by a simple kriging geostatistical interpolation. As previously stated, the rain gauge stations exhibiting a significant trend predominate in the case study, and their spatial distribution is highly uniform. In terms of trend direction, MMK tests show that a large proportion of rain gauge stations, approximately 72 %, show a positive trend. Negative trends appear to dominate the region's southern area, though still not significantly (Figure 4.3 (right panel)). Instead, the remaining portion is dominated by positive trends. The overall findings of the MMK test indicate that there is a generalized condition of significant increase in inter-annual variability almost across the entire analysed area.

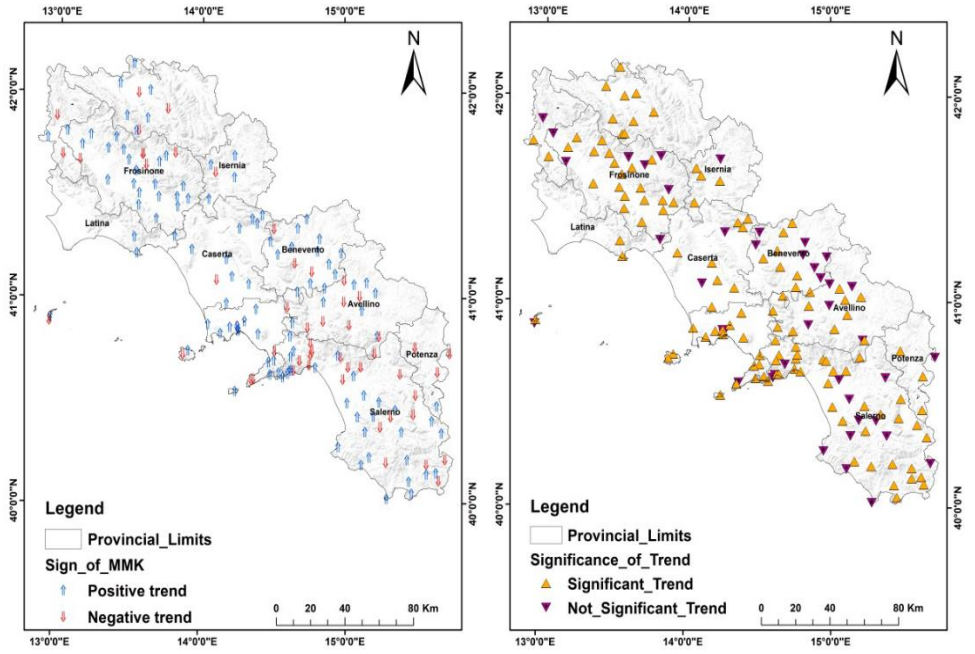

Figure 4.3. MMK significance (left panel) and sign (right panel) over the studied region (α = 5%).

Figure 4.4 depicts the magnitude of Sen's slope over the study area (α = 5%). The slope is expressed as a percentage of the annual increase or decrease in CV over the entire period of observations. The boxplot in Figure 4.4 illustrates the empirical distribution of Sen's slope values. The case study's minimum and maximum CV values are 0.36% (in absolute value)and 0.55%, respectively. The median value is approximately 0.06%. The interquartile range, which represents a measure of data dispersion, is only 0.19%. Only two outliers skew the data, one above and one below the 0.35% boxplot upper and lower fences. However apart from the overall generalized conditions of significant increase in inter-annual variability almost across the entire analyzed area as described by the MMK test results, the Sen's test results show a relatively moderate magnitude of the detected changes. There do not

appear to be well-organized spatial patterns of the magnitude of changes in CV, as there are in the case of the average CV spatial distribution.

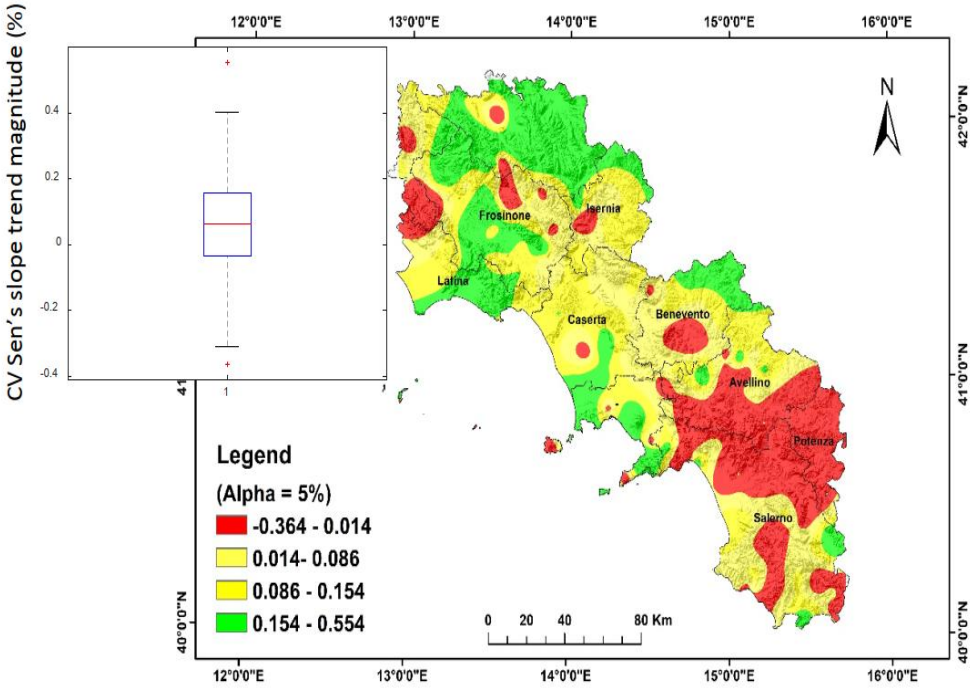

Figure 4.4. CV Sen's slope trend magnitude over the studied region (α = 5%). The slope is expressed as the percentage of annual increase or decrease in CV over the whole observations recording period.

Comparing Figures 4.1 and 4.4, it appears that areas with the lowest decrease in CV correspond to areas with the highest average CV values. In this regard, the rain gauge stations with the greatest average inter-annual variability appeared to be the least affected by temporal changes.Therefore, is not always a result that describes a phenomenon, but it could be due to a numerical correlation wherein the magnitude of interannual variability masks the possibility of detecting non-stationarity.

4.4.3 CV temporal patterns from 1918 to 2015, with comparisons to 1918-1999

As mentioned in section 4.2, Despite data availability (the stations share the same location in both datasets) and statistical homogeneity, only a subset of 30 stations for the period 1918-2015 were investigated. Given the small number of rain gauge stations in this subset, the emphasis was solely on temporal CV variability, with no spatial features derived. Table 4.2 shows the list of the subset of stations, as well as the results of the MMK test (significance level = 5%). Furthermore, the Pettitt test (Pettitt 1979) indicates that there is no break point at any of the subset studied stations. Table 4.2 also includes a summary (significance level = 5%).

The general tendency is still set on a large percentage of stations, approximately 64 percent, for which a significant trend in the CV temporal pattern was detected between 1918 and 2015. Furthermore, the trend is positive for the majority of stations, approximately 60%, during this period. This trend appeared to be consistent with the results reported in Table 4.1 for the larger set of 163 stations, where the percentage of stations exhibiting a significant and positive CV trend was only 17 % higher. Concerning the slope of the CV, an average value of 0.035 % was reported in the period 1918-2015, which is 40% lower than the average of about 0.06 % reported in the period 1918-1999.

Table 4.2. Mann-Kendall test and Sen test results for the sub-set of 30 gauged stations (α = 5%). Comparison between the periods 1918-1999 and 1918-2015. Yellow cells indicate the rain gauge stations for which a change in the sign of the trend was detected.

	Significance		Sign		Slope (%)	
	(1918-1999)	(1918-2015)	(1918-1999)	(1918-2015)	(1918-1999)	(1918-2015)
Agerola (Fraz. S.Lazzaro)	Trend	No_trend	Positive	Positive	0,222	0,134
Albanella (Ponte Barizzo)	Trend	No_trend	Positive	Negative	0,085	-0,015
Benevento (Genio Civile)	Trend	No_trend	Negative	Positive	-0,155	0,008
Capua	Trend	Trend	Positive	Positive	0,241	0,224
Caserta (Genio Civile)	Trend	Trend	Positive	Positive	0,064	0,063
Cassano Irpino	Trend	Trend	Negative	Negative	-0,246	-0,23
Cava Dei Tirreni	No_Trend	Trend	Negative	Negative	-0,063	-0,06
Ercolano (Oss. Vesuviano)	Trend	No_trend	Positive	Positive	0,319	0,086
Forino	Trend	Trend	Negative	Negative	-0,127	-0,096
Gragnano	Trend	Trend	Positive	Positive	0,3	0,268
Grazzanise	No_Trend	Trend	Negative	Negative	-0,066	-0,069
Luogosano	No_Trend	No_trend	Negative	Positive	-0,122	0,023
Maiori	Trend	Trend	Negative	Negative	-0,073	-0,068
Massalubrense (Turro)	Trend	Trend	Negative	Negative	-0,085	-0,126
Mercato S.Severino	Trend	Trend	Negative	Negative	-0,114	-0,091
Morcone	Trend	Trend	Positive	Positive	0,118	0,098
Morigerati	Trend	Trend	Positive	Positive	0,058	0,093
Napoli (Capodimonte)	No_Trend	No_trend	Negative	Negative	-0,055	-0,016
Paduli	No_Trend	No_trend	Positive	Positive	0,047	0,057
Pellezzano	Trend	Trend	Negative	Negative	-0,049	-0,044
Positano	Trend	Trend	Positive	Positive	0,28	0,198
Pozzuoli	Trend	No_trend	Positive	Negative	0,192	-0,023
Ravello	No_Trend	Trend	Positive	Positive	0,065	0,138
Roccadaspide	No_Trend	Trend	Positive	Positive	0,043	0,123
Rofrano	Trend	Trend	Positive	Positive	0,132	0,163
S.Angelo D'alife	No_Trend	No_trend	Positive	Positive	0,022	0,05
Sala Consilina	Trend	Trend	Positive	Positive	0,173	0,166

Salerno (Genio Civile) *	Trend	Trend	Negative	Negative	-0,047	-0,05
Torraca	Trend	No_trend	Negative	Positive	-0,061	0,011
Tramonti (Chiunzi)	Trend	No_trend	Positive	Positive	0,2	0,024
Average					**0,043**	**0,035**

The comparison of the results for the same subset of 30 stations between 1918-1999 and 1918-2015 provided in Table 4.3 only shows a very moderate impact of the last fifteen years of observation over the total length of the recording period.

Table 4.3. Summary of the Mann-Kendall test results for the sub-set of 30 gauged stations (α= 5%). Comparison between the periods 1918-1999 and 1918-2015.

	1918-1999 (%)	1918-2015 (%)
stations with significant trend	73	64
stations with not significant trend	27	34
stations with positive trend	57	60
stations with negative trend	43	40

Indeed, over the last fifteen years, there has been a very moderate increase in the percentage of stations showing a positive trend (from 57 % to 60 %), a decrease in the percentage of stations showing a significant trend (from 73 % to 64 %), and a moderate decrease in the CV slope (from 0.047 % to 0.035 %). In particular, for the CV slope, only 16% of the analysed stations experienced a change in slope sign (both positive to negative and negative to positive) over the last fifteen years (Yellow cells in Table 4.2).

4.5 Overall evaluation

As mentioned in section 4.1, in order to describe a general characterization of long-term climate variability for the investigated study area, and in accordance with the findings reported in the relevant literature, it was necessary to comment on the observed results about inter-annual variability in light of previous findings reported by the same authors about the annual precipitation regime and intra-annual precipitation variability for the same area. Longobardi and Villani (2010) conducted a study on long-term changes in annual precipitation using the same data-base and region as the proposed investigation (163 stations for the period 1918-1999). It was noticed that, across the entire region, the trend in annual precipitation appears to be predominantly negative, but that the significance of the changes only holds for a very small number of total rain gauge stations, approximately 9% in the case of negative trends and 27% in the case of positive trends. Subsequently, in Longobardi et al. (2016), the intra-annual variability of the precipitation regime, as outlined by the PCI index, was investigated for a larger data-base and a larger region, which included the current study area. It was revealed that, for the specific region, the trend in intra-annual precipitation variability is predominantly negative, but that the significance of the changes only maintains for a very small proportion of the total rain gauge stations, of about 11%. The overall outcomes of these studies over the region under consideration delineated a general, but not statistically significant, tendency toward a reduction in total precipitation and a general, but not statistically significant, tendency toward a more uniform distribution of total precipitation during the year (reduction in climate seasonality).

Figure 4.5 illustrates the comparison of the spatial distributions of mean annual precipitation, Precipitation Concentration Index, and average Coefficient of Variation. The orography of the region has a strong influence on the mean annual

precipitation spatial pattern, with the highest mountain reliefs running north-west to south-east, where the highest MAP values, between 1500 and 2000 mm, can be found. Besides that, the orography and distance from the coastline have a significant impact on the average PCI spatial distribution.

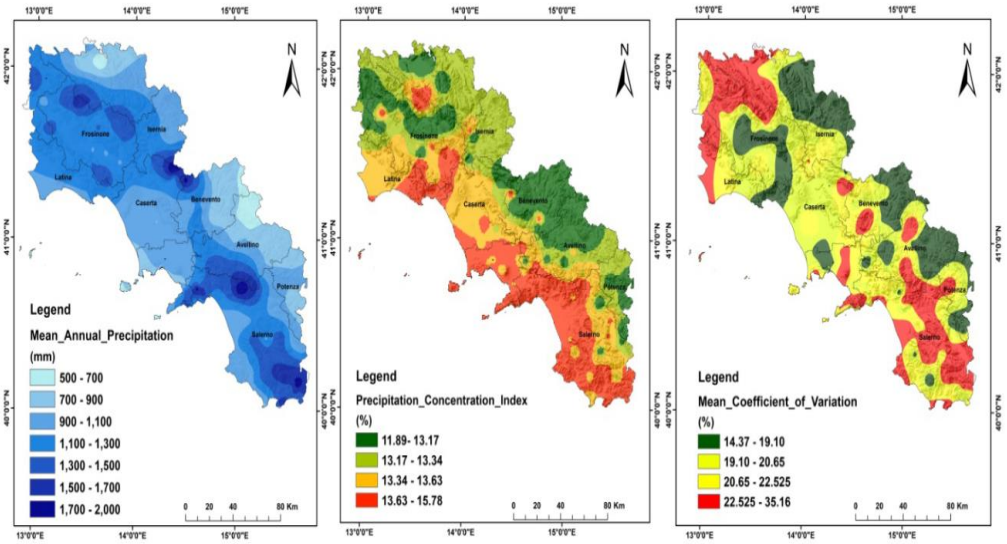

Figure 4.5 Spatial distribution of mean annual precipitation (left panel), Precipitation Concentration Index (middle panel) and Precipitation coefficient of variation (right panel).

Coastal areas have the highest PCI values, ranging from 13 to 16, whereas inland areas have average PCI values as low as 11. Whereas there appears to be a strong connection between the MAP and PCI spatial distributions across the region, the CV spatial distribution appears to be only partially influenced by the latter features. Evidently, higher CV values appear to be associated with higher MAP and PCI values, and vice versa, but the relationship between these variables is poor. This condition is also shown in Figure 4.6, where red dots represent observations, and a polynomial surface has been fitted to them. The goodness-of-fit is quite poor (R^2 =

0.20), but higher CV values appear to be associated with higher MAP and PCI values.

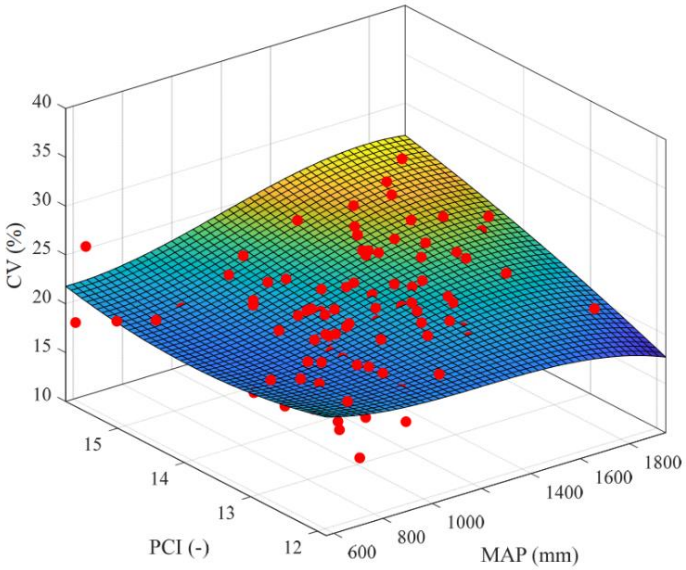

Figure 4.6. Relationship between MAP, PCI and CV for the studied region.

The specific findings reported for the region under investigation appeared to contradict the main findings illustrated in the relevant literature. Although some differences may influence the spatial distribution of the observed quantities due to interpolation issues, the main motivation is most likely represented by a limitation of the case study, which presents some rather characteristics of climatic homogeneity in general. A spatial extension of the rain gauge stations database is planned to investigate these specific features in greater depth.

4.6 Summary

In order to depict a general characterization of the long-term climate variability for the Campania region, located in the Mediterranean basin, an analysis of the precipitation coefficient of variation CV, assumed as index of inter-annual climate variability, was performed over the period 1918-2015 and compared with the results of a previous investigation about the annual precipitation regime and the intra-annual precipitation variability of the same region. Understanding the inter-annual precipitation variability from long term historical precipitation variability is necessary to plan mitigation strategies to face future climate change impacts in specific regions. In particular quantify the inter-annual precipitation variability is essential for a more realistic modelling of water resources availability under climate change scenario, which in turn results in a more effective quantification of socioeconomic impacts of planned complex water resources management tools.

The results of the current study can be summarized as in the following:

1. For what concerns the average CV characterization and spatial pattern, the findings illustrated a generalize conditions of statistically significant (73% of total stations) increase (72% of total stations) of inter-annual variability almost over the whole analyzed area, where a very moderate spatial consistency was however detected.
2. For what concerns the magnitude of the changes, the results of the analysis reported about a rather moderate intensity of the detected changes, with minimum and maximum CV patterns slope, expressed as the percentage of annual increase or decrease in CV over the whole observations recording, which amount respectively to -0.36% and 0.55%. Similarly, to the average CV characterization, no strong spatial consistency was detected, but rain gauge stations featured by

the largest average inter-annual variability seemed to be the less affected by temporal changes.

3. the effect of the last fifteen years of data, from 2000-2015 was only studied on a sub-set of stations because of data availability and statistical homogeneity. The comparative analysis of the statistical tests results for the period 1918-1999 and 1918-2015 showed, beyond the same general tendency (significant positive trends for the largest percentage of stations), that some quantitative difference between the two observed periods exists but that such difference appeared very moderate.

4. the relationship between average precipitation, intra-annual precipitation variability and inter-annual precipitation variability was not clearly identified for the studied region, but it was found that larger CV values appear associated to large MAP and large PCI values.

5. The main message that arises from the comparative analysis of average precipitation, intra-annual precipitation variability and inter-annual precipitation variability showed how, if the variations in the annual precipitation regime and in the intra-annual precipitation variability are poorly significant (respectively for 9% and 11% of total station), changes in inter-annual precipitation variability are strongly marked over the studied region.

The current work has increased the knowledge about the long-term climatological characterization of a specific area. It furthermore has contributed to extend the body of literature relevant to the use of historical observation aimed at the detection of changes in inter-annual variability within the Mediterranean basin, known to be one the most responsive region to climate changes. As a future perspective an extension to a spatially wider database (Longobardi, Buttafuoco et al. 2016) is foreseen to

overcome the climatic homogeneity issue which, in the opinion of the authors, dampened the significance of the link between CV,MAP and PCI.

Chapter 5

CONSTRUCTION OF GRIDDED CLIMATOLOGICAL DATASET FROM TWO DIFFERENT GAUGING NRTWORKS

5.1 Overview

Many hydrological research and modelling purposes rely on environmental data. The accuracy of various hydrological analyses, such as climate change studies, drought management, and water management, is heavily reliant on accurately estimating the spatial distribution of various climate data (precipitation, temperature, streamflow, etc.)(Moral 2010, Wu, Chen et al. 2019), It frequently requires a dense network of rain gauges with numerous stations and long-term measurements (Adhikary, Muttil et al. 2017, Xu, Tian et al. 2017, Tang, Behrangi et al. 2018). In the previous chapter interannual variability (for the Campania region) for the period 1918-1999 were evaluated. In addition, the knowledge about the long-term climatological characterization for a specific area has increased, it has also greatly expanded the body of literature on the use of historical observations to detect changes in inter-annual variability within the Mediterranean basin, which is known to be one of the most responsive regions to climate change.

The existence of serially incomplete data sets, the distribution of climate stations and the change in morphometric characteristics of the gauging stations after

1999 (typology, spatial location, etc.) are much more serious problems as they can lead to the rejection of entire data sets. These problems can be solved by establishing a unified archive of quality climate data that can be publicly accessible. Although many techniques for estimating missing data values have been used, such as (Schneider 2001, Teegavarapu and Chandramouli 2005). In this context, the current chapter reports on the reconstruction of climatological gridded data at 10x10 km resolution for the Campania region (southern Italy), based on a monthly data set of over 380 stations covering the entire region and parts of the surrounding regions from 1918 to 2019. As stated previously, this data was obtained from two different agencies: the Servizio Idrografico e Mareografico Nazionale S.I.M.N. and the Campania Civil Protection Department. Furthermore, the characteristics of the techniques used are carefully examined, and their performance is evaluated in order to reconstruct a new historical database.

5.2 Study Area and Dataset Used

The Campania Region was used as the case study to demonstrate the estimation of gridded climatological data. The details of the Campania region and its importance were described in Chapter 3. Similar to the inter-annual variability assessment, over 380 meteorological variables (i.e., rainfall, temperature) were used in the reconstruction of a historical database. The monthly time step was used in the reconstruction of the time series. The same data that was described and used in Chapter 4 were used in the current chapter to reconstruct climatological data for the Campania region.

5.3 Methodology Used for Reconstructing Gridded Climatological Database

The methodological framework for the climate reconstruction/regeneration study includes spatial interpolation methods, including four geostatistical kriging-based methods (OK, OCK, DK and EBK) and one deterministic method (IDW), as shown in Figure 5.1. This section provides an overview of these methods. Since variograms and their estimation methods are important components of kriging, they are grouped by kriging method. For more information on the methods used in the current study, see recent geostatistics references such as Journel and Huijbregts (1978), Isaaks and Srivastava (1989), Goovaerts (1997), Chilès and Delfiner (1999). give. Wackernagel (2003) and Webster and Oliver (2004). (2007).

5.3.1 Overview of interpolation methods

Surface modelling is a mathematical process by which a continuous surface is interpolated from a set of randomly distributed data (x, y, z). The result of this interpolation provides a structured data called "grid". The accuracy of the grid obtained depends on the starting data (number, distribution, etc.) but also on the algorithm used to calculate the grid points (Maron and Rihouey, 2002). Interpolation methods are numerous and vary greatly in complexity and efficiency (Drapeau, 2000). The selection of one or the other is logically conditioned by the expected representativeness of the results that we are looking for and the objectives that we set (Renard and Comby, 2006). Two approaches of interpolation methods, one deterministic and the other probabilistic, are possible and can be suitable to the problem to be treated (El morjani, 2003).

5.3.1.1 Deterministic methods

The so-called deterministic interpolation methods are based on mathematical functions that express either a weighting factor for the training values (inverse distance weighting) or a trend surface (polynomials, splines), or even a combination of both (Rogers, 2003).

- **The Inverse Distance Weighting (IDW)** method calculates, for each point to be estimated, the average of the experimental values of its neighbors, favoring the closest points; the weighting factors are therefore calculated in proportion to the inverse of the distance: **1 ÷ d**. This method makes it possible to obtain grids very quickly but creates circular zones around the observed values ("bull's eye" effect). This artifact can be smoothed by playing with the power and the neighborhood (El morjani, 2003).

  The IDW formula can be expressed as:

$$\sum_{i_1=1}^{n} w_{i_1}^{OCK} = 1; \sum_{i_2=1}^{m} w_{i_2}^{OCK} = 0 \quad \textbf{(5.1)}$$

$$P(r) = \sum_{j=1}^{N} W(r_j)\left(f(r_j)\right) \quad \textbf{(5.2)}$$

where PI = interpolated value at

$$W(r_j) = \frac{d_j r^{-p}}{\sum_{j=1}^{N} d_j r^{-p}} \quad \textbf{(5.3)}$$

And; $d_j(r) = \sqrt{(x - x_j)^2 + (y - y_j)^2}$ **(5.4)**

the distance between r and r_j; p = decay determining parameter.

A comprehensive discussion has been made by (Kravchenko and Bullock 1999) for the choice of parameter p, the effect of weight parameter for IDW interpolation is discussed by (Cecílio and Pruski 2003), a similar discussion has been made by

(Vicente-Serrano, Saz-Sánchez et al. 2003) over the importance of weight parameter in I.D.W. function for the prediction model.

- **The polynomial methods** constitute polynomial surfaces of a given order linking the training points, with, in Geostatistical Analyst, the possibility of adjusting the degree of locality (one polynomial surface per measurement in a given neighborhood) and globality (a single polynomial surface for the entire study area expressing the first-order trend).
- In the same way, the **Radial Basis Function (RBF)** method allows to interpolate or from randomly distributed data. This type of interpolation is made more flexible than polynomial interpolation by using a voltage parameter that controls the behavior of the interpolation function and the smoothing parameter (Drapeau, 2000). The RBF estimator can be thought of as a weighted linear function of the distance from grid point to data point plus a bias factor BF (Chilès & Delfiner, 1999)., for more details about the method see (Adhikary, Muttil et al. 2017).

However, these deterministic techniques have drawbacks: they ignore the spatial structure of the variable and thus produce very smooth interpolated surfaces; very specific local situations may be omitted (areas of high or very low values).
Finally, no statistical criteria to judge the accuracy of these maps are formulated. If we want to optimize the accuracy of the estimates, we will have to use other tools that will call upon probabilistic models (Despagne, 2006).

5.3.1.2 Probabilistic (geostatistical) methods

Geostatistics refers to the methods of probabilistic analysis to study spatially correlated phenomena called "regionalized phenomena". Geostatistical estimation methods are based on modelling the spatial structure from experimental data; the

parameters of the estimation depend on the spatial variability and the accuracy of the estimation is indicated by the estimation variance (De Fouquet, 1994). There is a series of geostatistical interpolation methods that can be performed in univariate (kriging) or multi-variate (co-kriging) mode (Rogers, 2003).

- **Ordinary Kriging**

Kriging methods have developed over the last thirty years in the mining industry and climatology in recent years. Kriging is a stochastic spatial interpolation method that considers both the geometric configuration of the observed points and the spatial structure of the estimated variable. There are three main types of Kriging: simple Kriging, Ordinary Kriging (OK), and Universal Kriging (Touazi, Laborde et al. 2004). The method, in general, is constructed in 5 steps: i) exploratory analysis (i.e., data visualization); ii) choice of the type of Kriging; iii) the so-called variography (Baillargeon 2005), i.e., the estimation of the variogram, its modelling and the choice of a model; iv) the realization of interpolations; (v) evaluating the quality of the best estimates, Kriging can also be used for the estimation of forecast errors. Nevertheless, what differentiates Kriging from the other previously described techniques is that it is the only method that considers the spatial dependency structure of the data. Thus, Kriging generates most accurate spatial predictions and estimates the more reliable errors than other stochastic methods. For the scientific community, Kriging could be the most appropriate interpolation method (Arnaud, Emery et al. 2001, Baillargeon 2005). We propose to test this by setting the four spatial interpolation methods in action, using the Campania Region as the experimental area. The ordinary Kriging us is given by:

$$\hat{Z}_{\mathrm{OK}}(\mathrm{s}_0) = \sum_{\mathrm{i}=1}^{\mathrm{n}} \mathrm{w}_{\mathrm{i}}^{\mathrm{OK}}\, \mathrm{Z}(\mathrm{s}_{\mathrm{i}}) \quad \text{with} \sum_{\mathrm{i}=1}^{\mathrm{n}} \mathrm{w}_{\mathrm{i}}^{\mathrm{OK}} = 1 \qquad \textbf{(5.5)}$$

$\hat{Z}_{\mathrm{OK}}(s_0)$ The estimated value of variable Z (i.e., Temperature, rainfall) at the unknown location s_0; ω_i^{OK} indicate the weights linked with the sampled location s_i s_0 concerning; and n is the number of sampling points used in prediction.

By solving the system of (n+1) simultaneous linear equations, the OK weight can be obtained as follow:

$$g(d) = \frac{1}{2\,N(d)} \sum_{i=1}^{N(d)} \left[Z(s_i + d) - Z(s_i) \right]^2, \text{for } j = 1; \ldots\ldots\ldots; n \; ; \quad \sum_{i=1}^{n} w_i^{OK} = 1 \qquad \textbf{(5.6)}$$

where $\gamma\left(s_i - s_j\right)$ is the variogram values between sampling locations s_i and s_j, $\gamma\left(s_j - s_0\right)$ is the variogram values between the sampling and the target location s_j s_0, and μ_1^{OK} is the Lagrange multiplier parameter.

As shown in Equation 2, it is clear that OK highly depends on the experimental variogram model $\gamma(d)$ that indicates the degree of spatial autocorrelation in datasets which are derived by;

$$g(d) = \frac{1}{2\,N(d)} \sum_{i=1}^{N(d)} \left[Z(s_i + d) - Z(s_i) \right]^2 \qquad \textbf{(5.7)}$$

$Z\left(s_i + d\right)^{Z(s_i)}$ The variable values at corresponding sampling locations $\left(s_i + d\right)$ and $\left(s_i\right)$, respectively, where d is the distance and N(d) is the number of data pairs.

Using equation 3, a variogram in the form of a cloud point is generated, as shown in Figure 5.1

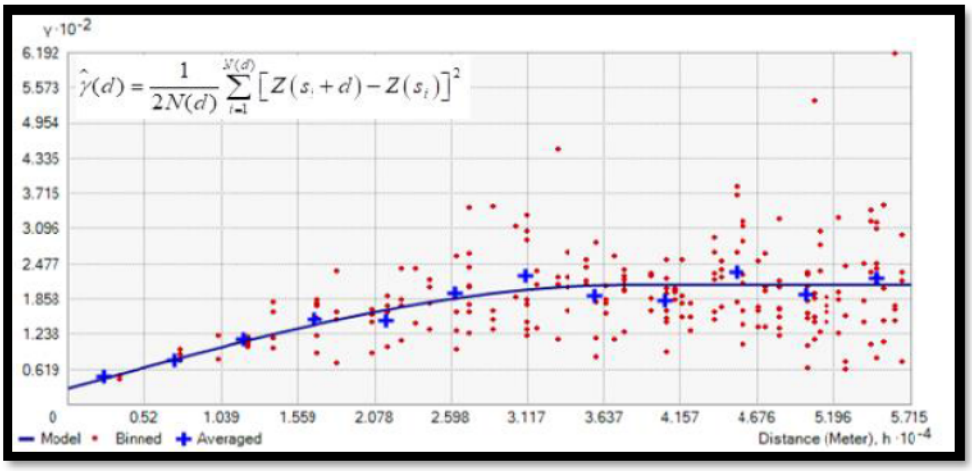

Figure 5.1: A typical experimental variogram based on the variogram cloud fitted by a typical variogram model with its parameters.

According to the literature (Johnston, Ver Hoef et al. 2001, Robertson 2008), Experimental variogram can be computed by subdividing the cloud variogram into several lags and then, estimating the mean of each lag interval. Hence, the resulted variogram model γ(d) will be then fitted to the experimental one. Depending on the form of experimental semi-variogram, different geostatistical models can be fitted to the experimental semi-variogram, such as spherical, exponential, Gaussian, circular, and linear, wherein hydrology Exponential, Gaussian, and spherical models are the most commonly used variogram for kriging applications (Adhikary, Yilmaz et al. 2015), the different models are presented as follow;

$$\text{Spherical model} \quad : y(d) = C_0 + C_1 \left\{ \frac{1.5d}{a} - 0.5\left(\frac{d}{a}\right)^3 \right\} \tag{5.8}$$

$$\text{Exponential model: } y(d) = C_0 + C_1 \left\{ 1 - \exp\left(\frac{-3d}{a}\right) \right\} \tag{5.9}$$

Gaussian model: $y(d) = C_0 + C_1 \left\{ 1 - \exp\left(\frac{-(3d)^2}{a^2} \right) \right\}$ **(5.10)**

Linear model: $y(d) = C_0 + C_1 \left\{ \frac{d}{a} \right\}$ **(5.11)**

Circular model: $y(d) = C_0 + C_1 \left\{ 1 - \frac{2}{\pi} \cos^{-1}\left(\frac{d}{a} \right) + \sqrt{1 - \frac{d^2}{a^2}} \right\}$ **(5.12)**

where, C_0 is the nugget coefficient, $C_0 + C_1$ = Sill, a range of the variogram model and d represents the distance of separation between two locations.

- **Detrended-Kriging (geo-regression)**

One method to improve data interpolation is co-kringing. The crux of this method is to extract maximum information from (covariate) variables related to the average annual precipitation. This procedure requires the estimation of cross-variograms that describe the relationship between the variable of interest and the covariates in space. (Phillips, Dolph et al. 1992) showed how this methodology is of particular interest in estimating the average annual precipitation, by using elevation as a covariate and presented an alternative technique of simple application, even when the number of covariates is greater than one, represented by geo-regression. It consists of the identification of a regression model, generally multiple and linear, through which one can estimate the value of the interest that varies according to the values of a set of covariates. The estimation is improved by combining this result with the residues, interpolated, to give a spatial distribution through ordinary Kriging. This technique is known as elevation-detrended Kriging (DK or Geo-Regression).

For the area in question, given the rather evident link found between the average annual precipitation and the topographic elevation, as previously indicated, a single covariate geo-regression model was chosen, represented by the elevation. The precipitation field, h(x) with x position in space, is described as:

$$h(x) = m[Z(x)] + W(x) + e(x) \quad \textbf{(5.13)}$$

where $\mu[Z(x)]$ is precisely the deterministic trend, estimated in correlation to the altimetric elevation, $W(x)$ is the random field with a small scale and mean zero structure and $\varepsilon(x)$ is purely a random error term.

The residues for each measuring station can be calculated as the difference between observations and estimation concerning the topographic elevation and can be interpolated by ordinary Kriging to generate the corresponding spatial distribution over the whole study area.

- **Co-Kriging**

Co-Kriging is a well-known approach in geostatistics and has been used in various fields such as the tracing of organic matter in the soil (Pei, Qin et al. 2010), climate variables (i.e., precipitation, temperature, etc.; (Khelfi, Touaibia et al. 2017)), and the determination of the soil organic matter content (Goovaerts 1999), estimate environmental variables such as groundwater pollutants (Hoeksema, Clapp et al. 1989, Desbarats, Logan et al. 2002, Guastaldi and Del Frate 2012). This method is a modification of Kriging with the possibility of using more than one variable in the prediction process. The Co-kriging is used to enhance the primary variable's prediction by using the auxiliary variable, assuming that the variables are correlated with each other (Isaaks and Srivastava 1989).

In our study, precipitation and temperature are considered primary variables, while altitude is the auxiliary variable. Like the OK method, the OCK aims to estimate the primary variable. The OCK estimator (Goovaerts 1997) considers a secondary variable (i.e., elevation), which is cross-correlated with the primary variable (i.e., precipitation) can be written as follows:

$$\hat{Z}_{OCK}(s_0) = \sum_{i_1=1}^{n} w_{i_1}^{OCK} Z(s_{i_1}) + \sum_{i_2=1}^{m} w_{i_2}^{OCK} V(s_{i_2}) \quad \textbf{(5.14)}$$

$$\text{with; } \sum_{i_1=1}^{n} w_{i_1}^{OCK} = 1; \sum_{i_2=1}^{m} w_{i_2}^{OCK} = 0 \quad \textbf{(5.15)}$$

- **Empirical Bayesian Kriging**

EBK is one of the special geostatistical interpolation methods that is able to interpolate time series in different spatial aspects, resulting in a valid kriging model (Baker, Kröger et al. 2015). The difference between the EBK and another geostatistical model is that it can automatically compute the model parameter through submission and simulations (Mirzaei, Sakizadeh et al. 2016), while other methods require a manual adjustment of the parameters. The basic idea of EBK method is to predict $Z_1(s)$ at an unknown location. The Empirical Bayesian kriging is given by (Goovaerts, AvRuskin et al. 2005); E.S.R.I., 2014b):

$$\gamma_{ebk} u_\alpha = \lambda u_\alpha Z u_\alpha + [1 - \lambda u_\alpha] m \quad \textbf{(5.16)}$$

where m is the population-weighted sample mean, $\lambda\mu_\alpha$ is the weight assigned to the rate observed at a location μ_α

These methods are applicable both to variables that indicate some homogeneity of features in space (stationary variables) and to variables whose spatial structure shows strong trends in certain directions (non-stationary variables) (Martin et al., 1989). The interpolation of measurements of climatological variables (rainfall, temperature) is very often performed using co-kriging. Several authors (Kumar, 2007; Sun et al., 2009) have also presented comparative studies on the effectiveness of deterministic and probabilistic interpolation methods. However, it would seem that, for climatological variables where elevation is an important factor,

kriging with an external drift digital terrain model is the most suitable (Desbarats et al., 2002).

5.3.2 Assessment of interpolation methods

The performance of different interpolation methods (OK, OCK, DK, EBK, and IDW) used in this study are evaluated and compared through cross-validation process. Cross-validation is a simple leave-one-out validation procedure in which observations are removed from the dataset one at a time and then re-estimated using the adopted model from the remaining observations. It provides significant proof of interpolation method performance measures. The performance of all interpolation methods for rainfall estimation is compared in this study using the Mean absolute error (MAE), percent bias error (PBE), root mean square error (RMSE), and coefficient of determination (R2) values between the observed and estimated variable values, which are given by the following Equations:

$$\mathrm{MAE} = \frac{1}{n}\sum_{i=1}^{n} \left|\hat{Z}(s_i) - z(s_i)\right| \quad \textbf{(5.17)}$$

The smaller the measurement error, the better is the model. In addition to these error measurements, Cross-Validation also delivers the Standardized Root Mean Square, which should be close to 1 to have a valid standard estimation error. A value greater than 1 indicates that the model is underestimating the variable to be predicted; vice versa, the model overestimates the variable.

$$\mathrm{RMSE} = \sqrt{\sum_{i=1}^{n} \frac{\left(\hat{Z}(s_i) - z(s_i)\right)^2}{n}} \quad \textbf{(5.18)}$$

The percent Bias represent the difference between the average values up or down from the observed values. The closer the PBIAS value is to zero, the smaller the bias between the predicted and observed values; therefore, the model describes the data

better. Overestimation occurs when the PBIAS value exceeds 0.0, and Underestimation occurs when the PBIAS value is less than 0.0. (Sorooshian, Duan et al. 1993).

$$BIAS(\%) = \frac{\sum_{i=1}^{n}(Q_{mod,i} - Q_{obs,i})}{\sum_{i=1}^{n} Q_{obs,i}} * 100 \quad \textbf{(5.19)}$$

The **Nash–Sutcliffe Efficiency coefficient (NSE)** was used to assess the forecast power model's quality (Nash and Sutcliffe 1970). The model would be better for forecasting if the value of NSE is closer to 1.

$$NSE = 1 - \frac{\sum_{i=1}^{n}(Q_{obs,i} - Q_{mod,i})^2}{\sum_{i=1}^{n}(Q_{obs,i} - \bar{Q}_{obs})^2} \quad \textbf{(5.20)}$$

In this chapter, different geostatistical and deterministic interpolation methods, including EBK, OK, OCK, DK and IDW, are used to estimate the spatial distribution of climatological variables (Precipitation and monthly mean temperature) in the Campania region of southern Italy. Several performance measures such as Nash-Sutcliffe efficiency criterion (NSE), standard deviation, MAE, RMSE, correlation coefficient, and percent bias are used to provide the accuracy of the interpolator that predicts the observed data accurately. Lower values of Stdev, MAE, RMSE and Bias with higher NSE value of an interpolator indicate better prediction by the corresponding method. Furthermore, according to (Kumar Adhikary, Muttil et al. 2016), if all the distributed points in the scatterplot are close to the 45° line with the highest correlation value between the expected and observed values, it represents a better prediction.

5.3.2.1 Rainfall spatial interpolation

Table 5.1 represents the different performance measures of the interpolation methods applied for monthly precipitation estimation over the study area. The different interpolation methods are compared in terms of performance to select the best interpolator for the study area. As can be seen in Table 5.1, the geostatistical interpolation methods (OK, OCK, DK, and EBK) perform better than the deterministic method (IDW) for estimating monthly climate data over the study area.

Table 5.1: Performance of different interpolation (IDW, OK, DK, OCK, and EBK) methods for monthly rainfall and temperature estimation in the study area

	Jan	Feb	Mar	Apr	May	Jun	Jul	Aug	Sep	Oct	Nov	Dec
	IDW											
NSE	0.53	0.48	0.47	0.50	0.58	0.69	0.58	0.26	0.45	0.59	0.48	0.47
StDev	28.3	22.8	19.7	17.6	14.3	10.8	7.6	6.5	11.2	23.4	28.8	31.3
MAE	19.53	18.34	15.33	13.64	10.07	5.70	4.61	6.10	9.52	15.43	22.98	24.68
RMSE	25.54	22.98	19.57	17.31	12.69	7.62	6.23	7.75	12.11	20.47	29.65	31.78
CC	0.73	0.70	0.69	0.71	0.76	0.83	0.76	0.54	0.67	0.77	0.70	0.69
PBIAS	1.93	1.89	1.74	1.46	1.52	1.42	0.57	1.92	1.51	1.63	1.92	2.11
	OK											
NSE	0.59	0.57	0.55	0.57	0.67	0.76	0.64	0.39	0.51	0.65	0.55	0.55
StDev	29.1	23.8	19.3	18.5	15.8	11.3	7.7	5.5	11.4	25.2	29.1	32.3
MAE	18.16	16.67	14.28	12.73	8.88	5.00	4.18	5.48	8.85	13.97	20.90	22.53
RMSE	23.66	20.94	18.01	16.08	11.18	6.69	5.81	7.05	11.42	18.73	27.69	29.27
CC	0.77	0.75	0.74	0.75	0.82	0.87	0.80	0.62	0.71	0.81	0.74	0.74
PBIAS	0.42	0.35	0.54	0.22	-0.14	-0.20	0.20	0.47	0.45	0.23	0.54	0.55
	OCK											
NSE	0.55	0.59	0.56	0.63	0.73	0.80	0.66	0.39	0.47	0.60	0.54	0.55
StDev	25.2	22.6	18.4	17.9	15.9	11.7	7.8	5.5	10.8	24.3	24.8	27.8
MAE	19.22	16.40	14.16	11.87	8.03	4.50	3.96	5.44	9.20	14.64	21.68	23.34
RMSE	24.80	20.50	17.84	14.88	10.18	6.03	5.60	7.02	11.89	20.06	27.90	29.42
CC	0.75	0.77	0.75	0.80	0.86	0.90	0.81	0.62	0.68	0.78	0.75	0.75
PBIAS	0.02	0.46	0.52	0.86	0.43	0.66	0.52	0.60	0.37	0.27	0.22	0.47

	DK											
NSE	0.58	0.59	0.58	0.62	0.72	0.80	0.63	0.38	0.48	0.61	0.54	0.57
StDev	28.3	23.4	19.6	17.7	15.2	11.6	7.4	5.7	11.4	25.2	28.8	30.7
MAE	18.44	16.28	13.67	11.89	8.04	4.48	4.17	5.45	9.13	14.66	21.04	22.25
RMSE	24.03	20.50	17.46	15.02	10.33	6.07	5.87	7.08	11.67	19.87	27.73	28.86
CC	0.76	0.77	0.76	0.79	0.85	0.90	0.79	0.62	0.70	0.78	0.74	0.75
PBIAS	0.65	0.51	0.53	0.46	0.33	0.40	0.27	0.65	0.35	0.19	0.55	0.61
	EBK											
NSE	0.57	0.54	0.53	0.53	0.64	0.74	0.63	0.38	0.48	0.63	0.52	0.52
StDev	29.7	23.8	19.4	18.4	15.9	12.1	8.0	5.2	10.8	24.9	29.0	31.6
MAE	18.68	17.22	14.40	13.09	9.06	5.09	4.31	5.58	9.16	14.16	21.56	23.21
RMSE	24.49	21.73	18.37	16.68	11.72	6.93	5.89	7.09	11.69	19.33	28.41	30.25
CC	0.75	0.73	0.73	0.73	0.80	0.86	0.79	0.62	0.69	0.79	0.72	0.72
PBIAS	0.51	0.28	0.19	0.20	0.03	-0.04	0.19	0.66	0.37	0.02	0.44	0.52

The OCK method provides the best results for the estimation of precipitation in the study area for all months considering all performance measures, especially in terms of variance (Figure 5.3) which is an important approach in geostatistical analysis (Guastaldi, Carloni et al. 2014). The DK method gives the second-best results, which are much more similar to the performance of the OCK method, but it is better than the OK method for estimating monthly precipitation and temperature over the study area, where IDW gives almost similar performance with a higher error in the precipitation estimation.

For IDW, EBK,OK,DK and OCK methods, the average NSE values for precipitation (Table 5.1) in the Campania region are 51,56,58,59, and 59% , respectively, whereas the average RMSE values are 17.81,16.88,16.38,16.21, and 16.34, respectively, and the average values of the mean absolute errors are 13.83,12.96,12.64,12.46 and 12.70 mm respectively.

For IDW, EBK, OK, DK and OCK methods, the average Correlation (CC) are 0.71, 0.75, 0.76, 0.77 and 0.77 respectively, whereas the average Bias values are

1.63,0.28,0.30,0.46 and 0.45. In addition, Figure 5.2 shows the results obtained by the analtsis carried out of the years 2009 and 2010. IDW appears to be the least reliable interpolation method as it gives the highest errors, as well as higher standard deviation and variance than the other methods. Ordinary Kriging and Ordinary CoKriging provide comparable mean error and RMSE values. However, it is evident that spherical CoKriging is preferable because it provides the lowest maximum prediction error, lower standard deviation, and most importantly, significantly smaller data variance. Therefore, it was decided to focus on Ordinary CoKriging (spherical model) for geostatistical analysis after these two applications.

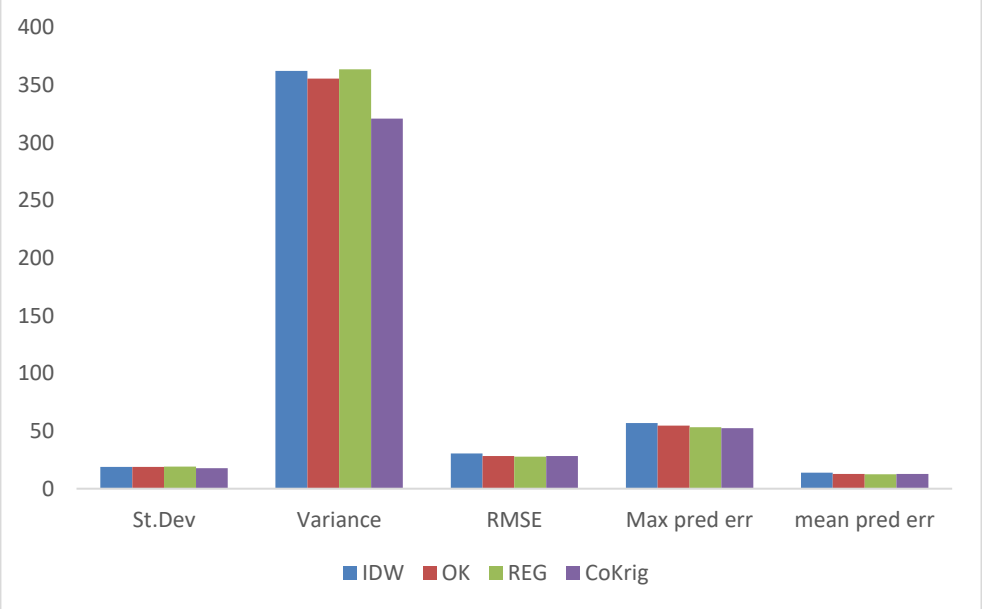

Figure 5.2: IDW, OCK and OK Comparison Test Results for spherical model

Moreover, in terms of variance, Figure shows that the ordinary cokriging present less variance than other interpolation methods, while in the summer period all models show a similar variance. This due to the lower scattered data

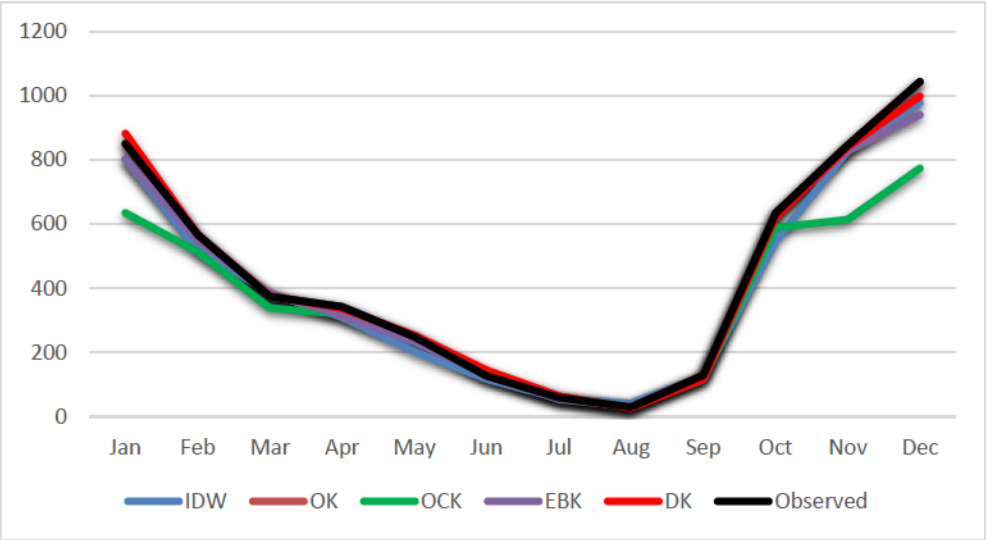

Figure 5.3: Variance of interpolated and observed values across the average months.

In the OCK and DK methods, the higher CC score implies that using elevation as a secondary variable brings more data under the kriging-based geostatistical analysis system in the rainfall estimation process. In addition, the Ok method is the one that most often reports a smaller maximum prediction error than the others, while the others report an average error of the same order of magnitude, which was confirmed earlier by the strong correlation between the predicted and observed values for the other methods.

5.3.2.2 Temperature spatial interpolation

As mentioned in section 5.3, the same methodology has been applied for the spatial prediction of the temperature. The two methods considered for spatial interpolation were Ordinary Kriging, which considers only the spatial variability of the temperature data, and Ordinary Cokriging, which on the other hand gives the possibility to use as auxiliary variable the elevation at which the thermometric stations providing the observations are located.

A further distinction was the choice of the model to be used for the definition of the semi variogram and therefore of the spatial autocorrelation of the data. To this purpose, two models that could best fit the case study were compared: the exponential model and the spherical model. To carry out the choice of the optimal model, two years were selected from the database (2009 and 2010) and, on the monthly averages, the Cross Validation results were performed. Cross Validation is a statistical technique used to evaluate the ability of a model to make the required predictions. Cross Validation results on monthly mean temperatures are shown in Figures 5.4 and 5.5. In particular it is evident that CoKriging always provides better results than Ordinary Kriging, regardless of the model used to describe the semivariogram. The standard deviation of the values predicted by the CoKriging method tends to be closer to the standard deviation of the observed values, compared to what is obtained by performing Kriging. In addition, the error parameters are significantly smaller using the CoKriging method, with respect to the mean error which is more or less similar for both methods.

Figure 5.4 Cross validation results on Monthly Mean Temperature for the year 2009

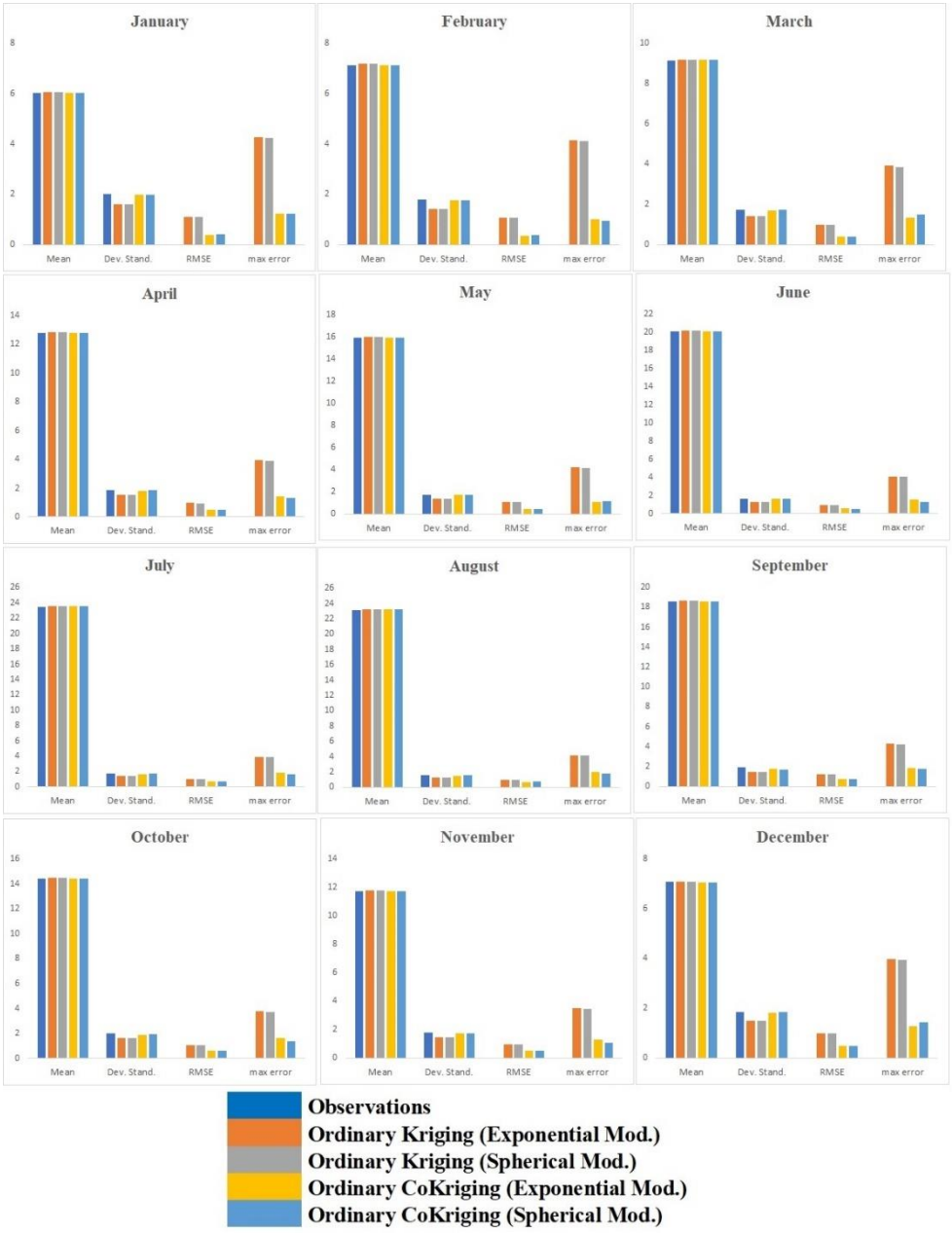

Figure 5.5: Cross validation results on Monthly Mean Temperature for the year 2010

The same gap is not found for the choice of function to model the semivariogram. It was not possible to find a dominant model between the exponential and the spherical, as far as monthly averages are concerned. For this reason, the same test was carried out on the long-term annual mean temperatures (Figure 5.6): in this scenario, it is evident that the exponential model gives better results in terms of error. Although the tests were carried out only on a small sample of data, these were sufficient to choose the Ordinary Cokriging method and the exponential model, used for the subsequent spatial interpolations.

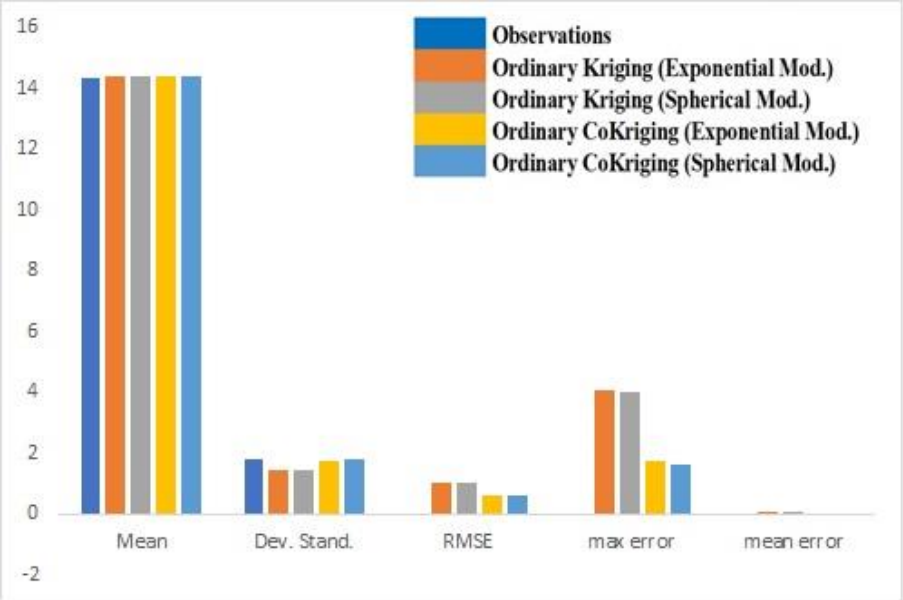

Figure 5.6: Cross validation results for the Mean Temperature

5.3.2.3 Variograms temporal pattern

The geostatistical analysis of climatological data (e.g., precipitation, temperature) requires the estimation of direct variogram models. In this analysis, an isotropic experimental variogram was calculated for each month using both rainfall

and temperature data, assuming equal spatial correlation in all directions and avoiding the effect of anisotropy on variogram parameters. Isotropy is a natural occurrence or data property in which directional influence is considered negligible and spatial dependence (autocorrelation) only varies with distance between two points (Johnston, Ver Hoef et al. 2001). Under the isotropic condition, the semi-variance is assumed to be the same for a given distance regardless of direction.

Firstly, directional experimental variograms are computed from each monthly rainfall dataset. Instead, the directional variograms are found to be noisy due to the lower number of gauge stations in the region under investigation. The directional effect is therefore neglected in the estimation of the experimental variogram. Furthermore, prior to modelling, problems in geostatistical data analysis such as non-normality, pattern, seasonality, and outlier behaviour must be resolved.

In this study, a statistical analysis of historical variogram parameters (Nugget, sill and range) times series using the Mann-Kendall and the Pettitt tests was performed for more realistic estimation. The values of the following analyzed variables are derived from the parameters of each variogram model fitted on experimental semi-variograms of either precipitation or temperature, excluding the main outliers found in each time series from 1918 to 2019 (Precipitation) and 1924 to 2019 (Temperature).

- Nugget_no_out: the nugget effect value, without outliers
- Sill_no_out: partial sill value of spherical structure, without outliers
- Range_no_out: range, without outliers
- Ratio_no_out: ratio between nugget effect and partial sill of spherical model, without outliers.

Table 5.2 represents statistical summary of parameters of precipitation variogram without outliers. It includes measures of mean, median, skewness,

variance, standard deviation, kurtosis as well as minimum and maximum values. The skewness has all positive values between 1.78 and 2.59 which represents that 90% of the values for each parameter are rightly skewed. Higher values of kurtosis also represent that the graph is heavily tailed towards right (Figure 5.7). This means that greater portion of the values fall under 2000 m. In figure 5.7., we plot histograms for each precipitation variogram parameter and found that this represents an asymmetric distribution with which is also proved by high skewness and kurtosis values.

Table 5.2: statistical summary of parameters of precipitation variograms' model without outliers

	Nugget no_out [mm2]	Partial_Sill no_out[mm2]	Range no_out[m]	Ratio_no_out
Min.	0	0	0	0
1st Qu.	66.53	265.8	18170	0.1427
Median	291.4	745.5	29260	0.51
Mean	622.6	1346	46280	0.7258
3rd Qu.	796.5	1812	57430	0.726
Max.	4955	9877	221400	14.02
IQR	7.299.787	1546.05	392.582.807	0.5832
sd	8.627.825	16.279.959	441.465.028	12.199
cv	13.858	12.091	0.9538	16.807
Skewness	2.332	21.503	20.173	57.758
Kurtosis	59.703	53.243	41.565	464.169
Observations	1236	1236	1236	1236
Outlier threshold	5000	10000	230000	20
No. of outliers	21	13	1	85

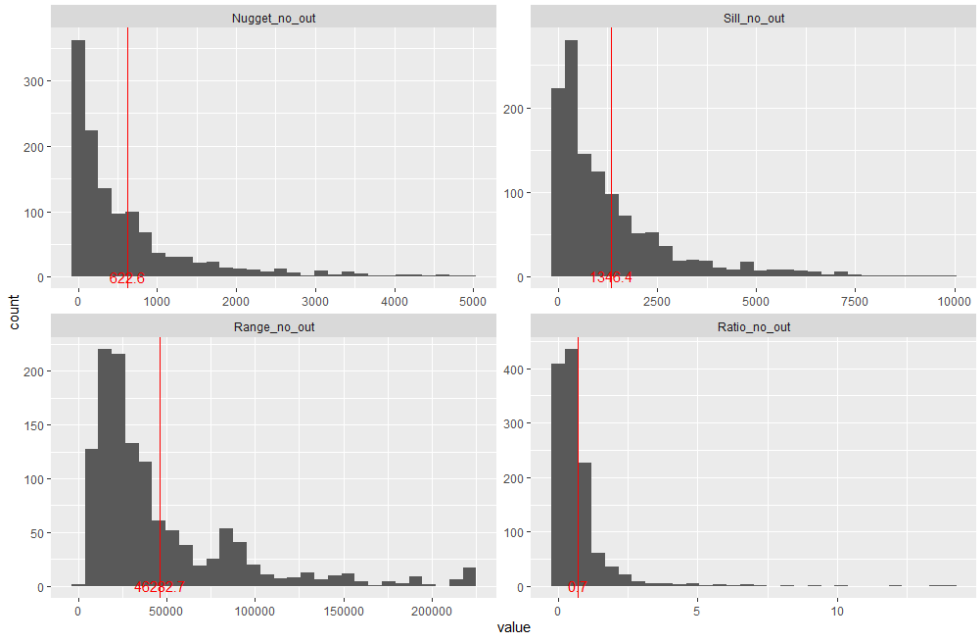

Figure 5.7: Frequency distribution of Precipitation variograms' parameters without outliers with mean values (red lines)

By Creating the Precipitation time series, the numeric vectors of variograms' parameters were converted into R time series objects, starting and ending each series by the first and last observation (from 1918 to 2020) with a monthly frequency (Figure 5.8). These graphs clearly depict that nugget and range represents tendency whereas, sill shows no tendency that means the amplitude does not vary or has no effect throughout the whole period. This is also proved by the Mann-Kandall and the Pettitt's test as shown in Table 5.3.

Table 5.3: statistical summary of the Mann-Kendall and Pettitt's test

	Mann Kendall			Pettitt's Test
	z	**n**	**p_value**	**Break Point**

Nugget	-6.33	1236	2.34E-10	**1999**
Sill	0.76	1236	0.45	**2003**
Range	-6.10	1236	0.00	**1997**

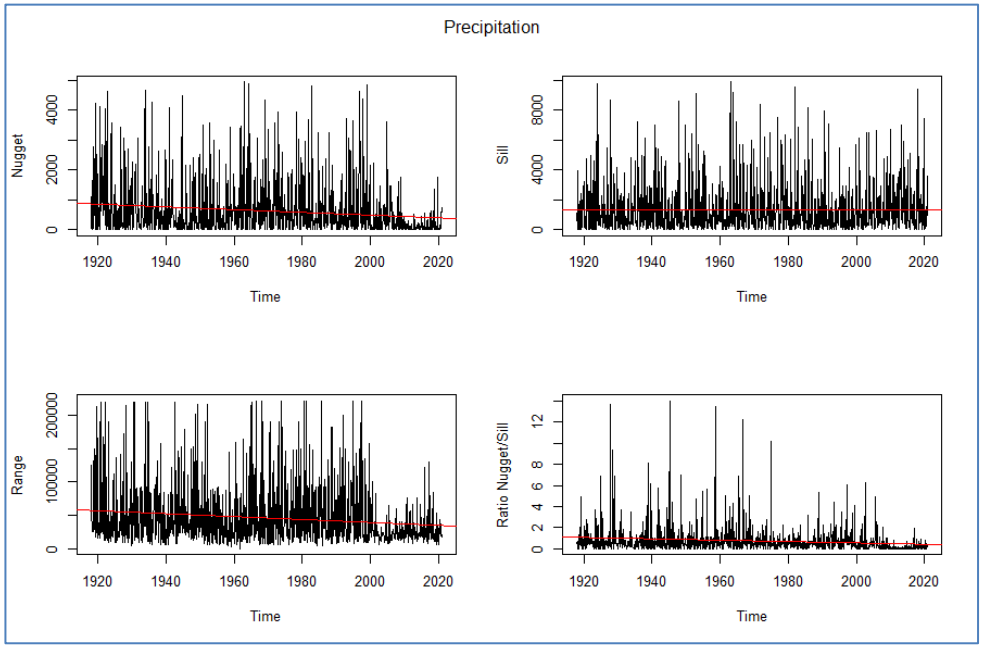

Figure 5.8: Time series plots of Precipitation variograms' parameters (no outliers) from 1918 to 2020 fitted by linear regression models (red line)

Cycle calculating across the years and cycle aggregating could highlight a year-on-year trend (Figure 5.9), that clearly describes that variogram's parameters acquire negative tendency from year 2000 which is due to the change of meteorological agencies in the region aforementioned in introduction, while the box plot across months could provide a sense on seasonal effect (Figure 5..A). Seasonal trends seem to be present in all model parameters, in particular the spatial variability components (nugget and partial sill) are less variable in summer months on average, while the range values tend to be more variable from July to October. These

behaviors could be highlighted also by plotting the month subseries for each variograms' parameters time series (Figure 5.10.B).

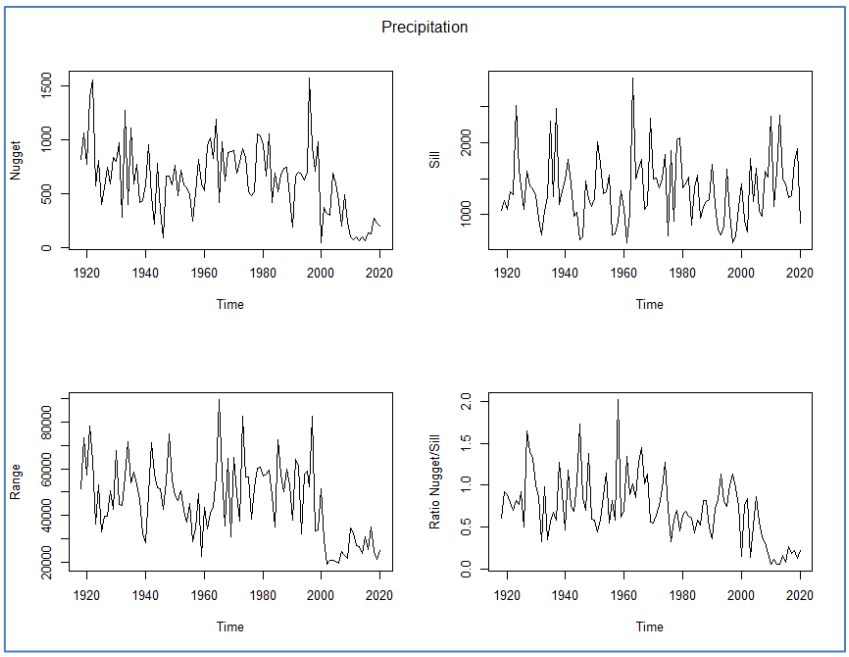

Figure 5.9: Aggregation of cycles of Precipitation variograms' parameters without outliers across the years

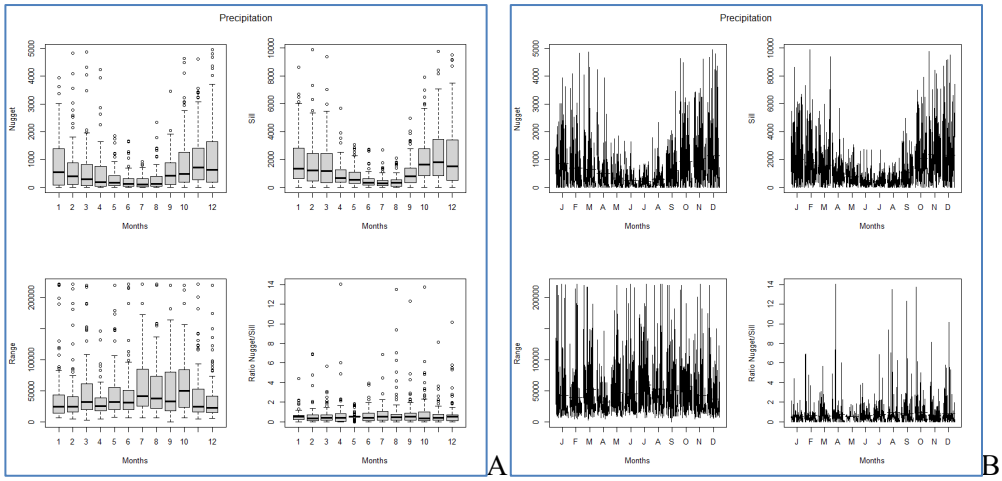

A B

Figure 5.10: Box plots (A) and month subseries (B) of Precipitation variograms' parameters without outliers across the months

In other hand, the same analysis was carried out for the temperature variogram's parameters where Outliers were removed from data. Table 5.4 represents statistical summary of parameters of temperature variogram without outliers. It includes measures of mean, median, skewness, variance, standard deviation, kurtosis as well as minimum and maximum values. The skewness has all positive values between such that nugget shows asymmetric distribution while sill and range depict symmetric distribution which means that sill and range are varying uniformly for temperature. Higher value of kurtosis for nugget represents that it is heavily tailed towards right whereas lower kurtosis value for sill and range represents the normal distribution (Figure 5.11).

Table 5.4: statistical summary of parameters of temperature variograms' model without outliers

	Nugget no_out [C°]	Partial_Sill no_out[C°]	Range no_out[m]	Ratio_no_out
Min.	0	0	22270	0
1st Qu.	0	3.63	43020	0
Median	0.235	7.565	58150	0.03
Mean	1.774	7.624	67530	0.3197
3rd Qu.	0.8525	9.542	88060	0.12
Max.	28.89	29.16	187100	16.63
IQR	0.8525	59.125	450.423.225	0.12
sd	43.262	50.994	31.602.176	14.084
cv	24.382	0.6689	0.468	4.405
Skewness	34.524	1.209	10.791	75.661
Kurtosis	125.074	23.502	12.249	654.136
Observations	1164	1164	1164	1164
Outlier threshold	30	30	180000	20000
No. of outliers	3	4	4	69

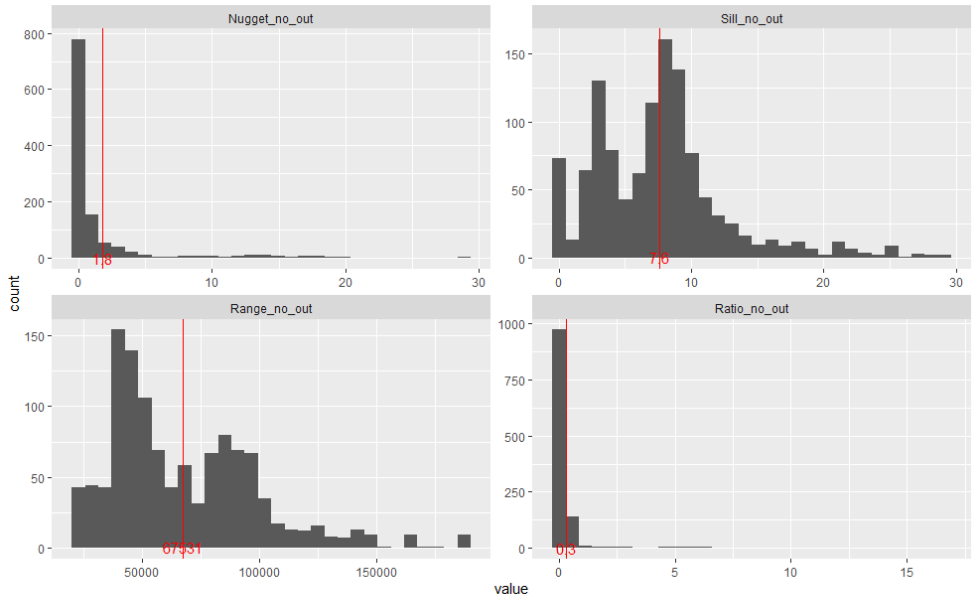

Figure 5.11: Frequency distribution of temperature variograms' parameters without outliers with mean values (red lines)

The numeric vectors of variograms' parameters were converted into R time series objects, starting and ending each series by the first and last observation (from 1924 to 2020) with a monthly frequency (Figure 5.11 and Table 5.4).

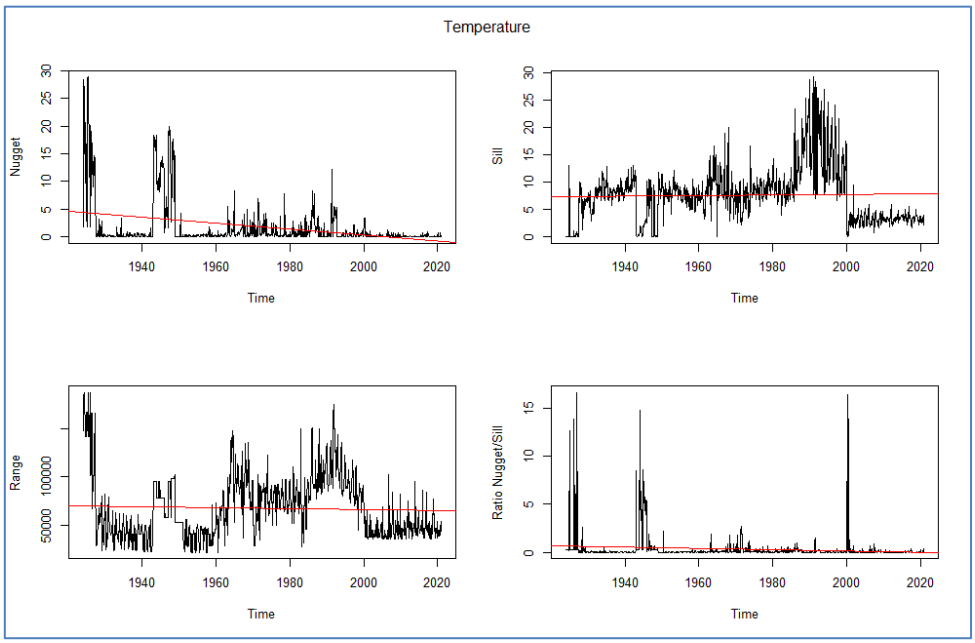

Figure 5.12: Time series plots of Temperature variograms' parameters (no outliers) from 1924 to 2020 fitted by linear regression models (red line)

Cycle calculating across the years and cycle aggregating could highlight a year-on-year trend (Figure 5.13) that clearly describes that variogram's parameters are greatly affected from 2000 due to the change of meteorological agencies, while the box plot across months could provide a sense on seasonal effect (Figure 5.14.A). In particular, Sill and Range monthly boxplots display a slight lower dispersion in spring and summer months (Figure 5.14.A). This could be highlighted also by plotting the month subseries for each variograms' parameters time series (Figure 5.14.B).

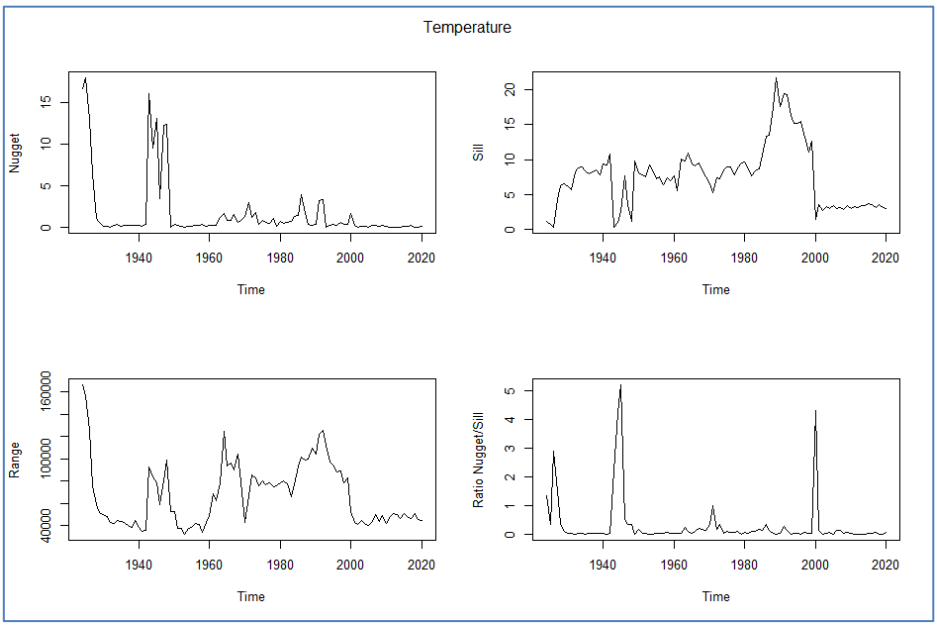

Figure 5.13: Aggregation of cycles of Temperature variograms' parameters without outliers across the years

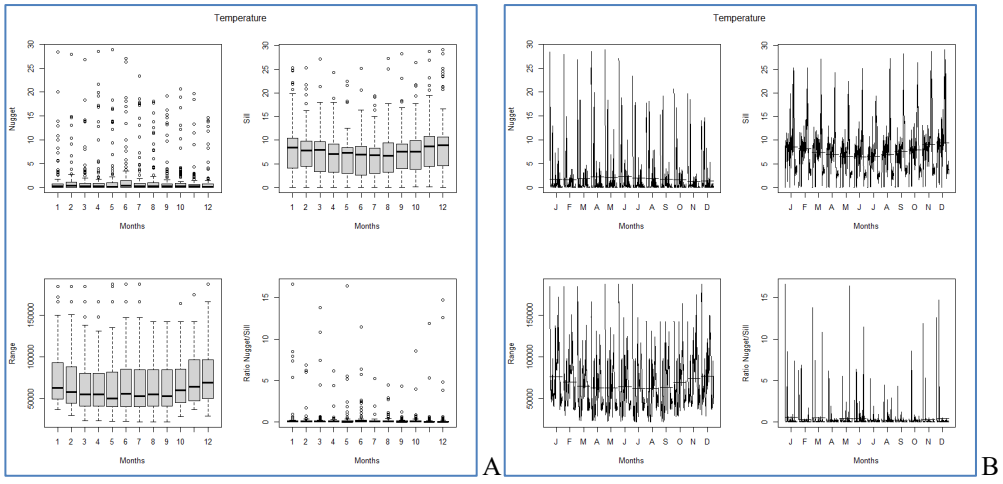

Figure 5.14: Box plots (A) and month subseries (B) of Temperature variograms' parameters without outliers across the months

Finally, by analyzing the ratio nugget to sell which indicates the spatial dependency of variables, There are three classifications used for model explanation: If the ratio is less than 25 %, it shows strong spatial dependence; if the ratio is in between 25 and 75 %, it indicates moderate spatial dependence; and if the ratio is more than 75 %, it represents weak spatial dependence, according to this it could be concluded that rainfall show a moderate spatial dependency while, it was not the case for temperature data where the ratio is less than 25% which mean a strong spatial dependency between samples.

5.3.3 From point data to grid data

After determining the most suitable geostatistical interpolator for the case study, we proceeded to the actual merging of the two databases. Given the different spatial and temporal consistency of the two historical series, it was deemed necessary to standardize them, moving from a set gauge station data to a grid-based representation. Therefore, beyond the ArcGIS 10.8 software and applying the Ordinary Cokriging method, prediction surfaces have been generated, starting from the monthly average rainfall and temperatures previously estimated based on observations collected by S.I.M.N. and the Civil Protection Functional Centre. This allowed the reconstruction of all those points of the Campania Region where there were no measurements. The spatial interpolation operation was performed again for all the months; 102 years (1918-2019 for precipitation) and 96 years (1924-2019 for temperatures) for which observations were available, for a total of 1224 and 1152 spatial interpolations for precipitation and temperature data respectively. The area obtained in ArcGIS through spatial interpolation is typically contained within a Geostatistical Layer, showing a fairly uniform area of predictions. In order to move to a grid representation, it was necessary to export the GALayers into Rasters. In

fact, a Raster is defined as an image composed of a grid with square meshes (pixels). For the case study in object, it was considered suitable to operate on a grid with meshes of 10 km2. In fact, while rain may be seen as a more localized meteorological phenomenon, the spatial distribution of climate variables covers larger areas; and having to subsequently put together the gridded data of rain and temperature for the calculation of different drought indicator that will be highlighted in the next chapter, a grid of 10 km^2 was the right compromise for both meteorological variable, a resolution of this type was appropriate for the meteorological phenomenon because it is a localized event (Molnar et al.,2000). Hence, when exporting to rasters, a cell size of 10,000 meters was set. Thus, the value assigned to each cell of the Raster in the output was nothing more than the average of all forecasts within that cell. In Figure 5.15, it is possible to observe both an example of the forecast surface resulting from the spatial interpolation and an example of the Raster.

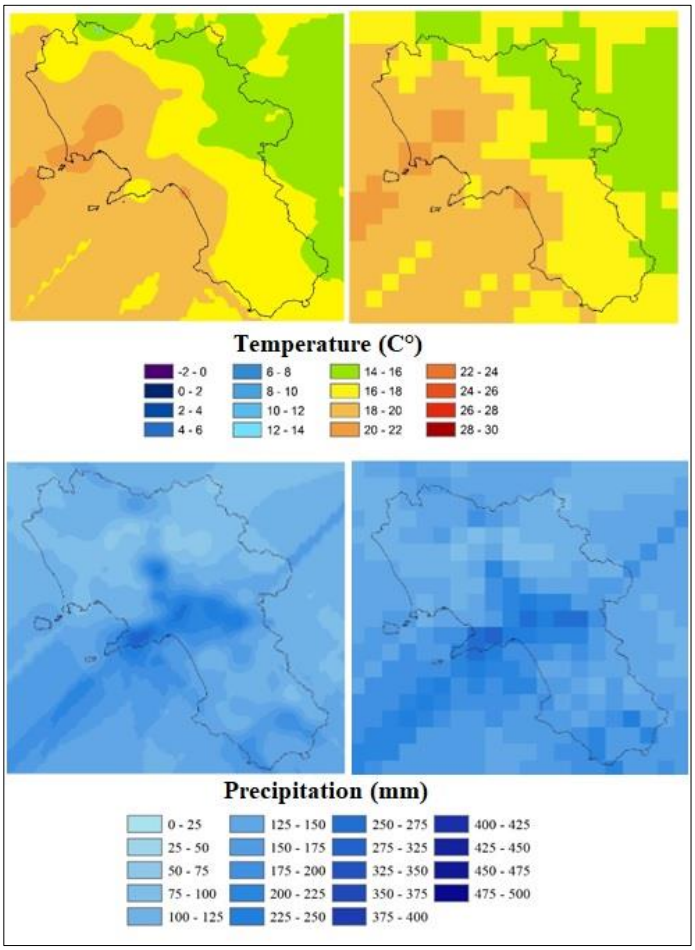

Figure 5.15: Sample of spatial interpolation and transformation to Raster

Finally, the shapefile of a grid (fishnet) was created to cover only the areas of interest in the Campania Region. This process was needed only to be able, after the creation of all the Rasters, to project the values of each pixel on the grid mesh barycentric points. This has allowed the extraction of data in Excel and the subsequent calculation of the drought indicators. As represented in Figure 5.16, the grid was made of 191 cells of 10x10 km.

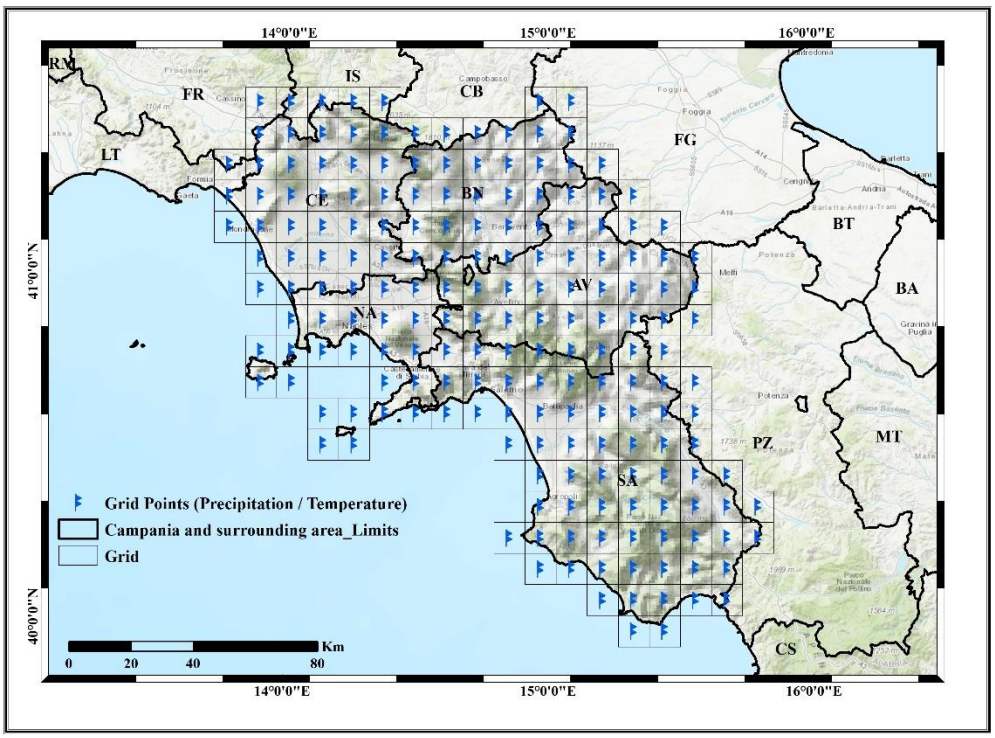

Figure 5.16 Gridded point Rainfall and temperature measurement in the Campania region

5.4 ERA5 versus Gridded datasets results

The most advanced global reanalysis data produced in Europe by ECMWF (ERA5 single levels (Hersbach et al., 2020)), was used in this study. Table 5.5 summarizes the main technical details of these reanalysis datasets.

Table 5.5. Main technical details of the reanalysis datasets used in this study.

Reanalysis dataset characteristics	ERA5
Data type	Gridded
Projection	Regular latitude-longitude grid
Horizontal coverage	Global
Horizontal resolution (atmosphere)	0.25° x 0.25°
Temporal coverage	1979 to present
Temporal resolution	Monthly

The ERA5 dataset is the fifth generation of ECMWF global reanalysis, succeeding ERA-Interim and covering the entire globe from 1979 to the present at a spatial resolution of approximately 30 km. By replaying the land component of the ERA5 climate reanalysis from 1981 to 2-3 months before the present, the ERA5-L dataset is generated for the entire globe with a native horizontal resolution of about 9 km (released on a regular 0.1 x 0.1 grid).

The ERA5 datasets were compared in the current thesis with the gridded datasets resulted above (precipitation and Temperature).

During the period 1979-2019, all of the gridded data sets were significantly positively correlated with ERA5 extracted datasets ($p < 0.01$). (Table 5.6).

Table 5.6. Evaluation results of the gridded datasets and the ERA5 monthly scales during 1979–2019

	RMSE	Pearson correlation	BIAS (%)
Precipitation	52,63	0,96	-0,94
Temperature	0,83	0,99	3,93

For monthly precipitation, gridded datasets showed a strong correlation with ERA5 precipitation (CC = 0.96) and the lowest underestimation (Bias = 0.94%), indicating higher accuracy measurements; however, a high root mean square error (RMSE = 52.63) was recorded. Temperature had a stronger correlation within ERA5 datasets (CC = 0.99) than precipitation, despite having a higher overestimation (Bias = 3.93%) and a lower root mean square error (RMSE=0.83). Indeed, the monthly precipitation and temperature scatterplots show that the resulting gridded datasets have high measurement accuracy (Figure 5.17).

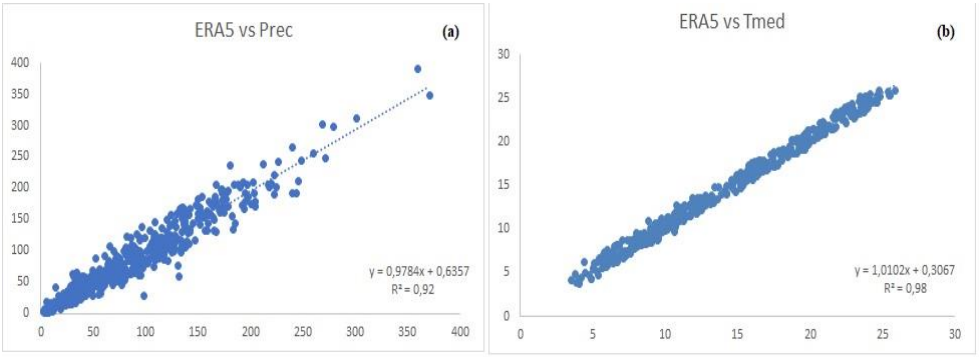

Figure 5.17. Scatterplots of monthly precipitation and temperature versus EA5 datasets: (a) ERA5 versus gridded precipitation (b) ERA5 versus gridded temperature during 1979–2019.

5.5 Overall evaluation

When choosing a spatial interpolation process, range, variance, and input data values are all essential performance metrics to be considered. The choice of a spatial interpolation technique is determined by many variable characteristics (range, variance, and relationship with other variables) (Collins and Bolstad 1996). These findings confirm (Kumar Adhikary, Muttil, et al. 2016) conclusions, that the data density, data measurement accuracy, data distribution, and spatial uncertainty have a significant influence on interpolation accuracy. Since IDW is an absolute interpolator, it provides a rough surface when the input data is highly variable. The created surface passes through the value at each gauge station, which captures local gradients but can result in absurdly steep gradients in areas with low network density, such as the south of the study area. In addition, IDW interpolation is readily influenced by disproportionate distributions of observational data points when each point is given the same weight even though it is in a cluster, which explains why the estimates for the boundary areas are less reliable. There were substantial differences in MAE and RMSE between IDW and other interpolators (Table 5.1), it was more likely to yield skewed estimates. Moreover, the IDW performs especially poorly for datasets with sudden shifts over short distances, whereas projected rainfall and temperature are declining for mountainous areas along the coast, this finding does not recommend the interpolator in the case of spaced data and complex orography. In station-sparse areas, IDW provided inaccurate results, as did most alternate smoothing techniques, such as predicting negative values of the variable in term of precipitation, which were usually rewritten to zero to prevent doubtful results.

In comparison to IDW, kriging is a somewhat more advanced interpolation strategy that specifically accounts for spatial variation and has a clear propensity to give lower RMSE, MAE, and PBIAS values. (Di Piazza et al. 2011) concluded that

Kriging was found to be superior to other traditional interpolation strategies such as RBF and IDW, which is consistent with the findings of this research. The differences in RMSE, MAE, and PBIAS between ordinary and empirical Bayesian kriging were small overall, but the Bayesian method had higher errors and less overlapping between observed and predicted values. One advantage of kriging is that it produces measurement errors that can be used to calculate interpolation uncertainty. This error information is very useful in analysing the efficiency of each function in the kriged map because it represents the density and distribution of control points as well as the degree of spatial similarity within the layer. The error map can also be used to decide where further detail is required, allowing further sampling to be prepared if needed. The advantage of using elevation as a covariate coincides with the findings of (Kumar Adhikary et al. 2016) and (Pellicone et al. 2019), who demonstrated that cokriging generated estimates with greater ‘precision' than kriging. Furthermore, cokriging and detrended kriging tend to reflect rainfall patterns more accurately in mountainous areas. Both approaches are the most time-consuming interpolation techniques since they involve fitting two semi-variograms and one semi-cross variogram for each sample, but they were the chosen technique in this study due to the high precision needed.

Both variance analysis and statistical comparisons showed that cokriging was more likely to have the best estimate of a continuous surface for temporal rainfall and temperature precision with less variance in the kriged map than detrended kriging, which generates a significant variance in the predicted map. When interpolating rainfall / temperature data, only elevation was viewed as a covariate, but other variables (e.g., distance to the coastline) would influence the variable conditions. Slope and aspect knowledge may be derived from the same digital elevation model used to calculate average altitude around meteorological stations and used as additional covariates to potentially boost rainfall prediction.

Therefore, after these analyses, it was decided to focus on the Ordinary Cokriging for the geostatistical analysis. Hence, the OCK method (the best interpolator) is used to produce a continuous rainfall/temperature dataset of monthly average rainfall/temperature for the entire Campania region which is shown in figure 5.17 and figure 5.18, respectively. In another hand, all the resulted variograms from 1918 to 2020 were tested in terms of tendency using the Mann Kendall and Pettitt's test, the analysis confirms that the tendency in all variogram's parameters (sill, range, and nugget) has no relation with the rainfall variability but with the changes occurred in the measurement structure as can be seen by Table 5.2. All the breaks point were highlighted between 1999 and 2003. At this point, the cokriging interpolator is the preferred approach to construct historical rainfall data from 1918 to 2019 and temperature data from 1924 to 2019.

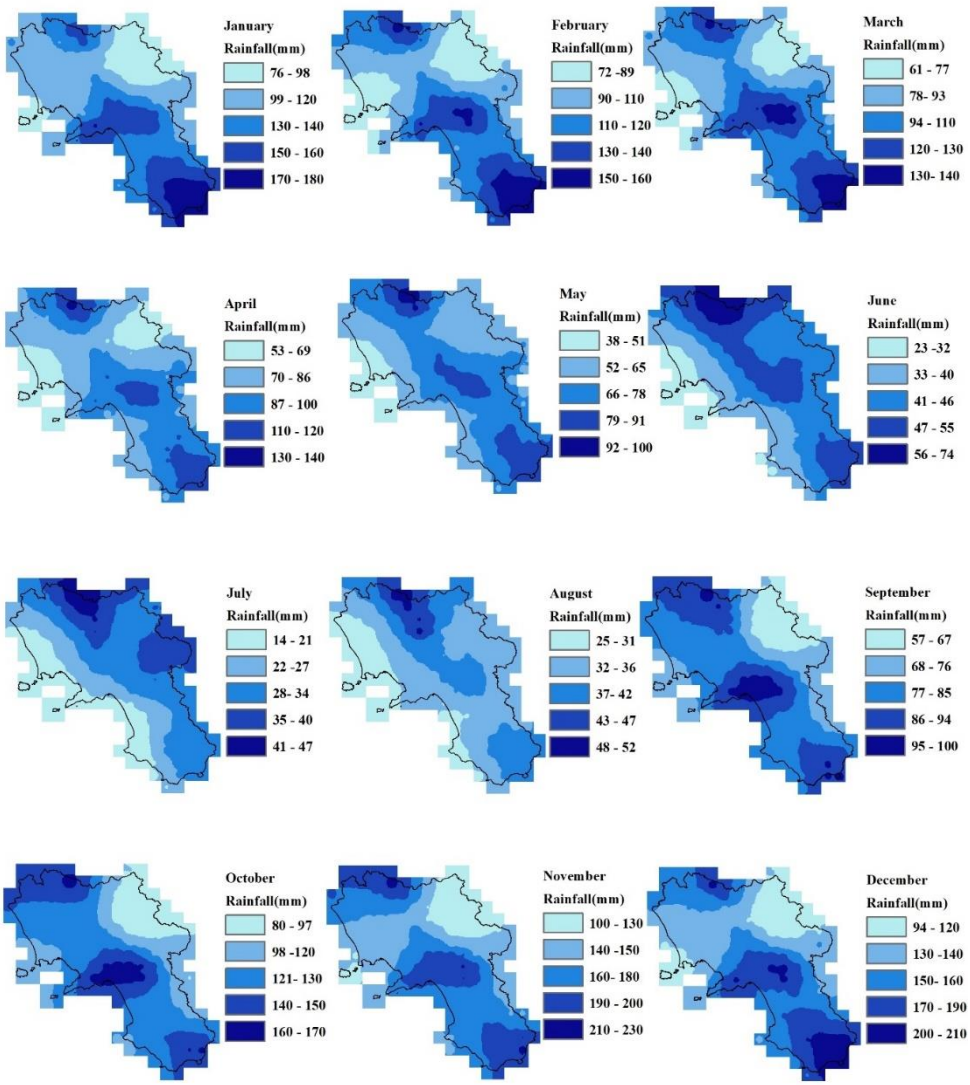

Figure 5.17 Spatial distribution of monthly rainfall in the Campania region using the ordinary cokriging (the best interpolator in this study) interpolation method

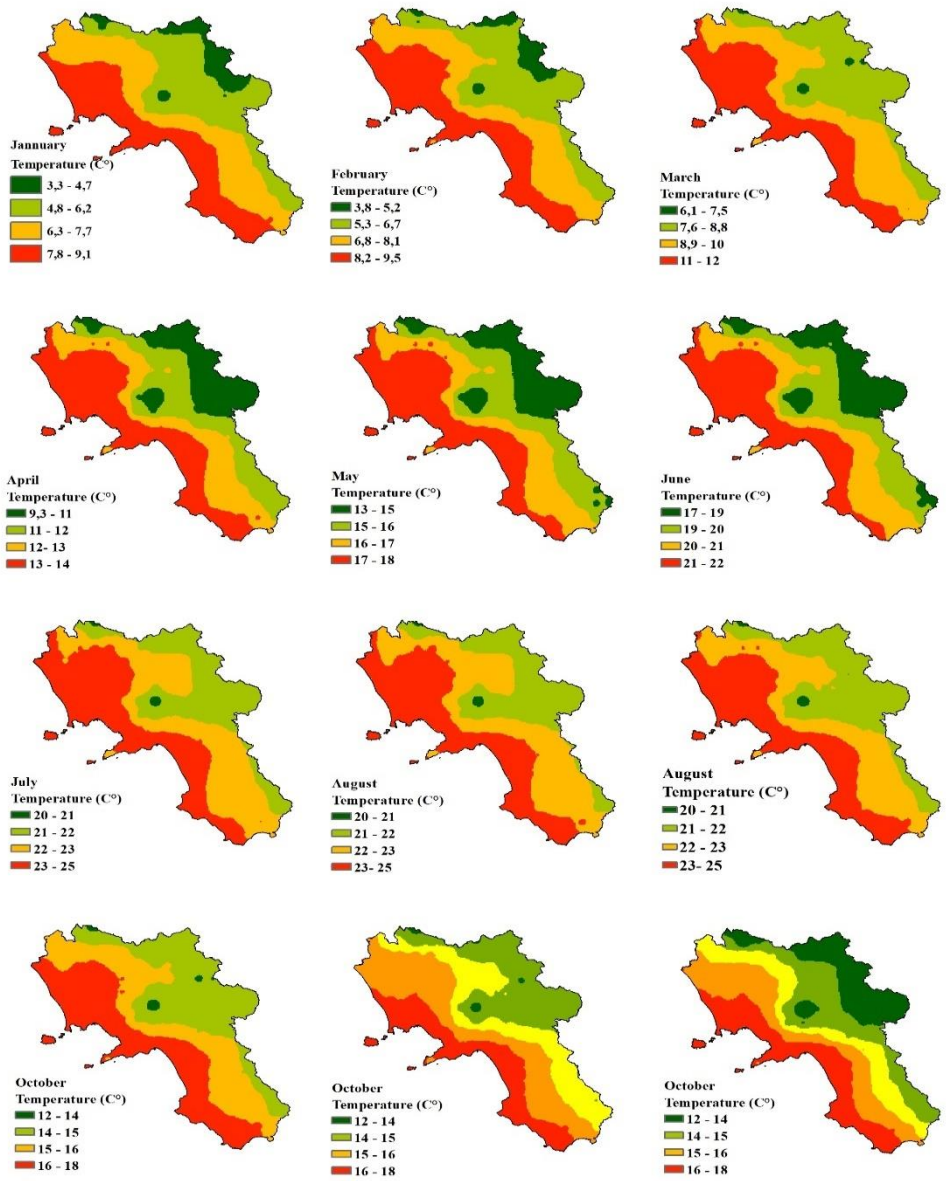

Figure 5.18 Spatial distribution of monthly temperature in the Campania region using the ordinary cokriging (the best interpolator in this study) interpolation method

5.6 Summary

In this study, the spatial distribution of monthly mean rainfall and temperature in the Campania region of southern Italy was estimated using four kriging-based geostatistical (EBK, OK, DK, and OCK) and one deterministic (IDW) interpolation method. The aim was to evaluate the results of these interpolation methods in order to select the best interpolation method for producing a high-quality continuous gridded rainfall/temperature dataset, initially not homogeneous, in the form of a rainfall/temperature chart at the regional scale. In addition to rainfall/temperature data, elevation data from a DEM of the study area is used as a secondary attribute in the cokriging analysis using the OCK and DK methods. The results show that geostatistical methods outperform deterministic methods for spatial interpolation of rainfall/temperature over a century in a morphologically complex region like Campania. The IDW approach produced the worst results for the sample field, whereas the cokriging methods (OCK and DK) performed better than other geostatistical methods. OCK outperformed all other interpolators by producing more reliable rainfall estimates for all monthly data over a century. OCK had the lowest prediction errors and uncertainty, as well as the highest correlations between predicted and measured monthly average rainfall/temperature. As a result, OCK emerged as the best interpolator in this study for estimating the spatial distribution of rainfall/temperature in the study area. The findings show that adding elevation as an auxiliary variable to rainfall/temperature data improves the variable prediction in mountainous areas with complex orography. As a result, the current study recommends using OCK to generate continuous climate variables maps, particularly in areas with high spatial variation in rainfall and elevation.

Chapter 6

EVALUATION OF SELECTED DROUGHT INDICES AND DROUGHT CONDITIONS

6.1 Overview

Drought indices are widely used all over the world to assess and quantify drought conditions. As discussed in Section 2.1, most drought indicators were developed for a specific region and may not be directly applicable to other regions due to the inherent complexity of the drought phenomenon, different hydro-climatic conditions, and different area characteristics (Redmond, 2002; Smakhtin and Hughes, 2007; Mishra and Singh, 2010). The suitability of some existing drought indicators for various climatic regions around the world has been investigated, with details available in Keyantash and Dracup (2002), Heim Jr (2002), Smakhtin and Hughes (2004), and Morid et al (2006). However, no such study had been conducted in the Campania region (southern Italy), which is known as the driest inhabited region in the Italian territory (Polemio and Casarano 2008).

(Polemio and Casarano 2008) stated that the 5-year average deviation has been continuously negative since 1983, they also noted a prevailing increasing trend in observed temperature in Campania region, in addition, their results show a slight prevalence of increasing trends in the Campania region where an increase of temperature starting from about 1980 were observed. Longobardi and Villani (2010) noted that the trend in rainfall in the Campania region appears to be predominantly

negative, both on an annual and seasonal scale, with the exception of the summer period, when it appears to be positive; they also noted that over the entire period (1918-1999), positive and negative trends were significant for 9 and 27% of total stations, respectively, and over the last 30 years, a negative trend is significant for 97 % of total stations. Droughts are more prevalent in southern Italy than elsewhere in the Mediterranean basin, and they have become more frequent in the last 50 years, particularly in the south-eastern part of the country (Piccarreta, Capolongo et al. 2004, Capra, Scicolone et al. 2012, Buttafuoco, Caloiero et al. 2015). For these reasons, it is worthwhile to investigate the suitability of existing drought indicators for use in drought management in southern Italy; these drought indicators are primarily designed for use in other parts of the world.

This chapter's work is an important component of a current research project aimed at assessing drought conditions for water resource management in the Campania region. Water resource management in this area is critical to the Campanian community and the surrounding area, as described in Section 3.4.2. Selecting a suitable drought index to use in defining drought conditions in the Campania region is thus a critical issue for this project. The first step in this chapter was to evaluate two existing drought indicators based on water cycle components (rainfall, temperature, and evapotranspiration) from various drought perspectives (i.e., meteorological, hydrological, and agricultural). They were widely used rainfall-based drought indicators, namely, the standardized precipitation index (SPI) and the Standardized Precipitation Evapotranspiration Index (SPEI). In addition, and as a second part of the current chapter three existing drought indicators namely Normalized Difference Vegetation Index (NDVI), Enhanced Vegetation Index (EVI), and Normalized Difference Water Index (NDWI), based on remote sensing from the agricultural drought perspective were evaluated to study drought-related vegetation stress.

SPI has been used in Italian territory in the past, as mentioned in Section 2.2 (Capra, Scicolone et al. 2012, Brunetti, Maugeri et al. 2014, Bonaccorso, Cancelliere et al. 2015, Buttafuoco, Caloiero et al. 2015), but only a few studies used SPEI and other vegetation indices in Italy to date, except for a few studies carried out by (Bonaccorso and Cancelliere 2015, Colangelo, Camarero et al. 2017). This is one of the first studies in Italy to assess the suitability of existing drought indicators for drought management in a southern Italian area, using an in-situ measurement database comprising a centennial period from 1918 to 2019 and a historical database of vegetation indexes spanning a long period from 1984 to 2020. Section 2.2 discussed the qualitative assessment of the above-mentioned selected drought indicators. The current chapter aims to perform a quantitative assessment of these indicators for the Campania region. The chapter begins with a brief description of the study area and the data used in this study (detailed in Chapter 5), followed by the methodology used to develop the five drought indicators chosen. The indices are then analyzed and evaluated. The study's summary is provided at the end of the chapter.

6.2 Study Area and Data Used

The Campania region was used in this study. The details of the area and the importance of its water resources for Campanian people and surrounding areas were elaborated in Chapter 3. Three meteorological variables (i.e., rainfall, temperature, and potential evapotranspiration) which have effects on droughts were used in the evaluation of drought indicators. Measurement locations of these data were shown in Figure 5.15, and the data processing to obtain the monthly values as described in Chapter 5. Data from 1918 to 2019 (102 years) and from 1924 to 2019 (96 years)

were used in this study which was available from the previous chapter for all three variables.

6.3 Methodology Used for Evaluation of Drought Indices

6.3.1 Standardized Precipitation Index

The SPI drought index is computed for any given location using the cumulative rainfall record over a specified timescale and the probability density function "Gamma," which fits only positive and null values (McKee et al., 1993; Husak et al., 2007). According to previous studies and the literature, rainfall time series are first fitted to the Gamma distribution and then standardized by transformation into a normal distribution (Caloiero et al., 2018; Martinez et al., 2019; Stagge et al., 2015; Zhou and Liu, 2016). The following equation can be used to express the probability density function for the Gamma distribution:

$$g(x) = \frac{1}{\beta^{\alpha}\Gamma(\alpha)} x^{\alpha-1} e^{-x/\beta}$$

where α, β and x are respectively the shape parameter, the scale parameter and the amount of precipitation (α, β and x > 0). Γ(α) is the gamma function expressed as follows:

$$\Gamma(\alpha) = \int_0^{\infty} y^{\alpha-1} e^{-y}\ dy$$

Parameters $\hat{\alpha}$ and $\hat{\beta}$ are assessed through the maximum likelihood method (McKee et al., 1993; Liu et al., 2016):

$$\hat{\alpha} = \frac{1}{4A}\left(1 + \sqrt{1 + \frac{4A}{3}}\right) \quad \text{and} \quad \hat{\beta} = \frac{\hat{x}}{\hat{\alpha}}\ ,$$

Where: $A = ln(\bar{x}) - \frac{1}{n}\sum_n ln(x)$

for n observations. By integrating the density of probability function g(x), the cumulative probability G(x) is obtained:

$$G(x) = \int_0^x g(x)\,dx = \frac{1}{\hat{\beta}^{\hat{\alpha}}\Gamma(\hat{\alpha})}\int_0^x x^{\hat{\alpha}-1}e^{-x/\hat{\beta}}dx$$

Given that the Gamma distribution is not defined for x values equal to zero and that instead the cumulative rainfall series may contain null values, the cumulative distribution is re-defined as follows:

$$H(x) = q + (1 - q)\,G(x)$$

where q is the probability of zero precipitation. Then, the value of the SPI can be obtained through the approximation proposed in Abramowitz and Stegun (1964) which converts the cumulative distribution H(x) to a normal random variable Z:

$$Z = SPI = \begin{cases} -\left(t - \dfrac{c_0 + c_1 t + c_2 t^2}{1 + d_1 t + d_2 t^2 + d_3 t^3}\right) per\ 0 < H(x) \leq 0{,}5 \\ +\left(h - \dfrac{c_0 + c_1 h + c_2 h^2}{1 + d_1 t + d_2 t^2 + d_3 t^3}\right) per\ 0{,}5 < H(x) \leq 1 \end{cases}$$

$$t = \begin{cases} \sqrt{ln\left(\dfrac{1}{(H(x))^2}\right)} per\ 0 < H(x) \leq 0{,}5; \\ \sqrt{ln\left(\dfrac{1}{(1 - H(x))^2}\right)} per\ 0{,}5 < H(x) \leq 1 \end{cases}$$

Where: $c_0 = 2{,}515517$ $c_1 = 0{,}802853$

$d_1 = 1{,}432788$ $d_2 = 0{,}189269$

As discussed in Section 2.2.5, SPI values can be calculated for multiple monthly time scales of interest (e.g., 3-, 6-, 12-, 24-, and 48-month time scales). In this study,

however, SPI was calculated using a monthly time step. Table 6.1 displays the SPI threshold ranges used to define drought conditions (McKee et al., 1993).

Table 6.1: Drought classification based on SPI (McKee *et al.*, 1993)

2.00 or more	Extremely wet
1.50 to 1.99	Very wet
1.00 to 1.49	Moderately wet
0.99 to -0.99	Near normal
-1.00 to -1.49	Moderate drought
-1.50 to -1.99	Severe drought
-2.00 or less	Extreme drought

6.3.2 Standardized Precipitation Evapotranspiration Index

The SPEI, developed by Vicente-Serrano et al. (2010), has the advantage of considering the effects of temperature variability on drought in relative terms to the SPI (Naumann et al., 2014). The SPEI is calculated by subtracting precipitation from potential evapotranspiration (PET) and fitting the data to a log-logistic PDF.

In this section, we summarize the steps involved in calculating the SPEI using monthly precipitation and temperature data. Vicente Serrano et al. (2010) presented a detailed procedure for estimating the SPEI.

Step 1: Estimate the water surplus or deficit in month *j (Dj)* using the difference between precipitation *(P_j)* and potential evapotranspiration *(PET_j)*.

$D_j = P_j - PET_j$

The Thornthwaite (1948) method is used to calculate potential evapotranspiration, which requires the monthly temperature, latitude, day, and month.

Step 2: Calculate the cumulative difference ($X_{i,j}^{k}$) in a given month *j* and year *i* over a timescale *k*. For example, based on a 12-month timescale, the cumulative difference for a month in a particular year can be calculated as follows:

$$X_{i,j}^{k} = \sum_{l=13-k+j}^{12} D_{i-1,l} + \sum_{l=1}^{j} D_{i,j} \text{ if } j < k,$$

$$X_{i,j}^{k} = \sum_{l=j-k+1}^{j} D_{i,l}, \text{ if } j \geq k$$

Step 3: Fit the cumulative difference to a log-logistic distribution as follows:

$$F(X) = \left[1 + \left(\frac{\alpha}{x-\gamma}\right)^{\beta}\right]^{-1}$$

where F (X) is the cumulative probability function of a three-parameter log-logistic distribution and, and represent the scale, shape, and origin parameters. The L-moment procedure (Hosking, 1990) is used for model fitting because it is one of the most robust and simple approaches.

Step 4: Calculate the SPEI using the estimated F(X). The SPEI can be estimated using the standardized values of F(X) and the classical approximation of Abramowitz and Stegun (1964), as described by Vicente Serrano et al (2010). Table 6.2 shows the estimated drought index for moderate, extreme, and very extreme cases. In this study, we focused on the SPEI with various lag times, such as 1, 3, 6, 12, 24, and 48 months.

Table 6.2: Drought classification based on SPEI

2.00 or more	Extremely wet
1.50 to 1.99	Very wet
1.00 to 1.49	Moderately wet
0.99 to -0.99	Near normal
-1.00 to -1.49	Moderate drought
-1.50 to -1.99	Severe drought
-2.00 or less	Extreme drought

6.3.3 Normalized Difference Vegetation Index

The NDVI is a widely used remote sensing index (Bhandari, Kumar, & Singh, 2012). The ratio of TOA (top of atmosphere) reflectance of a red band (ρ_{red}) around 0.66 µm and a near-infrared (NIR) band (ρ_{nir}) around 0.86 µm is used to calculate NDVI. A densely vegetated area's NDVI will tend toward positive values, whereas water and built-up areas will have near zero or negative values see table 6.1. Braun and Herold (2004) define NDVI as follows:

$$\mathrm{NDVI} = \frac{\rho_{\mathrm{nir}} - \rho_{\mathrm{red}}}{\rho_{\mathrm{nir}} + \rho_{\mathrm{red}}}$$

The figure 6.1 depict actual values, but real vegetation is much more varied.

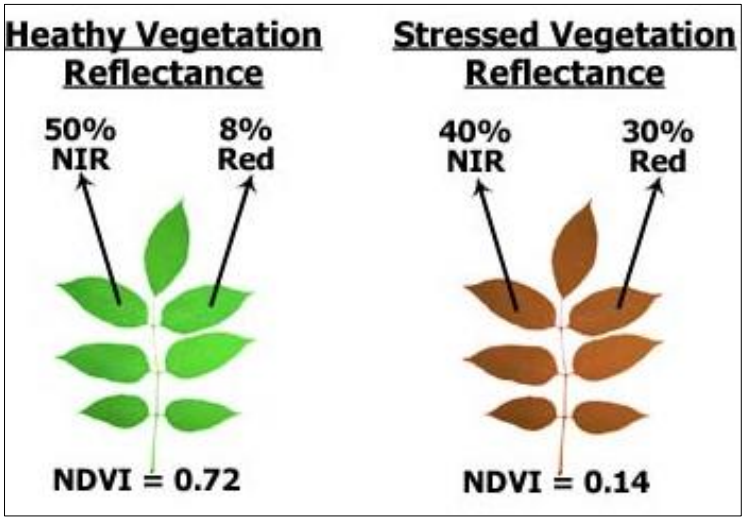

Figure 6.1. Robert Simmon illustration. (Measuring Vegetation (NDVI & EVI) (nasa.gov)).

Table 6.1 classification of vegetation presence based on the NDVI

Range	Classe
<0	Water
0-0,03	Barre soil
0,03-0,3	Sparse vegetation
0,3-0,5	Moderate vegetation
0,5-1	Dense vegetation

6.3.4 Enhanced Vegetation Index

The enhanced vegetation index (EVI) was created as a suitable alternative vegetation index to address some of the NDVI's limitations. EVI is more sensitive to differences in plant canopy such as leaf area index (LAI), canopy structure, plant phenology, and stress than NDVI, which generally responds only to the amount of

chlorophyll present. NASA adopted EVI as a standard MODIS product with the launch of the MODIS sensors, which is distributed by the USGS.

EVI is calculated as follow:

$$EVI = 2.5 * \frac{(NIR - RED)}{\left(NIR + C_1^* RED - C_2 * BLUE + L\right)}$$

where NIR, RED, and BLUE are atmospherically corrected (or partially atmospherically corrected) surface reflectance, and C_1, C_2, and L are coefficients to correct for atmospheric condition (i.e., aerosol resistance). For the standard MODIS EVI product, L=1, C1=6, and C2=7.5. (Measuring Vegetation (NDVI & EVI) (nasa.gov)).

Table 6.2 classification of vegetation presence based on the EVI

Pixel Range	Classe
<0	Stressed vegetation
0-0,2	No vegetative cover
0,2-0,8	Healthy vegetation cover
0,8-1	high vegetative cover

6.3.5 Normalized Difference Water Index

As it mentioned in section 2.2.2, McFeeters (1996) proposed the NDWI index. Its primary application today is to detect and monitor minor changes in the water content of bodies of water. The NDWI is calculated as follows:

$$\mathrm{NDWI} = (\rho\mathrm{PIR} - \rho\mathrm{MIR}) / (\rho\mathrm{PIR} + \rho\mathrm{MIR})$$

Where; ρ MIR: Reflectance in the mid-infrared band.

ρ PIR: Reflectance in the near infrared band.

The logic is the same here for the reason of being NDWI indices value from -1 to 1.

The NDWI maximizes water reflectance by absorbing a maximum of wavelength and minimizes NIR reflectance by absorbing a maximum of wavelength. As a result, having positive values enhances water features while having zero or negative values suppresses vegetation and soil.

6.3.6 Run Theory and Drought Characteristics

To characterize the meteorological drought features of the selected area, the occurrence of drought events was assessed for each cell of the gridded dataset using the SPI and SPEI thresholds, and the average over the observation period was shown. To detect the behavior of the region in response to moderate and extremely severe drought conditions, two different SPI and SPEI thresholds were used, SPI≤ -1, SPEI ≤ -1 and SPI≤ -2, SPEI ≤ -2. (See Table 6.1). The accumulation period's impact was investigated. In addition, three drought characteristics were chosen (Guo et al., 2018; Wang et al., 2019; Fung et al., 2020). These are mean drought duration (MDD), mean drought severity (MDS), and mean drought intensity (MDP). MDD and MDS were estimated using the SPI and SPEI data in conjunction with the "run theory" proposed by Yevjevich (1967) and Wang et al. (2019):

$$\mathrm{MDD} = \frac{\sum_{i=1}^{N} \mathrm{DD}_i}{N}$$

$$\mathrm{MDS} = \frac{\sum_{i=1}^{N} \mathrm{DS}_i}{N}$$

$$\mathrm{DS}_i = \sum_{\mathrm{DD}_i} \mathrm{SPI}$$

where, considering a given SPI/SPEI threshold, DD is the period with continuous (negative) SPI/SPEI values below the given threshold (i.e., drought spell duration in the run theory), i is the number of the sequence of DD, N is the total

number of drought spells observed during the studied period, and DSi is the drought severity value associated with the period DD_i (Figure 6.3)

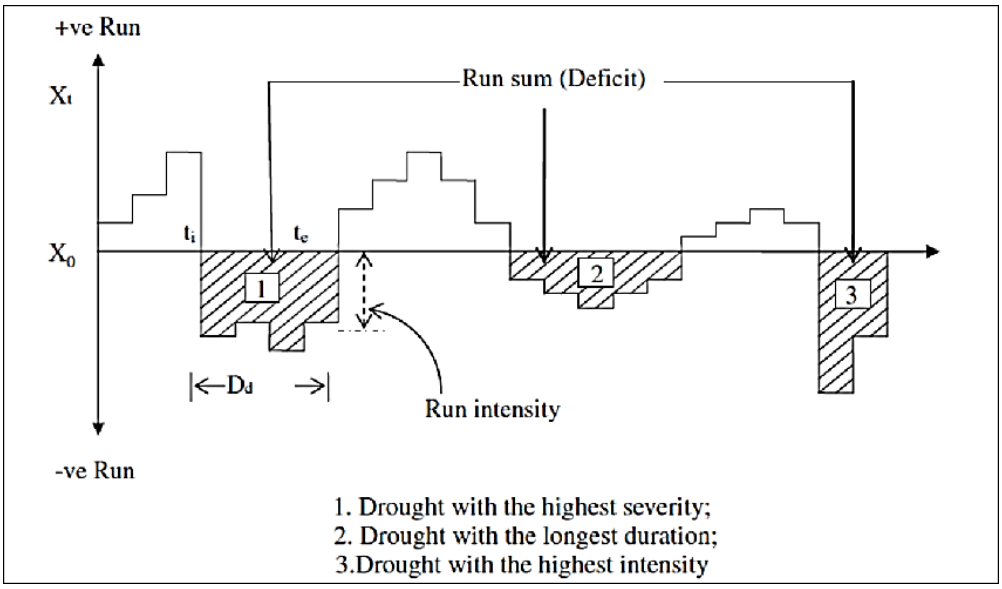

Figure 6.3 Drought characteristic identification using the "run theory" (Yevjevich, 1967).

Only events with DD 3 months were accounted for. Furthermore, the mean drought intensity MDP was calculated as the ratio of MDS to MDD (Li et al., 2017). As with the computation of MDD, MDS, and MDP, the two different thresholds, SPI/SPEI ≤ -1 and SPI/SPEI ≤ -2, were considered. The effects of the accumulation scale as well as the spatial patterns were studied.

6.3.7 Remote Sensing and Google Earth Engine (GEE)

Google Earth Engine is a cloud computing platform that processes satellite imagery as well as other geospatial and observational data. It gives users access to a large database of satellite imagery as well as the computational power required to analyze the images (Gardner 2010).

It permits the monitoring of dynamic changes in agriculture, natural resources, and climate through the use of geospatial data from the Landsat satellite program, which passes over the same locations on the Earth every sixteen (16) days (Jenner 2013). In collaboration with GCS (Google Cloud Storage), GEE has evolved into a platform that makes Landsat and Sentinel-2 (Figure6.4) data easily accessible to researchers "New Public Application of Landsat Images Released".

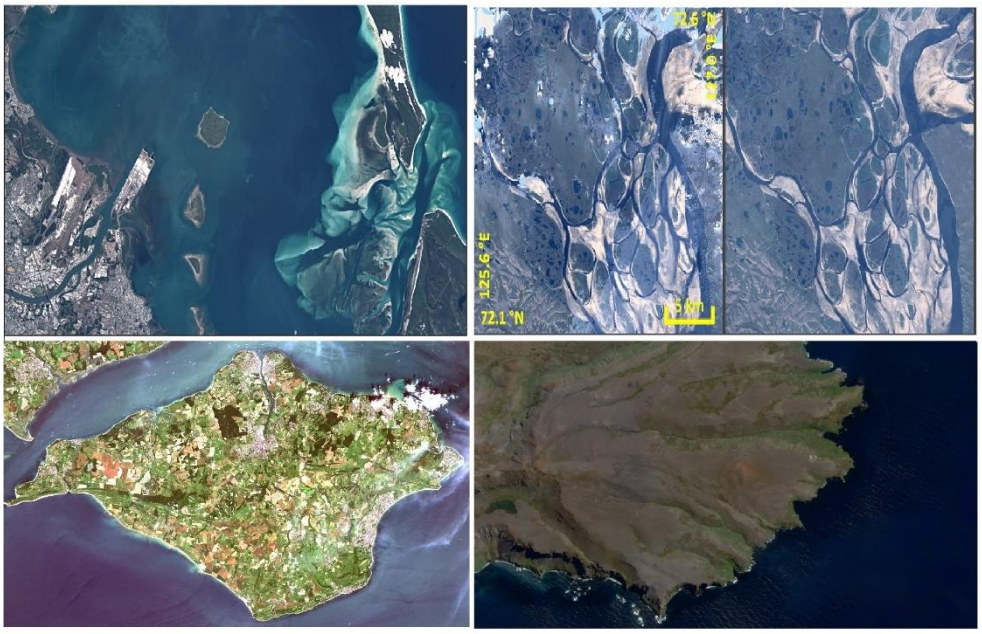

Figure 6.4 Image collections in the GEE

GEE offers a data catalogue as well as computers for analysis (Figure 6.5) , allowing scientists to collaborate with data, algorithms, and visualizations (Gorelick 2013).

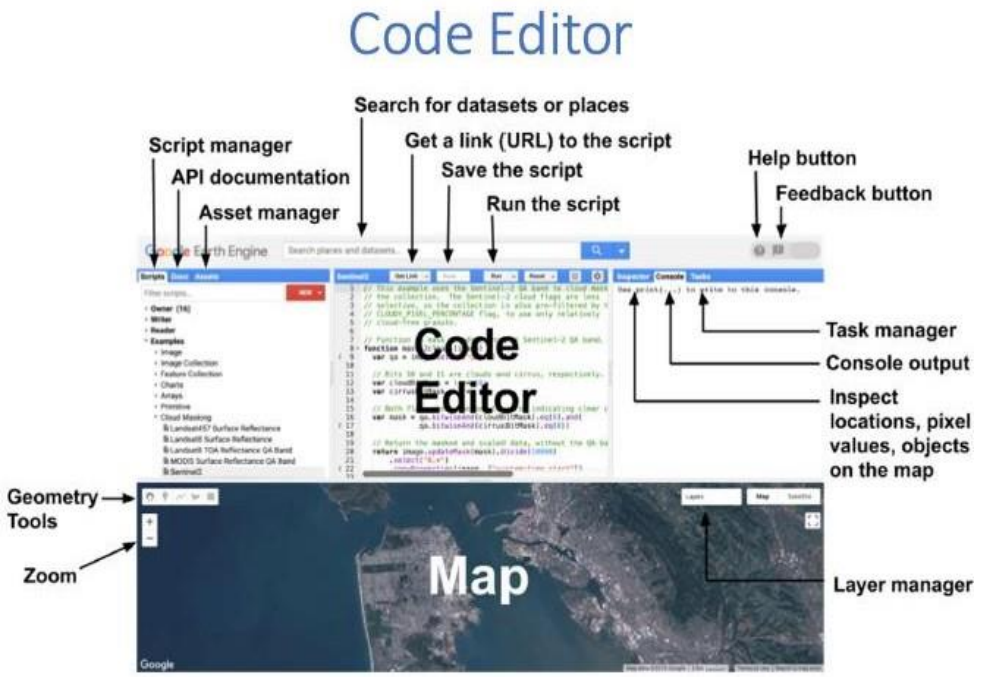

Figure 6.5. The GEE program interface

The platform includes a graphical user interface for developing applications as well as Python and JavaScript application programming interfaces for making requests to servers.

In 2013, researchers from the University of Maryland used Earth Engine to create the first high-resolution global forest cover and loss maps, revealing an overall loss in global forest cover (Hansen et al., 2013). Other early Earth Engine applications covered a wide range of topics, such as global surface water Pekel et al., 2016),increases in vegetation around Mount Everest Lobell et al. (2015), and the annual Forest Landscape Integrity Index (Tsai et al., 2018). Since then, Earth Engine has been used to create hundreds of scientific journal articles in a variety of fields such as forestry and agriculture, hydrology, natural disaster monitoring and assessment, urban mapping, atmospheric and climate sciences, and soil mapping.

6.4 Temporal Analysis

6.4.1 Standardized Precipitation Index

The temporal patterns of the SPI time series in the investigated region at various timescales have the potential to provide insights into the temporal variation of droughts in the Campania region. As an example, Figure 6.7 depicts SPI 6, SPI 12, and SPI 24 for two grid data cells (Figure 3.1). The left panels show an example from the southern coastal area, while the right panels show an example from the northern inland area.

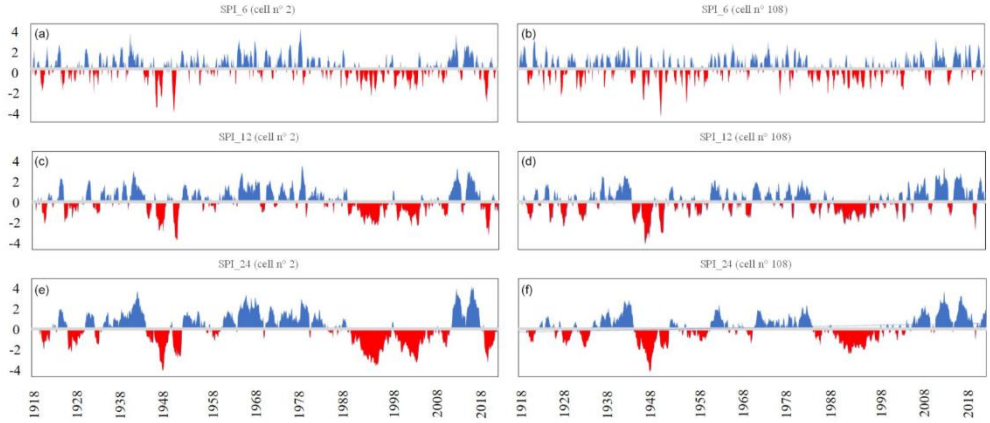

Figure 6.7 SPI_6, SPI_12 and SPI_24 for cell no. 2 (southern area – **a**, **c**, **e**) and cell no. 108 (northern area – **b**, **d**, **f**).

Figure 6.7 highlights the drought periods that affected the Campania region around 1940–1950 and 1990–2010. This finding appears to be consistent with the findings of a European-scale assessment study, which stated that the period between 1985 and 1995 was characterized by the widest spread of extreme drought events, with most of them mainly located on the Iberian Peninsula, southern Europe, the Balkans, and western Turkey (Bonaccorso et al., 2013). Drought severity appears to be less pronounced in the northern inland areas, particularly when the longest

accumulation timescale is considered. Drought severity appears to be less pronounced in the northern inland areas, particularly when the longest accumulation timescale is considered. Drought tends to be more persistent in the southern areas than in the northern ones, which have also been impacted only slightly by the region's drought conditions since 2015. More information on the spatial variability of drought features will be discussed in following section.

To investigate temporal trends, sign, significance, and magnitude in SPI time series over the studied period, the modified Mann–Kendall (MMK) test and the Sen's slope estimator were used. The relevant MMK results for trend sign and significance (significance level = 5%) are depicted in Figures 6.8 and 6.9.

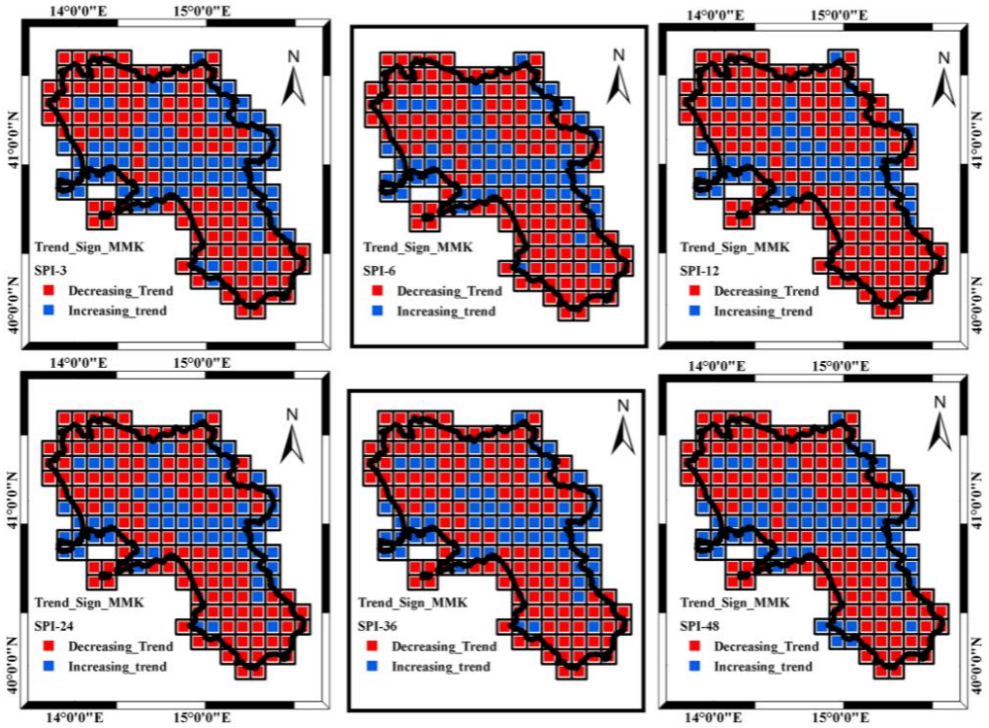

Figure 6.8: SPI MMK test sign for the different accumulation scales (α= 5 %).

From SPI 3 to SPI 12, the downward trend becomes dominant in the study area, especially in the north-western and southern sectors (Figure 6.8), which correspond to the area with the highest mean annual precipitation and the highest precipitation downward trend (Longobardi and Villani, 2010). For the SPI 24 to SPI 48, the proportion of negative to positive trends remains nearly identical, with negative values still dominating in more than 60% of the cells. Concerning the trend's significance (Figure 6.9), the MMK test demonstrated how a very large proportion of the gridded SPI showed a significant trend over the different timescales, particularly from the SPI 3 accumulation scale to the SPI 24 accumulation scale (Figure 6.9). The negative trend is especially noticeable for SPI 3, SPI 6, and SPI 12, with a percentage of grid cells of around 55 percent for both SPI 3 and SPI 6 and 65 percent for SPI 12. In terms of trend spatial distribution, the SPI 24 is the most significant, accounting for nearly 70% of the grid cells. Beyond this scale, temporal variations did not appear to be significant.

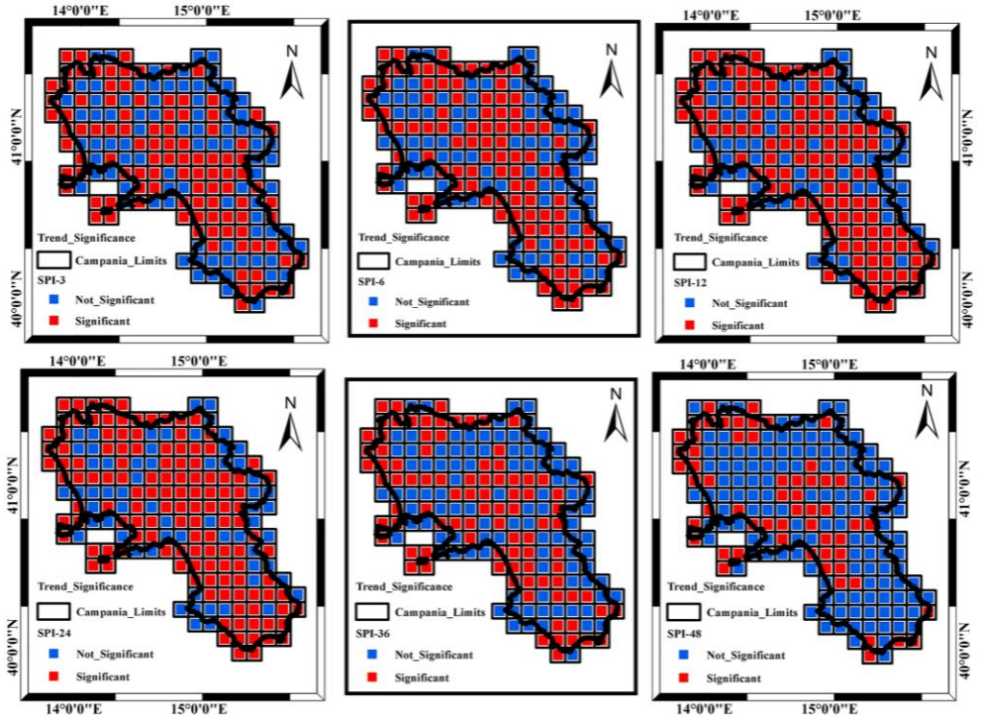

Figure 6.9: SPI MMK test significance (α= 5 %) for the different accumulation scales.

Because the region's groundwater systems have long delay times and are thus potentially impacted by SPI accumulated on a large scale, climate temporal variations are unlikely to have a significant impact on those systems (Longobardi and Van Loon, 2018). On a national scale, the obtained results were well in line with the general overview outlined in previous research by Delitala et al. (2000) and Bordi et al. (2001) for other regions of southern Italy (Sardinia, Sicily, and Puglia), and were also in perfect agreement with the results provided by Buttafuoco and Caloiero (2014) for the Calabria region in southern Italy.

At the local scale, the modified Mann–Kendall trend test findings are also consistent with previous climatological studies on precipitation regime investigation (Longobardi and Villani, 2010; Longobardi et al., 2016). Indeed, annual and

seasonal precipitation in the region were found to have a generalized negative trend over the last century, despite the fact that the downward tendencies, contrary to the SPI tendencies, were significant for a very small number of rain gauge stations.

Figure 6.10 depicts the magnitude of the trend in the SPI time series as determined by Sen's estimator. In accordance with the MMK test results, the trend was dominantly negative across the region, which is consistent with the trend sign depicted in Figure 6.8, with the exception of a west–east transect at the region's middle latitudes, which corresponds to an area with moderate mean annual precipitation values and the lowest downward precipitation trends (Longobardi and Villani, 2010).

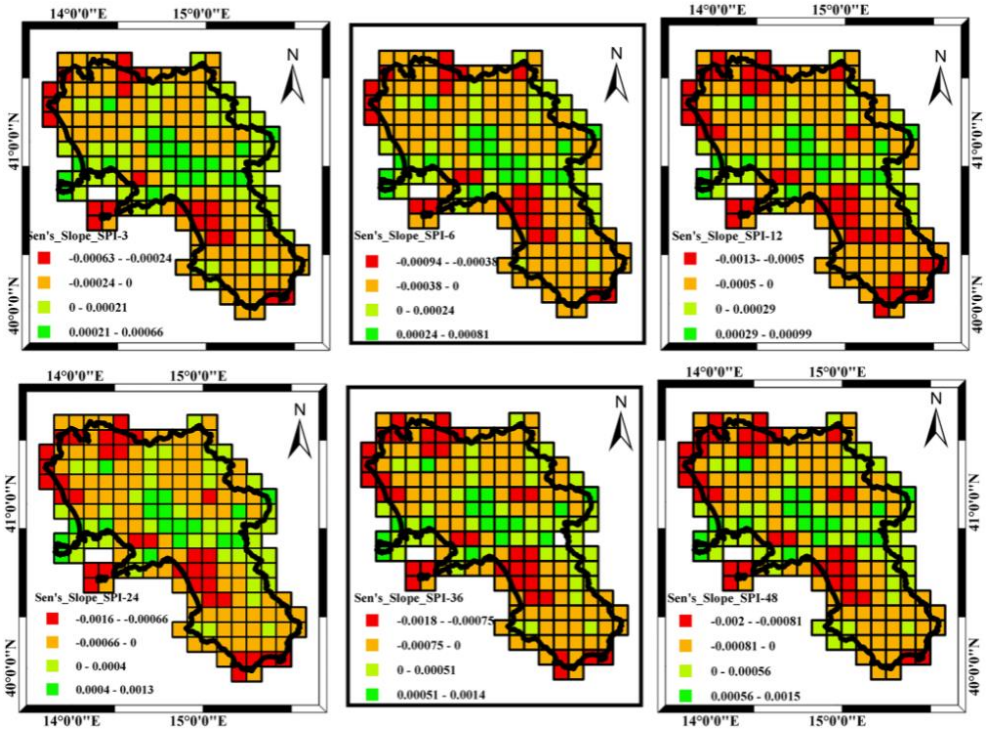

Figure 6.10: SPI Sen's slope for the different accumulation timescales.

However, the overall tendency toward drier conditions was moderate, with an amplification with increasing accumulation timescale. In the case of SPI 6, the increase in the SPI index is approximately 10% over a ten-year period. It rises by up to 15% and 24% in ten years for SPI 12 and SPI 48, respectively. On the spatial scale, the variability in the minimum and maximum assessed trend increases as the accumulation timescale increases.

6.4.2 Standardized Precipitation Evapotranspiration Index

The patterns of the SPEI time series in the studied region at different timescales have the potential to provide insights into the temporal variation of droughts in the Campania region. Figure 6.11 depicts SPEI 6, SPEI 12, and SPEI 24 for two grid data cells as an example (Figure 3.1). The examples on the left are from the southern coastal area, while the examples on the right are from the northern inland area.

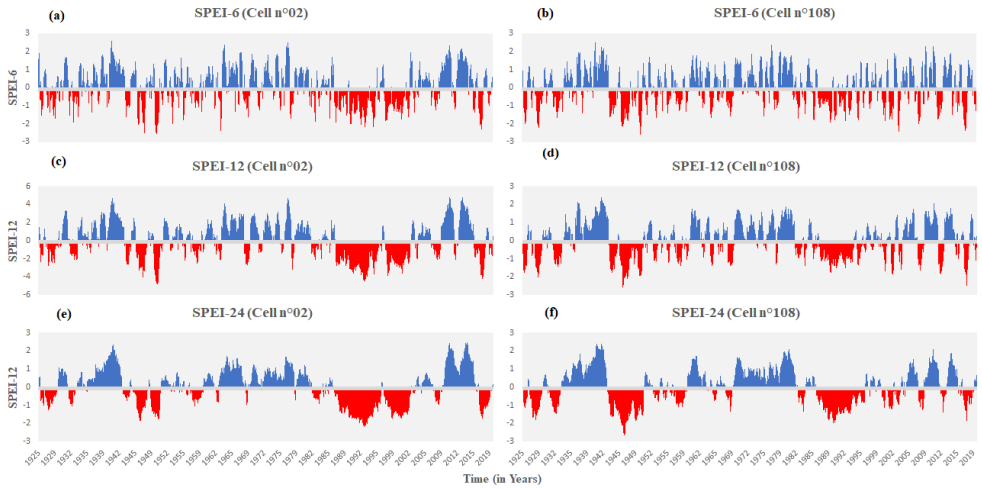

Figure 6.11: SPEI_6, SPEI_12 and SPEI_24 for cell no. 2 (southern area – **a**, **c**, **e**) and cell no. 108 (northern area – **b**, **d**, **f**).

Figure 6.11 depicts the drought periods that affected the Campania region in the years 1940–1950 and 1990–2010. This finding confirms the SPI index results in section 6.4.1, and it appears to be consistent with the findings of a European-scale assessment study, which stated that the period between 1985 and 1995 was characterized by the widest spread of extreme drought events, with the majority of them primarily located on the Iberian Peninsula, southern Europe, the Balkans, and western Turkey (Bonaccorso et al., 2013). Drought severity appears to be less noticeable in the northern inland areas, especially when the longest accumulation timescale is assessed. Drought is more persistent in the south than in the north, which has also been impacted only slightly by the region's drought conditions since 2015.

The modified Mann–Kendall (MMK) test and the Sen's slope estimator were used, as mentioned in section 6.4.1, to investigate temporal trends, sign, significance, and magnitude in SPEI time series over the studied period. Figures 6.8 and 6.9 show the relevant MMK results for trend sign and significance (significance level = 5%).

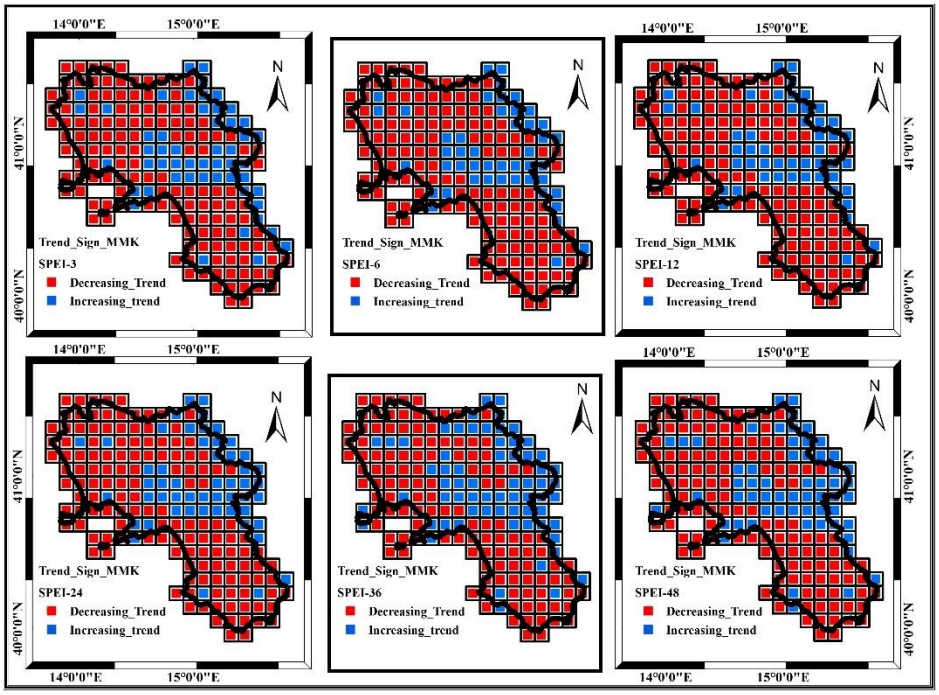

Figure 6.12 SPEI MMK test sign for the different accumulation scales (α= 5 %).

From SPEI 3 to SPEI 12, the downtrend dominates and its percentage increases as the time scale increases in the study area, particularly in the north-western and southern sectors (Figure 6.12), which correspond to the area with the highest mean annual precipitation and the highest precipitation downward trend (Longobardi and Villani, 2010). The proportion of negative to positive trends remains nearly identical from SPI 24 to SPI 48, with negative values dominating in more than 70% of the cells. Concerning the trend's significance (Figure 6.13), the MMK test demonstrated how a very large proportion of the gridded SPI showed a significant trend over the different timescales, particularly from the SPI 3 accumulation scale to the SPI 24 accumulation scale (Figure 6.9). The negative trend is especially noticeable for SPI 3, SPI 6, and SPI 12, with a percentage of grid cells of around 55 percent for both SPI 3 and SPI 6 and 65 percent for SPI 12. In terms of

trend spatial distribution, the SPI 24 is the most significant, accounting for nearly 70% of the grid cells. Beyond this scale, temporal variations did not appear to be significant.

Concerning the significance of the trend (Figure 6.13), the MMK test revealed that a very large proportion of the gridded SPEI showed a significant trend across timescales, particularly from the SPEI 3 accumulation scale to the SPEI 12 accumulation scale (Figure 6.13). The negative trend is most noticeable for SPEI 3, SPEI 6, SPEI 12, and SPEI 24, with grid cell percentages of 64, 67, 71, and 65 percent, respectively. The SPEI 12 is the most significant in terms of trend spatial distribution, by almost 72 percent of the grid cells. Temporal variations did not appear to be significant above this scale.

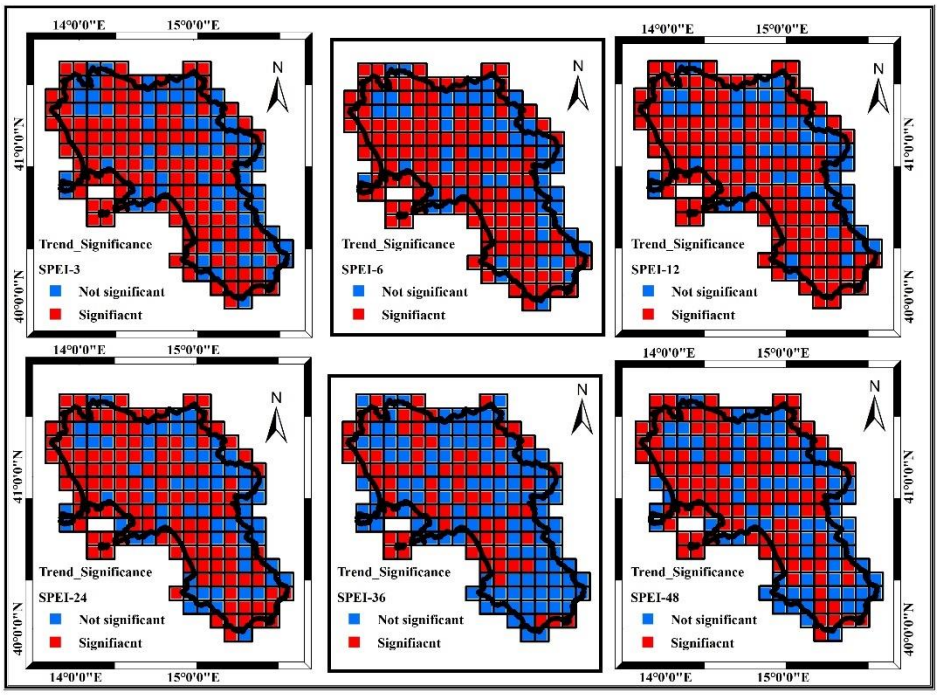

Figure 6.13 SPEI MMK test significance (α= 5 %) for the different accumulation scales.

The results of the modified Mann–Kendall trend test were well in line with prior climatological studies on precipitation and temperature regime investigation (Toreti, Desiato et al. 2008, Longobardi and Villani, 2010; Longobardi et al., 2016). Indeed, according to previous studied carried out in the region by (Longobardi and Villani, 2010; Longobardi et al., 2016), annual and seasonal precipitation in the region were found to have a generalized negative trend over the last century, despite the fact that the downward tendencies were significant for a very small number of rain gauge stations, contrary to the SPEI tendencies.

The magnitude of the trend in the SPEI time series as determined by Sen's estimator is represented in Figure 6.14. According to the MMK test results, the trend was predominantly negative across the region, which corresponds to the trend sign depicted in Figure 6.12, except for a Northeast part and some central cells of the studied area, which corresponds to an area with moderate mean annual precipitation values and the lowest downward precipitation trends (Longobardi and Villani, 2010).

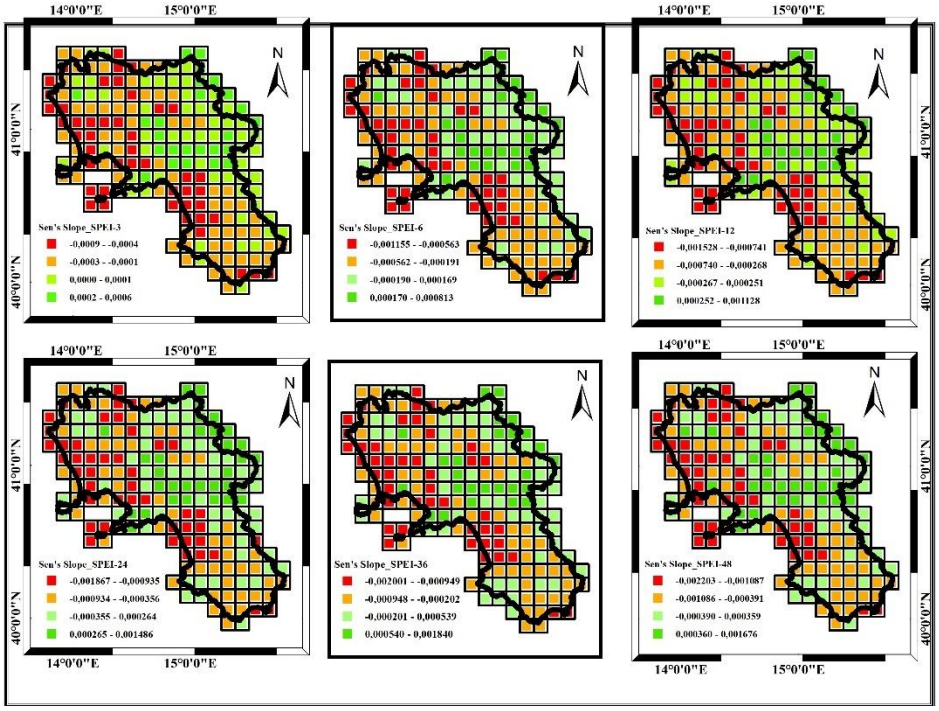

Figure 6.14 SPEI Sen's slope for the different accumulation timescales.

The overall tendency toward drier conditions, on the other hand, was moderate, with an amplification with increasing accumulation timescale. In addition, the variability in the minimum and maximum assessed trend increases as the accumulation timescale increases on the spatial scale.

6.5 Drought Characteristics Assessment

6.5.1 Standardized precipitation index

Figures 6.15 and 6.16 highlight the total number of drought events detected in the SPI time series from 1918 to 2019 for moderate drought conditions and

extremely severe drought conditions of threshold SPI≤ -1 and SPI≤ -2, respectively at each grid point for all accumulation scales considered. In the case of moderate drought events (figure 6.15), the SPI 3 was found to be associated with the greatest number of droughts, on average 95, for the entire period of observation across the 191 grid cells. Drought frequency decreased with increasing accumulation scale, given the large theoretical autocorrelation in SPI time series for the larger accumulation scale, with the SPI 24 to SPI 48 patterns approximately identical among them (Figure 6.15). The findings appeared to be in good agreement with those of other authors (McKee et al., 1993; Buttafuoco et al., 2015; Marini et al., 2019; Fung et al., 2020). Except for the lower number compared to moderate events, extremely severe drought episodes reflected very similar behavior (figure 6.16). The average number of drought events in the case of SPI 3 for the threshold SPI ≤ -2 was 27 for the entire observation period across the 191 grid cells. In terms of spatial patterns, while a moderate correlation was observed for small clusters of cells, no clear concentration of drought event occurrence in a specific area was discovered.

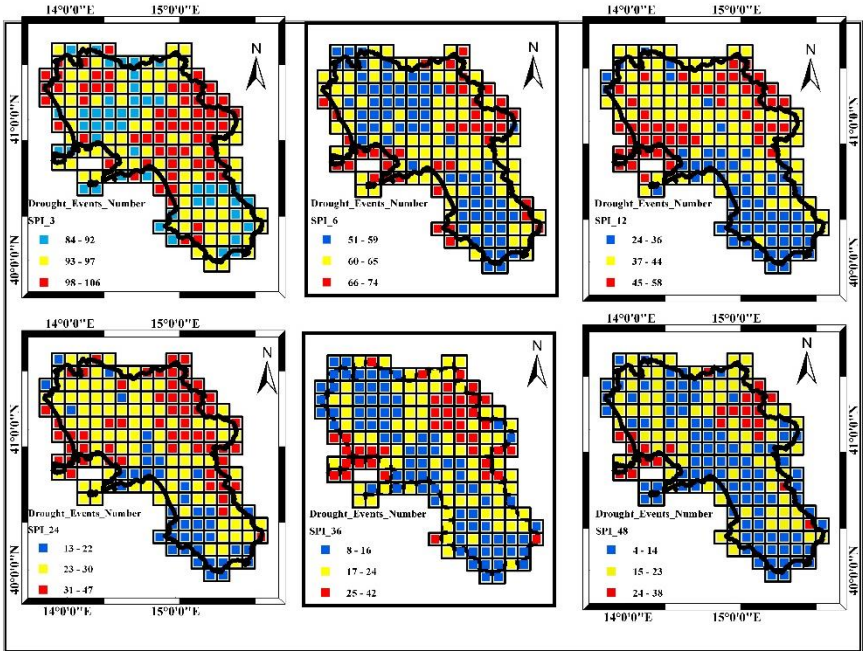

Figure 6.15 Number of drought events for the different accumulation timescales over the whole period of observation 1918–2019 (threshold SPI≤ -1).

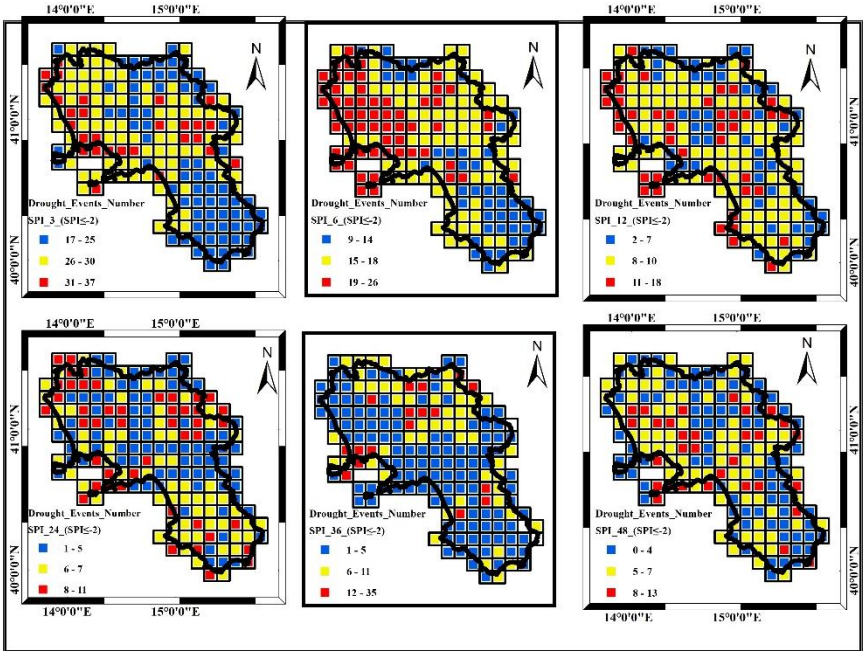

Figure 6.16 Number of drought events for the different accumulation timescales over the whole period of observation 1918–2019 (threshold SPI≤ -2).

More perspectives are therefore obtained from the analysis of the MDD, MDS, and MDP, as displayed in Figures 6.17, 6.18 and 6.19 with reference to an SPI≤ -1 threshold value.

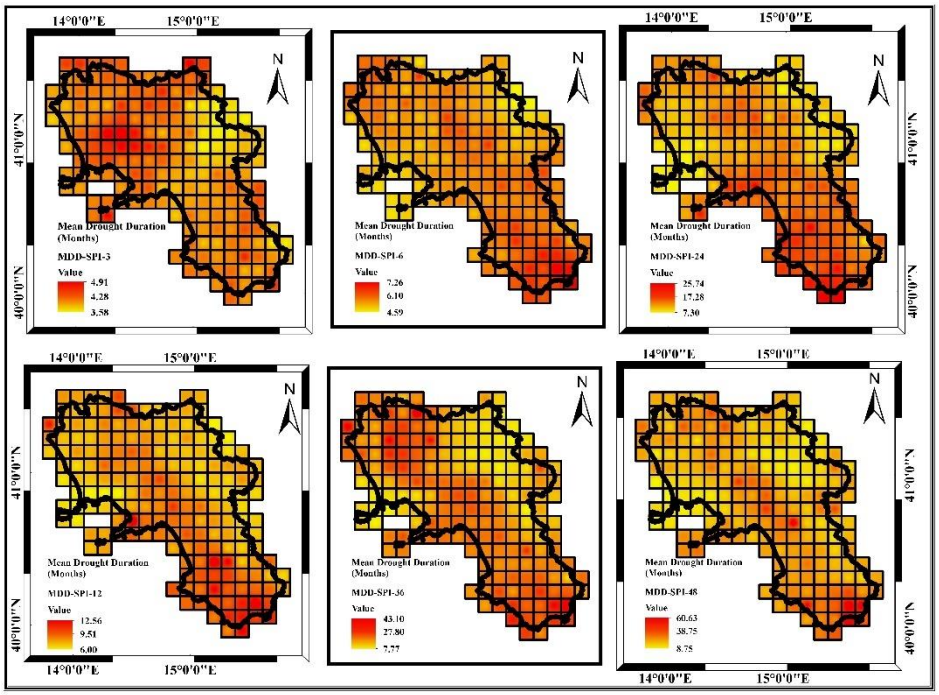

Figure 6.17 MDD (mean drought duration) for the different accumulation periods considered (SPI ≤−1).

In terms of the MDD (figure 6.17), besides what occurred with drought frequency, the mean drought duration increased with accumulation timescale, ranging from 4 to 5 months for the SPI 3 to 8 to 60 months for the SPI 48. The MDD spatial behavior was also influenced by the accumulation timescale (figure 6.17). The average MDD values affected nearly the entire region in the case of SPI 3 and SPI 6. The largest MDD values were found along a northwest to southeast transect in the case of SPI 12, SPI 24, SPI 36, and SPI 48, and more clearly in the southern areas of the region under investigation. Northern sections are the most impacted at the smallest timescales (SPI 3). For longer accumulation timescales, the maximum

values detected in the southern region were mainly caused by severe drought periods that occurred in the region in 1990, 2003, and 2017.

In terms of the MDS (Figure 6.18), the drought severity increased due to the MDD characteristics, with the accumulation timescale ranging from 6 to 8 for the SPI 3 to 11 to 90 for the SPI 48 (Figure 6.18). The accumulation timescale, as in the case of MDD, seemed to influence the spatial pattern of MDS. MDS showed a significant severity in the northern area for SPI-3, whereas from SPI-12 to SPI-48, MDS severity moved from the northern to southern areas and almost disappeared with an even distribution set at an almost constant value (about -10).

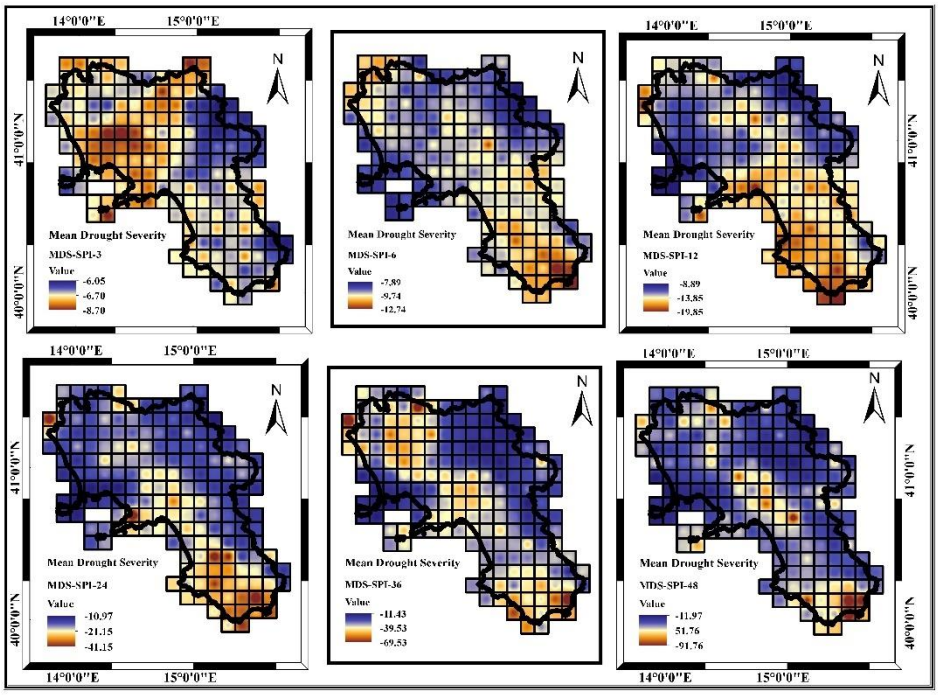

Figure 6.18: MDS (mean drought severity) for the different accumulation periods considered (SPI ≤−1).

In the case of the MDP (Figure 6.19), as previously demonstrated for the MDD and MDS, the minimum (about -1.5 on average) and maximum (about -2.3 on average) values appeared similar for the different accumulation timescales and were likely more marked for the lower accumulation scales where MDP's largest peaks are concentrated in the northern area. The spatial pattern, on the other hand, was found to be particularly complex, with no clear tendency related to the accumulation timescale (figure 6.19). Moreover, the highest peaks for the SPI-3 to SPI-6 are located in the northern areas of the region. With the exception of some coastline cells in the north of the region, there was a general tendency for a dominant low peak spatial distribution from SPI-24 to SPI-48. In addition, The SPI 12 reflected a neutral condition, with marked minimum and maximum SPI values distributed across the region.

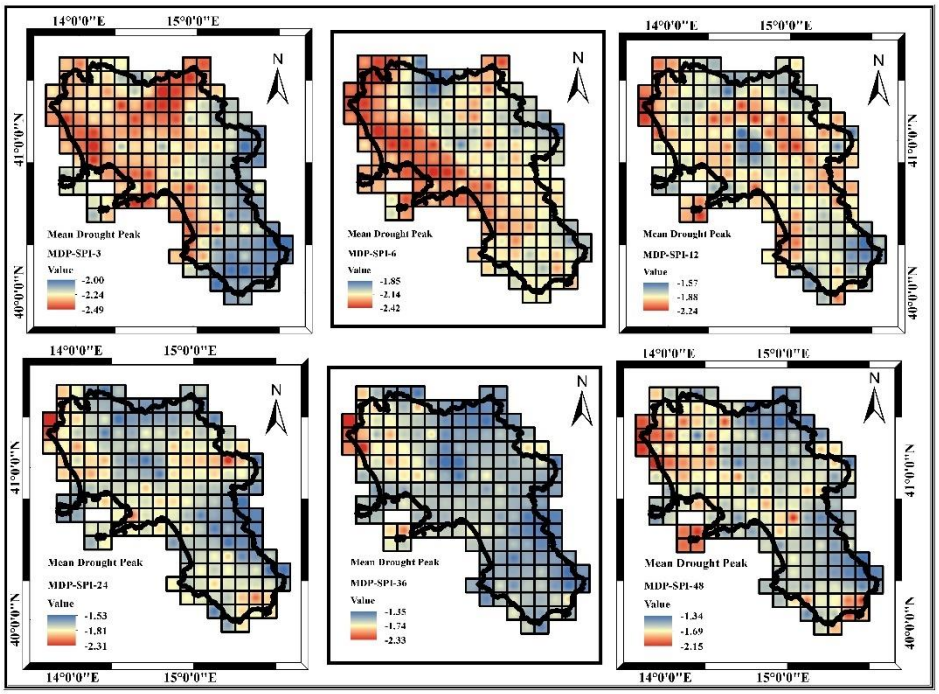

Figure 6.19 MDP (mean drought peak) for the different accumulation periods considered (SPI ≤−1).

By increasing the threshold for SPI values, from SPI 1 to SPI 2, it was possible to investigate the region's extremely severe drought conditions. In terms of the MDD (figure 6.20), the average drought duration increased with accumulation timescale, ranging from 3 months for the SPI 3 to 47 months for the SPI 48.

When compared to moderate drought events, the mean drought duration for each accumulation scale decreased for extremely severe events. In term of spatial distribution, in case of extreme drought condition (SPI ≤ -2), the same consideration provided for the case of SPI ≤−1 was held.

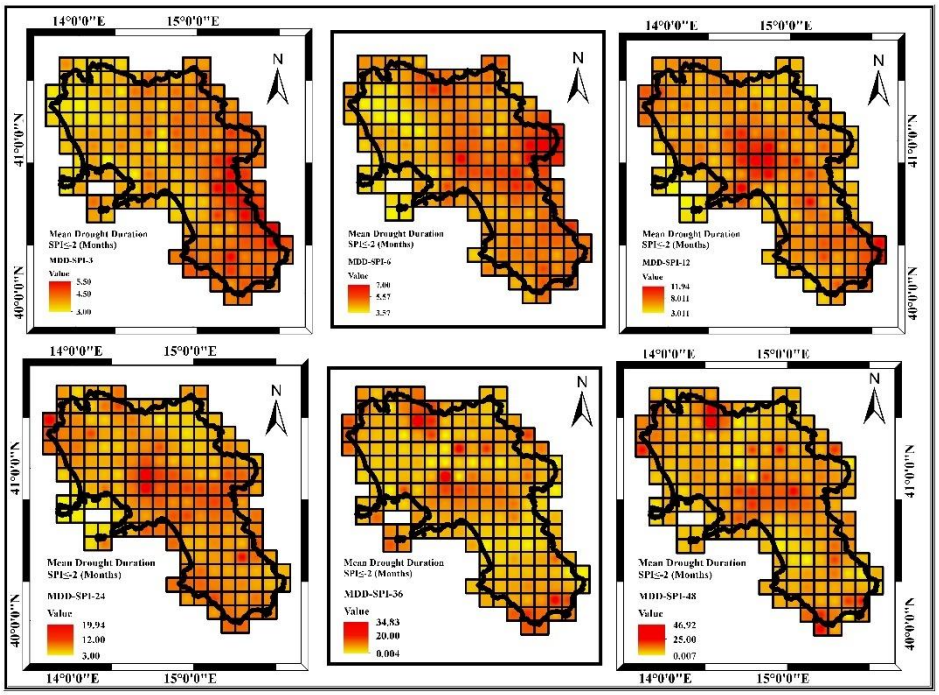

Figure 6.20: MDD (mean drought duration) for the different accumulation periods considered (SPI ≤−2).

The drought severity increased with the accumulation timescale ranging from 16 for the SPI 3 to 109 for the SPI 48, with reference to the MDS and thus to the MDD (figure 6.21). In comparison to moderate drought events, the mean drought severity increased for each accumulation scale during extremely severe drought events. More about the spatial pattern of MDS, it emerged as a common feature that the highest MDS values appeared in the region's center, with some spot cells located on the region's extreme southern and northern coastlines. The lower SPI 3 provided an exception.

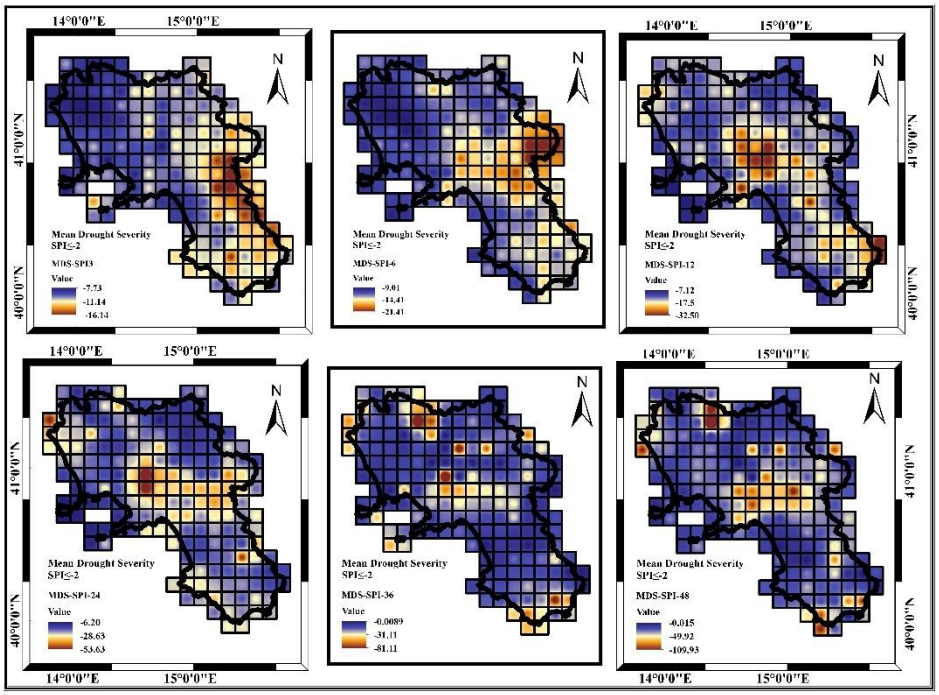

Figure 6.21: MDS (mean drought severity) for the different accumulation periods considered (SPI ≤−2).

In the end, unlike the MDD and MDS, the minimum (about -2.5 on average) and maximum (about -3.5 on average) values for the different accumulation

timescales of MDP appeared similar and likely more pronounced for the lower accumulation timescales (-4.09 for SPI 6), (figure 6.22). The spatial pattern was found to be particularly complex, with no clear tendency related to the accumulation timescale (figure 6.22). Larger peaks remained concentrated in the central cells of the region, but the area covered changed with accumulation timescale, becoming more moderate for the larger SPI accumulation scale. In the case of the largest accumulation periods, SPI 36 and SPI 48, a large peak appeared to spread throughout the region.

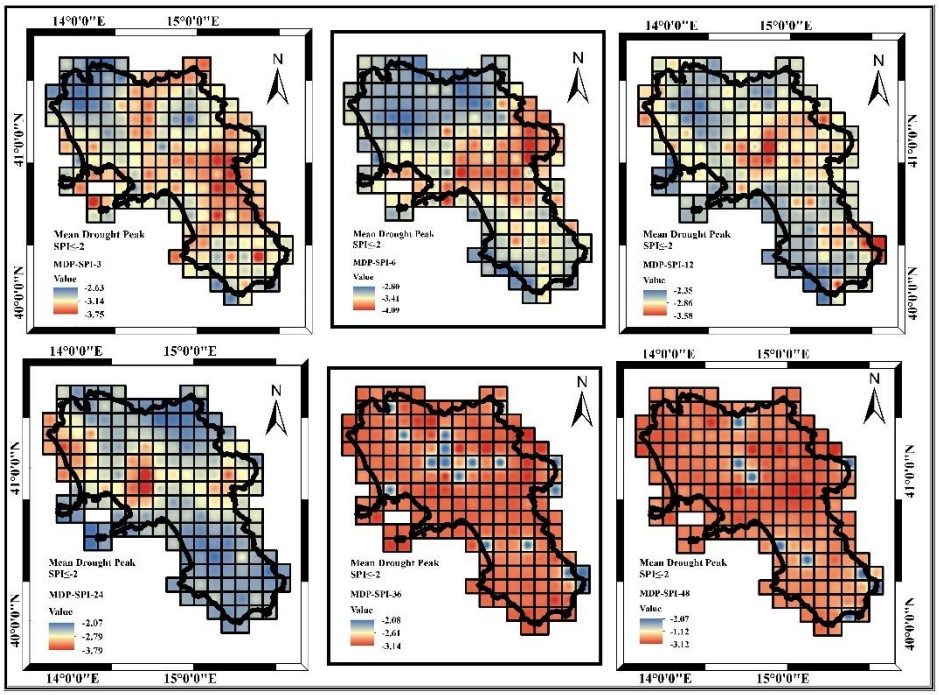

Figure 6.22: MDP (mean drought peak) for the different accumulation periods considered (SPI ≤ -2).

6.5.2 Standardized Precipitation Evapotranspiration Index

Figures 6.23 and 6.24 show the total number of drought events detected in the SPEI time series from 1924 to 2019 for moderate and extremely severe drought conditions of SPEI≤ -1 and SPEI≤ -2, respectively, at each grid point for all accumulation scales considered. In the case of moderate drought events (figure 6.23), the SPEI-3 was found to be associated with the greatest number of droughts, on average around 90, over the entire observation period across the 191 grid cells. Drought frequency decreased with increasing accumulation scale, given the large theoretical autocorrelation in SPEI time series for larger accumulation scales, with the SPEI 24 to SPEI 48 patterns seeming to be pretty much identical (Figure 6.23). The results appeared to be in good agreement with the SPI temporal pattern (section 6.5.1). Furthermore, these findings are consistent with those of other authors (McKee et al., 1993; Buttafuoco et al., 2015; Marini et al., 2019; Fung et al., 2020). With the exception of a lower number when compared to moderate events, extremely severe drought episodes exhibited very similar behavior (figure 6.24). For the entire observation period across the 191 grid cells, the average number of drought events in the case of SPEI-3 for the threshold SPEI ≤ -2 was however almost 10. In terms of spatial patterns, while there was a moderate correlation for small clusters of cells, large clusters seemed to be concentrated in the northeastern part of the region, indicating a clear concentration of drought event occurrence.

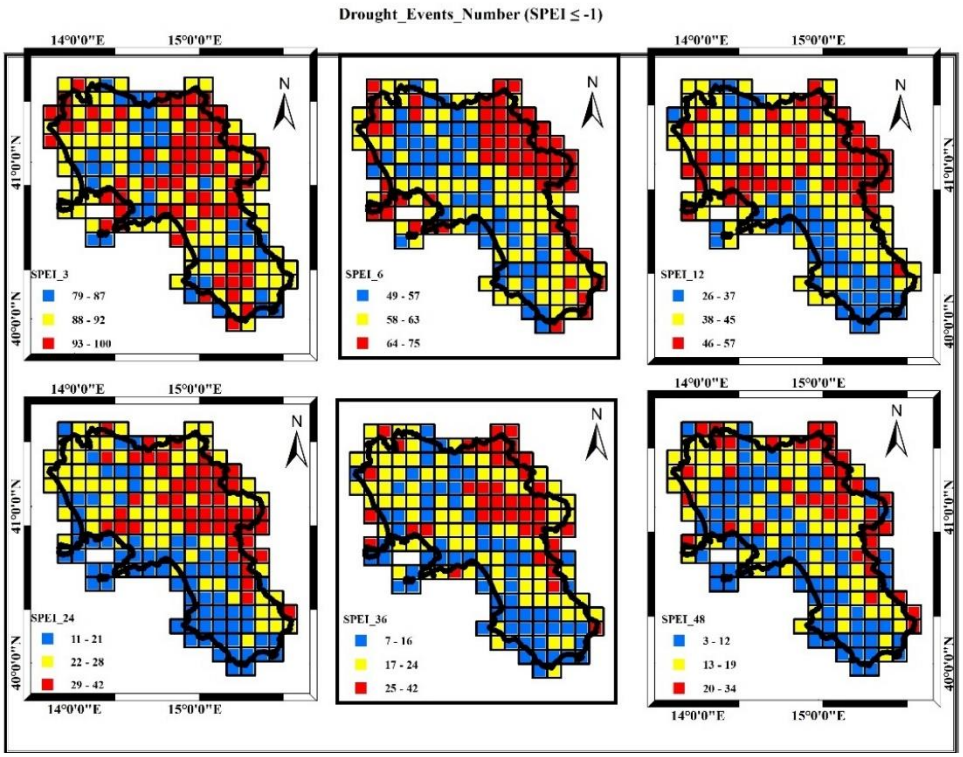

Figure 6.23: Number of drought events for the different accumulation timescales over the whole period of observation 1924–2019 (threshold SPEI≤ -1).

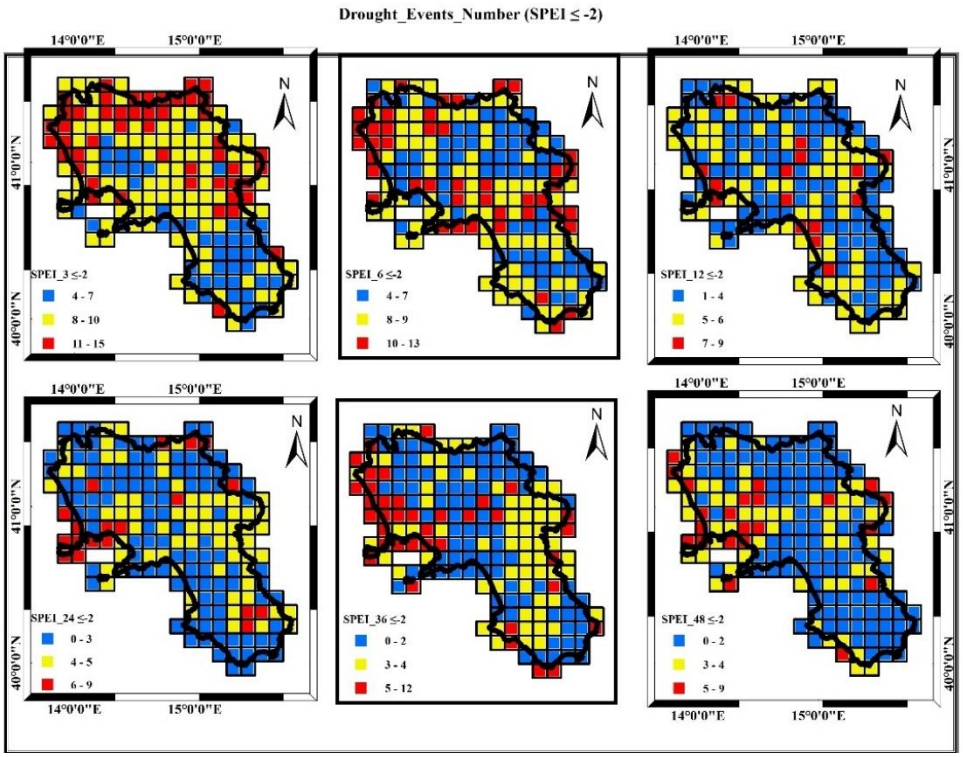

Figure 6.24: Number of drought events for the different accumulation timescales over the whole period of observation 1924–2019 (threshold SPEI≤ -1).

The analysis of the MDD, MDS, and MDP, as shown in Figures 6.25, 6.26, and 6.27 with reference to an SPEI ≤ -1 threshold value, yields more perspectives. In terms of MDD (Figure 6.25), in addition to what occurred with drought frequency, the average duration of drought increased with accumulation time scale, ranging from 4-5 months for SPEI 3 to 9-167 months for SPEI 48. The spatial behavior of MDD was also influenced by the accumulation time scale (Figure 6.25). average MDD values affected almost the entire region in the case of SPI 3 and SPI 6, while minimum values were detected in the northern region except for some cells in the southern part of the region for SPI 12. The largest MDD values were found along a northwest to southeast transect in the case of SPEI 24, SPEI 36, and SPEI 48, and most

clearly in the southern areas of the study region. The northern sections are most affected at the smallest time scales (SPEI 3, and SPEI-12 in particular). As mentioned in section 6.5.1, for longer accumulation time scales, the maximum values detected in the southern region are primarily caused by the severe drought periods that occurred in the region in 1990, 2003, and 2017.

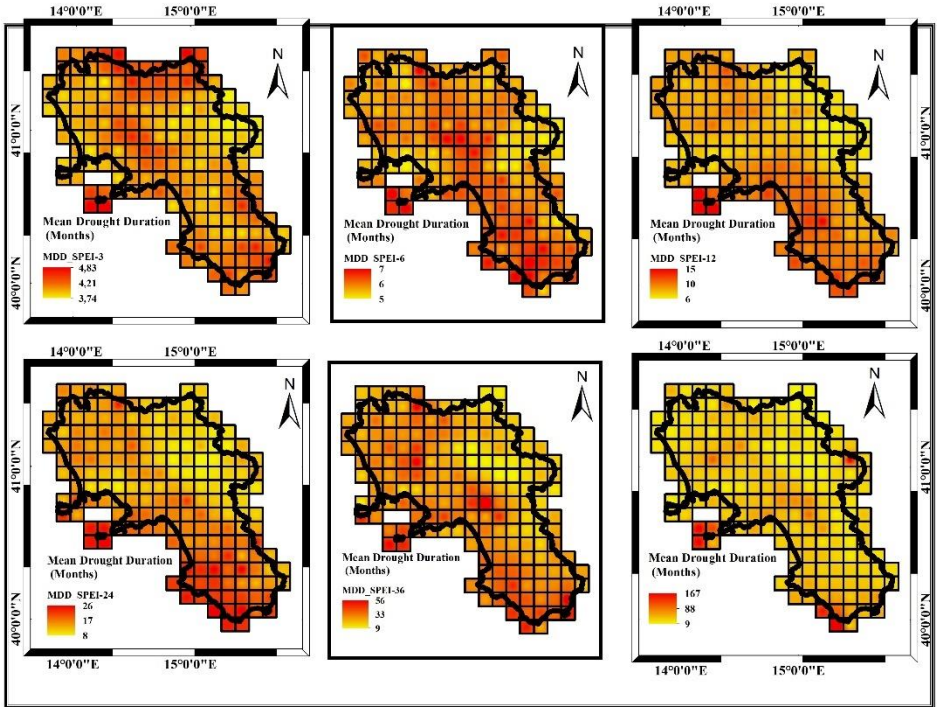

Figure 6.25 MDD (mean drought duration) for the different accumulation periods considered (SPEI ≤−1).

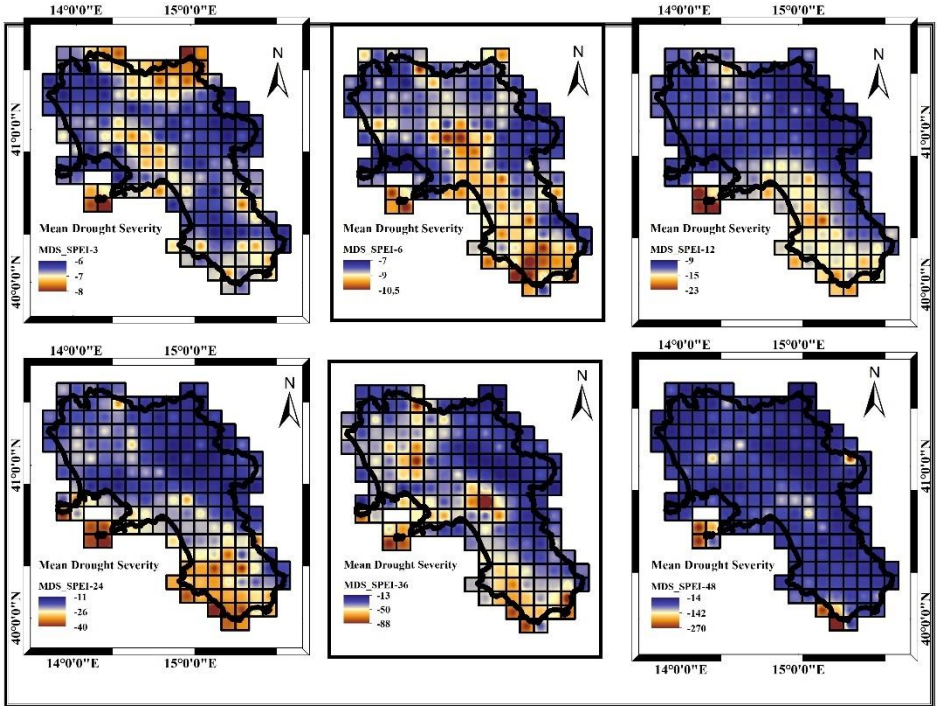

Figure 6.26: MDS (mean drought severity) for the different accumulation periods considered (SPEI ≤ -1).

The drought severity increased due to the MDD characteristics, with the accumulation timescale ranging from 6 to 8 for the SPEI-3 to 14 to 270 for the SPEI-48, according to the MDS (Figure 6.26). As with MDD, the accumulation timescale appeared to influence the spatial pattern of drought severity. MDS showed a significant severity in the northern area for SPI-3, whereas from SPI-12 to SPI-48, MDS severity moved from the northern to southern areas and almost disappeared with an even distribution set at an almost constant value (about -14), except some cells in the Napoli and Cilento coastal areas where the severity indicates maximal values over 200.

In the case of the MDP (Figure 6.27), as previously demonstrated for the MDD and MDS, the minimum (about -1.5 on average) and maximum (about -1.92 on average) values appeared similar for the different accumulation timescales and were likely more pronounced for lower accumulation timescales where MDP's largest peaks are concentrated in the northern, central, and east northern areas. The spatial pattern, on the other hand, was discovered to be extremely complex, with no clear tendency related to the accumulation timescale (figure 6.27). Furthermore, the highest SPEI-3 to SPEI-6 peaks were located in the region's northern and central areas. With the exception of some coastline cells in the region's north, there was a general tendency for a dominant low peak spatial distribution from SPEI-24 to SPEI-48. Besides that, the SPEI 12 reflected a neutral condition, with marked minimum and maximum SPI values distributed across the region.

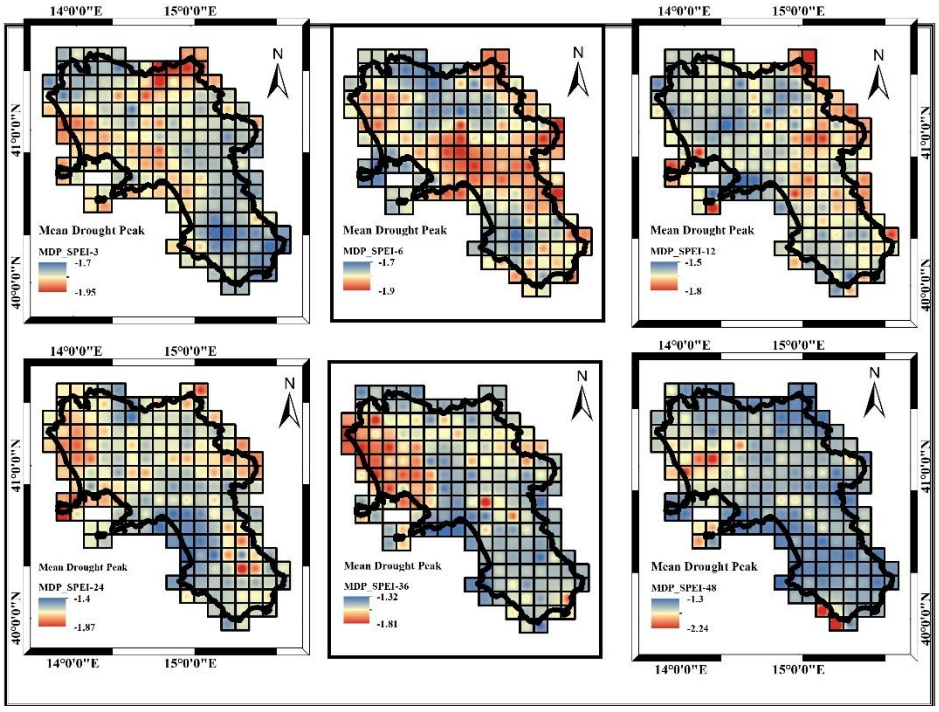

Figure 6.27: MDP (mean drought Peak) for the different accumulation periods considered (SPEI ≤−1).

As mentioned in section 6.5.1, it was possible to investigate extreme severe drought conditions in the region by increasing the threshold for SPEI values from SPIE≤ -1 to SPI≤ -2. The average drought duration increased with accumulation timescale in terms of the MDD (figure 6.28), ranging from 3 months for the SPEI-3 to 29 months for the SPI-36, with an exception for the SPEI-48, which had a maximum value of 23 months. The mean drought duration for each accumulation scale decreased for extremely severe events when compared to moderate drought events. In terms of spatial distribution, in the case of extreme drought (SPEI≤ -2), the same consideration as in the case of SPEI≤ -1 was adapted.

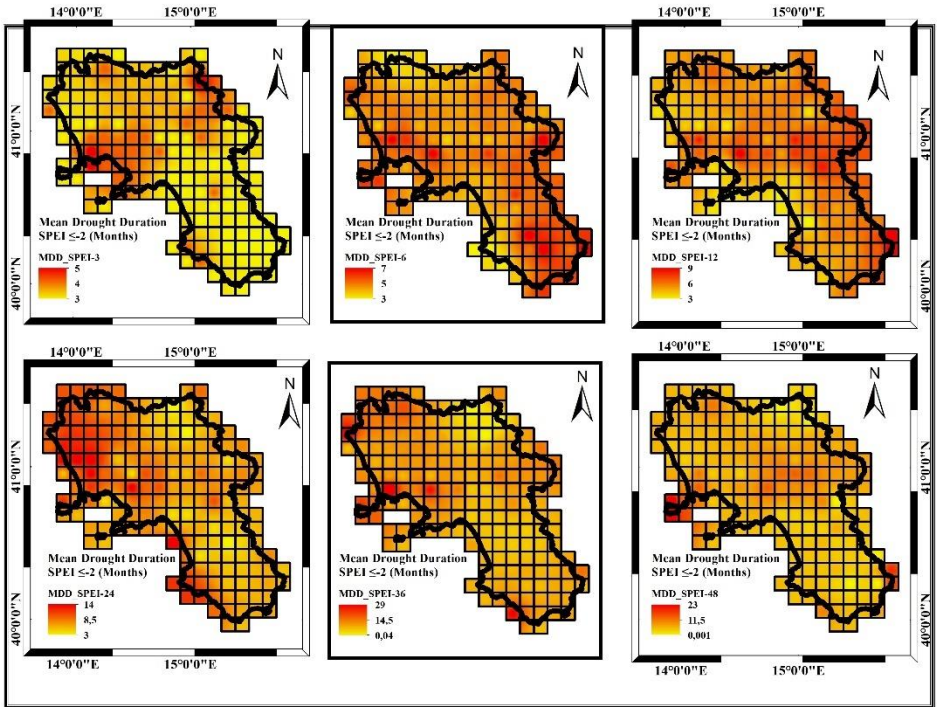

Figure 6.28 MDD (mean drought duration) for the different accumulation periods considered (SPEI ≤−2).

Consequently, the severity of the drought increased with the accumulation timescale, which ranged from 13 for the SPEI-3 to 50 for the SPEI-48 in terms of MDS and thus MDD (figure 6.29). In comparison to moderate drought events, the mean drought severity increased for each accumulation scale during extremely severe drought events. More on the spatial pattern of MDS, it occurred as a common feature that the highest MDS values appeared in the region's south-eastern for the smallest scale accumulation. besides that, the maximum value of MDS appeared in the region's north-western area for the largest scale accumulation, with some spot cells located on extreme southern coastlines of the region.

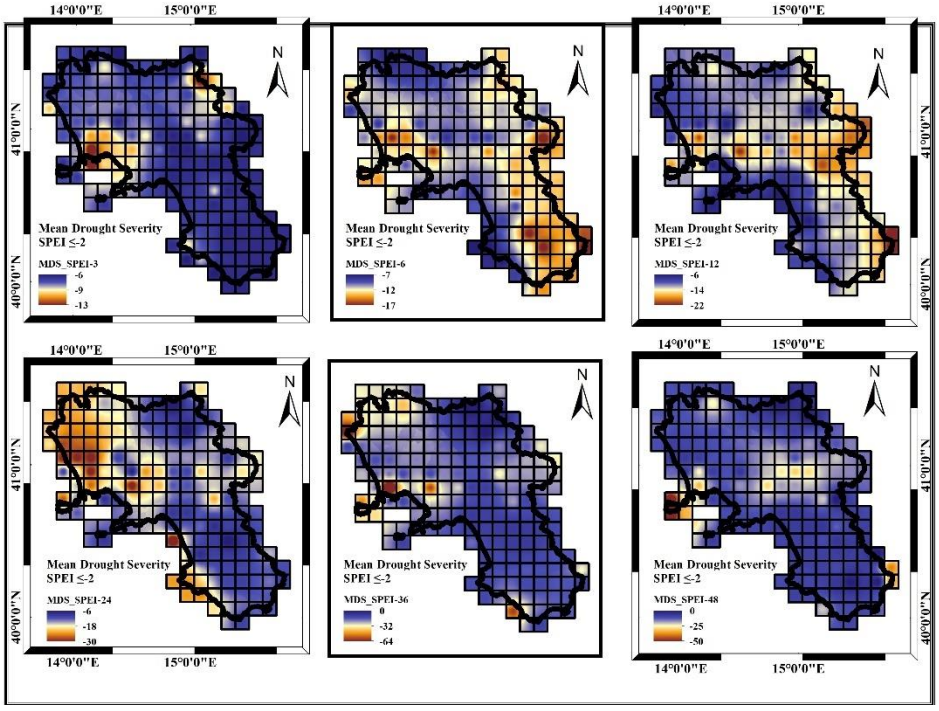

Figure 6.29: MDS (mean drought severity) for the different accumulation periods considered (SPEI ≤−2).

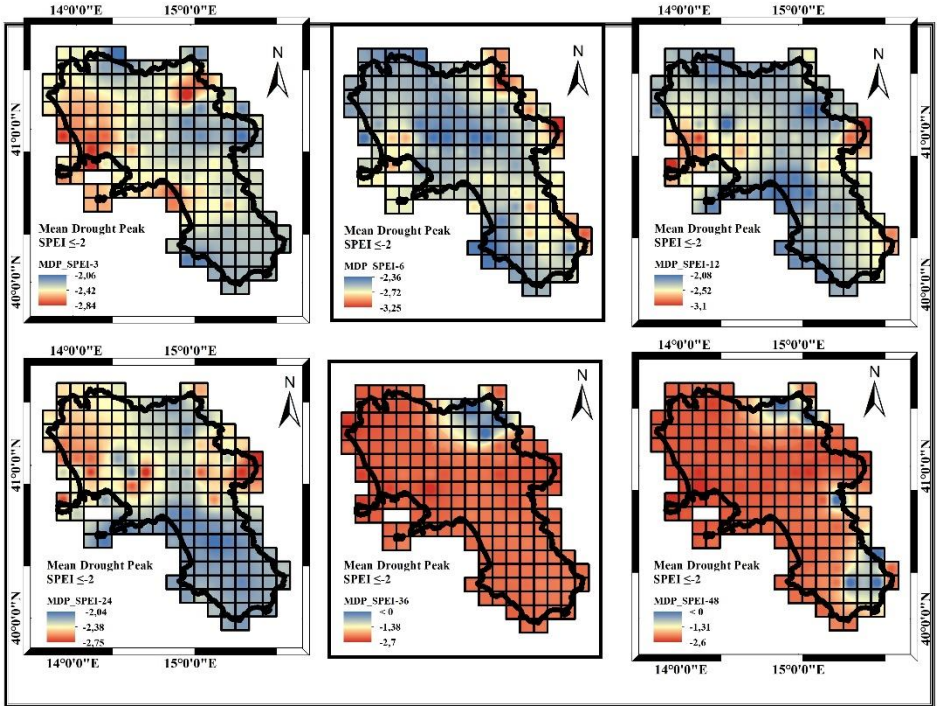

Figure 6.30: MDP (mean drought Peak) for the different accumulation periods considered (SPEI ≤ -2).

Finally, unlike the MDD and MDS, the MDP's minimum (about -1.4 on average) and maximum (about -2.9 on average) values for the various accumulation timescales appeared similar, and likely more pronounced for the lower accumulation timescales (-3.25 for SPEI 6). (Figure 6.30). The spatial pattern was discovered to be particularly complex, with no noticeable tendency related to the accumulation timescale (figure 6.22). Greater peaks remained concentrated in the region's north-western and north-eastern cells, but the area covered changed with accumulation timescale, becoming more moderate for the larger SPEI accumulation scale. In the case of the largest accumulation periods, SPEI 36 and SPEI 48, a large peak of -2.6

on average covered almost the entire study area, which is not the case when studying SPI patterns.

6.6 Assessment of the relationship between SPI and SPEI

Pearson correlation coefficient (PCC), also known as the product-moment correlation coefficient, was used to test the linear relationship between SPI and SPEI. According to Adler et al., 2010 and Giavarina (2015), PCC is the most commonly used statistical technique for determining how strongly two variables are related to one another. This is assisted by research from different fields of study that have successfully worked on and/or used PCC as a tool to test linear relationships between variables or methods (Hines et al., 1987, Artusi et al., 2002, Tsakiris et al., 2007).

Figure 6.31 shows that SPI and SPEI had a strong and significant relationship at all time scales ($r \geq 0.7$, $p < 0.01$).

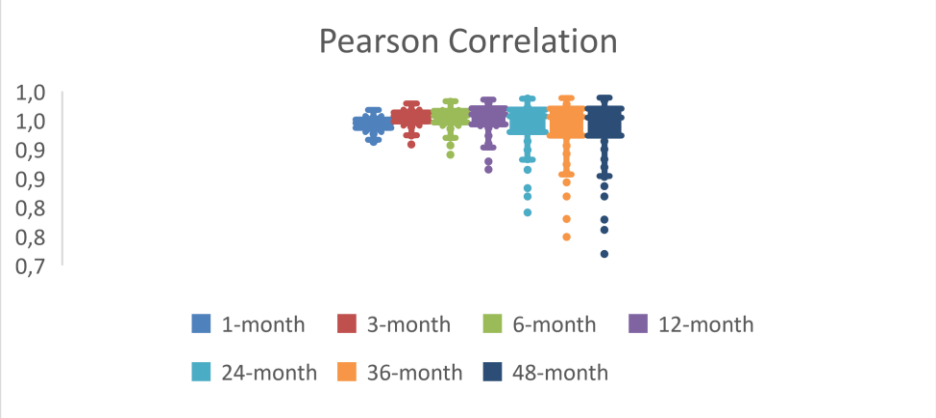

Figure 6.31: Pearson correlation coefficient (PCC) for different time scales

Figure 6.32 compares the SPEI and SPI in terms of drought characteristics (duration, severity, and peak). In terms of duration, the graph shows nearly identical results for both indices. Because the durations have a similar distribution, the two

indices describe the drought in the same way in terms of timing. In terms of severity, the figure shows that the SPI is possibly more severe than the SPEI; additionally, the SPI has a slightly higher interquartile range, indicating that its distribution is heavier in the center; these differences result from the distribution type used in the calculation of the SPEI (Log-logistic distribution). In addition, overall, the average values of the peaks are very similar to each other. In terms of average values, perhaps the SPI has a slightly wider interquartile range, and it is always may due to the distribution fact.

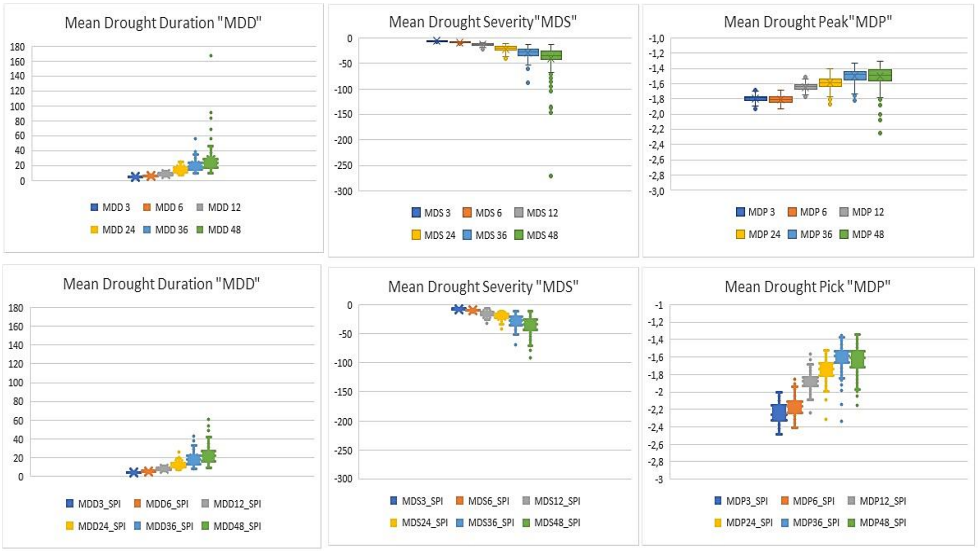

Figure 6.32: Drought characteristics for both indices SOI and SPEI (first row correspond to SPEI and the second to SPI)

Moreover, figure 6.33 shows an example about how SPI and SPEI behave within a drought event in different time scales (drought event of 2017). The figure shows that SPI is slightly more severe than SPEI, this was due to the consistent lack of rain since December 2016, especially during spring 2017 (http://edo.jrc.ec.europa.eu/).

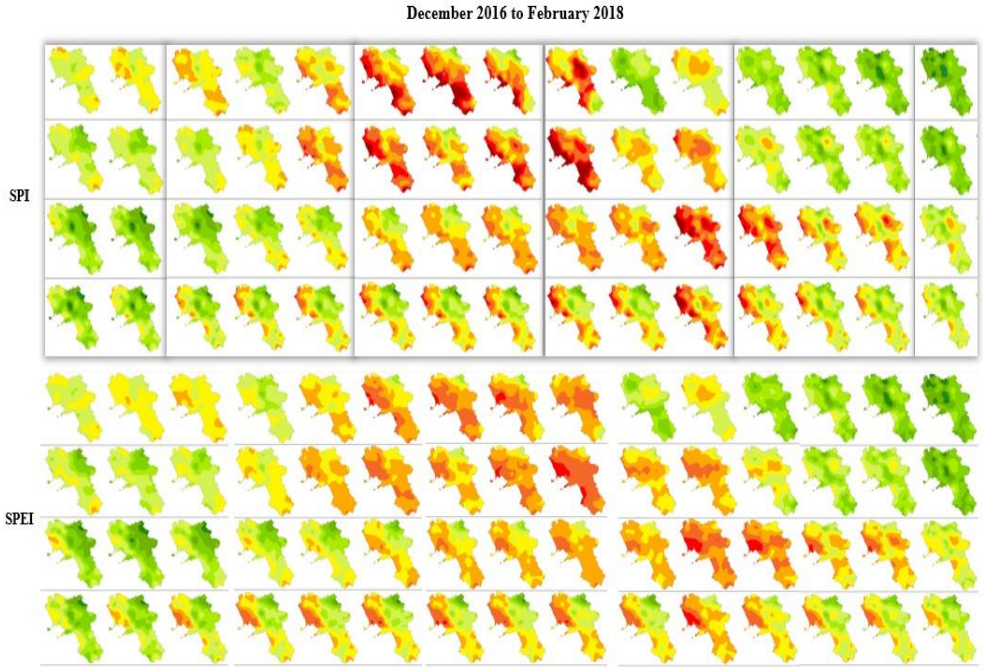

Figure 6.33: Drought event of the 2017 by SPI and SPEI indexes

6.7 Overall evaluation

Concerning the drought temporal features, the trend was found to be dominantly negative, and the percentage of impacted cells increased with accumulation scale. It remained almost similar for SPI/SPEI time series computed over 24 months or longer intervals. The significance was also found to be particularly evident approaching 70 % of grid cells for SPI_24/SPEI_24. Beyond this timescale threshold, significance in temporal variability strongly decreased. The SPI increase over time, ranging from about 10 % in 10 years for the case of SPI/SPEI_6 and 24 % for the SPI/SPEI_48. In the case of moderate dry conditions, MDD increased with the accumulation timescale, ranging from about 5 months for the SPI_6 to 60 months for the SPI_48 where for the SPEI MDD ranging from 4-5

months for SPEI 3 to 9-167 months for SPEI 48. Accordingly, MDS increased with accumulation scale, moving from about −10 in the case of SPI_6 to about −50 in the case of SPI_48, and from -6 in the case of SPEI_3 to -270 for the SPEI_48. MDP did not change significantly for both indices with the accumulation scale and was particularly pronounced in the case of the shorter temporal scales. Extremely severe events were featured by shorter durations and larger severity compared to the moderate drought events but were much less frequent (over 75 % less then).

In term of spatial pattern, the negative trends appeared to occur along a northwest to southeast transect, whereas positive trends were focused along a west–east transect at the middle latitude of the region. These areas are respectively featured by large mean annual precipitation coupled with the largest negative trends and by low to moderate mean annual precipitation and lowest negative trends. Those two regions are quite different in terms of orography. While the first is characterized by mountainous relief approaching or close to the coastline, the second features a large plain devoted to agricultural practices, crossed by the longest river of the region, the Volturno River, which probably represents an access corridor to atmospheric weather systems. The complex orography of the region appears then to impact both the average precipitation spatial distribution and the relevant temporal variability. The accumulation timescale affected the MDD spatial behavior. At the lowest accumulation scale, the northern area appeared to be more affected, whereas large MDD values were detected along a northwest to southeast transect and were however more evident in the southern sectors of the region. The maximum values detected in the southern area for the longer accumulation timescale were mainly caused by severe drought periods occurring in 1990, 2003 and 2017 in the region. The MDS spatial pattern was also affected by accumulation scale. It showed a concentration on the northern region area for the shorter temporal scales and instead a constant spatial distribution for the longer temporal scales, with an exception for a

northwest to southeast transect and for the southern sectors of the region where the largest MDS values were detected. In the end, the MDP spatial pattern was found to be particularly complex and did not show a clear tendency related to the accumulation timescale. At least for the shorter timescale, the largest drought peaks seemed concentrated on the norther inland area of the region, which overall could be addressed as an area potentially prone to agricultural drought stress.

6.8 Summary

Drought is defined as a prolonged period of lower-than-normal water availability. It is a recurring and global phenomenon, but the Mediterranean Basin is regarded as a particularly vulnerable environment in this regard. The primary goal of this study was to assess drought characteristics in the Campania region of southern Italy by analyzing the spatial and temporal pattern characteristics of SPI time series computed at different accumulation scales over a centennial period from 1918 to 2019. To describe the temporal trend significance and magnitude, the modified Mann–Kendall test and Sen's test were used. Furthermore, for both moderate (SPI≤ -1) and extremely severe (SPI≤ -2) drought conditions, the "run theory" (Yevjevich, 1967) was used to illustrate the frequency, duration, peak, and severity of drought events. The current study demonstrated how historical in situ long-term measurements are critical for understanding historical drought conditions and planning mitigation strategies to deal with future climate change impacts. As a result of the findings of this study, it is possible to conclude that SPI and SPEI performs similarly in the Campania region. However, the relationship and agreement analyses revealed that SPI can be used in place of SPEI at all time scales and vice versa, despite the fact that the two indices agreed to some extent. Hence, in the absence of temperature data and/or appropriate analysis tools to perform SPEI, it is safe to

conclude that SPI can be used to assess drought in the study area at all investigated time scales.

Chapter 7

DROUGHT HOT SPOT ANALYSIS USING LOCAL INDICATORS OF SPATIAL AUTOCORRELATION

7.1 Overview

The following work aims to analyse drought as seen through the SPI and SPEI climate indicators and water stress on vegetation measured through the NDVI vegetation index, limiting considerations to the Campania Region, in order to delineate any connections that are present between the two drought phenomenon.

7.2 Assessment of different historical drought events in the Campania Region

7.2.1 Comparison of SPEI and NDVI

7.2.1.1 Drought event of the year 2003

One of the most well-known and severe droughts to affect Italy - and the rest of Europe - was the summer of 2003, when there was an extraordinary heatwave

with average temperatures exceeding 40°C. According to reports, the event lasted from May to the end of August. Figures 7.1-7.9 depict the temporal evolution of the 2003 drought in terms of SPEI aggregated at various time scales.

The meteorological drought, as depicted by the SPEI on a three-month scale, began in March 2003, a few months earlier than what was reported in the bibliographic record. In fact, small yellow "spots" can be seen near the border with Basilicata. The phenomenon appears to end in October 2003, restoring normalcy (green), but then resumes with less intensity until February 2004, when the last signs of a moderate drought appear (orange). In this case, the drought peaks in July 2003, with drought values ranging from severe to extreme (orange, red, and dark red) in the provinces of Caserta and Naples.

The 6-month scale depicts an agricultural drought that began in March 2003 with moderate SPEI values (yellow) and ended between February and April 2004 with very mild (yellow) and localized effects in small areas. The most severe moment occurred in August 2003, surpassing the severity of the SPEI 3 peak. The indicator's extreme values cover the entire Campania Region (dark orange and red).

On a 12-month scale, the drought begins slowly and almost invisible between May and July 2003; however, it quickly expands, reaching the most critical effects on the hydrological compartment in January 2004, when the Provinces of Caserta and Naples are characterized by moderate to severe dry conditions. The return to normalcy occurs after April 2004, when the effects of moderate drought are still visible (orange).

This was also a drought that affected almost the entire Campania Region, with the effects being most severe along the Tyrrhenian coast. The Apennines are rarely affected by the drought event, with the exception of a few instances, such as August 2003 (6 months scale) with extreme values (dark red) and other rare instances with moderate SPEI values (orange).

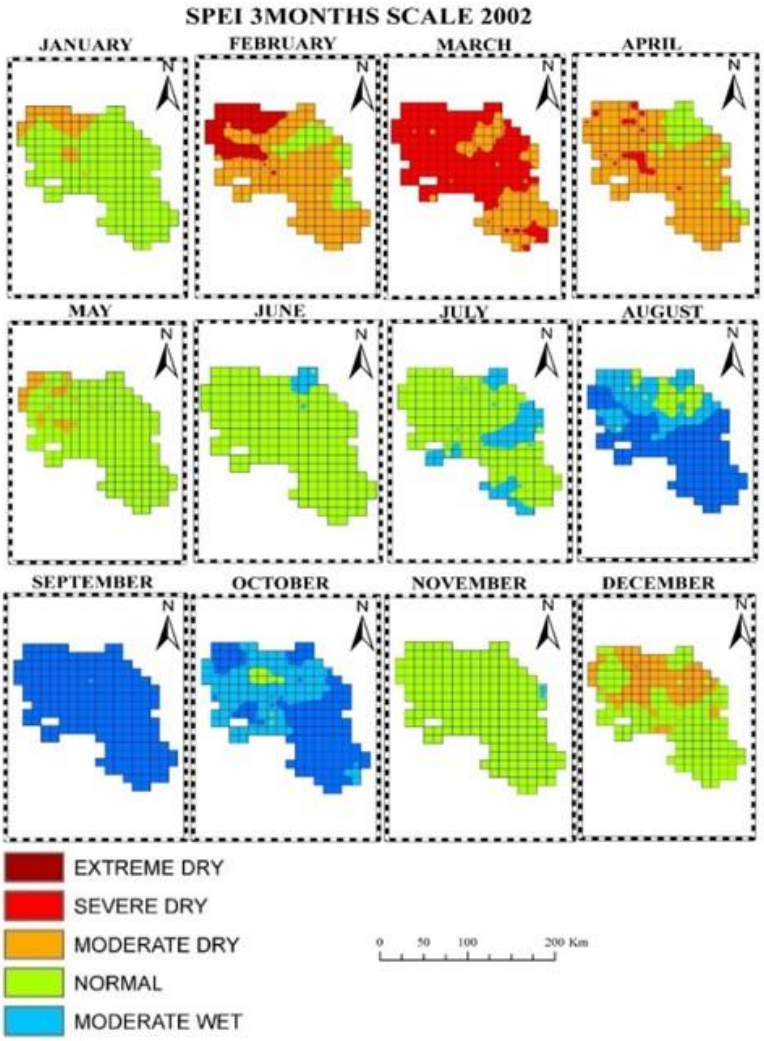

Figure 7.1: SPEI map of the year 2002 on a 3-month scale

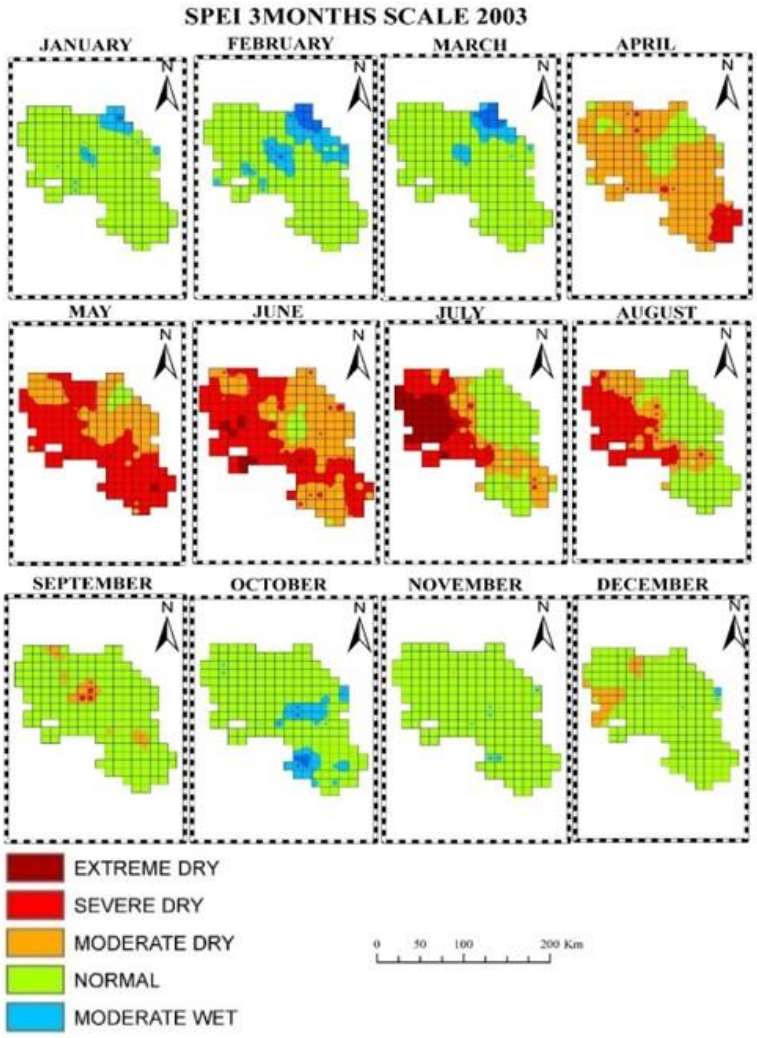

Figure 7.2: SPEI map of the year 2003 on a 3-month scale

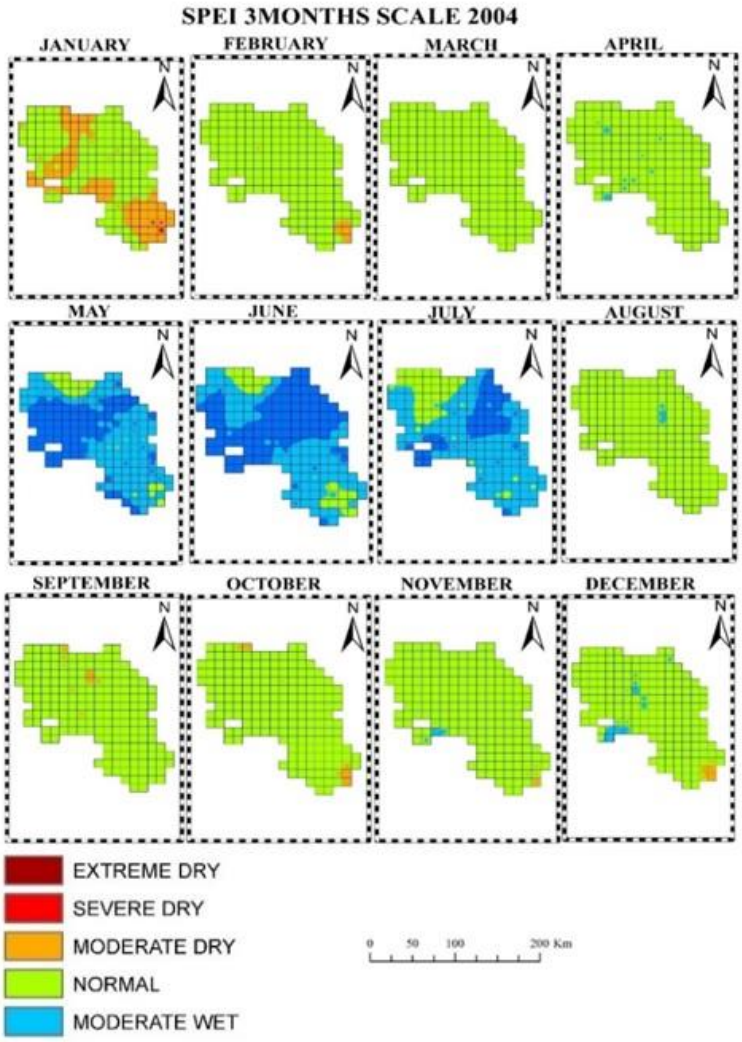

Figure 7.3: SPEI map of the year 2004 on a 3-month scale

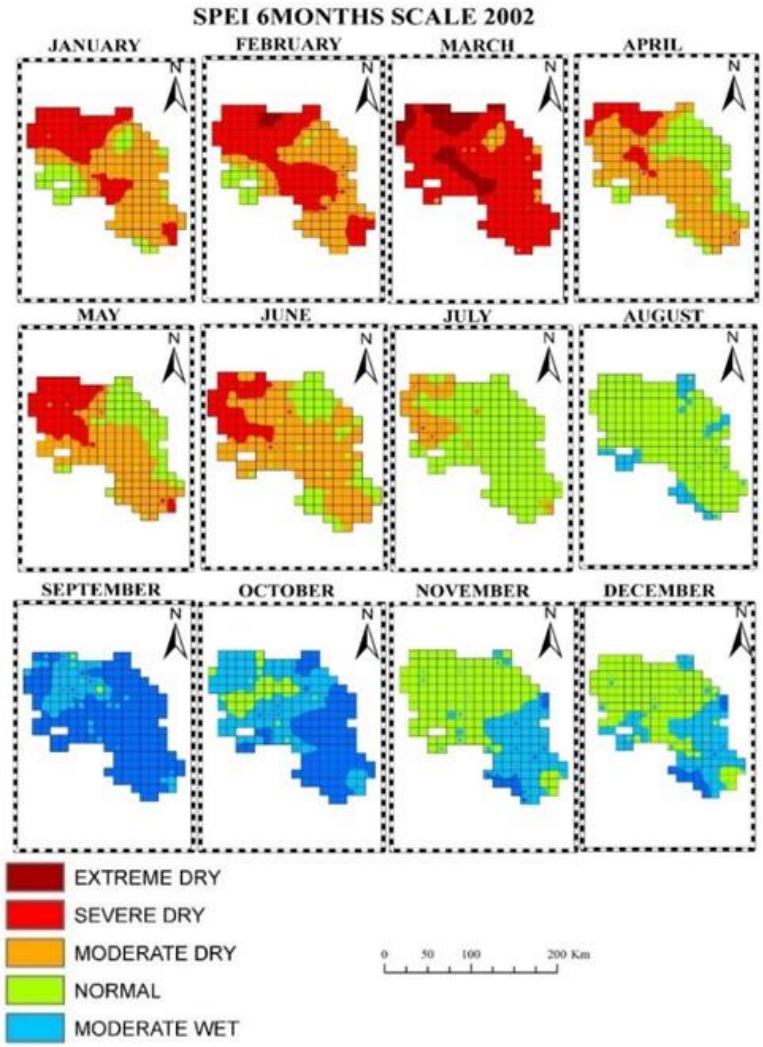

Figure 7.4: SPEI map of the year 2002 on a 6-month scale

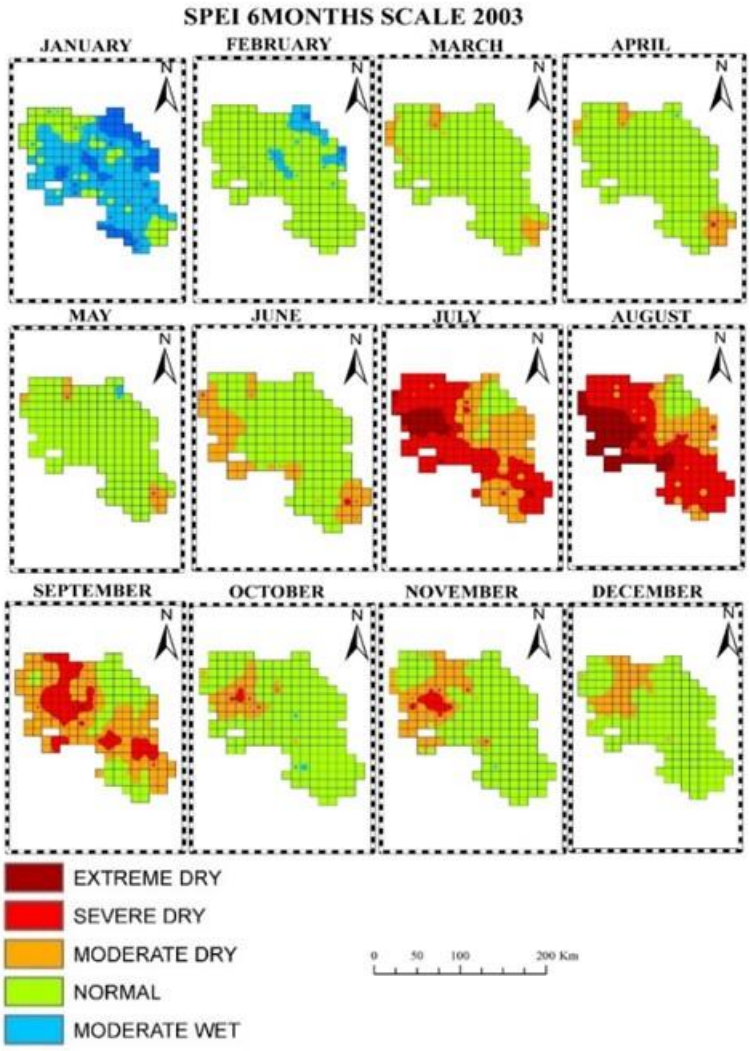

Figure 7.5: SPEI map of the year 2003 on a 6-month scale

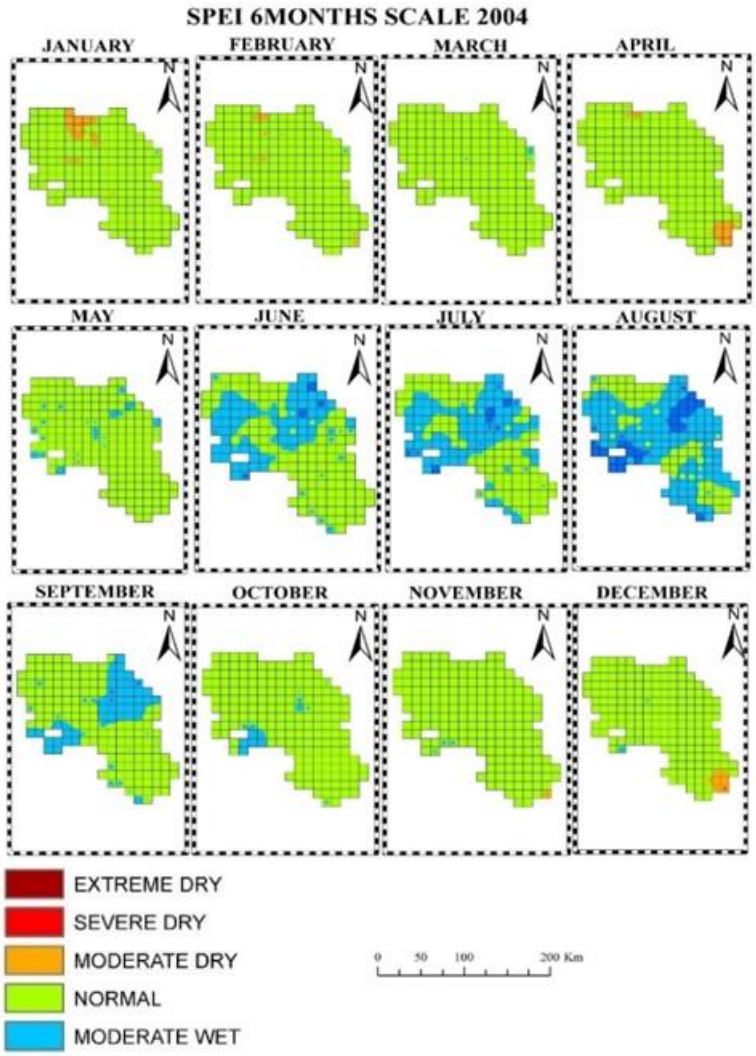

Figure 7.6: SPEI map of the year 2004 on a 6-month scale

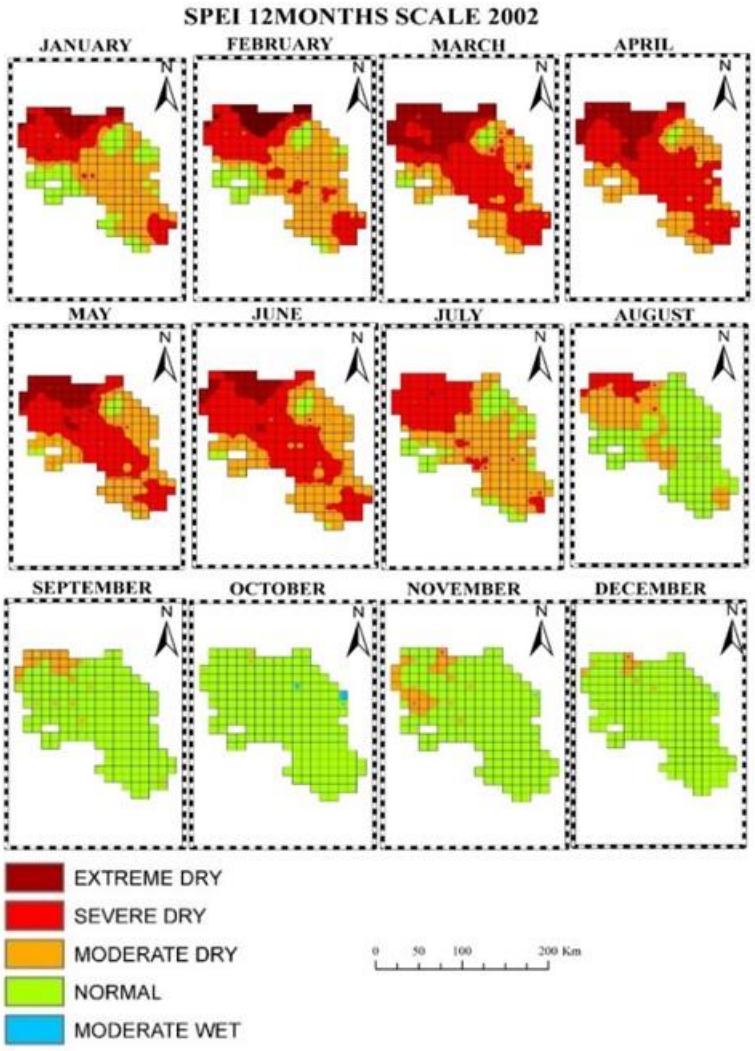

Figure 7.7: SPEI map of the year 2002 on a 12-month scale

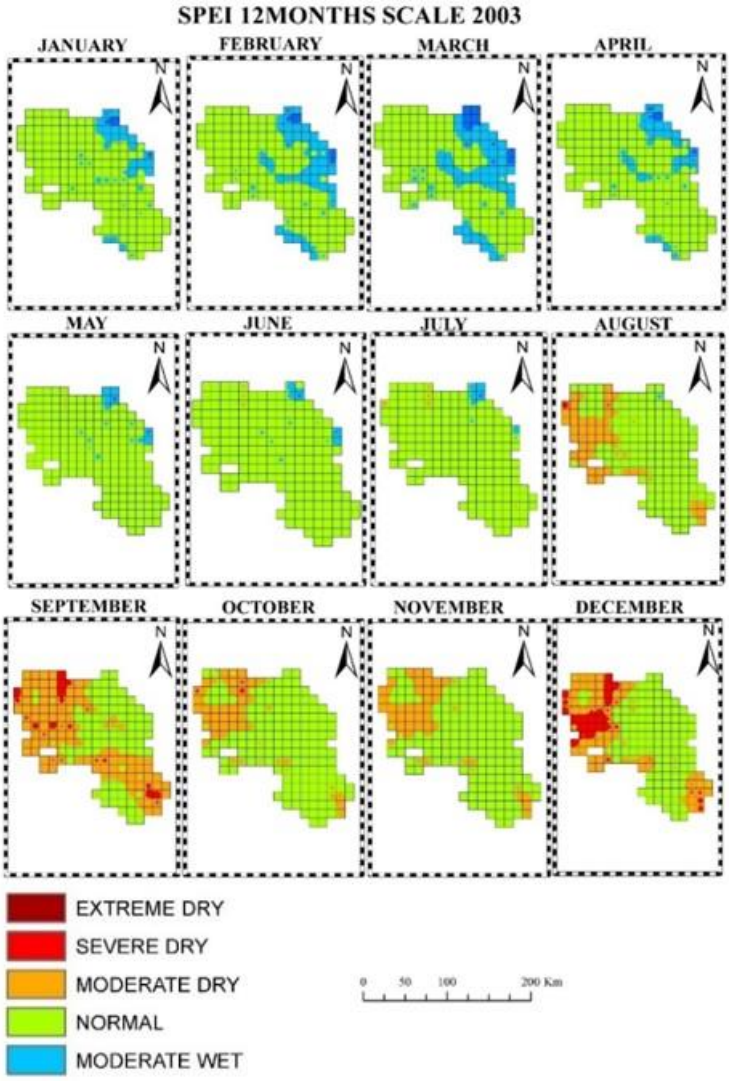

Figure 7.8. SPEI map of the year 2003 on a 12-month scale

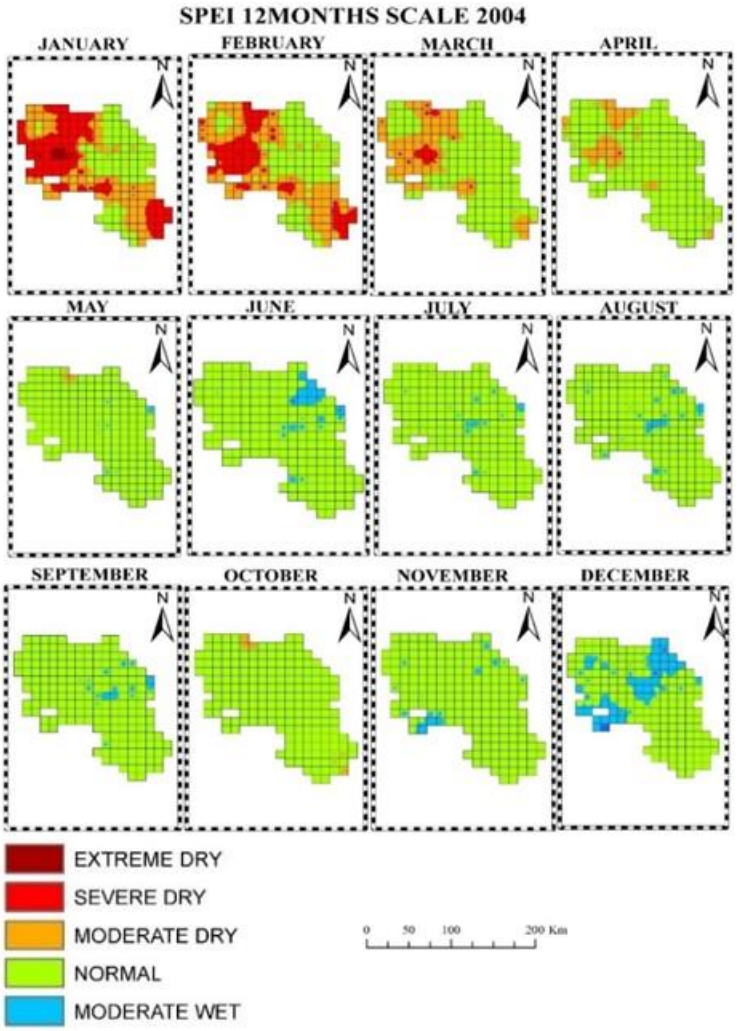

Figure 7.9: SPEI map of the year 2004 on a 12-month scale

The NDVI maps (Figure 7.10-7.12) show, on the one hand, the seasonality of the vegetation, while, on the other hand, only in 2003 is there a slight reduction of dense vegetation (dark green), but during the winter period there is a condition of scarcity (green) and severe scarcity (light green) until February 2004. The Mediterranean bush is not uniform across the entire coastal territory; in fact, because

of the different conformity of the ground, it allows different types of plants to grow, which also depends on rainfall; in places where it is scarcer, the vegetation becomes more rugged.

Because vegetation growth is comparable to that of a normal year, it is impossible to say definitively that meteorological drought corresponds to vegetation stress.

EVI (Figure 7.13-7.15) shows that there is no green cover in the area perpendicular to the Apennines in February 2004, as there was in February 2002. This phenomenon, however, does not appear to be related to the 2003 drought.

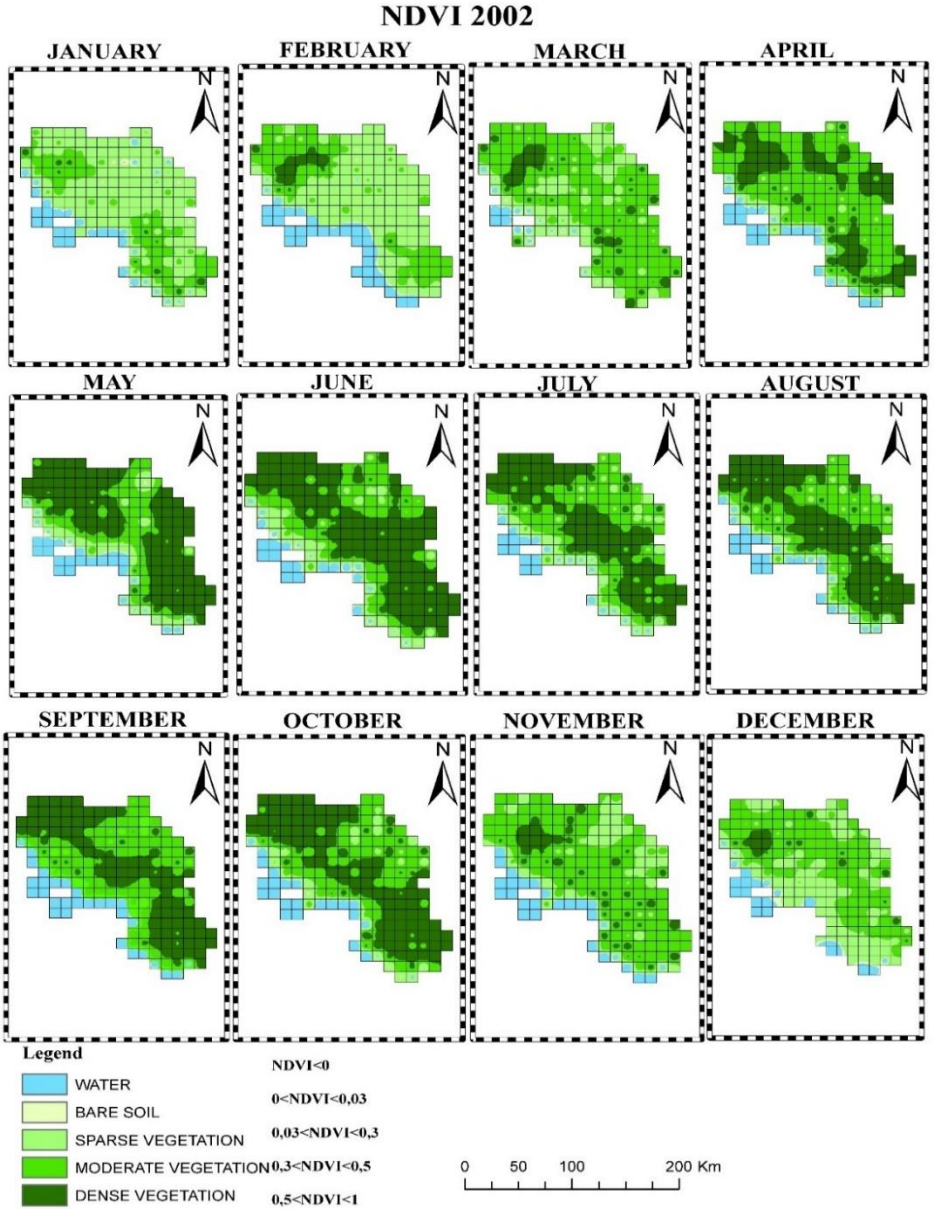

Figure 7.10: NDVI map of the year 2002

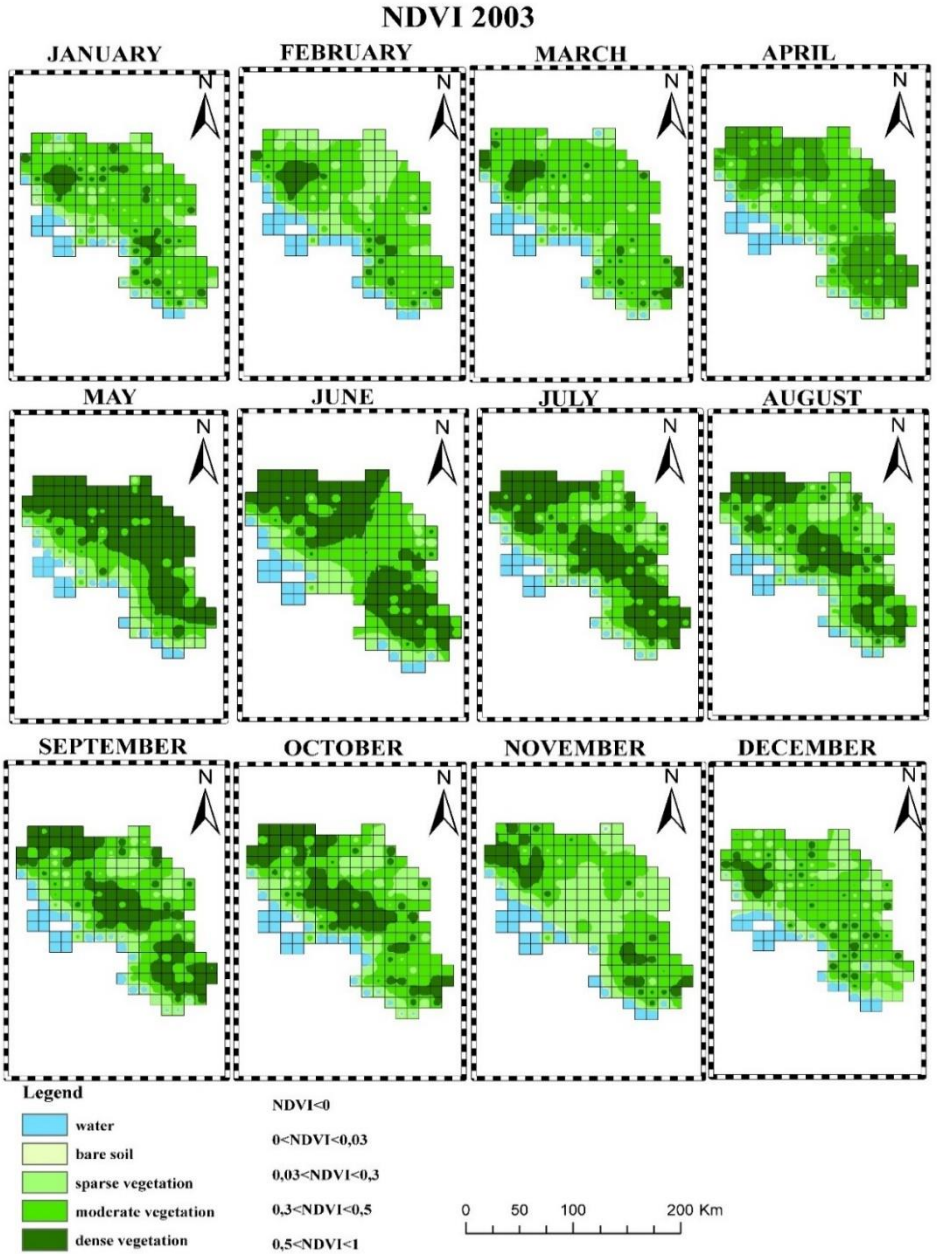

Figure 7.11: NDVI map of the year 2003

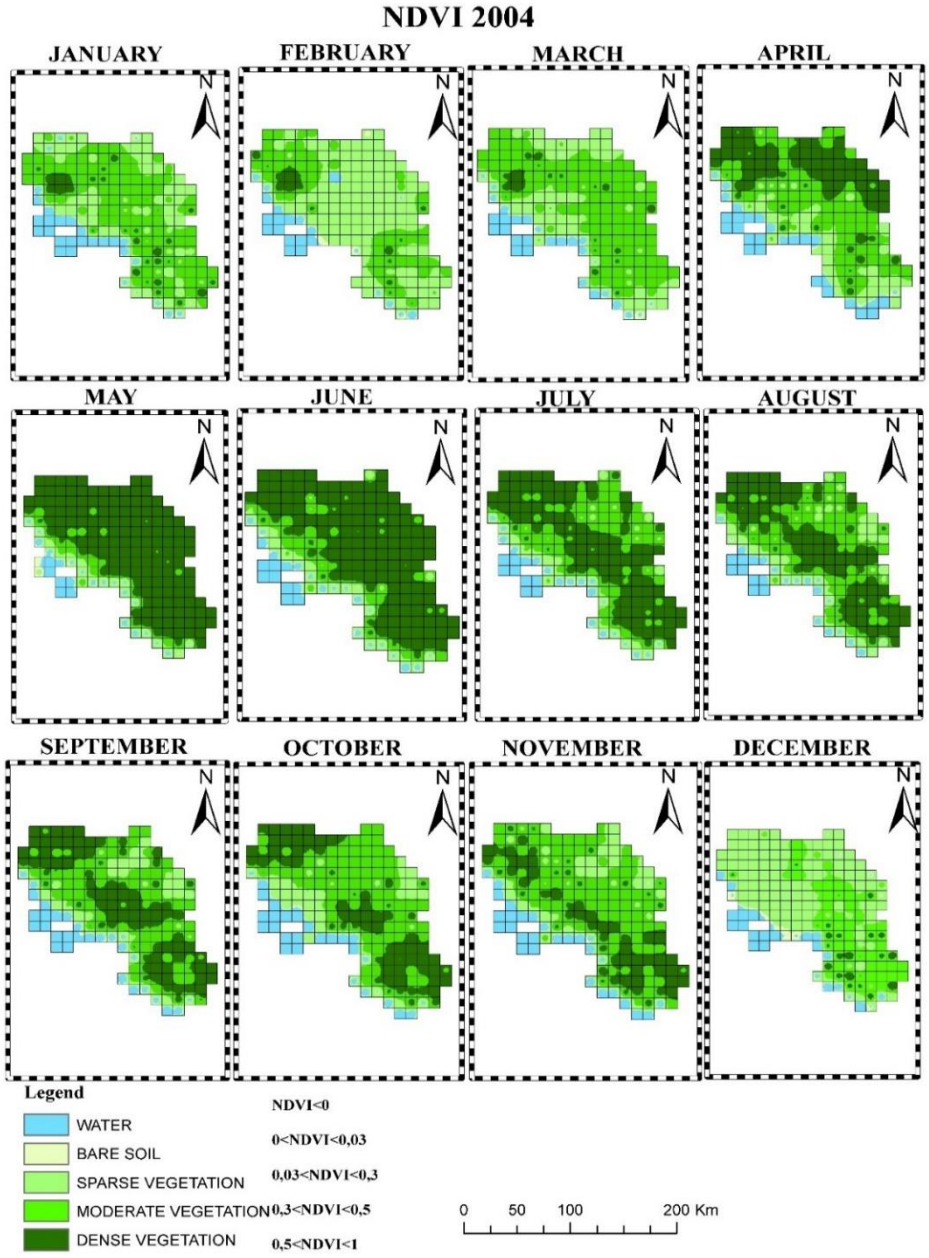

Figure 7.12: NDVI map of the year 2004

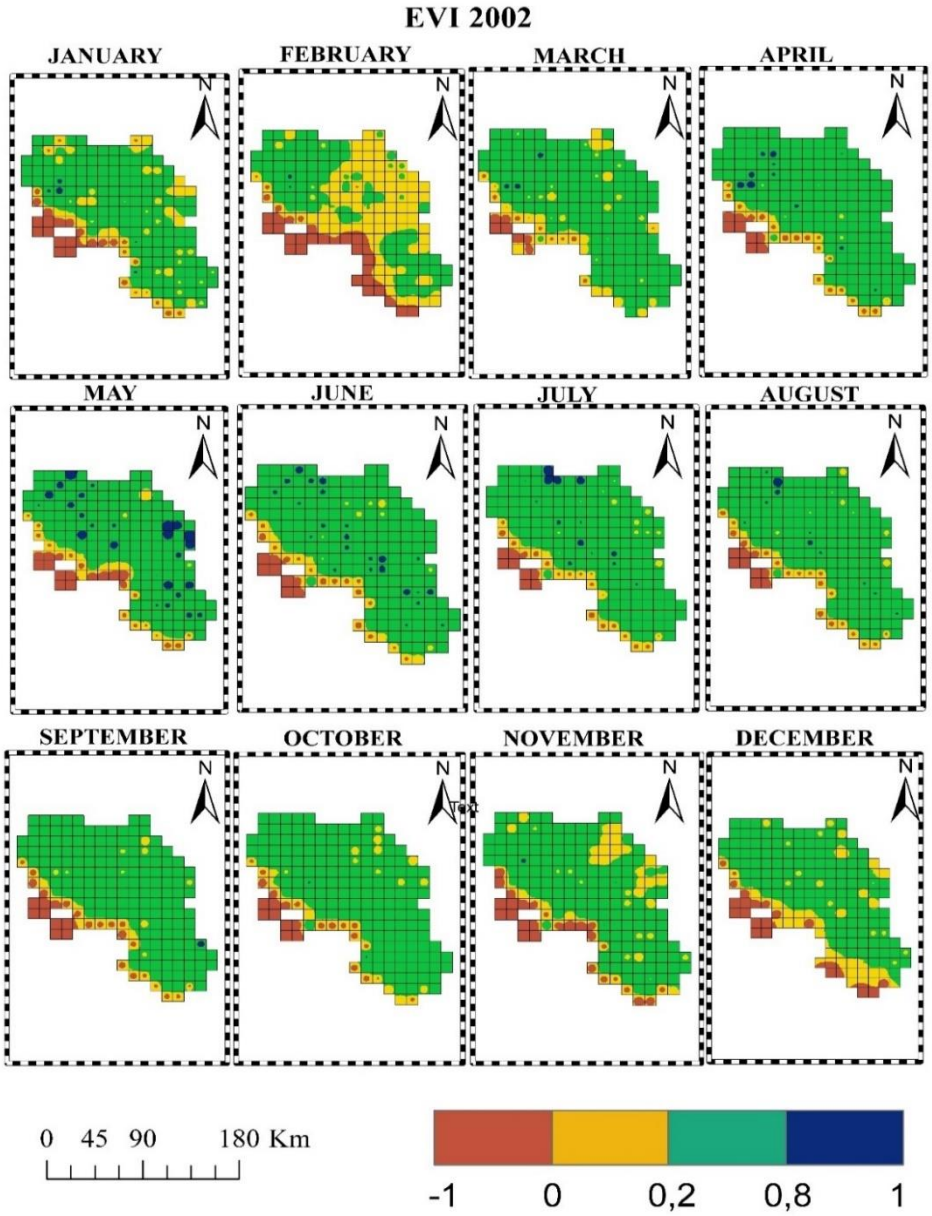

Figure 7.13: EVI map of the year 2002

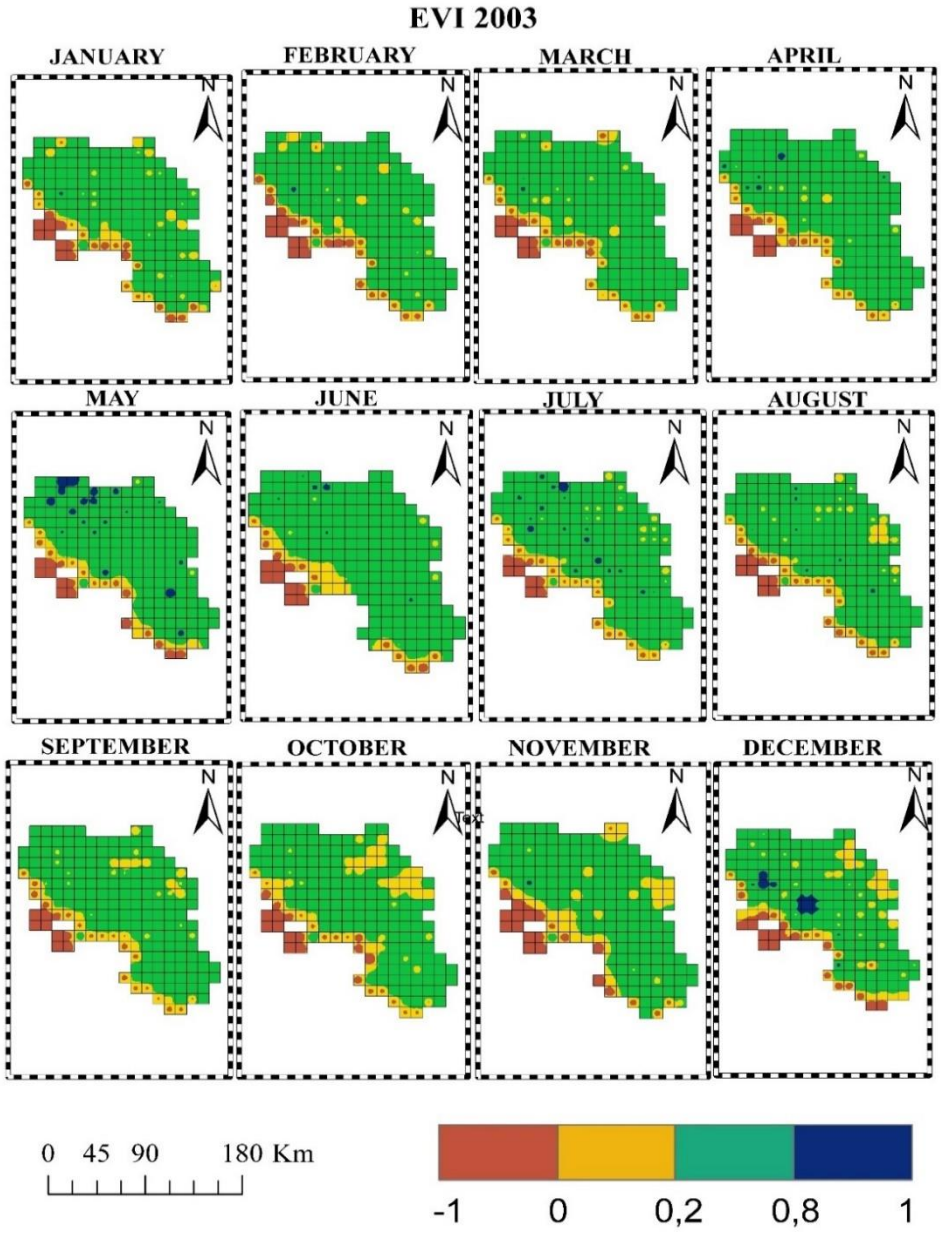

Figure 7.14: EVI map of the year 2003

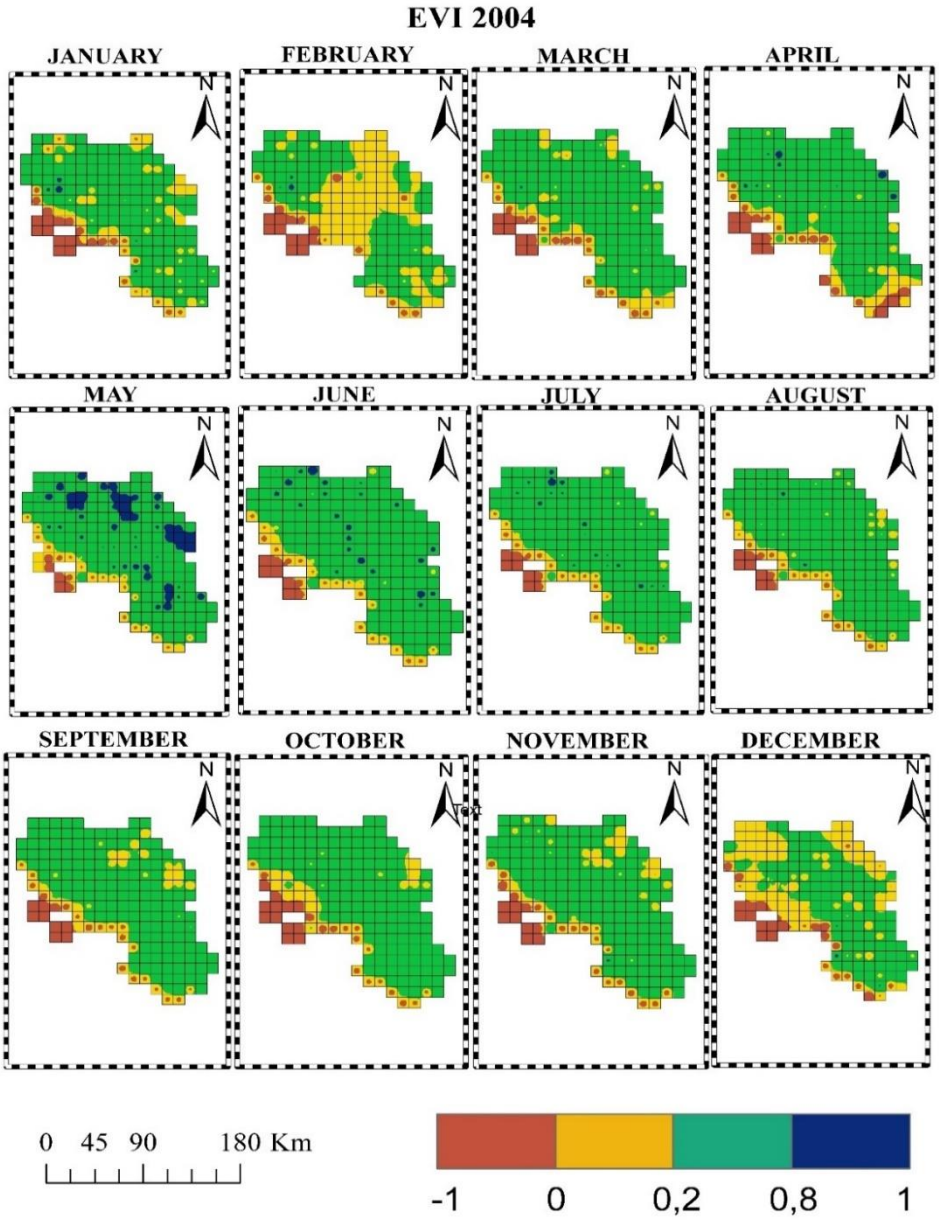

Figure 7.15: EVI map of the year 2004

7.2.1.2 Drought event of the year 2017

The 2017 drought began in December 2016 as a result of a large rainfall deficit, which was concentrated in both winter and the following spring. Furthermore, there were heat waves of unprecedented magnitude in the summer, with temperatures reaching 40°C. As a result of this event, many regions were forced to declare a state of water crisis, and the government declared a national emergency.

For smaller time scales, the SPEI index perfectly illustrates the effects of different drought declines since December 2016, but the duration of the drought event does not match the information collected.

On a 3-month scale, the meteorological drought will continue until December 2017, after which the study region will turn green. Between May and July of this year, the most severe effects are visible. During these months, severe to extreme SPEI index values (red and dark red) cover almost the entire Campania Region, with only moderate (orange) values in the Apennines. The most severe values are found along the Tyrrhenian coast, specifically in Caserta, Salerno, and, to a lesser extent, Naples.

At the 6-month aggregation scale, agricultural drought continues into January 2018, with areas still experiencing moderate drought (orange). The severity of the storm peaked in August of 2017. During the peak month, the entire Campania Region is in a critical situation, with very extreme conditions (dark red) in the Provinces of Caserta and Salerno.

The 12-month scale captures the effects of the 2015 drought on the hydrological compartment, which lasted until the end of 2016 with moderate drought conditions (orange with small areas of red) localized along the Tyrrhenian coast; the drought gradually expands spatially, until it subsides in February 2018. The most severe conditions can be attributed to the month of October 2017, when very extreme

drought conditions (dark red) were observed for the first time at the highest aggregation scales, primarily in the Province of Caserta.

The 2017 drought event affected a large area, completely affecting the Campania Region, with very severe effects on the Tyrrhenian coast and less severe internal effects towards the Apennines..

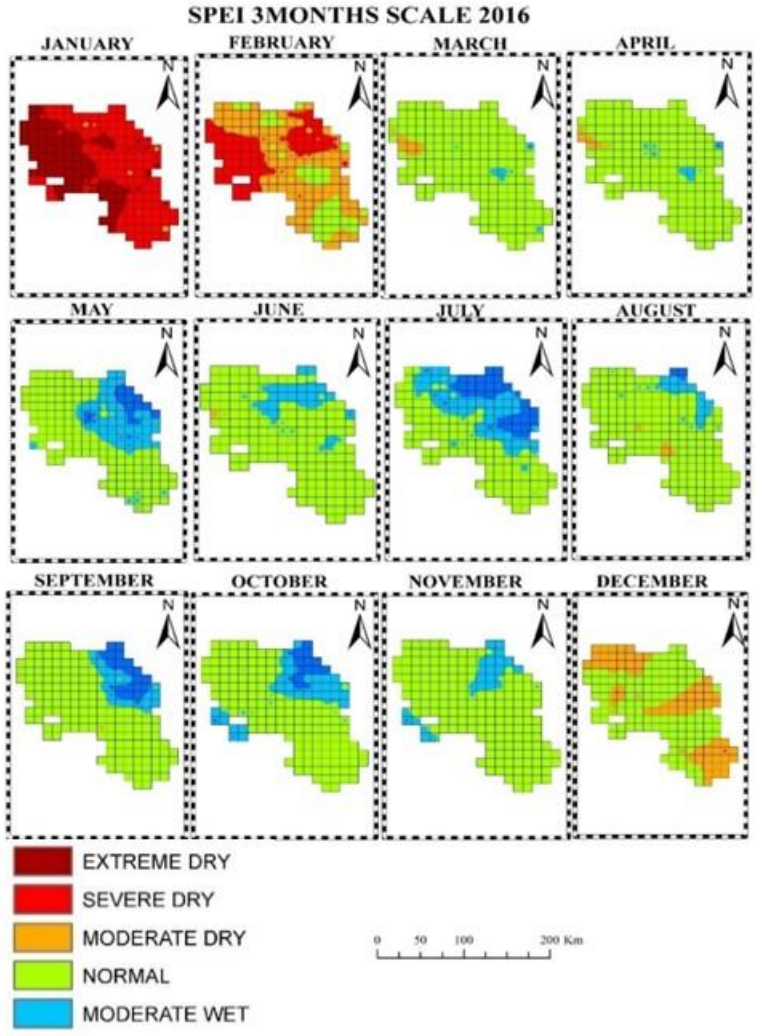

Figure 7.16. SPEI map of the year 2016 on a 3-month scale

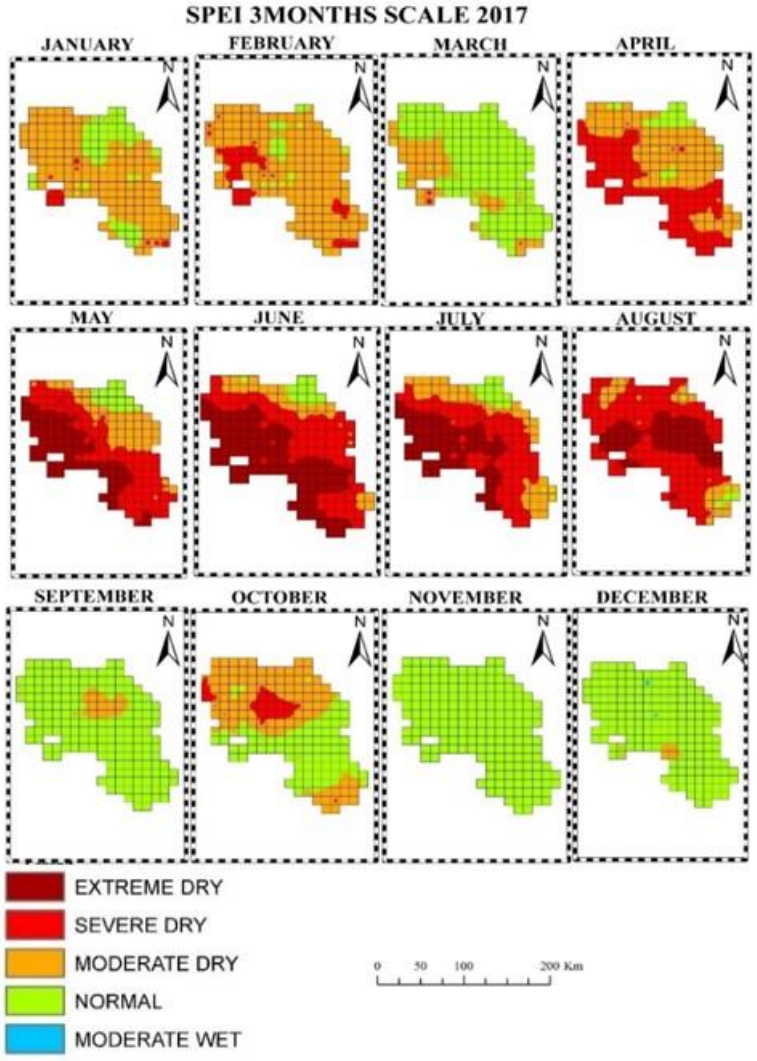

Figure 7.17. SPEI map of the year 2017 on a 3-month scale

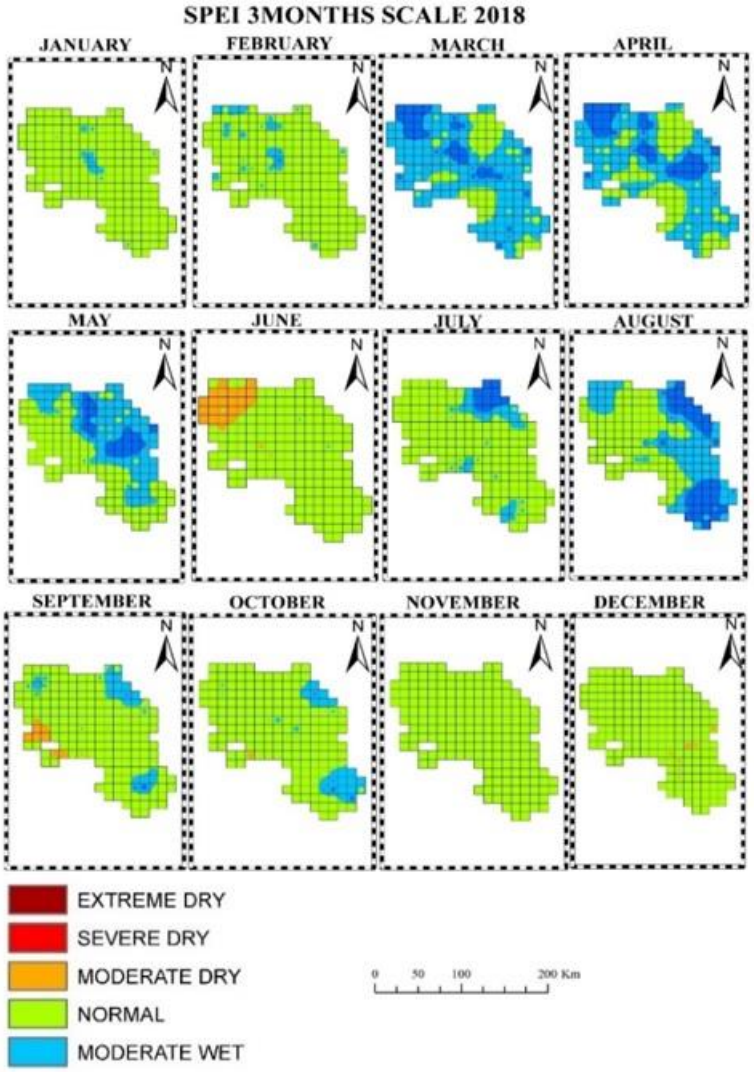

Figure 7.18. SPEI map of the year 2018 on a 3-month scale

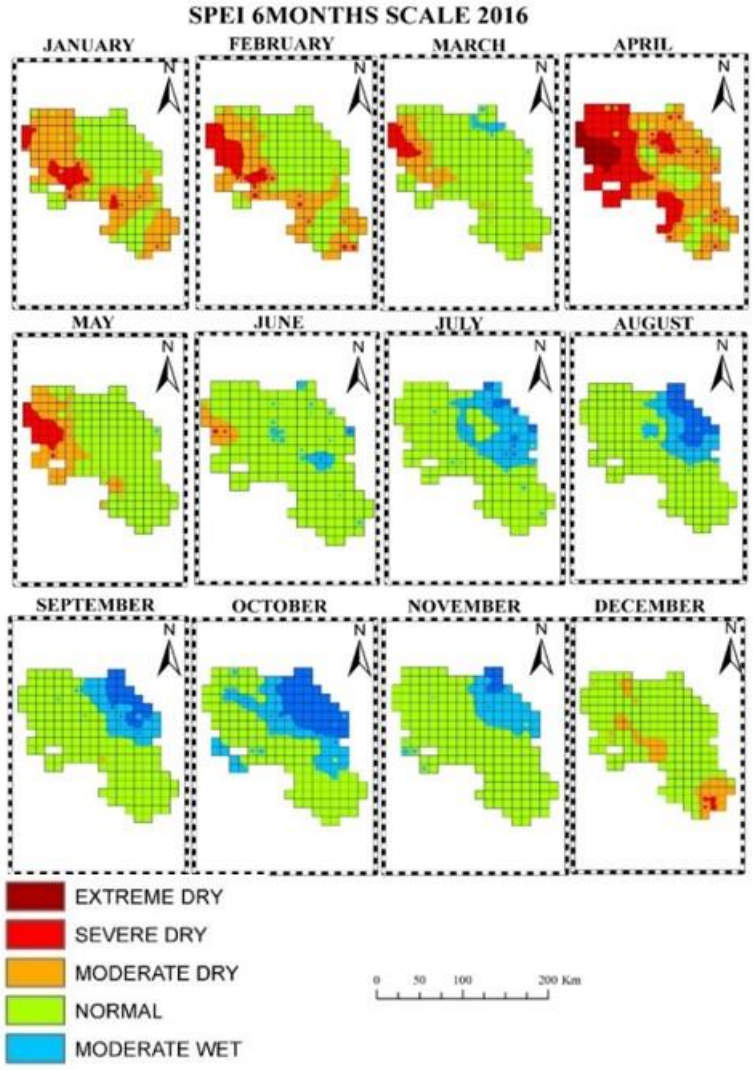

Figure 7.19. SPEI map of the year 2016 on a 6-month scale

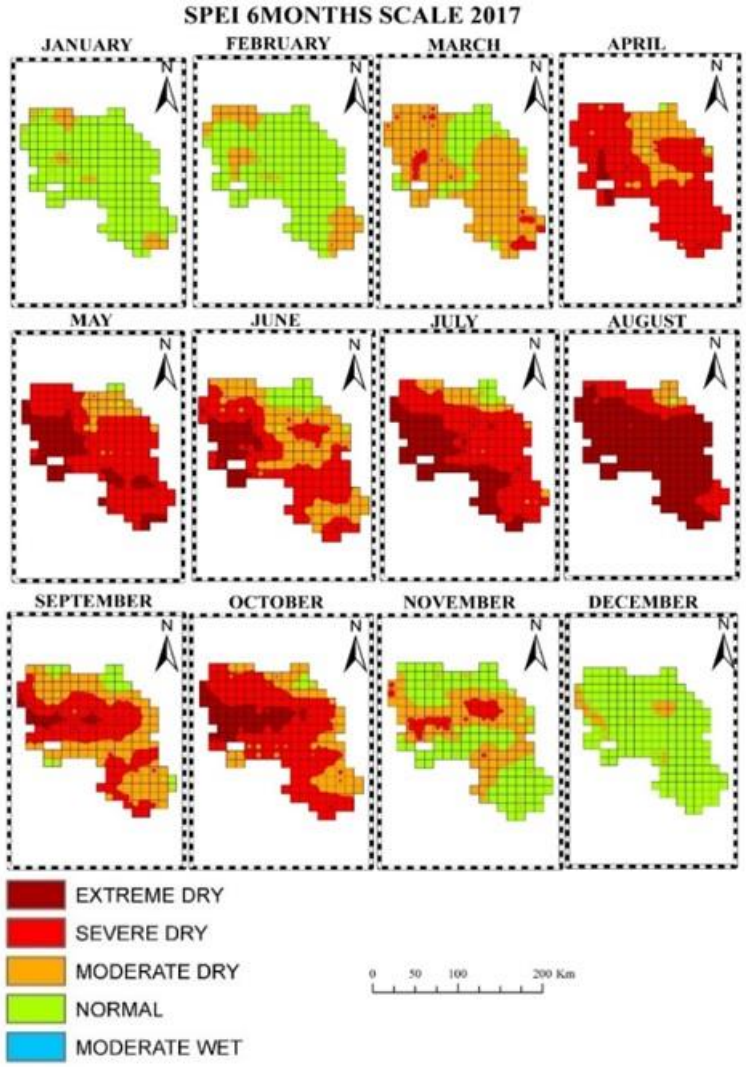

Figure 7.20. SPEI map of the year 2017 on a 6-month scale

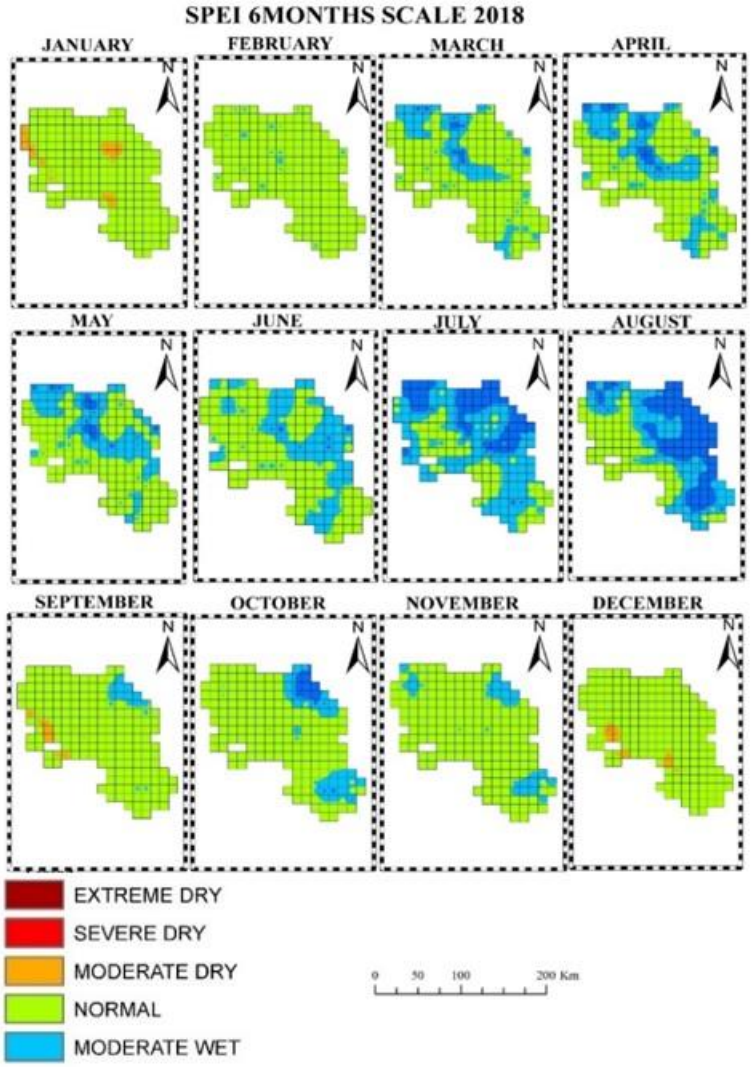

Figure 7.21. SPEI map of the year 2018 on a 6-month scale

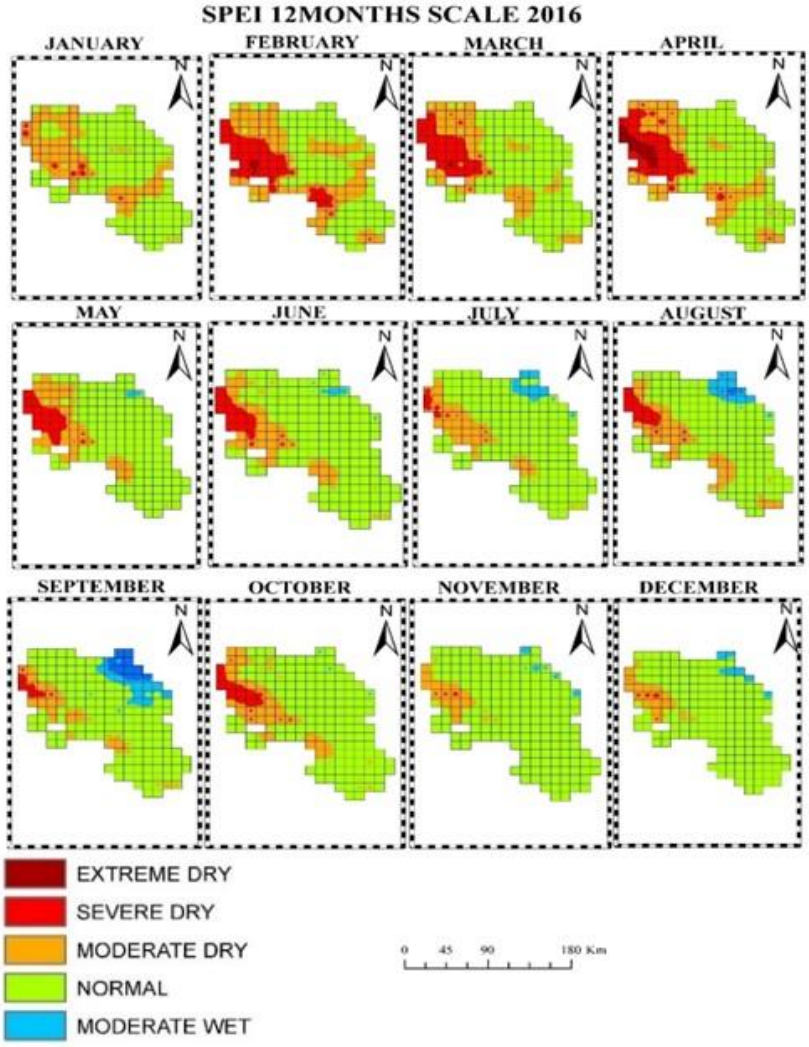

Figure 7.22. SPEI map of the year 2016 on a 12-month scale

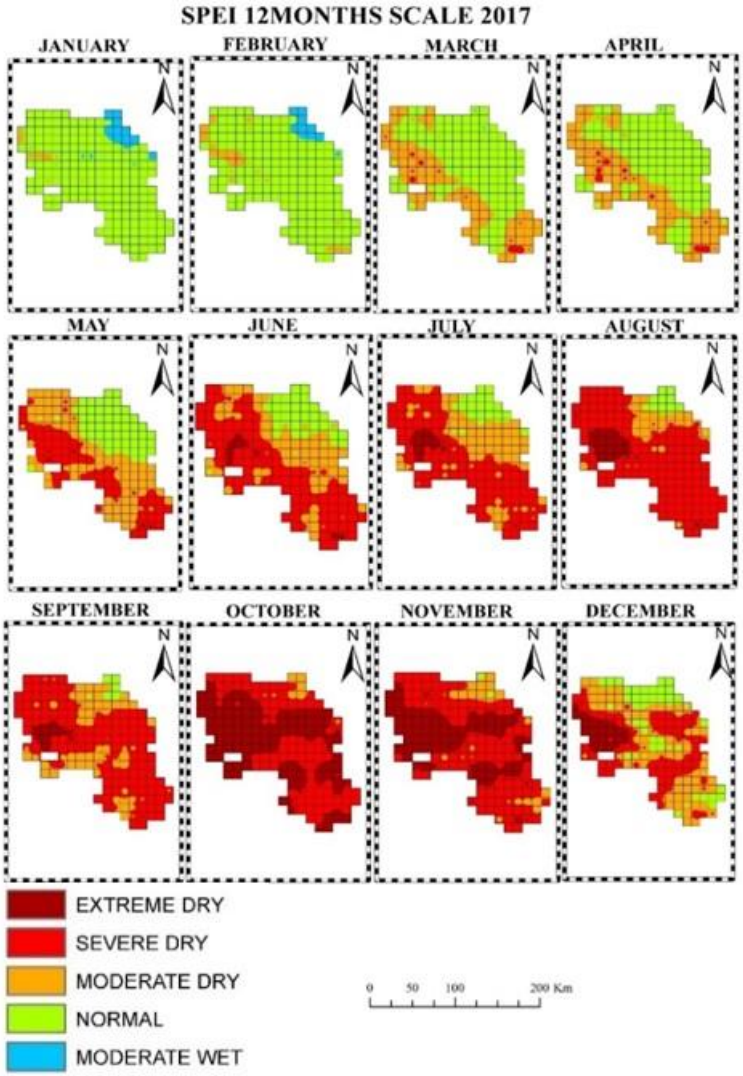

Figure 7.23. SPEI map of the year 2017 on a 12-month scale

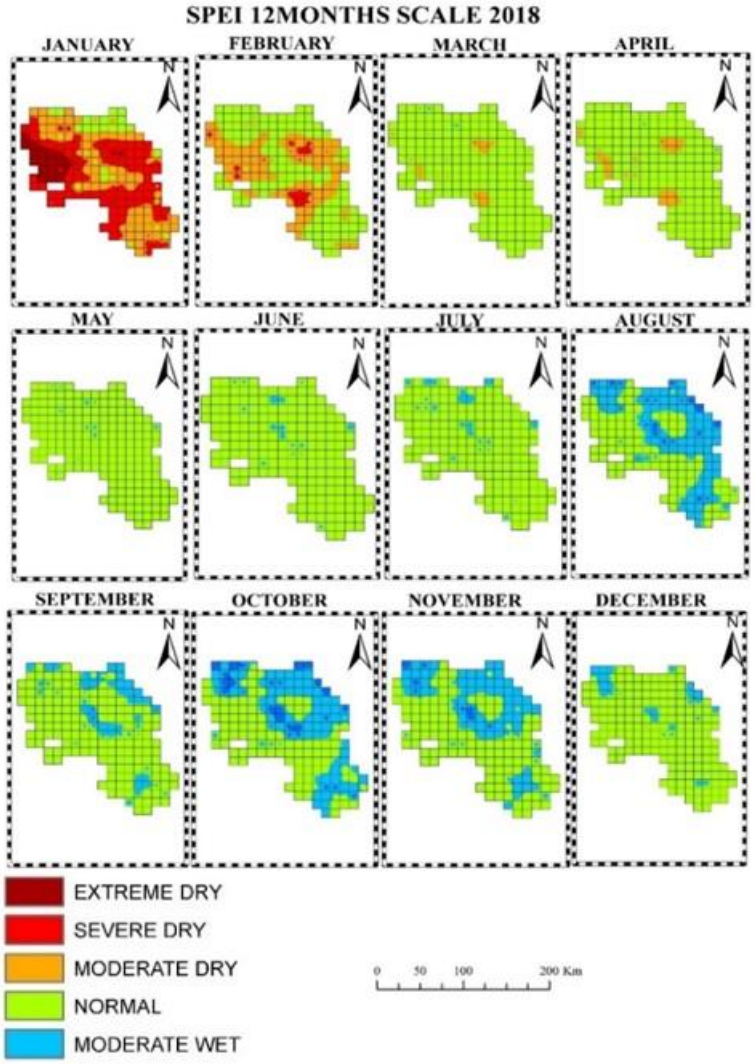

Figure 7.24. SPEI map of the year 2018 on a 12-month scale

The NDVI and EVI for this drought event show no signs of vegetation stress or loss of green cover. This also results in insufficient information for the year 2003, because it was a very dry year compared to 2017, and a more severe effect on

vegetation should have been obtained; thus, vegetation indices (NDVI and EVI) do not reflect drought conditions.

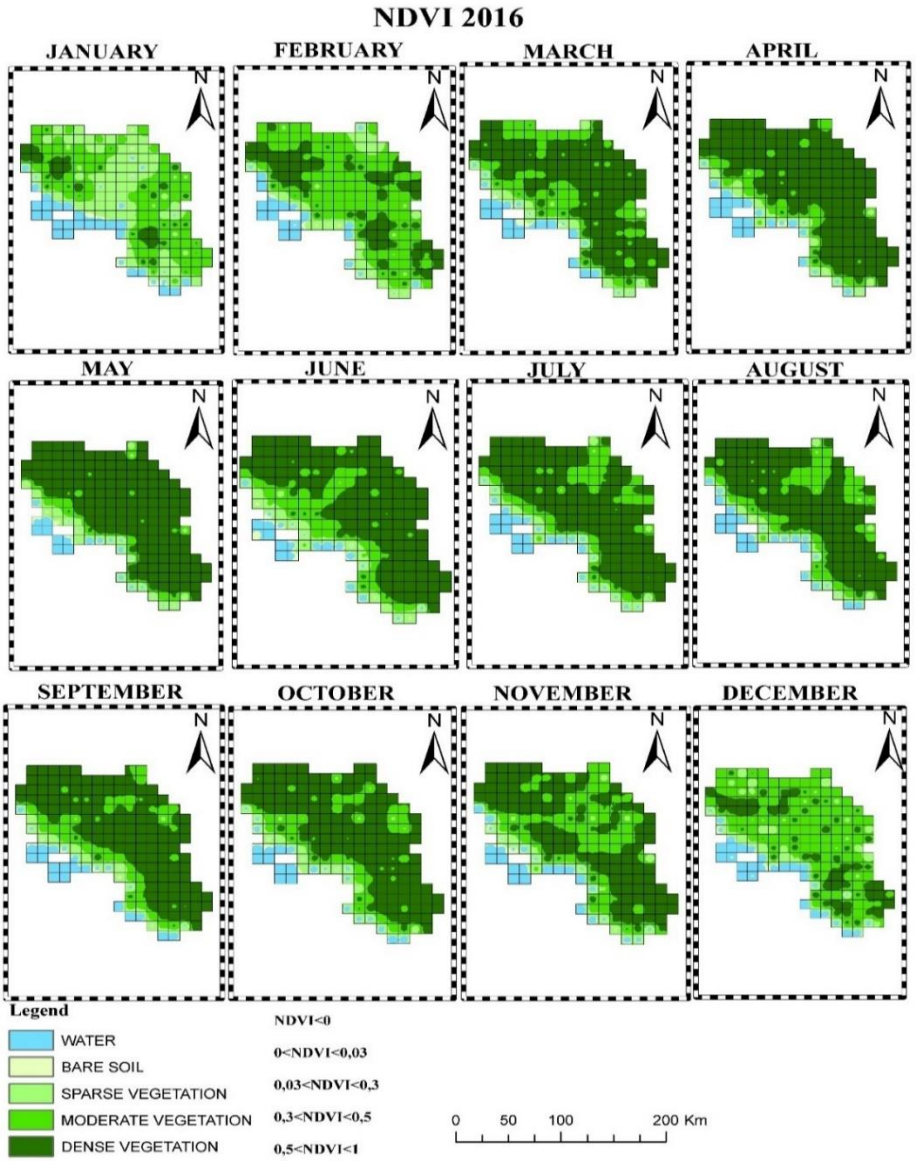

Figure 7.25. NDVI map of the year 2016

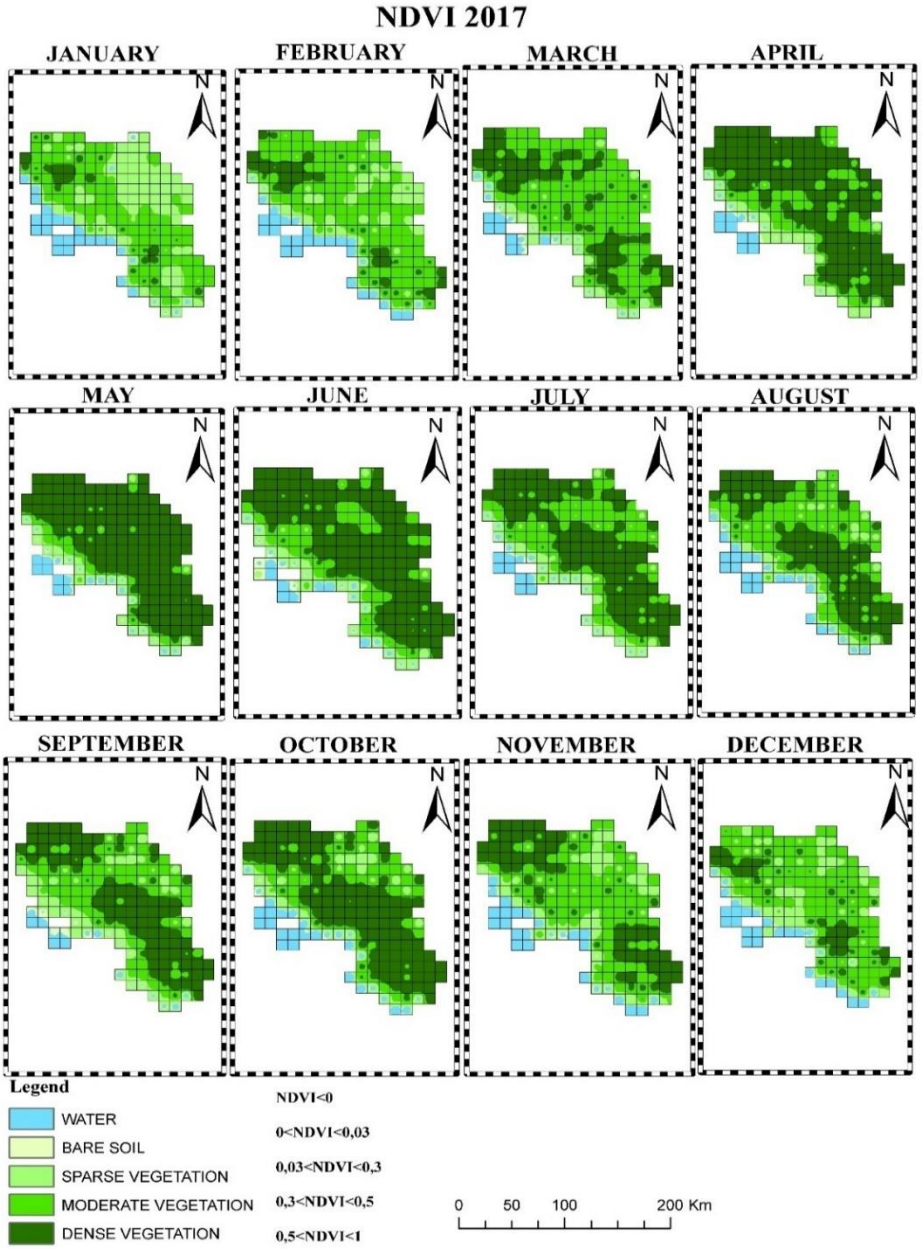

Figure 7.26. NDVI map of the year 2017

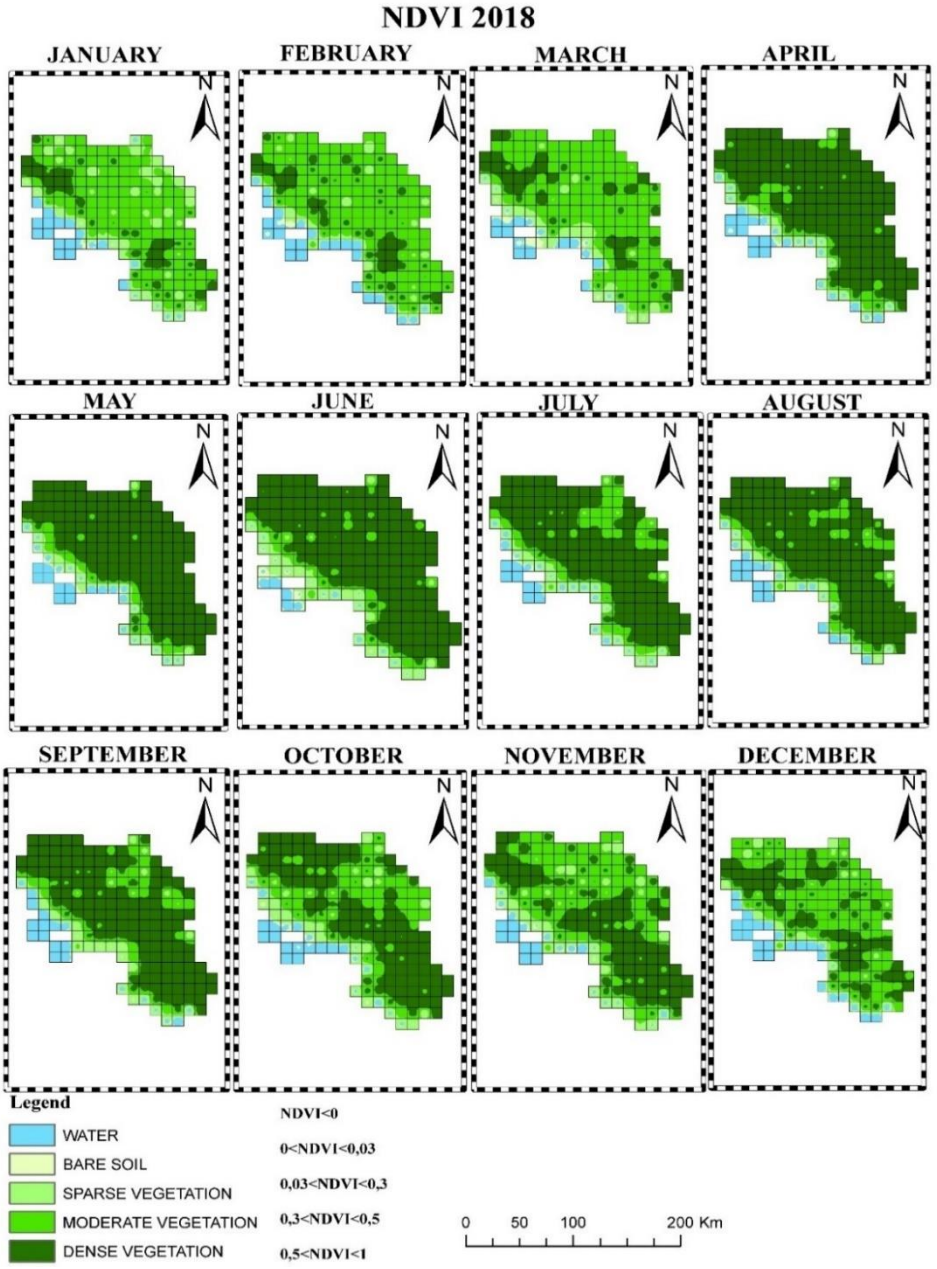

Figure 7.27. NDVI map of the year 2018

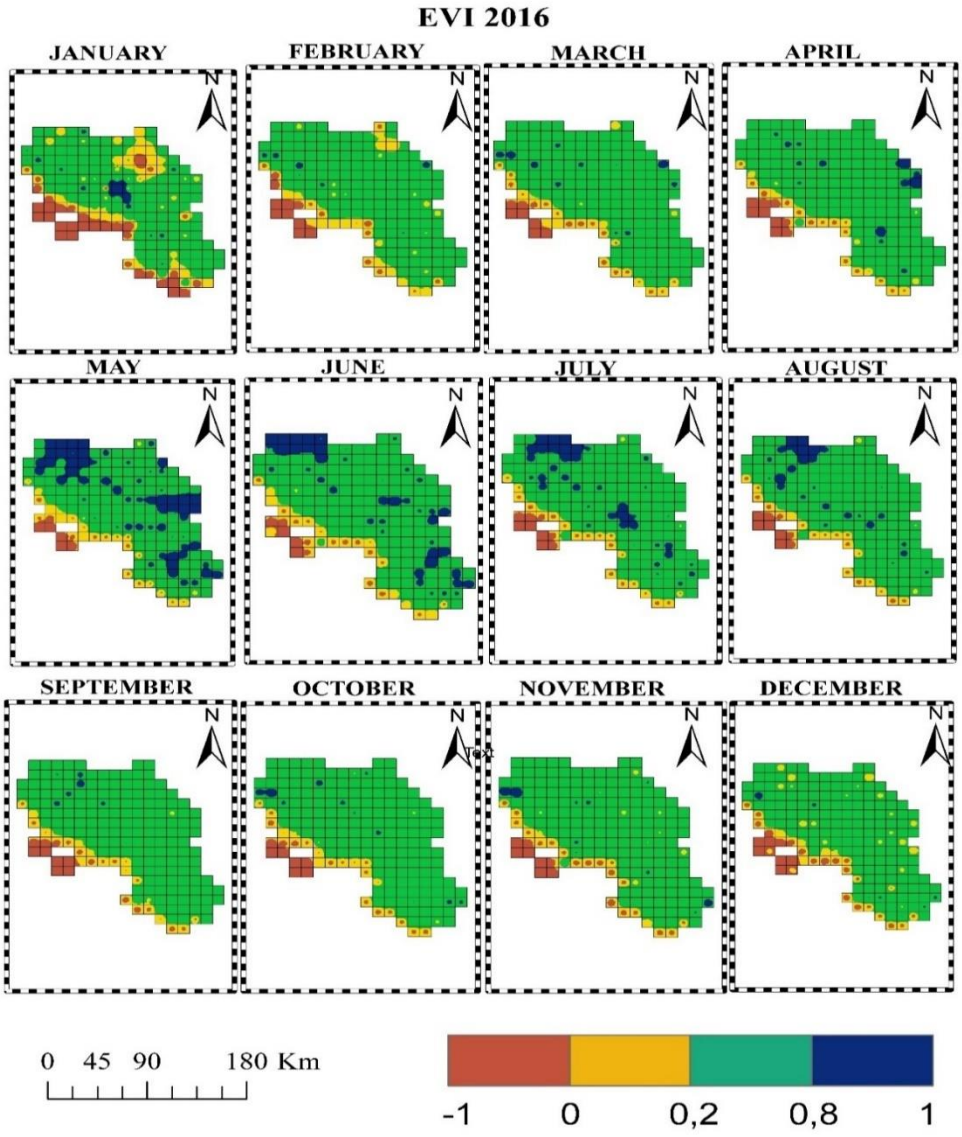

Figure 7.28. EVI map of the year 2016

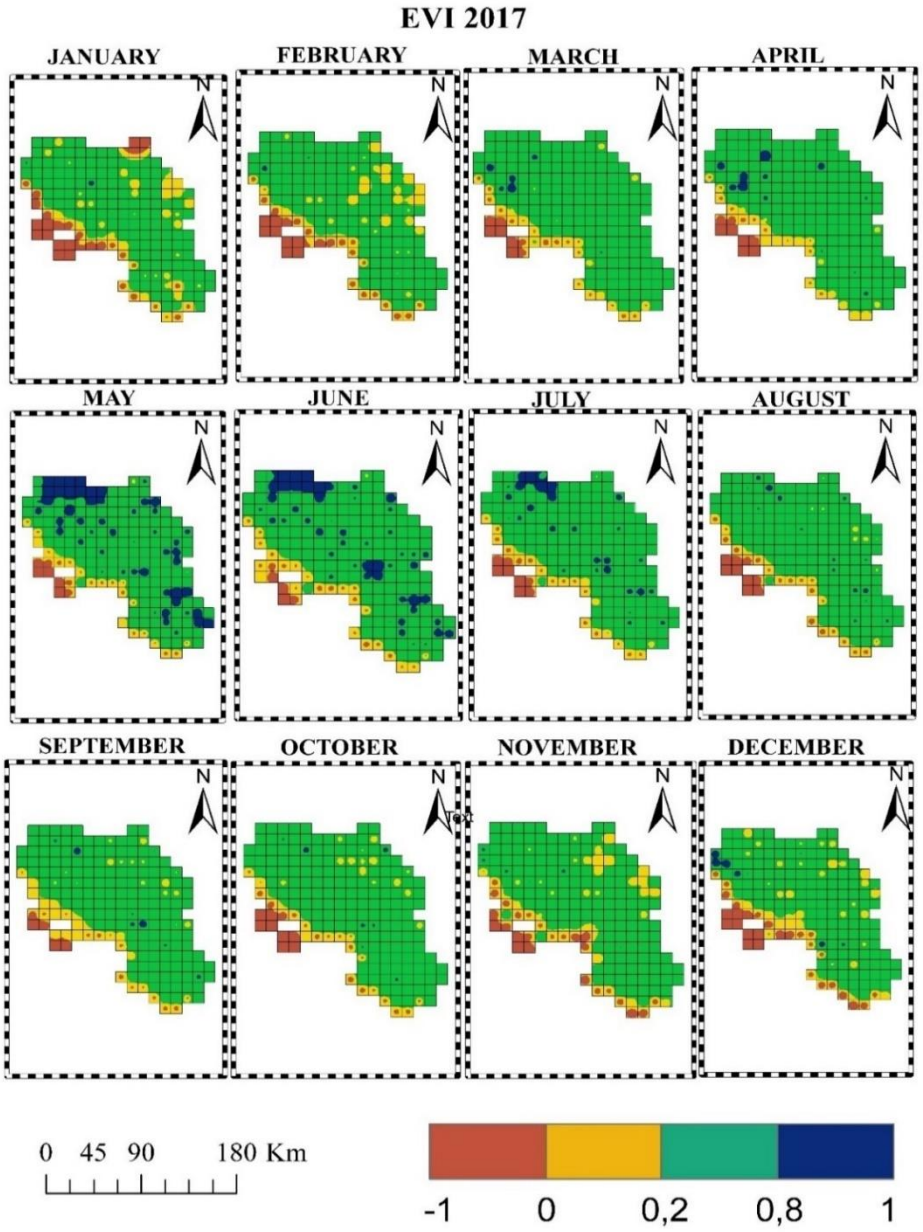

Figure 7.29. EVI map of the year 2017

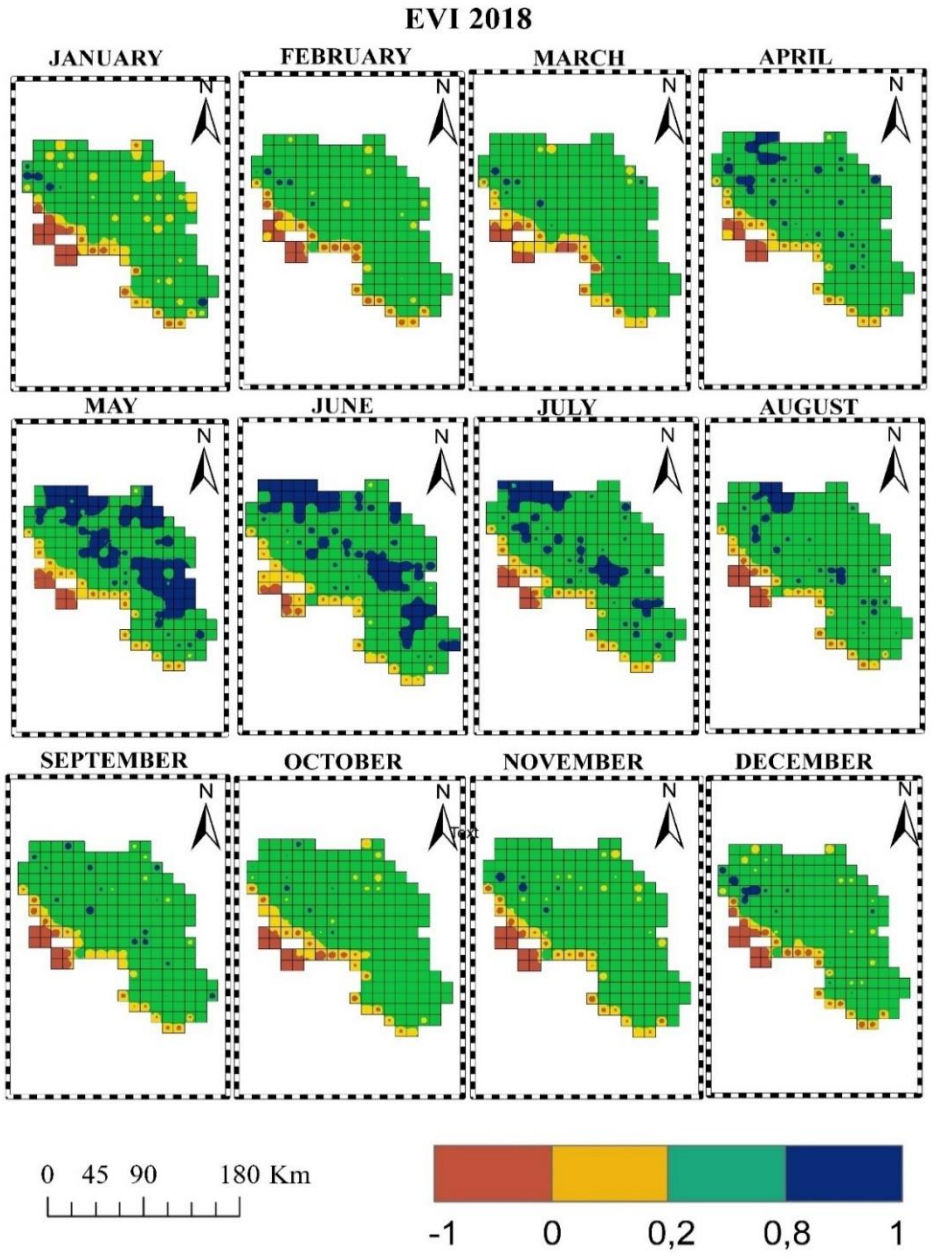

Figure 7.30. EVI map of the year 2018

The analysis of the NDVI and SPEI maps revealed the need to observe the phenomenon in a limited time span in order to observe primarily the ground effects of the meteorological phenomenon because the hydrological responses of the basin are placed in different time horizons. As a result, considering the year preceding and following the drought year does not allow for considerations about the effect on vegetation, as will be seen in the following.

The EVI index, which provides information on vegetation health, was obtained through remote sensing, but it did not add to the information provided by the NDVI. The NDVI and EVI were obtained using remote sensing in the same way, except that once the effect of the atmosphere is removed, the EVI provides more information if the study area is smaller than the one considered here. In fact, viewing the image at a scale of 30 meters yields a more detailed distribution of the data and, as a result, greater spatial variability of the index. This observation narrowed the scope of the study to areas that are not intended for anthropogenic human activity but are affected by water scarcity in terms of water balance. The wooded areas, grazing areas, bushes, sclerophyllous vegetation areas, and shrubby vegetation areas have been identified using the land use map from the "Corine Land Cover" inventory. These areas are highlighted in green in Figure 7.31. This observation narrowed the scope of the study to areas that are not intended for anthropogenic human activity but are affected by water scarcity in terms of water balance. The wooded areas, grazing areas, bushes, sclerophyllous vegetation areas, and shrubby vegetation areas have been identified using the land use map from the "Corine Land Cover" inventory. These areas are highlighted in green in Figure 7.31.

CORINE Land Cover (CLC) inventory began in 1985. (The reference year 1990). The updates were created in the years 2000, 2006, 2012, and 2018. It is made up of a land cover inventory divided into 44 classes. For area phenomena, CLC uses a minimum mapping unit (MMU) of 25 hectares (ha) and a minimum width of 100m

for linear phenomena. The initiative's main goal is to dynamically verify the state of the environment in the community, to provide support for the development of common policies, to monitor their effects, and to propose any corrective measures..(https://www.isprambiente.gov.it/it/attivita/suolo-e-territorio/copertura-del-suolo/corine-land-cover)

We move from a comprehensive regional analysis to a regional scale analysis that is limited to forested areas. These areas' NDVI and SPEI maps have been represented to evaluate both the temporal evolution of vegetation and the effects of drought on the density of vegetative land cover. It is important to note that the seasonality of vegetation has a significant impact on land cover because the maximum coverage of leaves of the canopy of trees of any type occurs during the summer period, while there is a loss of green during the autumn period, and then we observe a lower green coverage through remote sensing and, as a result, through the indices. This phenomenon is not related to a lack of water resources in comparison to the budget because there is more rainfall in the autumn season than in the summer season, but it is related to climatic characteristics.

Rainfall in Mediterranean environments is highly seasonal, occurring primarily in autumn and winter, during the vegetative resting season. In addition, there is a clear distinction between the summer-spring season and the rest of the year in terms of solar radiation and temperatures, which govern evapo-transpirative processes. We distinguish between modeling the vegetation growing season and the dormant (or resting) season to describe the seasonality of climate forcings.

Because the map analysis revealed that the vegetation cover of a drought year showed no significant difference from the normal year, a six-month average (May-October) was used to compare the difference to the normal year average. The maps did not show a clear difference; however, it was possible to see it through the

probability distribution, which showed vegetation water stress due to an extreme drought phenomenon.

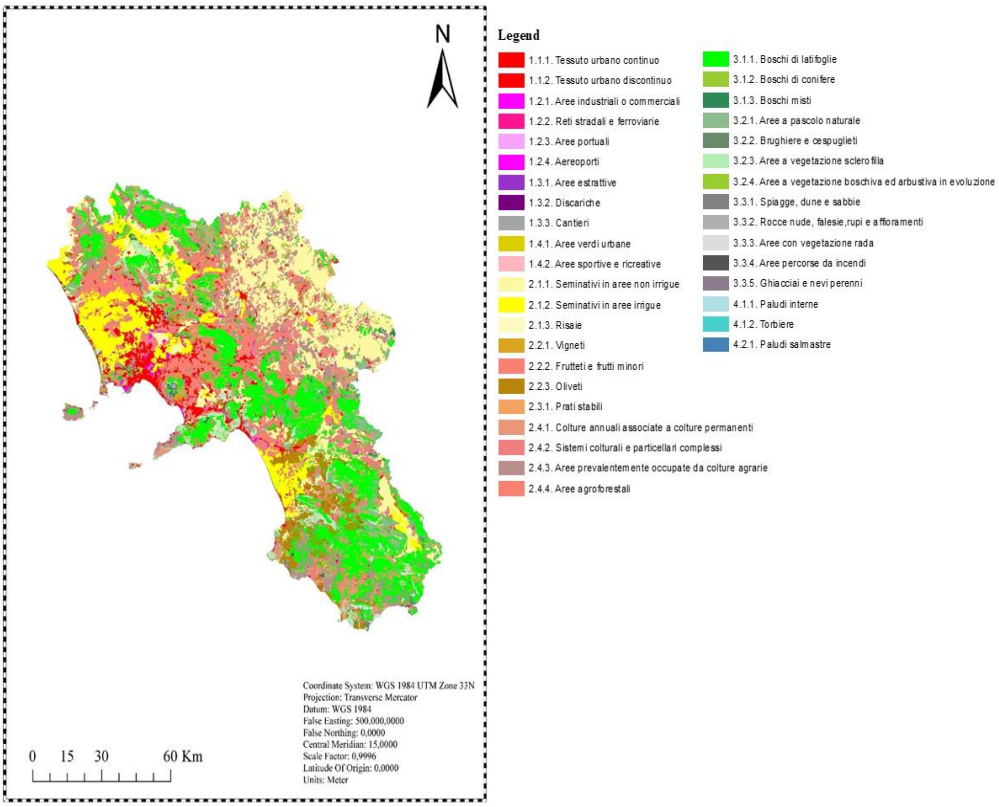

Figure 7.31 Corine Land cover use map

The extraction of non-irrigated areas yielded the same results as the maps shown in Figures 7.1-7.30 of this study. This is because, while extracting the areas affected by potential water stress, the grid scale remains constant, and thus the maps obtained now only allow us to focus on the areas potentially tested by drought. As a result, a six-monthly average of both NDVI and SPEI was calculated for the drought year. It should be noted, however, that taking a year before and after the drought year had no additional value in determining the ground effect of the drought event.

As shown in Figure 7.32, the six-month average (May-October) for 1996 was compared to that of 2003, and similarly, the average of the normal year was compared to that of 2017.

The average NDVI map for 1996 shows moderate vegetation and dense vegetation in an area that runs parallel to the Apennines. As seen in the average SPEI, this type of vegetation is associated with a normal condition.

In a drought year, such as 2003, the average NDVI map becomes increasingly dark green (dense vegetation), once again in the area parallel to the Apennines. The 2003 mean SPEI indicates moderate drought in Caserta and Naples.

In 2017, the mean NDVI shows many areas of dense vegetation (dark green) in most of the region; however, the SPEI shows severe drought (red) primarily affecting the Provinces of Naples, Avellino, and Salerno, all against an orange background, indicating that the rest of the region is characterized by moderate drought.

When only the 1996 NDVI average map and the 2003 NDVI average map are used, an increase in dense vegetation areas is seen in 2003. Similarly, it can be seen when comparing the average NDVI 1996 map to the average NDVI 2017 map. Even though there is a severe drought, the vegetative cover appears dense.

It should be remembered that the semester observed is the semester of vegetation growth, so observing vegetation during its growth period may be insignificant. The effects on vegetation were observed during the winter semester, i.e., October-March. Because the vegetation is in the dormant (or resting) phase this semester, it should have a lower vegetative cover than in the growth phase.

A six-month average (October-March) for the year 1996 and for the year 2017 of the NDVI was again carried out, as we want to observe the effect of that drought period on a later time, keeping the spatial context unchanged (Figure 7.33).

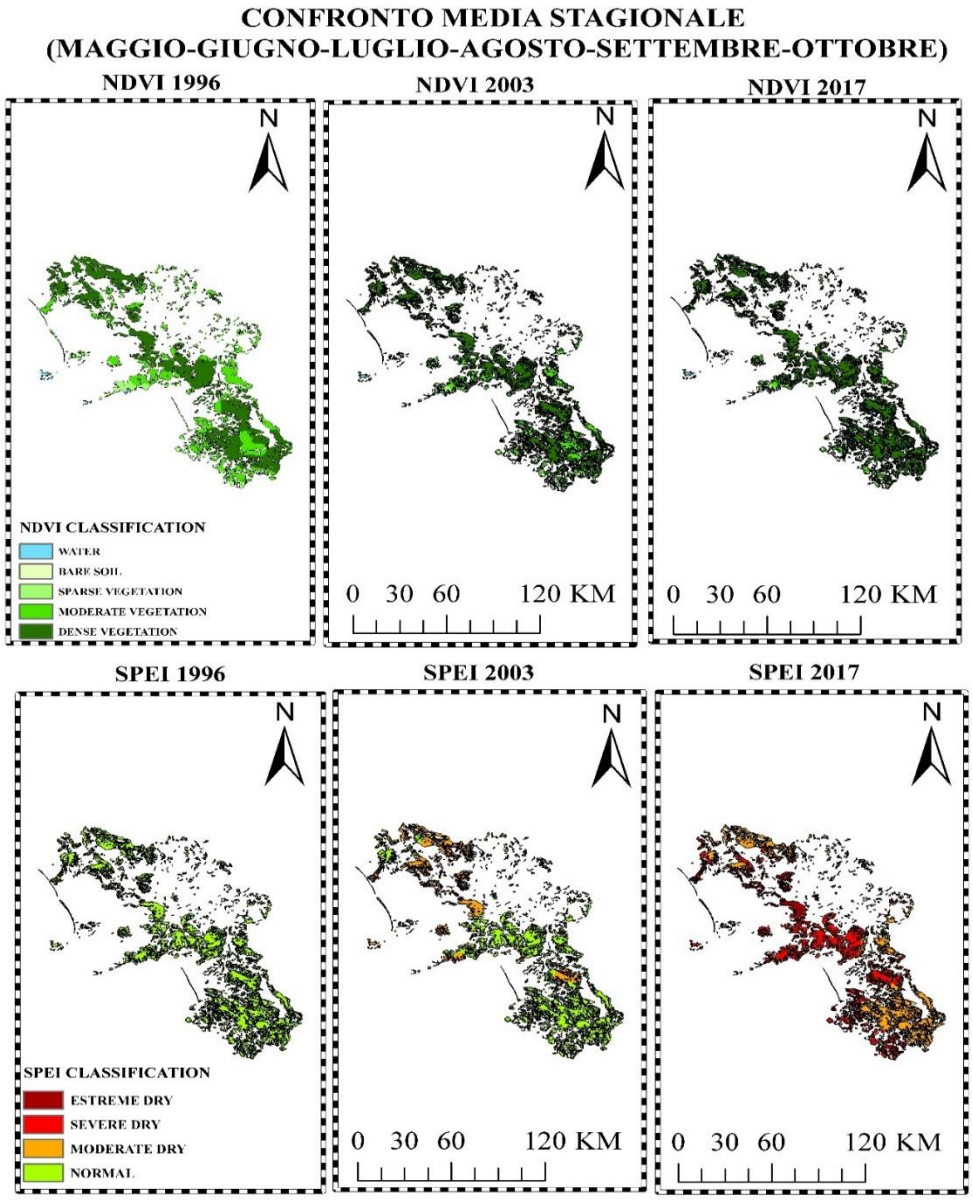

Figure 7.32 Comparison map of NDVI averages and SPEI averages.

In the 1996 average map, it is evident that the entire region is characterized by green i.e., moderate vegetative cover. The same cannot be said for the year 2017. In fact, in the year 2017, we observe a vegetation that is still moderate (green), however, we notice more those darker green areas that indicate a dense cover.

This analysis led to consider only the year in which the drought event was most extreme, hence the choice to represent in Figure 7.33 the average NDVI only for the years 1996 and 2017 in order to compare what occurs in a normal year and what occurs following the drought event.

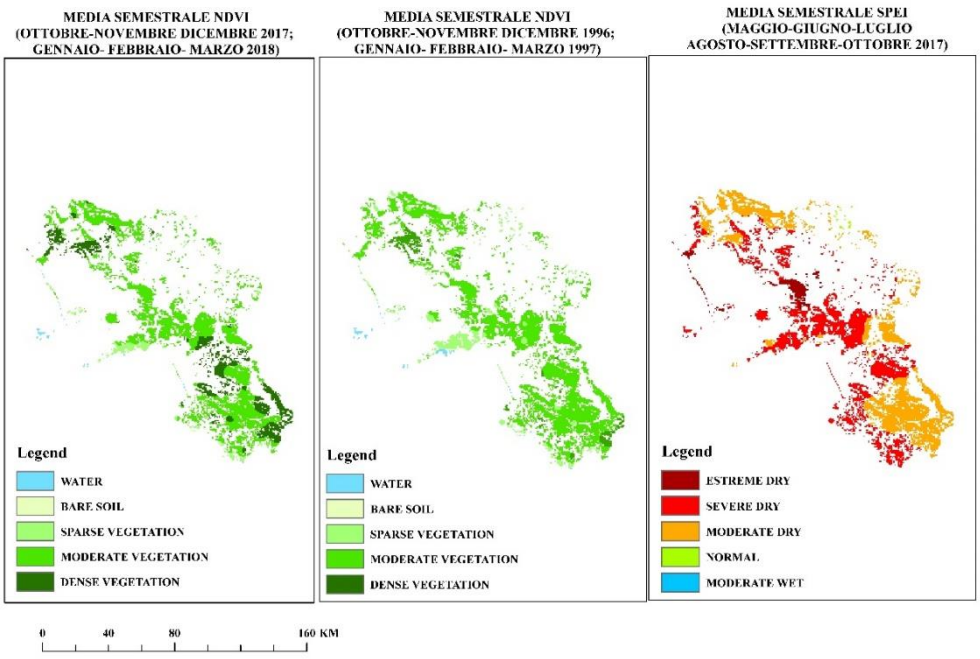

Figure 7.33 Comparison map of the NDVI averages and the SPEI averages for the half-year October-March.

Because what is visually observed when comparing the frames is not exhaustive, further statistical analysis was required to interpret the maps. The

datasets required to obtain the empirical probability distributions for the seasonal averages from May to October were obtained.

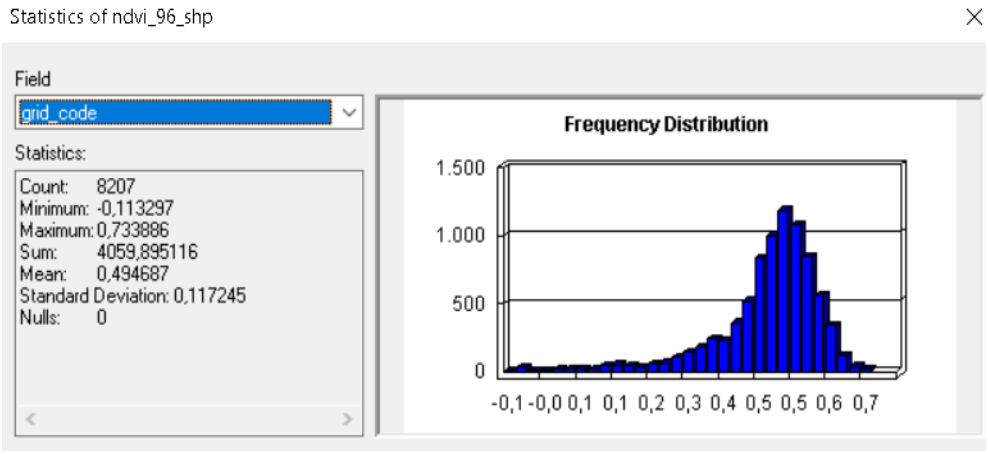

Figure 7.34. Empirical distribution year 1996 Average NDVI semester May-October

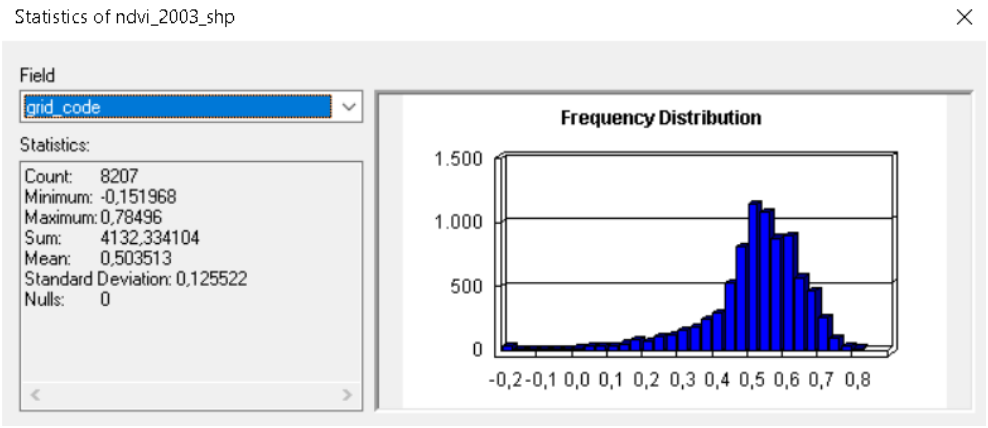

Figure 7.35 Empirical distribution year 2003 Average NDVI semester May-October

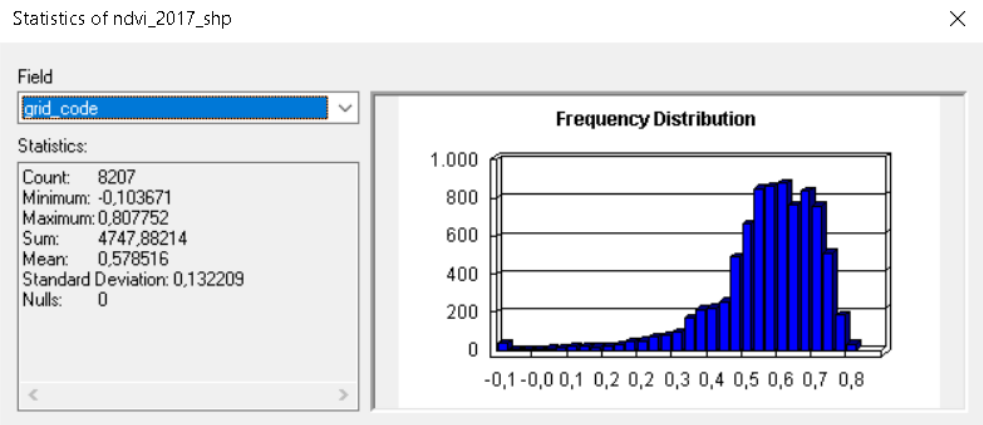

Figure 7.36 Empirical distribution year 2017 Average NDVI semester May-October

When comparing drought and normal years, the probability density shown in Figure 7.34 is used as a reference. The probability density for the year 2003 is more pointed. The modal value is concentrated around 0.55, which represents dense vegetation in the NDVI classification. Similarly, the modal value is observed between 0.5 and 0.7 in the 2017 distribution, which also has a wider range of values; in fact, the probability distribution differs from that of 2003 because it is more flattened. Furthermore, the density of larger values (closer to the unit value) is higher in the 2017 distribution than in 2003.

When we compare the distributions from 2003 and 2017, we notice a similarity in the frequency distribution of the data as well as the modal value.

This outcome was predictable because the drought phenomenon in 2003 was not as severe as it was in 2017, when not only were extreme drought values of the SPEI recorded, but the phenomenon also affected the entire region.

An analogy with a non-drought year cannot be drawn for the year 2017. The drought was significant; however, the NDVI showed a trend of vegetation growth; in fact, the highest probability density occurs for the highest NDVI values.

Discussion of the results

The results reported in the preceding paragraph show a weak correlation between the two indices, whether observing the drought period, observing the subsequent period, or observing only forests and all those areas with natural irrigation. It can be seen that NDVI and SPEI are not in a cause-effect relationship.

These results were obtained for two reasons: the first is the climatic condition of the last 30 years, and the second is the very low correlation between NDVI and SPEI.

Moreover, the correlation between NDVI and precipitation (P), NDVI and SPEI at each aggregation scale was calculated. The results were compiled in Table 7.1

Table 7.1. The correlation between the SPEI and NDVI

	Correlation index
NDVI-P	0,25
NDVI-SPEI_3	-0,01
NDVI-SPEI_6	-0,005
NDVI-SPEI_12	-0,006

The correlation between the meteorological indices SPEI and NDVI vegetation is rather low, in fact, the values of the correlation indices are approximated to 0 (no correlation), at different scales of aggregation and this justifies why in times of drought the values of NDVI are not low. Slightly more significant is the correlation between NDVI and precipitation, so the long- and short-term trend of both precipitation and NDVI will be considered later.

Climate condition over the past 30 years.

The temporal analysis of the SPEI showed that in the long term there is a decrease in the index associated with decreasing precipitation and increasing temperatures. In fact, this can be seen in Figure 7.38 which for the period from 1924 to 2019 shows a decreasing trend in the trend function (in red), thus towards a drier climate.

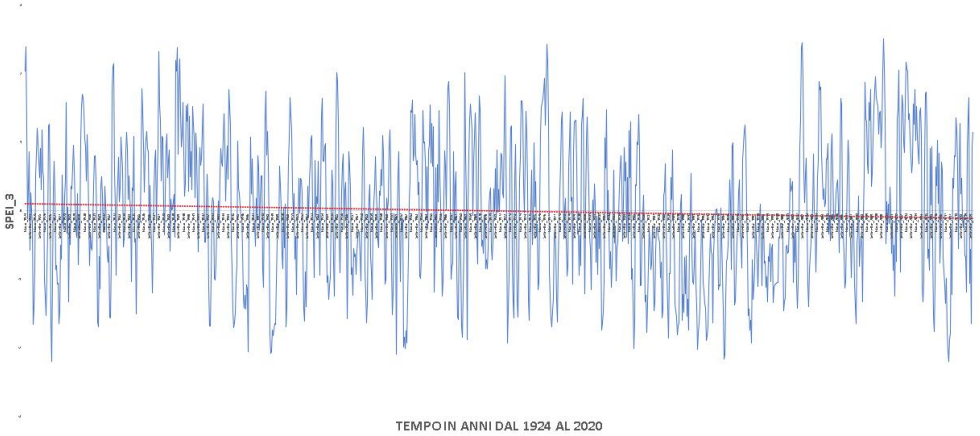

Figure 7.37 Evolution of the SPEI over the last 100 years.

The climate trend over the past 30 years, however, is toward a wet climate as seen in the precipitation figure 7.37. In particular, the trend curve is increasing over time, so precipitation is higher. The data we have for the NDVI index is for the last 30 years. The NDVI trend appears to be increasing, although in some areas of the region this trend is less pronounced.

As a result, if precipitation increases, the NDVI index becomes increasing rather than stationary, and the vegetation cover increases. Looking at the last 30 years rather than the scale of events, we can see that the index has been increasing. This is why, even after an extreme drought event like the one in 2017, the NDVI

continues to rise. What can be seen is that the curve's points are both lower and higher than the trend curve. These large differences are typical of the Mediterranean climate, which has a year with less precipitation followed by a year with more precipitation. The representation of NDVI and precipitation for three different cells can be seen in the three graphs below (figures 7.38-7.40). However, having only the last 30 years of data available limits the ability to determine the trend of NDVI versus precipitation. If one were to examine the NDVI dataset for the last 100 years, one would most likely notice a similar trend to that of precipitation for the last 100 years, resulting in a decrease in the vegetation index.

Figure 7.38 Trend of cell 36 precipitation and NDVI

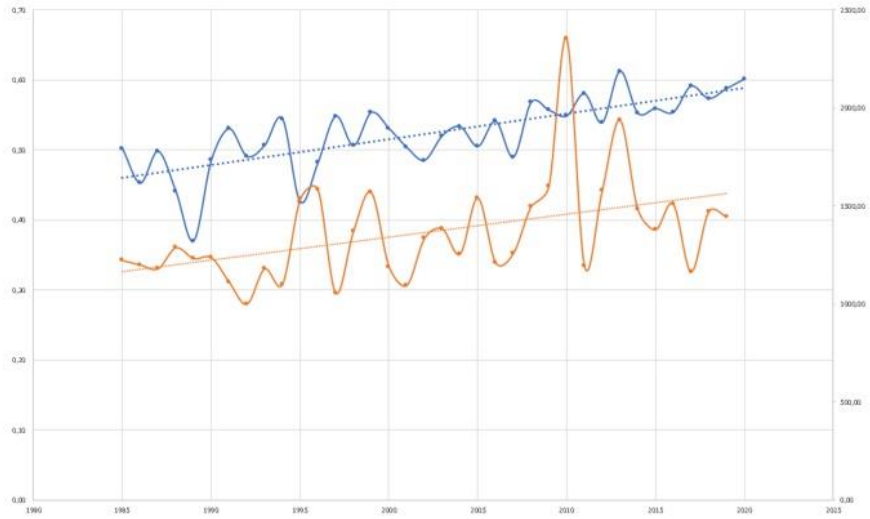

Figure 7.39 Trend of cell 85 precipitation and NDVI

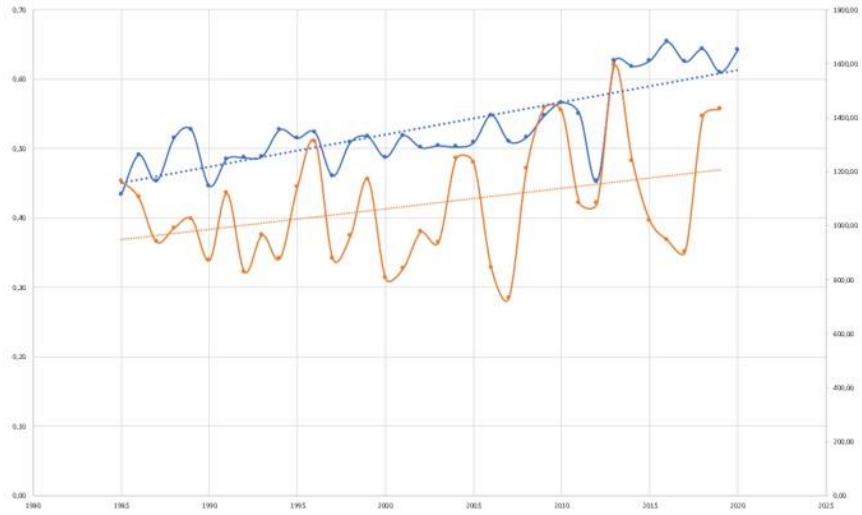

Figure 7.40 Trend of cell 186 precipitation and NDVI

7.3 SPATIAL AUTOCORRELATION OF HISTORICAL EVENTS

The application of Spatial Autocorrelation has the utility of identifying, through Moran's Index, the presence of a dependence in the data, both in values above the mean and for those below it, (Chieppa, 1994).

After we have studied durations and intensities, we want to find out if the different events studied have similar characteristics in terms of spatial aggregation, that is, if there are areas that are increasingly affected by drought and how these are affected.

By using spatial autocorrelation maps it was possible to evaluate how much the various points on the grid influence each other; we will have Moran indices, mostly positive, which determine the presence of autocorrelation.

It can be high, so **High-High** represented by the red color, or low, so **Low-Low** represented by the blue color; in addition, on the grid there are many points represented by gray color or those points that are not significant (points that do not depend on the neighbor).

7.3.1 The Drought event of 1962, 1989 and 2003

With respect to the consideration of the drought event, some thoughts can be made regarding spatial autocorrelation. Using the local indicator of spatial association (LISA) method, several spatial autocorrelation maps resulted.

Analyzing the 1962,1989 and 2003 events and comparing the drought maps, obtained by SPI and SPEI, with these maps obtained by LISA (Figure 7.41-7.49), we could make some considerations. The first thing to say is that first of all, many points on the grid are not significant (gray color). It is possible, moreover, to observe that in the areas characterized by moderate and severe drought conditions it happens

that the spatial autocorrelation between the points on the grid is of the Low-Low type (blue color), i.e. a low autocorrelation that does not mean that Moran's I index is negative but simply means that the influence of the various neighboring points is not high.

On the other hand, for the areas characterized by drought conditions in the norm it happens that the spatial autocorrelation between the points on the grid is of the High-High type (red color), i.e., a high autocorrelation, meaning that the influence of the various neighboring points is high.

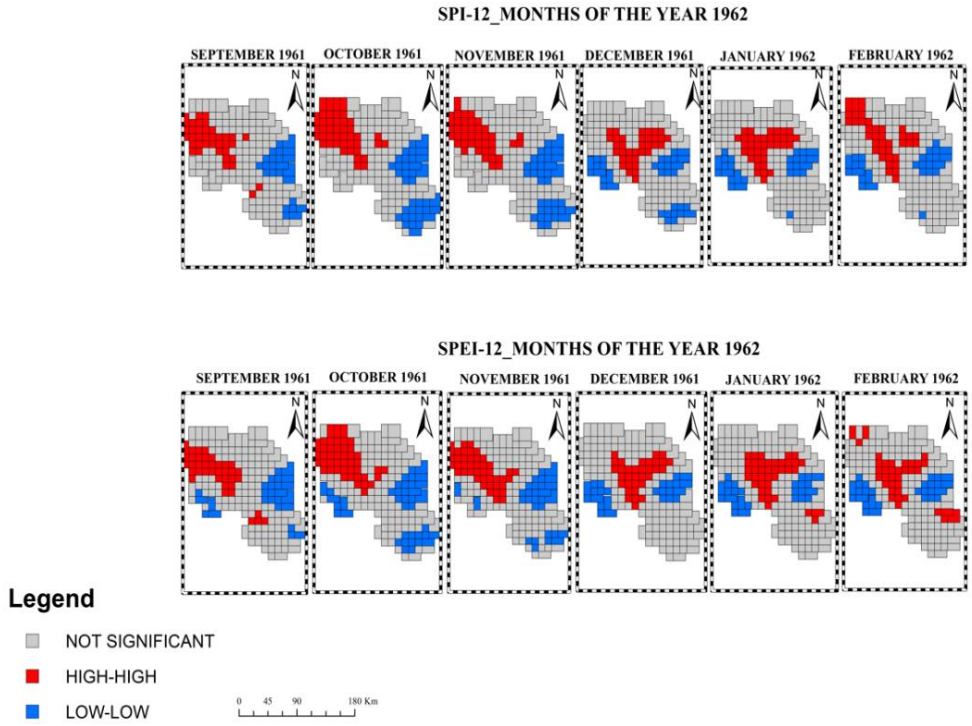

Figure *7.41* - Spatial autocorrelation maps using LISA (September 1961 - February 1962)

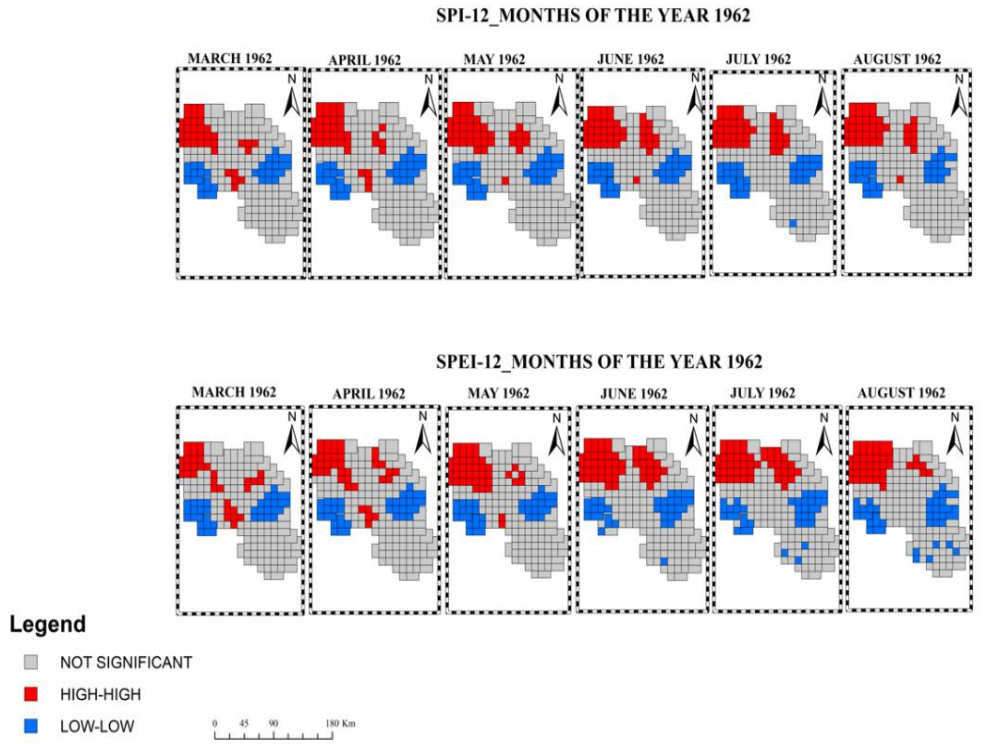

Figure *7.42* - Spatial autocorrelation maps using LISA (March 1962 - August 1962)

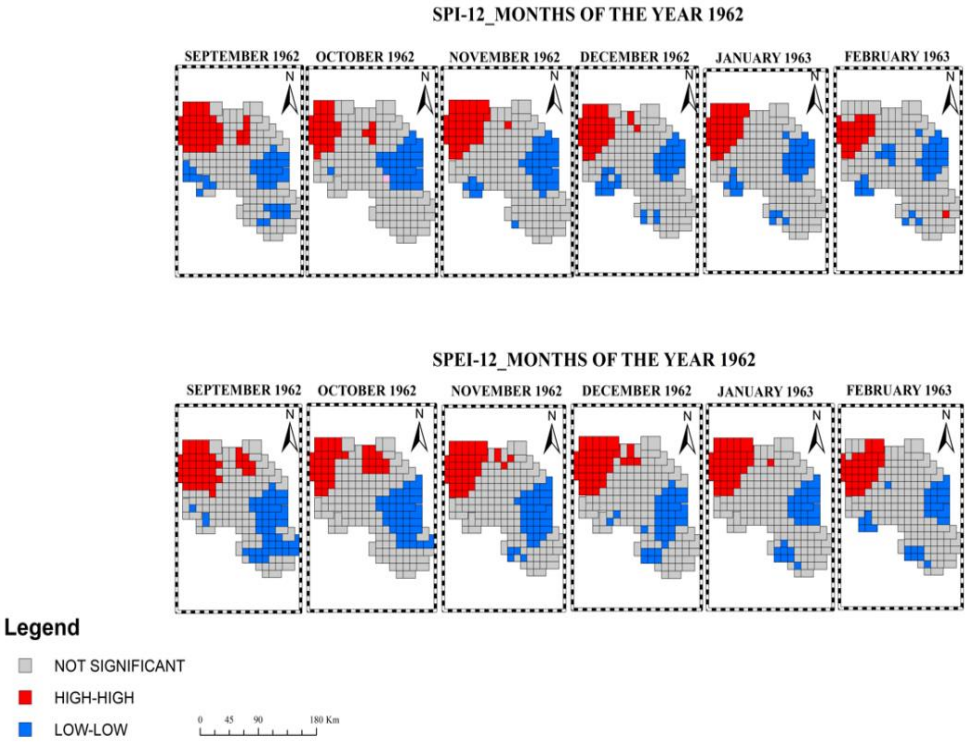

Figure ***7.43*** Spatial autocorrelation maps using LISA (September 1962 - February 1963)

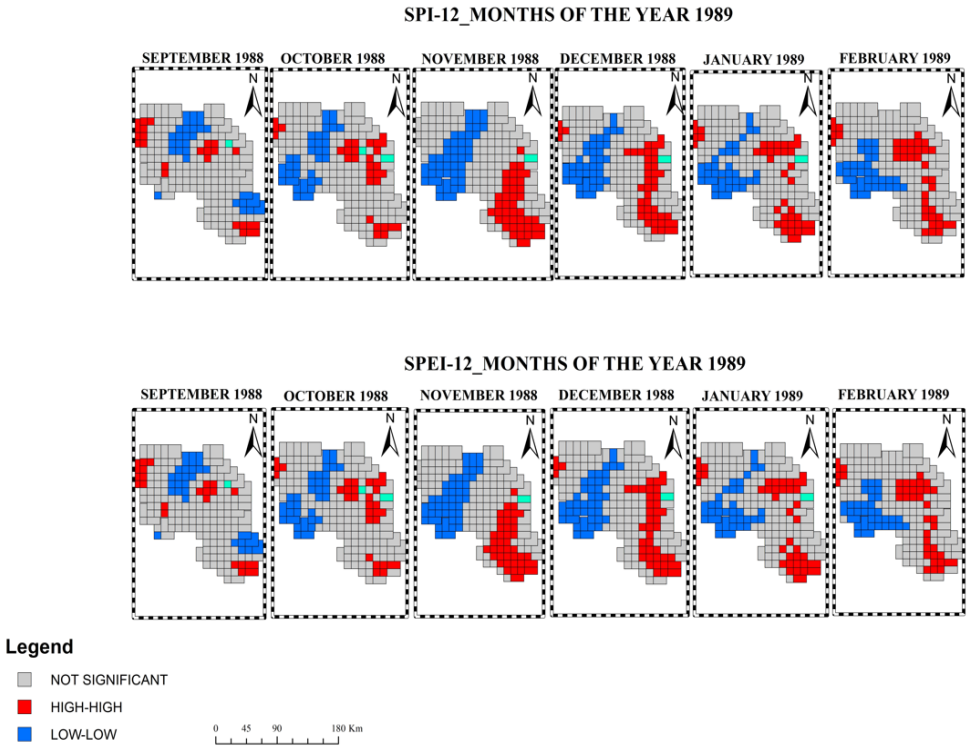

Figure *7.44* - Spatial autocorrelation maps using LISA (September 1988 - February 1989)

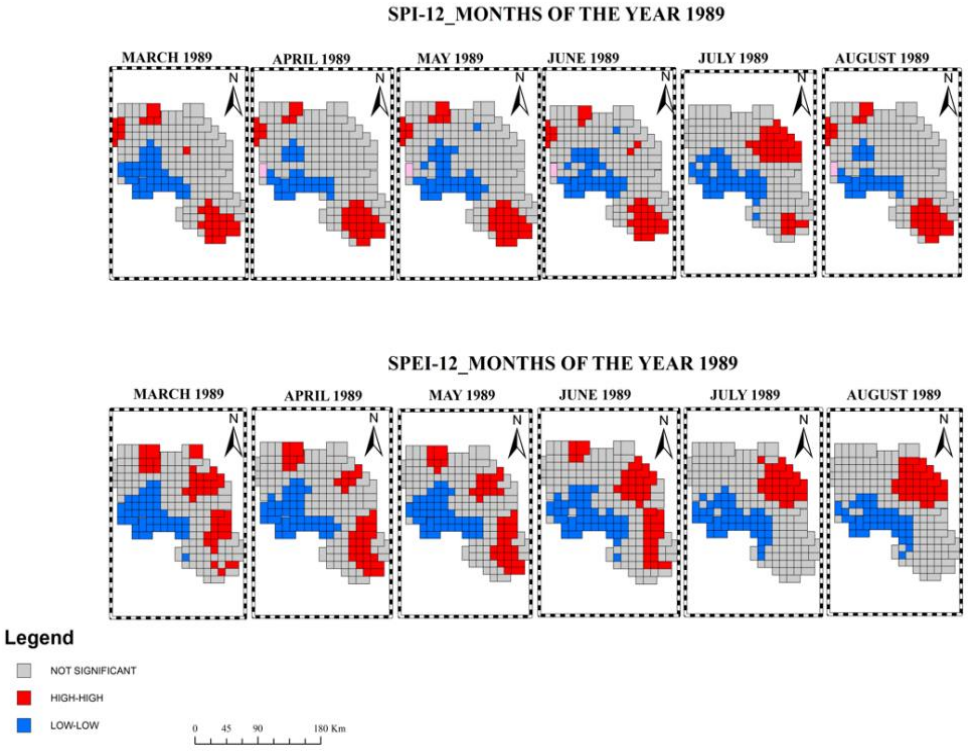

Figure *7.45* - Spatial autocorrelation maps using LISA (March 1989 - August 1989)

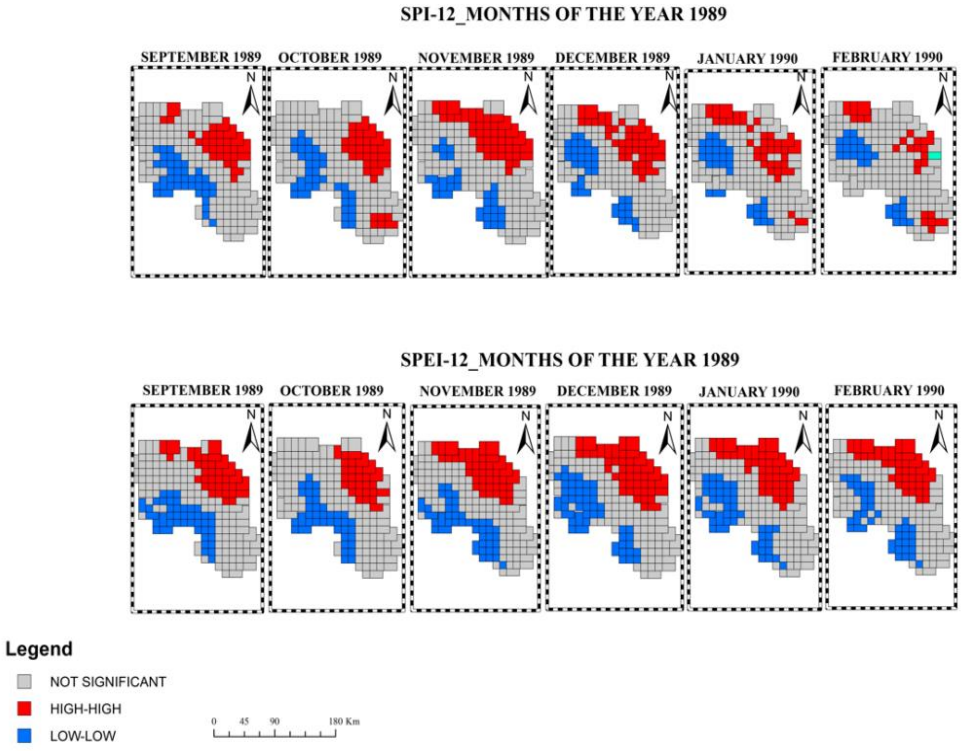

Figure *7.46* - Spatial autocorrelation maps using LISA (September 1989 - February 1990)

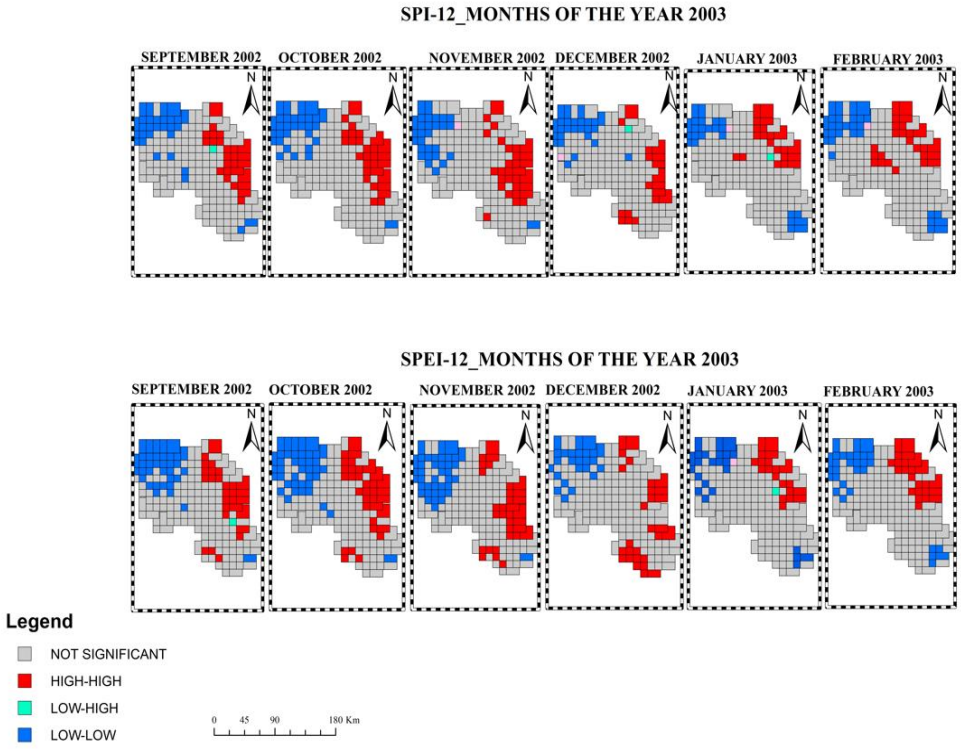

Figure *7.47* - Spatial autocorrelation maps using LISA (September 2002 - February 2003)

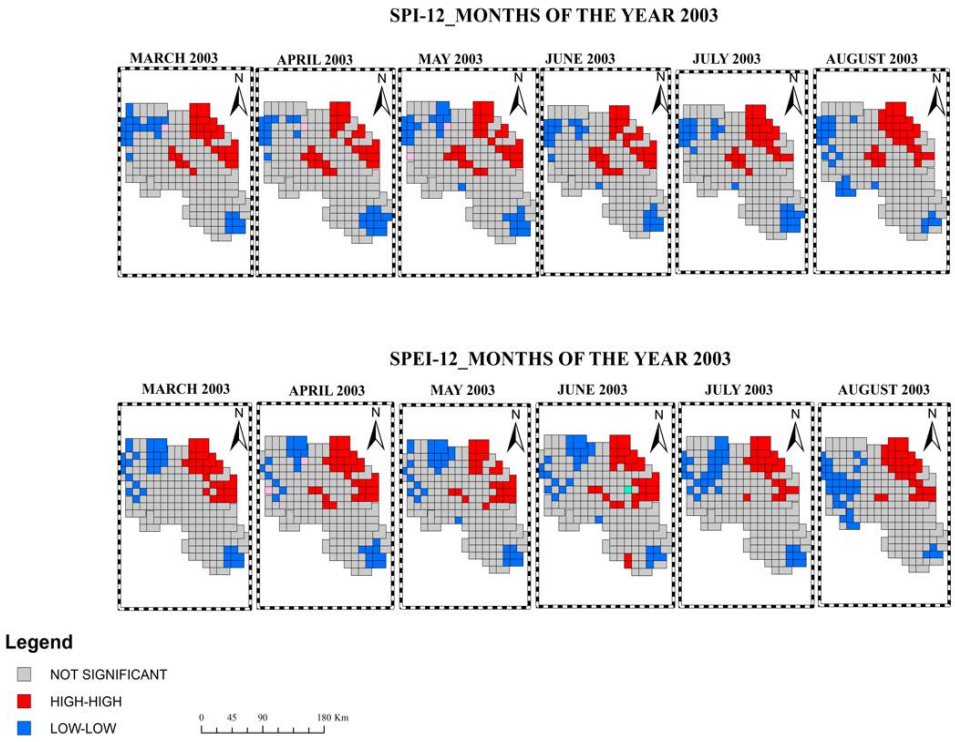

Figure ***7.48*** - Spatial autocorrelation maps using LISA (March 2003 - August 2003)

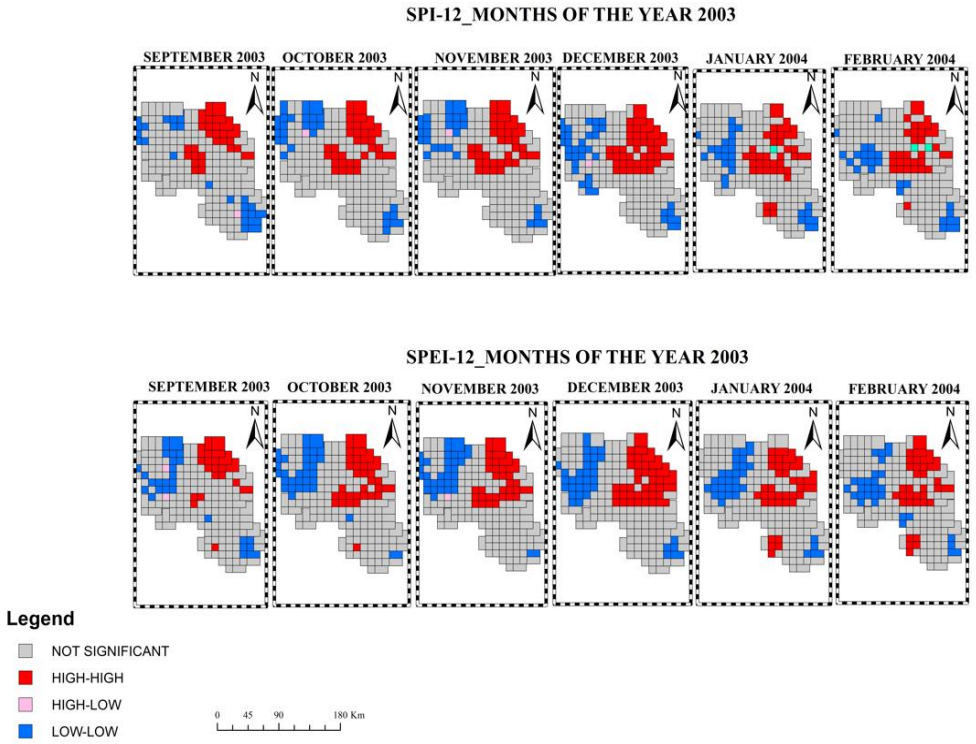

Figure *7.49* - Spatial autocorrelation maps using LISA (September 2003 - February 2004)

7.3.2 The Drought event of 2017

Looking at the 2017 event and comparing the drought maps to the spatial autocorrelation maps, some observations can be made. The sequence of frames is shown in Figures 7.50-7.52. First, we can make that many points on the grid are not significant (gray color).

Referring to past experiences, i.e., the 62', 89' and 03' events, we would have expected many clusters representing low spatial autocorrelation (blue color) since in

this drought event the whole Campania region was affected, but this was not the case.

We can say that, therefore, the points on the grid are correlated but not significantly. We always have areas with high spatial correlation, High-High, (red color) there where the drought event was little or no, but the areas with low spatial correlation, Low-Low, (blue color) in this case refer to areas where the drought has occurred at extreme levels.

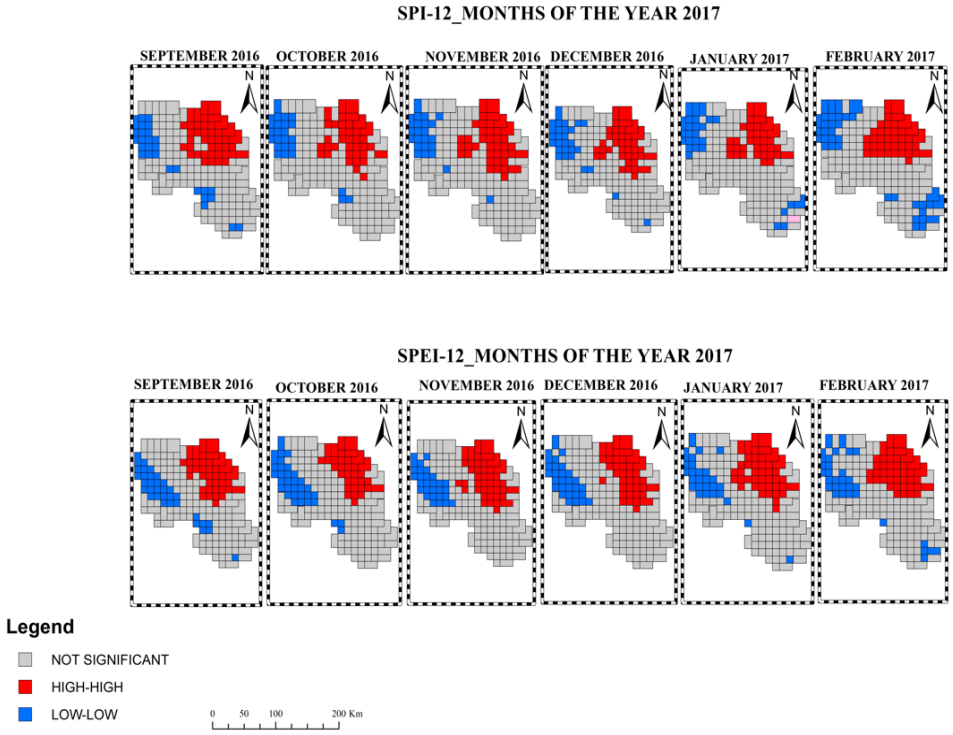

Figure *7.50* - Spatial autocorrelation maps using LISA (September 2016 - February 2017)

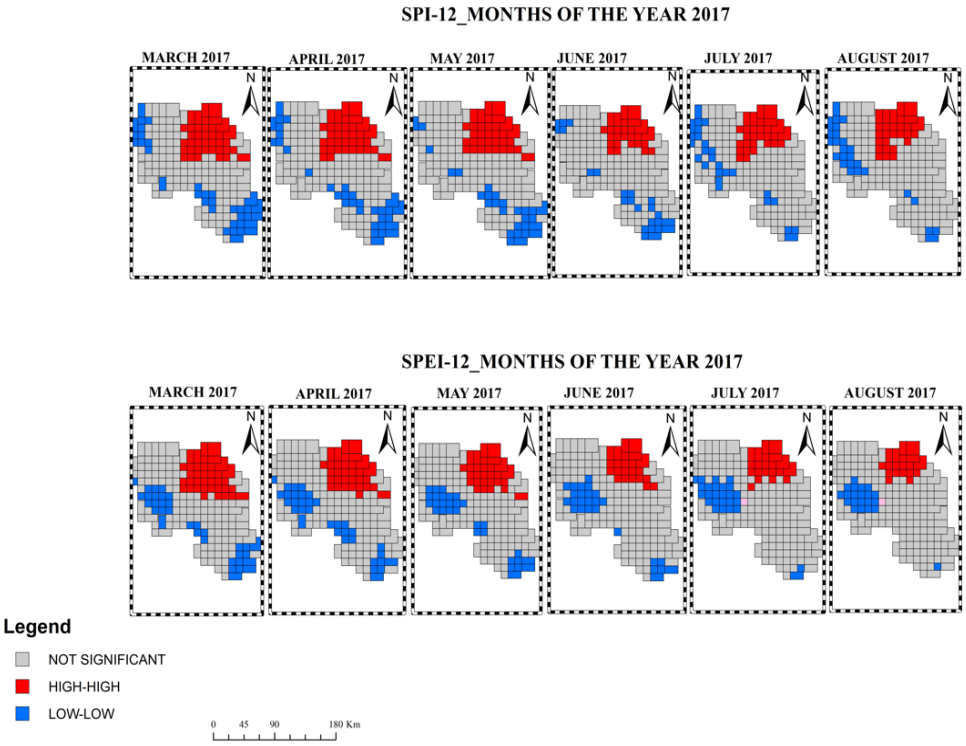

Figure *7.51* - Spatial autocorrelation maps using LISA (March 2017 - August 2017)

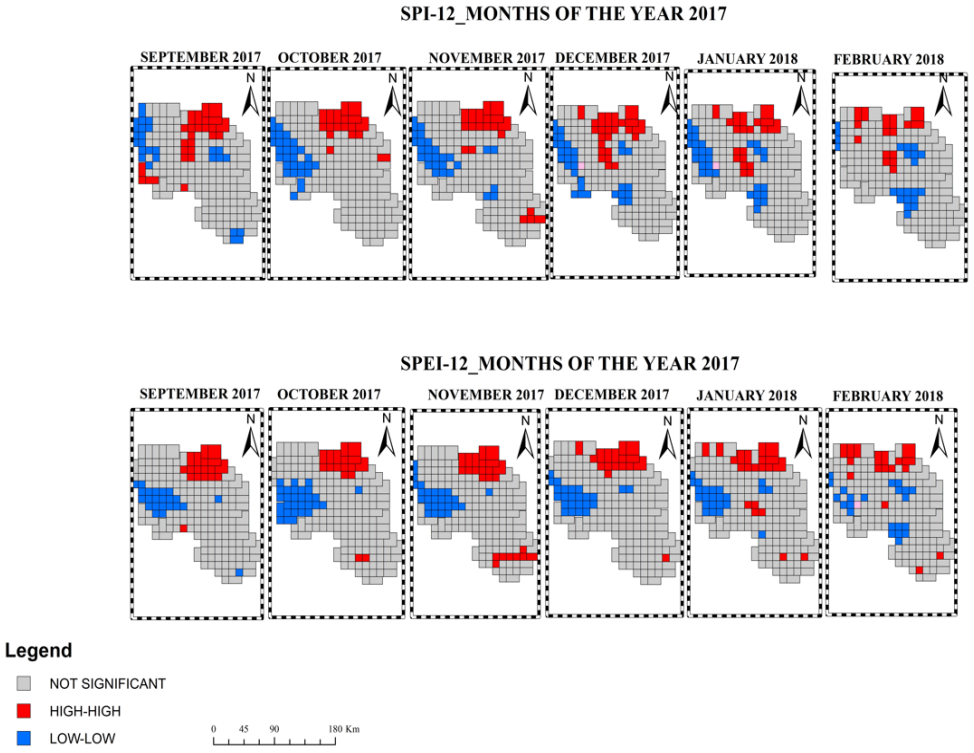

Figure 7.52 - Spatial autocorrelation maps using LISA (September 2017 - February 2018)

7.4 SPATIAL AUTOCORRELATION OF MEAN ANNUAL PRECIPITATION

After having analyzed the effect of the spatial autocorrelation on the drought indices, we thought it appropriate to also consider the spatial trend of the average annual precipitation over the Campania region (Figure 7.53).

Analyzing the following maps, some considerations came out; first of all, it is possible to highlight that where rainfall is high (dark blue color) the spatial autocorrelation will be High-High (red cluster) and, consequently, where rainfall is scarce (light blue color) also the autocorrelation will be Low-Low (blue cluster).

Always observing the maps, it was noted that the rainfall and therefore the autocorrelation are high in areas where there are morphometric relief, that is, in the hinterland of the region. It is well known for a complex orography; the altitude of the region varies well above 2000 m a.s.l. (above sea level) in the Apennine Mountains to the coast. The region is characterized by a complex climate pattern because of the orography. It could be, therefore, mostly the relief that provides high spatial autocorrelation where it is present and low autocorrelation where it is not.

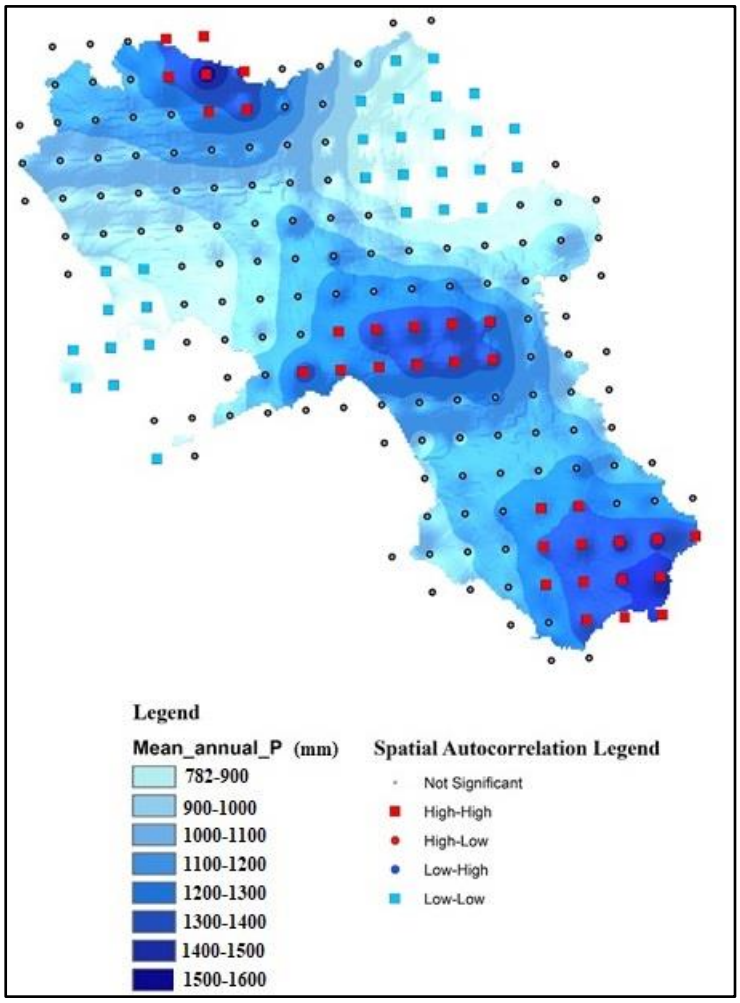

Figure 7.53. Maps of the spatial autocorrelation of the average annual rainfall using LISA

7.5 Overall evaluation

Investigating and understanding the phenomenon of drought becomes critical if we are to aim for sustainable management of the water resource. Climate change must push society to change in turn by identifying better management strategies for infrastructure and resources on the ground. The goal must be to increase the efficiency of the works already present on the territory and those to be built in the future, to drastically reduce waste and consumption. The purpose of this study was to assess the health of forests based on the drought events that characterized Campania in the period of 2003 and 2017.

This study showed a correlation of vegetation stress by NDVI, with the meteorological phenomenon of drought by SPEI; however, the impact of drought is underappreciated when NDVI and EVI index values from a drought year are compared to those from a normal year. Exploring the maps of the NDVI and EVI is not the only way to assess the phenomenon. In fact, another way may be to look at agricultural land use (nonagricultural use was considered in this thesis work) and measure the impact on the ground by considering the moisture content index of surface states that is obtained through remote sensing. It will, then, be necessary to reduce the scale of the case study, for example, considering a 30mx30m mesh grid, because land use varies from meter to meter.

Throughout concluding, the NDVI can represent the evolution of vegetation; however, due to limitations caused by both the low correlation of the same with the SPEI index and the limited time horizon for which NDVI data are available, it is not possible to state that there is a water deficit for vegetation due to the rainfall deficits shown by the SPEI because the climatic condition of the Campania Region fits into a sub-humid climate; perhaps if it had been arid a greater.

Chapter 7: DROUGHT HOT SPOT ANALYSIS USING LOCAL INDICATORS OF SPATIAL AUTOCORRELATION

The study of spatial autocorrelation was also significant, as it is a very effective technique for analyzing the spatial distribution of variables while assessing the extent to which they are influenced by and related to neighboring elements. Spatial autocorrelation was used to determine whether the various events studied have similar spatial aggregation characteristics, that is, whether there are areas that are increasingly affected by drought and how these are affected.

For the 1962,1989 and 2003 events, it was immediately noticeable that in the areas characterized by moderate and severe drought conditions the spatial autocorrelation between the points on the grid was low, i.e., Low-Low. Therefore, large low-low clusters were formed on the maps, which thus went to define that autocorrelation was present but not in a high manner. Whereas, in areas characterized by drought conditions that were within the normal range, the spatial autocorrelation was of the High-High type, i.e., high, so much so that these large, red-colored clusters were formed on the maps, which therefore went to define that autocorrelation was present and was also very high. Based on the previous events' experiences, we would have expected large blue clusters, and thus very low spatial autocorrelation of the points, for the 2017 event, but this was not the case. Small blue clusters appeared only in areas where the drought was extremely severe, while small red clusters appeared in areas where the drought was moderate to severe. In addition, the average annual rainfall was subjected to a spatial correlation analysis. It was deduced from this that where there are morphometric reliefs, in the region's hinterland, we will have high rainfall and indices characterized by drought under normal conditions. As a result, the spatial autocorrelation in these areas will be of the High-High type, that is, very high. In contrast, where there are no morphometric reliefs, we can see that precipitation is low and drought indices are moderate or extreme. As a result, the spatial autocorrelation will be Low-Low, that is, low.

In Addition, according to Fotheringham, (2009), Local variants of spatial

regression models, such as spatial lag and spatial error models, can be formulated to model both spatial non-stationarity and spatial dependency at the same time. This model allows not only the relationships within the model to vary spatially but also the degree of spatial dependence. in either the dependent variable or the residuals. The often-subjective nature of the definition of a spatial weights matrix, representing the scale of the spatial dependency being measured, remains a weakness in calculating any spatial autocorrelation statistic. To some extent, local spatial models address this issue by determining an optimal spatial weights matrix based on model goodness of fit. What is surprising is that a geographically weighted version of a spatial lag model, which would allow for a more objective estimation of local spatial autocorrelation statistics via estimates of local parameters on the lagged dependent variable term, is not used more frequently.

Chapter 8

SUMMARY AND CONCLUSIONS AND RECOMMENDATIONS

8.1 Summary and Conclusions

The main aim of this study was to assess drought conditions in the Campania region, southern Italy. Moreover, the study performed a detailed evaluation of existing Drought Indices to investigate their usefulness under different climatic conditions for which they were not originally developed for. The aim of the study was achieved by undertaking the following tasks:

1. Selection of the study area, and data collection and processing
2. Review and evaluation of the existing Drought Indices
3. Analysis of inter-annual precipitation variability
4. Reconstruction of historical gridded database
5. Evaluation of drought indices and drought conditions
6. Assessment of different historical drought events

A brief summary and the conclusions drawn from each of these tasks are presented in the following sections.

8.1.1 Selection of Study Area, and Data Collection and Processing

The Campania region, Southern Italy was selected as the case study in this research. It was chosen because the management of water resources in this region has great importance, since it is a major source of water supply for the region and its limitrophe area. Almost all population (approximately 6 million) depends on the water resources of this region. Moreover, the water resources of the study area support a range of uses valued by the Campanian community, including urban water supply, agricultural and horticultural industries, and downstream user requirements, as well as flow requirements for maintaining environmental flows. Therefore, the assessment of the drought conditions can be a useful tool for the management of water resources in the Campania region.

Data related to several hydro-meteorological variables (i.e., rainfall, potential evapotranspiration…etc.) were collected or computed for the Campania region. These data were required for the computation of different drought indicators. The required data were collected for this study from a number of organizations such as SIMN of Naples and the Civil protection department. Data used for the drought indicators were obtained from chapter 5 they were from 1918-2019 (102 years). Data processing was carried out to obtain the area representative monthly values as drought indicators were developed in this study using a monthly time step. Monthly drought indicators are suitable for operational purposes and have lower sensitivity to observational errors (McKee et al., 1993). Several historical droughts recorded in Campania including 1962,1989, 2003, and 2017 onwards were used in this study to evaluate the drought indicators.

8.1.2 Review And Evaluation of Existing Drought Indices

There are many drought indices that have been developed in the past

around the world to define drought conditions. Limited use of drought indices has been carried for the Campania region in the past, and therefore the usefulness of the existing drought indices was first reviewed in this study.It was found that majority of the drought indicators had been developed for specific regions, and therefore may not be directly applicable to other regions due to different hydro-climatic conditions. Moreover, it was also found that the researchers and professionals are confronted with the ambiguity of the drought definition. Some researchers and professionals argue that drought is just deficiency in rainfall and should be defined with the rainfall as the single variable.

Drought is classified into four types: meteorological, agricultural, hydrological, and socioeconomic. These droughts may not occur at the same time, but meteorological drought is the driving force behind the others. It is characterized by a reduction or poor distribution of rainfall in a given region for an extended period of time. However, many others believe that the definition of drought should consider significant components of the water cycle (such as rainfall, streamflow, and temperature), because the drought depends on numerous factors, such as water supplies and demands, hydrological and political boundaries, and antecedent conditions. Therefore, an evaluation study of the existing drought indicators was performed in this research to investigate whether they are applicable to a region, in this case the Campania region, for which these drought indices were not specifically developed.

A quantitative assessment of four existing drought indicators selected from different drought perspectives (i.e., meteorological, hydrological, and agricultural), was first conducted in this study to investigate how well these drought indicators can define the historical droughts in the Campania region.

The selected drought indicators namely, *Standardized Precipitation Index (SPI), Standardized Precipitation Evapotranspiration Index (SPEI), Normalized Difference Vegetation Index (NDVI)* and *The Enhanced Vegetation Index (EVI)*. Thereafter, an evaluation of these drought indicators was carriedout based on both qualitative and quantitative assessments to select the most appropriate drought index for defining drought conditions in the Campania region.

8.1.3 Regional Changes in Interannual Precipitation Variability

Quantifying inter-annual precipitation variability is critical for more realistic modeling of water resource availability under climate change scenarios, which leads to a more effective quantification of the socioeconomic impact of planned complex water resource management tools.

The results show a generalized condition of statistically significant increase of inter-annual variability almost over the whole analyzed area, where a very moderate spatial consistency was however detected. In addition, the magnitude of the changes reported about a rather moderate intensity of the detected changes, with minimum and maximum CV patterns slope, expressed as the percentage of annual increase or decrease in CV over the whole observations recording. Moreover, no strong spatial consistency was detected, but rain gauge stations featured by the largest average inter-annual variability seemed to be the less affected by temporal changes.

Because of data availability and statistical homogeneity, the effect of the last fifteen years of data, from 2000 to 2015, was only studied on a subset of stations. A comparison of the statistical test results for the periods 1918-1999 and 1918-2015 revealed that, aside from the same general tendency (significant positive trends for the greatest percentage of stations), there is some quantitative difference between the two observed periods, but it appears to be very minor.

The relationship between average precipitation, intra-annual precipitation variability and inter-annual precipitation variability was not clearly identified for the studied region, but it was found that larger CV values appear associated to large MAP and large PCI values.

The primary point from the comparative analysis of average precipitation, intra-annual precipitation variability, and inter-annual precipitation variability is that, while variations in the annual precipitation regime and intra-annual precipitation variability are not statistically significant changes in inter-annual precipitation variability were indeed.

8.1.4 Reconstruction Of Gridded Climatological Data from The Two Database

The spatial distribution of monthly mean rainfall and temperature in the Campania region of southern Italy was estimated in this study using four kriging-based geostatistical interpolation methods (EBK, OK, DK, and OCK) and one deterministic (IDW). The goal is to compare the results of these interpolation methods in order to choose the best interpolation method for producing a high-quality continuous gridded rainfall/temperature dataset, which is initially heterogeneous, in the form of a rainfall/temperature chart at the regional scale. Elevation data from a DEM of the study area is used as a secondary attribute in the cokriging analysis using the OCK and DK methods, in addition to rainfall/temperature data. Geostatistical methods outperform deterministic methods for spatial interpolation of rainfall/temperature over a century in a morphologically complex region like Campania, according to the results. The IDW method yielded the worst results for the sample field, while cokriging methods (OCK and DK) outperformed other geostatistical methods. OCK outperformed all other

interpolators over a century by producing more reliable rainfall estimates for all monthly data. OCK had the smallest prediction errors and uncertainty, as well as the strongest correlations between predicted and measured monthly average rainfall/temperature. In this study, OCK proved to be the best interpolator for estimating the spatial distribution of rainfall/temperature in the study area. The results show that incorporating elevation as an auxiliary variable into rainfall/temperature data improves variable prediction in mountainous areas with complex orography. As a result, the current study suggests that OCK be used to generate continuous climate variable maps, particularly in areas with high spatial variation in rainfall and elevation. The comparison of the resulting OCK datasets with those of the ERA5 database revealed a high correlation between both datasets, confirming the accuracy of the geostatistical model's precipitation and temperature predictions over the Campania region.

8.1.5 Evaluation Of Drought Indices and Drought Conditions

In terms of drought temporal features, the trend was found to be prevalently negative, and the percentage of impacted cells increased with accumulation scale. It was nearly identical for SPI/SPEI time series calculated over 24 months or longer intervals. The significance was also discovered to be especially evident near 70% of grid cells for SPI 24/SPEI 24. Beyond this timescale threshold, the significance of temporal variability decreased dramatically. As a result, MDS increased with accumulation scale, rising from around 10 for SPI 6 to around 50 for SPI 48, and from -6 for SPEI 3 to -270 for SPEI 48. MDP did not change significantly with the accumulation scale for both indices, and this was especially noticeable with the shorter temporal scales. Extremely severe events had shorter durations and greater severity than moderate drought events, but they were much less common (over 75% less frequent). The region's complex orography appears to have an impact on both

the average precipitation spatial distribution and the relevant temporal variability. The accumulation timescale influenced the spatial behavior of the MDD. At the lowest accumulation scale, the northern area appeared to be more affected, whereas large MDD values were detected along a northwest to southeast transect but were more visible in the region's southern sectors. The maximum accumulation timescale values detected in the southern area were primarily caused by severe drought periods in the region in 1990, 2003, and 2017. The SPEI findings confirms the results reported by the SPI index, the main message in the current study is that we can not ignore the effect of temperature and evapotranspiration when evaluating drought conditions in a specific area. The accumulation scale had an effect on the MDS spatial pattern as well. Apart from a northwest to southeast transect and the southern sectors of the region where the highest MDS values were detected, it showed a concentration on the northern region area for the shorter temporal scales and a constant spatial distribution for the longer temporal scales. Finally, the MDP spatial pattern was discovered to be particularly complex, with no clear tendency related to the accumulation timescale. The largest drought peaks appeared to be concentrated on the region's northern inland area, which could be addressed as an area potentially prone to agricultural drought stress on a shorter timescale.

8.1.6 Drought Hot Spot Analysis Using Local Indicators of Spatial Autocorrelation

From the current research, we stated that the NDVI can reflect the evolution of vegetation; however, due to limitations caused by both the low correlation with the SPEI index and the restricted time horizon for which NDVI data are available, it was not possible to detect a link between SPEI and NDVI. This can be reflected to the climatic conditions of the Campania Region which would have been present fits into a sub-humid climate; perhaps if it had been arid, a greater vegetation stress. This study states that the SPEI and SPI indices adequately represent and describe drought phenomena, providing significant indications of their severity and temporal extent.

Drought is a multi-scalar phenomenon that has occurred over time in an ever-changing manner, even within the same year, as seen in the SPI and SPEI maps, and its spatial evolution is difficult to predict. As a result, studying spatial autocorrelation was also necessary to determine whether and how the points on the grid were related to one another. It was concluded from this that when the drought phenomenon occurs, the spatial autocorrelation is of the Low-Low type, whereas when the drought phenomenon does not occur, the autocorrelation is of the High-High type.

8.2 Limitation Of the Study and Recommendations for Further Research

Some limitations of the present study can be discussed and recommendations can be suggested for future studiesto alleviate them.

As was discussed in section 1.4.2 several data were not available such

as the soil moisture data, stream flow storage reservoir volume …etc., for that we could not test different drought indicators for instance the Palmar (1965) index (PDSI) or the aggregated drought index (ADI). The latter is a multivariate drought index that comprehensively considers all physical forms of drought (i.e., meteorological, hydrological, and agricultural). It takes into account the most important eight variables that define the hydrologic cycle: rainfall, potential evapotranspiration, streamflow, storage reservoir volume, soil moisture content, snow water content, groundwater flow, and temperature. Keyantash and Dracup used six influential variables for ADI formulation: rainfall, potential evapotranspiration, streamflow, storage reservoir volume, soil moisture content, and snow water content (2004). These variables except the rainfall and evapotranspiration were not considered in this study. According to Keyantash and Dracup (2004), groundwater flow was excluded from this study for three reasons: (1) data on historic groundwater levels were not easily accessible for this catchment; (2) groundwater flow into heterogeneous aquifers across the catchment is difficult to assess; and (3) groundwater recharge/depletion is a slow process that occurs over longer time scales. For what concern the drought indicator derived from remote sensing (NDVI, EVI), it could be better to test these indicators on micro area for example river, agricultural lands …etc., as it was mentioned in section 7.5 the NDVI and the EVI could not highlight the drought at large scale. In addition, it should be noted that the spatial autocorrelation needs to be developed for different section in the study area, the Analytic Hierarchy Process AHP could be an efficient process to better locate drought in the study area, however, Using pair-wise comparison matrices, AHP can be used to calculate the weights for each criterion and drought type. Individual drought categories and overall drought vulnerability maps should be created using the weighted overlay technique and the

corresponding criteria. In the current research we could not apply the process for the lack of different parameters.

Last but not least, there is no community or private sector preparedness or training for drought management, as there is for disaster response training. Water companies are required by law to revise their drought plans on an annual basis to reflect changing conditions in water supply and demand.

REFERENCES

Abramowitz, M., and Stegun, I. A.: Handbook of mathematical functions with formulas, graphs, and mathematical tables, US Government printing office, 1964.

Adhikary, S. K., Muttil, N., & Yilmaz, A. G. (2017). Cokriging for enhanced spatial interpolation of rainfall in two Australian catchments. *Hydrological processes*, *31*(12), 2143-2161.

Adhikary, S. K., Yilmaz, A. G., & Muttil, N. (2015). Optimal design of rain gauge network in the Middle Yarra River catchment, Australia. *Hydrological processes*, *29*(11), 2582-2599

AghaKouchak, A., Chiang, F., Huning, L. S., Love, C. A., Mallakpour, I., Mazdiyasni, O., ... & Sadegh, M. (2020). Climate extremes and compound hazards in a warming world. *Annual Review of Earth and Planetary Sciences*, *48*, 519-548..

Arnaud, M., Emery, X., De Fouquet, C., Brouwers, M., & Fortier, M. (2001). L'analyse krigeante pour le classement d'observations spatiales et multivariées. *Revue de statistique appliquée*, *49*(2), 45-67.

Bachmair, S., Tanguy, M., Hannaford, J., & Stahl, K. (2018). How well do meteorological indicators represent agricultural and forest drought across Europe?. *Environmental Research Letters*, *13*(3), 034042.

Baillargeon, S. (2005). Le krigeage: revue de la théorie et application à l'interpolation spatiale de données de précipitations.

Baker, B. H., Kröger, R., Brooks, J. P., Smith, R. K., & Czarnecki, J. M. P. (2015). Investigation of denitrifying microbial communities within an agricultural drainage system fitted with low-grade weirs. *Water research*, *87*, 193-201.

Belayneh, A., & Adamowski, J. (2012). Standard precipitation index drought forecasting using neural networks, wavelet neural networks, and support vector regression. *Applied computational intelligence and soft computing*, *2012*.

Bonaccorso, B., Aronica, G.T.: Estimating Temporal Changes in Extreme Rainfall in Sicily Region (Italy), Water Resour Manag, 30 (15), 5651-5670, 2016.

Bonaccorso, B., & Cancelliere, A. (2015, April). Exploiting teleconnection indices for probabilistic forecasting of drought class transitions in Sicily region (Italy). In *EGU General Assembly Conference Abstracts* (p. 15030).

Bonaccorso, B., Cancelliere, A., & Rossi, G. (2015). Probabilistic forecasting of drought class transitions in Sicily (Italy) using standardized precipitation index and North Atlantic oscillation index. *Journal of Hydrology*, *526*, 136-150.

Bonaccorso, B., Peres, D. J., Cancelliere, A., & Rossi, G. (2013). Large scale probabilistic drought characterization over Europe. *Water Resources Management*, *27*(6), 1675-1692.

Bordi, I., Frigio, S., Parenti, P., Speranza, A., and Sutera,: The analysis of the Standardized Precipitation Index in the Mediterranean area: regional patterns, ANN GEOPHYS-ITALY., 44, 2001.

Boulariah, O., Longobardi, A., Nobile, V., Sessa, M. and Villani, P.: Long term monthly precipitation database reconstruction for drought assessment. In: "ClimRisk2020: Time for Action! Raising the ambition of climate action in the age of global emergencies" – SISC Seventh Annual Conference, 21-23 October 2020, 2020

Boulariah O, Longobardi A, Meddi M (2017) Hydroclimate temporal variability in a coastal Mediterranean watershed: the Tafna basin, North-West Algeria. EGU General Assembly Conference Abstracts 17462

Brunetti, M., Maugeri, M., Nanni, T., Simolo, C., & Spinoni, J. (2014). High-resolution temperature climatology for Italy: interpolation method intercomparison. *International Journal of Climatology*, *34*(4), 1278-1296.

Buttafuoco, G., and Caloiero,: Drought events at different timescales in southern Italy (Calabria), J MAPS., 10, 529-537, 2014.

Buttafuoco, G., Caloiero, T., & Coscarelli, R. (2015). Analyses of drought events in Calabria (Southern Italy) using standardized precipitation index. *Water Resources Management*, *29*(2), 557-573.

Caloiero, T., Veltri, S., Caloiero, P., and Frustaci, F.: Drought analysis in Europe and in the Mediterranean basin using the standardized precipitation index, Water., 10, 1043, 2018.

Caloiero, T., Veltri, S., A.: Drought assessment in the Sardinia Region (Italy) during 1922–2011 using the standardized precipitation index, J APPL GEOPHYS., 176, 925-935, 2019.

Capra, A., & Scicolone, B. (2012). Spatiotemporal variability of drought on a short–medium time scale in the Calabria Region (Southern Italy). *Theoretical and applied climatology*, *110*(3), 471-488.

Califano, F., Mobilia, M., & Longobardi, A. (2015). Heavy rainfall temporal characterization in the peri-urban Solofrana river basin, Southern Italy. *Procedia Engineering*, *119*, 1129-1138.

Cecílio, R. A., & Pruski, F. F. (2003). Interpolação dos parâmetros da equação de chuvas intensas com uso do inverso de potências da distância. *Revista Brasileira de Engenharia Agrícola e Ambiental*, *7*, 501-504.

Chandniha, S. K., Meshram, S. G., Adamowski, J. F., & Meshram, C. (2017). Trend analysis of precipitation in Jharkhand State, India. *Theoretical and Applied Climatology*, *130*(1), 261-274.

Colangelo, M., Camarero, J. J., Borghetti, M., Gazol, A., Gentilesca, T., & Ripullone, F. (2017). Size matters a lot: drought-affected Italian oaks are smaller and show lower growth prior to tree death. *Frontiers in Plant Science*, *8*, 135.

Colella, M., M. Ripa, A. Cocozza, C. Panfilo and S. J. J. o. E. M. Ulgiati (2021). "Challenges and opportunities for more efficient water use and circular wastewater management. The case of Campania Region, Italy." **297**: 113171.

Conrad, V. (1941). The variability of precipitation. *Monthly Weather Review*, *69*(1), 5-11.

Cook, B. I., Anchukaitis, K. J., Touchan, R., Meko, D. M., and Cook, E. R.: Spatiotemporal drought variability in the Mediterranean over the last 900 years, J. Geophys. Res. Atmos., 121, 2060-2074, 2016.

Delitala, A. M., Cesari, D., Chessa, P. A., and Ward, M. N.: Precipitation over Sardinia (Italy) during the 1946–1993 rainy seasons and associated large-scale climate variations, INT J CLIMATOL., 20, 519-541, 2000.

Di Lena, B., Vergni, L., Antenucci, F., Todisco, F., Mannocchi, F.: Analysis of drought in the region of Abruzzo (Central Italy) by the Standardized Precipitation Index, Theor. Appl. Climatol 115, 41-52, 2014

Desa, U. N. (2019). World population prospects 2019: Highlights. *New York (US): United Nations Department for Economic and Social Affairs*, *11*(1), 125.

Desbarats, A. J., Logan, C. E., Hinton, M. J., & Sharpe, D. R. (2002). On the kriging of water table elevations using collateral information from a digital elevation model. *Journal of Hydrology*, *255*(1-4), 25-38.

Diaz, V., Corzo, G., Van Lanen, H. A., & Solomatine, D. P. (2019). Spatiotemporal drought analysis at country scale through the application of the STAND toolbox. In *Spatiotemporal analysis of extreme hydrological events* (pp. 77-93). Elsevier.

Dracup, J. A., Lee, K. S., and Paulson Jr, E. G.: On the definition of droughts, Water Resour. Res.,16, 297-302, 1980

European drought center., http://europeandroughtcentre.com/, last access: 10 December 2020

Dünkeloh, A., & Jacobeit, J. (2003). Circulation dynamics of Mediterranean precipitation variability 1948–98. *International Journal of Climatology: A Journal of the Royal Meteorological Society*, *23*(15), 1843-1866.

Fatichi, S., Ivanov, V. Y., & Caporali, E. (2012). Investigating interannual variability of precipitation at the global scale: Is there a connection with seasonality?. *Journal of climate*, *25*(16), 5512-5523.

Fattoruso G, *Longobardi A, Pizzuti A, Molinara M, Marocco C, de Vito S, Tortorella F, Di Francia G (2017) Evaluation and design of a rain gauge network using a statistical optimization method in a severe hydro-geological hazard prone area. AIP Conference Proc AIP Publishing, 020055*

Fava, F., Gardossi, L., Brigidi, P., Morone, P., Carosi, D. A., & Lenzi, A. (2021). The bioeconomy in Italy and the new national strategy for a more competitive and sustainable country. *New Biotechnology*, *61*, 124-136.

Fischer, E. M., & Knutti, R. (2015). Anthropogenic contribution to global occurrence of heavy-precipitation and high-temperature extremes. *Nature climate change*, *5*(6), 560-564.

Forootan, E., Khaki, M., Schumacher, M., Wulfmeyer, V., Mehrnegar, N., van Dijk, A. I., ... & Mostafaie, A. (2019). Understanding the global hydrological droughts of 2003–2016 and their relationships with teleconnections. *Science of the Total Environment*, *650*, 2587-2604.

Fung, K., Huang, Y., and Koo, C.: Assessing drought conditions through temporal pattern, spatial characteristic and operational accuracy indicated by SPI and SPEI: case analysis for Peninsular Malaysia, NAT HAZARDS., 103, 2071-2101, 2020

Gajbhiye, S., Meshram, C., Mirabbasi, R., & Sharma, S. K. (2016). Trend analysis of rainfall time series for Sindh river basin in India. *Theoretical and applied climatology*, *125*(3), 593-608.

Ganguli, P., and Reddy, M. J.: Evaluation of trends and multivariate frequency analysis of droughts in three meteorological subdivisions of western India, INT J CLIMATOL., 34, 911-928, 2014.

Gardner, T. (2010). Google unveils satellite platform to aid forest efforts. Reuters.

Giorgi, F. (2006). Climate change hot-spots. *Geophysical research letters*, *33*(8).

Giorgi F, Bi X (2005) Regional changes in surface climate interannual variability for the 21st century from ensembles of global model simulations. Geophys Res Lett 32

Giorgi, F., & Lionello, P. (2008). Climate change projections for the Mediterranean region. *Global and planetary change*, *63*(2-3), 90-104.

Goovaerts, P. (1997). *Geostatistics for natural resources evaluation*. Oxford University Press on Demand.

Goovaerts, P., AvRuskin, G., Meliker, J., Slotnick, M., Jacquez, G., & Nriagu, J. (2005). Geostatistical modeling of the spatial variability of arsenic in groundwater of southeast Michigan. *Water Resources Research*, *41*(7).

Goovaerts, P. (1999). Geostatistics in soil science: state-of-the-art and perspectives. *Geoderma*, *89*(1-2), 1-45.

Gorelick, N. (2013). Google earth engine. EGU general assembly conference abstracts, American Geophysical Union Vienna, Austria.

Gouveia, C., Trigo, R. M., Beguería, S., Vicente-Serrano, S. M.: Drought impacts on vegetation activity in the Mediterranean region: An assessment using remote sensing data and multi-scale drought indicators, GLOBAL PLANET CHANGE .,151, 15- 27, 2017.

Gamelin, F. X., Baquet, G., Berthoin, S., Thevenet, D., Nourry, C., Nottin, S., & Bosquet, L. (2009). Effect of high intensity intermittent training on heart rate variability in prepubescent children. *European journal of applied physiology*, *105*(5), 731-738.

Guastaldi, E., & Del Frate, A. A. (2012). Risk analysis for remediation of contaminated sites: the geostatistical approach. *Environmental Earth Sciences*, *65*(3), 897-916.

Gutiérrez, A. P. A., Engle, N. L., De Nys, E., Molejón, C., & Martins, E. S. (2014). Drought preparedness in Brazil. *Weather and Climate Extremes*, *3*, 95-106.

Guo, H., Bao, A., Liu, T., Ndayisaba, F., Jiang, L., Kurban, A., and De Maeyer, P.: Spatial and temporal characteristics of droughts in Central Asia during 1966–2015, SCI TOTAL ENVIRON.,624, 1523-1538, 2018

Haile, G. G., Tang, Q., Li, W., Liu, X., & Zhang, X. (2020). Drought: Progress in broadening its understanding. *Wiley Interdisciplinary Reviews: Water*, *7*(2), e1407.

Hamed, K. H., & Rao, A. R. (1998). A modified Mann-Kendall trend test for autocorrelated data. *Journal of hydrology*, *204*(1-4), 182-196.

Hamed, K. H. (2008). Trend detection in hydrologic data: the Mann–Kendall trend test under the scaling hypothesis. *Journal of hydrology*, *349*(3-4), 350-363.

Hamilton, L. C., & Keim, B. D. (2009). Regional variation in perceptions about climate change. *International Journal of Climatology: A Journal of the Royal Meteorological Society*, *29*(15), 2348-2352.

Hao, Z., Singh, V. P., & Hao, F. (2018). Compound extremes in hydroclimatology: a review. *Water*, *10*(6), 718.

Hayes, M. J., Alvord, C., & Lowrey, J. (2002). *Drought indices*. National drought mitigation center, University of Nebraska.

Hasegawa, A., Gusyev, M., and Iwami, Y.: Meteorological drought and flood assessment using the comparative SPI approach in Asia under climate change, J. Disaster Res. .,11, 1082-1090, 2016.

He, C., & Li, T. (2019). Does global warming amplify interannual climate variability?. *Climate Dynamics*, *52*(5), 2667-2684.

He, M., & Gautam, M. (2016). Variability and trends in precipitation, temperature and drought indices in the State of California. *Hydrology*, *3*(2), 14.

Heim Jr, R. R. (2002). A review of twentieth-century drought indices used in the United States. *Bulletin of the American Meteorological Society*, *83*(8), 1149-1166.

Hoeksema, R. J., Clapp, R. B., Thomas, A. L., Hunley, A. E., Farrow, N. D., & Dearstone, K. C. (1989). Cokriging model for estimation of water table elevation. *Water Resources Research*, *25*(3), 429-438.

Husak, G. J., Michaelsen, J., and Funk, C.: Use of the gamma distribution to represent monthly rainfall in Africa for drought monitoring applications, INT J CLIMATOL.,27, 935-944, 2007

Inoue, T., Yaida, Y. A., Uehara, Y., Katsuhara, K. R., Kawai, J., Takashima, K., ... & Kenta, T. (2021). The effects of temporal continuities of grasslands on the diversity and species composition of plants. *Ecological Research*, *36*(1), 24-31.

IPCC (2014). "Climate Change 2013: The Physical Science Basis: Working Group I Contribution to the Fifth Assessment Report of the Intergovernmental Panel on Climate Change." Cambridge: Cambridge University Press.

IPCC (2021). "Climate change 2021: The physical science basis. Contribution of working group I to the sixth assessment report of the Intergovernmental Panel on Climate Change (V Masson-Delmotte, P Zhai, A Pirani, SL Connors, C Péan, S Berger, N Caud, Y Chen, L Goldfarb, MI Gomis, et al., Eds.). Cambridge University Press." Cambridge University Press.

Isaaks, E. H., & Srivastava, M. R. (1989). *Applied geostatistics* (No. 551.72 ISA).

Jenner, L. (2013). NASA-NASA's Goddard Space Flight Center.

Johnston, K., Ver Hoef, J. M., Krivoruchko, K., & Lucas, N. (2001). *Using ArcGIS geostatistical analyst* (Vol. 380). Redlands: Esri.

Kendall, M. G. (1948). Rank correlation methods.

Keyantash, J., & Dracup, J. A. (2002). The quantification of drought: an evaluation of drought indices. *Bulletin of the American Meteorological Society*, *83*(8), 1167-1180.

Khelfi, M. E. A., Touaibia, B., & Guastaldi, E. (2017). Regionalisation of the "intensity-duration-frequency" curves in Northern Algeria. *Arabian Journal of Geosciences*, *10*(20), 1-13

Kravchenko, A., & Bullock, D. G. (1999). A comparative study of interpolation methods for mapping soil properties. *Agronomy journal*, *91*(3), 393-400.

Lazoglou, G., Anagnostopoulou, C., Tolika, K., & Kolyva-Machera, F. (2019). A review of statistical methods to analyze extreme precipitation and temperature events in the Mediterranean region. *Theoretical and Applied Climatology*, *136*(1), 99-117.

Lehmann, J., Mempel, F., & Coumou, D. (2018). Increased occurrence of record-wet and record-dry months reflect changes in mean rainfall. *Geophysical Research Letters*, *45*(24), 13-468.

LI, X.-X., JU, H., Sarah, G., YAN, C.-R., Batchelor, W.D., LIU, Q.: Spatiotemporal variation of drought characteristics in the Huang-Huai-Hai Plain, China under the climate change scenario, J. Integr. Agr., 16 (10), 2308-2322, 2017.

Littell, J. S., Peterson, D. L., Riley, K. L., Liu, Y., and Luce, C. H.: A review of the relationships between drought and forest fire in the United States, GLOB CHANGE BIOL., 22, 2353-2369, 2016.

Liu, Z., Wang, Y., Shao, M., Jia, X., and Li, X.: Spatiotemporal analysis of multiscalar drought characteristics across the Loess Plateau of China, J HYDROL.,534, 281-299, 2016

Longobardi, A., and Mautone, M.: Trend analysis of annual and seasonal air temperature time series in southern Italy, in: Engineering Geology for Society and Territory-Volume 3, Springer, 501-504, 2015.

Longobardi, A., Buttafuoco, G., Caloiero, T., & Coscarelli, R. (2016). Spatial and temporal distribution of precipitation in a Mediterranean area (southern Italy). *Environmental earth sciences*, *75*(3), 1-20.

Longobardi, A., & Van Loon, A. F. (2018). Assessing baseflow index vulnerability to variation in dry spell length for a range of catchment and climate properties. *Hydrological Processes*, *32*(16), 2496-2509.

Longobardi, A., & Villani, P. (2010). Trend analysis of annual and seasonal rainfall time series in the Mediterranean area. *International journal of Climatology*, *30*(10), 1538-1546.

Longobardi, A., & Boulariah, O. (2022). Long-term regional changes in inter-annual precipitation variability in the Campania Region, Southern Italy. *Theoretical and Applied Climatology*, *148*(3), 869-879.

Luterbacher, J., Xoplaki, E., Casty, C., Wanner, H., Pauling, A., Küttel, M., ... & Ladurie, E. L. R. (2006). Mediterranean climate variability over the last centuries: a review. *Developments in Earth and environmental Sciences*, *4*, 27-148.

Marini, G., Fontana, N., & Mishra, A. K. (2019). Investigating drought in Apulia region, Italy using SPI and RDI. *Theoretical and applied climatology*, *137*(1), 383-397.

Martinez, C., Goddard, L., Kushnir, Y., & Ting, M. (2019). Seasonal climatology and dynamical mechanisms of rainfall in the Caribbean. *Climate dynamics*, *53*(1), 825-846.

Martino, G. D., Fontana, N., Marini, G., & Singh, V. P. (2013). Variability and trend in seasonal precipitation in the continental United States. *Journal of Hydrologic Engineering*, *18*(6), 630-640.

MANN, H. (1945). Non-parametric tests against trend. Econometria.

McKee, T. B., Doesken, N. J., & Kleist, J. (1993, January). The relationship of drought frequency and duration to time scales. In *Proceedings of the 8th Conference on Applied Climatology* (Vol. 17, No. 22, pp. 179-183).

Mathbout, S., Lopez-Bustins, J. A., Martin-Vide, J., Bech, J., & Rodrigo, F. S. (2018). Spatial and temporal analysis of drought variability at several time scales in Syria during 1961–2012. *Atmospheric Research*, *200*, 153-168.

Meddi, M. M., Assani, A. A., & Meddi, H. (2010). Temporal variability of annual rainfall in the Macta and Tafna catchments, Northwestern Algeria. *Water Resources Management*, *24*(14), 3817-3833.

Mirzaei, R., & Sakizadeh, M. (2016). Comparison of interpolation methods for the estimation of groundwater contamination in Andimeshk-Shush Plain, Southwest of Iran. *Environmental Science and Pollution Research*, *23*(3), 2758-2769.

Mishra, A. K., & Singh, V. P. (2010). A review of drought concepts. *Journal of hydrology*, *391*(1-2), 202-216.

Mishra, A. K., & Singh, V. P. (2011). Drought modeling–A review. *Journal of Hydrology*, *403*(1-2), 157-175.

Mishra, V., Tiwari, A. D., Aadhar, S., Shah, R., Xiao, M., Pai, D. S., & Lettenmaier, D. (2019). Drought and famine in India, 1870–2016. *Geophysical Research Letters*, *46*(4), 2075-2083.

Mondal, A., Kundu, S., & Mukhopadhyay, A. (2012). Rainfall trend analysis by Mann-Kendall test: A case study of north-eastern part of Cuttack district, Orissa. *International Journal of Geology, Earth and Environmental Sciences*, *2*(1), 70-78.

Moral, F. J. (2010). Comparison of different geostatistical approaches to map climate variables: application to precipitation. *International Journal of Climatology: A Journal of the Royal Meteorological Society*, *30*(4), 620-631.

Nicholls, N., & Wong, K. K. (1990). Dependence of rainfall variability on mean rainfall, latitude, and the Southern Oscillation. *Journal of climate*, 163-170.

Nash, J. E., & Sutcliffe, J. V. (1970). River flow forecasting through conceptual models part I—A discussion of principles. *Journal of hydrology*, *10*(3), 282-290.

Ntale, H. K., & Gan, T. Y. (2003). Drought indices and their application to East Africa. *International Journal of Climatology: A Journal of the Royal Meteorological Society*, *23*(11), 1335-1357.

Observatory(EDO), E. D. (2018). "Timeline of Drought Events."

Oliver, J. E. (1980). Monthly precipitation distribution: a comparative index. *The Professional Geographer*, *32*(3), 300-309.

Pachauri, R. K., & Meyer, L. A. (2014). Climate Change 2014: Synthesis Report. Contribution of Working Groups I, II and III to the Fifth Assessment Report of the Intergovernmental Panel on Climate Change.

Palmer, W. C. (1965). *Meteorological drought* (Vol. 30). US Department of Commerce, Weather Bureau.

Palmer, W. C. (1968). Keeping track of crop moisture conditions, nationwide: the new crop moisture index.

Papalexiou, S. M., & Montanari, A. (2019). Global and regional increase of precipitation extremes under global warming. *Water Resources Research*, *55*(6), 4901-4914.

Pei, T., Qin, C. Z., Zhu, A. X., Yang, L., Luo, M., Li, B., & Zhou, C. (2010). Mapping soil organic matter using the topographic wetness index: A comparative study based on different flow-direction algorithms and kriging methods. *Ecological Indicators*, *10*(3), 610-619.

Pettitt, A. N. (1979). A non-parametric approach to the change-point problem. *Journal of the Royal Statistical Society: Series C (Applied Statistics)*, *28*(2), 126-135.

Pendergrass, A. G., Knutti, R., Lehner, F., Deser, C., & Sanderson, B. M. (2017). Precipitation variability increases in a warmer climate. *Scientific reports*, *7*(1), 1-9.

Phillips, D. L., Dolph, J., & Marks, D. (1992). A comparison of geostatistical procedures for spatial analysis of precipitation in mountainous terrain. *Agricultural and forest meteorology*, *58*(1-2), 119-141.

Piccarreta, M., Capolongo, D., & Boenzi, F. (2004). Trend analysis of precipitation and drought in Basilicata from 1923 to 2000 within a southern Italy context. *International Journal of Climatology: A Journal of the Royal Meteorological Society*, *24*(7), 907-922.

Pierleoni, A., Camici, S., Brocca, L., Moramarco, T., & Casadei, S. (2014). Climate change and decision support systems for water resource management. *Procedia Engineering*, *70*, 1324-1333.

Preziosi, E., Del Bon, A., Romano, E., Petrangeli, A. B., & Casadei, S. (2013). Vulnerability to drought of a complex water supply system. The upper Tiber basin case study (Central Italy). *Water resources management*, *27*(13), 4655-4678.

Ramos, M. C., & Martínez-Casasnovas, J. A. (2006). Trends in precipitation concentration and extremes in the Mediterranean Penedes-Anoia region, NE Spain. *Climatic Change*, *74*(4), 457-474.

Raymond, F., Ullmann, A., Camberlin, P., Oueslati, B., & Drobinski, P. (2018). Atmospheric conditions and weather regimes associated with extreme winter dry spells over the Mediterranean basin. *Climate Dynamics*, *50*(11), 4437-4453.

Robertson, G. P. (2008). GS: Geostatistics for the Environmental Sciences. Gamma Design Software, Plainwell, MI.

Rodriguez-Puebla, C., Encinas, A. H., Nieto, S., & Garmendia, J. (1998). Spatial and temporal patterns of annual precipitation variability over the Iberian Peninsula. *International Journal of Climatology: A Journal of the Royal Meteorological Society*, *18*(3), 299-316.

Ronco, P., Zennaro, F., Torresan, S., Critto, A., Santini, M., Trabucco, A., ... & Marcomini, A. (2017). A risk assessment framework for irrigated agriculture under climate change. *Advances in Water Resources*, *110*, 562-578.

Rossi, G. (2020). Paradigm Change in Water Resources Development in Italy. In *Water Resources of Italy* (pp. 29-53). Springer, Cham.

Rouse Jr, J. W., Haas, R. H., Schell, J. A., & Deering, D. W. (1973, December). Paper a 20. In *Third Earth Resources Technology Satellite-1 Symposium: The Proceedings of a Symposium Held by Goddard Space Flight Center at Washington, DC on* (Vol. 351, p. 309).

Ruffault, J., Martin-StPaul, N., Pimont, F., & Dupuy, J. L. (2018). How well do meteorological drought indices predict live fuel moisture content (LFMC)? An assessment for wildfire research and operations in Mediterranean ecosystems. *Agricultural and Forest Meteorology*, *262*, 391-401.

Sa'adi, Z., Shahid, S., Ismail, T., Chung, E. S., & Wang, X. J. (2019). Trends analysis of rainfall and rainfall extremes in Sarawak, Malaysia using modified Mann–Kendall test. *Meteorology and Atmospheric Physics*, *131*(3), 263-277.

Salvador, C., Nieto, R., Linares, C., Díaz, J., & Gimeno, L. (2020). Effects of droughts on health: Diagnosis, repercussion, and adaptation in vulnerable regions under climate change. Challenges for future research. *Science of the Total Environment*, *703*, 134912.

Santos, L. D. C., José, J. V., Alves, D. S., Nitsche, P. R., Reis, E. F. D., & Bender, F. D. (2017). Space-time variability of evapotranspiration and precipitation in the State of Paraná, Brazil. *Revista Ambiente & Água*, *12*, 743-759.

Searls, D. T. (1964). The utilization of a known coefficient of variation in the estimation procedure. *Journal of the American Statistical Association*, *59*(308), 1225-1226.

Sen, P. K. (1968). Estimates of the regression coefficient based on Kendall's tau. *Journal of the American statistical association*, *63*(324), 1379-1389.

Sillmann, J., Daloz, A. S., Schaller, N., & Schwingshackl, C. (2021). Extreme weather and climate change. In *Climate Change* (pp. 359-372). Elsevier.

Sobral, B. S., de Oliveira-Junior, J. F., de Gois, G., Pereira-Júnior, E. R., de Bodas Terassi, P. M., Muniz-Júnior, J. G. R., ... & Zeri, M. (2019). Drought characterization for the state of Rio de Janeiro based on the annual SPI index: trends, statistical tests and its relation with ENSO. *Atmospheric research*, *220*, 141-154.

Sohoulande Djebou, D. C., & Singh, V. P. (2016). Impact of climate change on precipitation patterns: A comparative approach. *International Journal of Climatology*, *36*(10), 3588-3606.

Sorooshian, S., Duan, Q., & Gupta, V. K. (1993). Calibration of rainfall-runoff models: Application of global optimization to the Sacramento Soil Moisture Accounting Model. *Water resources research*, *29*(4), 1185-1194.

Spinoni, J., Barbosa, P., De Jager, A., McCormick, N., Naumann, G., Vogt, J. V., ... & Mazzeschi, M. (2019). A new global database of meteorological drought events from 1951 to 2016. *Journal of Hydrology: Regional Studies*, *22*, 100593.

Spinoni, J., Naumann, G., Vogt, J. V., & Barbosa, P. (2015). The biggest drought events in Europe from 1950 to 2012. *Journal of Hydrology: Regional Studies*, *3*, 509-524.

Spinoni, J., Naumann, G., Vogt, J. V., & Barbosa, P. (2015). The biggest drought events in Europe from 1950 to 2012. *Journal of Hydrology: Regional Studies*, *3*, 509-524.

Stagge, J. H., Kohn, I., Tallaksen, L. M., & Stahl, K. (2015). Modeling drought impact occurrence based on meteorological drought indices in Europe. *Journal of Hydrology*, *530*, 37-50.

Stagge, J. H., Kingston, D. G., Tallaksen, L. M., & Hannah, D. M. (2017). Observed drought indices show increasing divergence across Europe. *Scientific Reports*, *7*(1), 1-10.

Swain, S., & Hayhoe, K. (2015). CMIP5 projected changes in spring and summer drought and wet conditions over North America. *Climate Dynamics*, *44*(9), 2737-2750.

Tallaksen, L. M., & Van Lanen, H. A. (Eds.). (2004). Hydrological drought: processes and estimation methods for streamflow and groundwater.

Tsakiris, G., & Vangelis, H. J. E. W. (2005). Establishing a drought index incorporating evapotranspiration. *European water*, *9*(10), 3-11.

Tang, G., Behrangi, A., Long, D., Li, C., & Hong, Y. (2018). Accounting for spatiotemporal errors of gauges: A critical step to evaluate gridded precipitation products. *Journal of hydrology*, *559*, 294-306.

Taverniers, I., De Loose, M., & Van Bockstaele, E. (2004). Trends in quality in the analytical laboratory. II. Analytical method validation and quality assurance. *TrAC Trends in Analytical Chemistry*, *23*(8), 535-552.

Tigkas, D., Vangelis, H., & Tsakiris, G. (2015). DrinC: a software for drought analysis based on drought indices. *Earth Science Informatics*, *8*(3), 697-709.

Toreti, A., & Desiato, F. (2008). Temperature trend over Italy from 1961 to 2004. *Theoretical and Applied Climatology*, *91*(1), 51-58.

Touazi, M., Laborde, J. P., & Bhiry, N. (2004). Modelling rainfall-discharge at a mean inter-yearly scale in northern Algeria. *Journal of Hydrology*, *296*(1-4), 179-191.

Tramblay, Y., & Somot, S. (2018). Future evolution of extreme precipitation in the Mediterranean. *Climatic Change*, *151*(2), 289-302.

Tramblay, Y., Koutroulis, A., Samaniego, L., Vicente-Serrano, S. M., Volaire, F., Boone, A., ... & Polcher, J. (2020). Challenges for drought assessment in the Mediterranean region under future climate scenarios. *Earth-Science Reviews*, *210*, 103348

Van Loon, A. F. (2015). Hydrological drought explained. *Wiley Interdisciplinary Reviews: Water*, *2*(4), 359-392.

van Ginkel, M., & Biradar, C. (2021). Drought early warning in agri-food systems. *Climate*, *9*(9), 134.

Vicente-Serrano, S. M., Saz-Sánchez, M. A., & Cuadrat, J. M. (2003). Comparative analysis of interpolation methods in the middle Ebro Valley (Spain): application to annual precipitation and temperature. *Climate research*, *24*(2), 161-180.

Vogt, J. V., & Somma, F. (Eds.). (2013). *Drought and drought mitigation in Europe* (Vol. 14). Springer Science & Business Media.

Wang, J., Lin, H., Huang, J., Jiang, C., Xie, Y., & Zhou, M. (2019). Variations of drought tendency, frequency, and characteristics and their responses to climate change under CMIP5 RCP scenarios in Huai River Basin, China. *Water*, *11*(10), 2174.

Wilhite, D. A., & Glantz, M. H. (1985). Understanding: the drought phenomenon: the role of definitions. *Water international*, *10*(3), 111-120.

Wilhite, D. A., Sivakumar, M. V., & Pulwarty, R. (2014). Managing drought risk in a changing climate: The role of national drought policy. *Weather and climate extremes*, *3*, 4-13.

World Meteorological Organization. (1989). Calculation of monthly and annual 30-year standard normals. *WCDP 10, WMO-TD 341*.

Wood, E. F., Schubert, S. D., Wood, A. W., Peters-Lidard, C. D., Mo, K. C., Mariotti, A., & Pulwarty, R. S. (2015). Prospects for advancing drought understanding, monitoring, and prediction. *Journal of Hydrometeorology*, *16*(4), 1636-1657.

Wu, S., Chen, L., Wang, N., Xu, S., Bagarello, V., & Ferro, V. (2019). Variable power-law scaling of hillslope Hortonian rainfall–runoff processes. *Hydrological Processes*, *33*(22), 2926-2938.

Xu, R., Tian, F., Yang, L., Hu, H., Lu, H., & Hou, A. (2017). Ground validation of GPM IMERG and TRMM 3B42V7 rainfall products over southern Tibetan Plateau based on a

high-density rain gauge network. *Journal of Geophysical Research: Atmospheres*, *122*(2), 910-924.

Yevjevich, V. M. (1967). *Objective approach to definitions and investigations of continental hydrologic droughts, An* (Doctoral dissertation, Colorado State University. Libraries).

Yue, S., & Wang, C. (2004). The Mann-Kendall test modified by effective sample size to detect trend in serially correlated hydrological series. *Water resources management*, *18*(3), 201-218.

Zhang, L., & Zhou, T. (2015). Drought over East Asia: a review. *Journal of Climate*, *28*(8), 3375-3399.

Zhou, H., & Liu, Y. (2016). SPI based meteorological drought assessment over a humid basin: Effects of processing schemes. *Water*, *8*(9), 373.

.